
Madm Controls

Synapse Development and Stability

Inauguraldissertation

zur
Erlangung der Würde eines Doktors der Philosophie
vorgelegt der
Philosophisch-Naturwissenschaftlichen Fakultät
der Universität Basel

von

Ingrid Daniela Kieweg
(aus Bad Wimsbach-Neydharting, Österreich)

Basel, 2014

Originaldokument gespeichert auf dem Dokumentenserver der Universität Basel edoc.unibas.ch



Dieses Werk ist unter dem Vertrag „Creative Commons Namensnennung-Keine kommerzielle Nutzung-Keine Bearbeitung 3.0 Schweiz“ (CC BY-NC-ND 3.0 CH) lizenziert. Die vollständige Lizenz kann unter creativecommons.org/licenses/by-nc-nd/3.0/ch/ eingesehen werden.

Genehmigt von der Philosophisch-Naturwissenschaftlichen Fakultät
auf Antrag von:

Prof. Dr. Silvia Arber
Dr. Jan Pielage
Prof. Dr. Heinrich Reichert

Basel, den 24.06.2014

Prof. Dr. Jörg Schibler (Dekan)



Namensnennung-Keine kommerzielle Nutzung-Keine Bearbeitung 3.0 Schweiz
(CC BY-NC-ND 3.0 CH)

Sie dürfen: Teilen — den Inhalt kopieren, verbreiten und zugänglich machen

Unter den folgenden Bedingungen:



Namensnennung — Sie müssen den Namen des Autors/Rechteinhabers in der von ihm festgelegten Weise nennen.



Keine kommerzielle Nutzung — Sie dürfen diesen Inhalt nicht für kommerzielle Zwecke nutzen.



Keine Bearbeitung erlaubt — Sie dürfen diesen Inhalt nicht bearbeiten, abwandeln oder in anderer Weise verändern.

Wobei gilt:

- ☒ **Verzichtserklärung** — Jede der vorgenannten Bedingungen kann **aufgehoben** werden, sofern Sie die ausdrückliche Einwilligung des Rechteinhabers dazu erhalten.
- ☒ **Public Domain (gemeinfreie oder nicht-schützbarer Inhalte)** — Soweit das Werk, der Inhalt oder irgendein Teil davon zur Public Domain der jeweiligen Rechtsordnung gehört, wird dieser Status von der Lizenz in keiner Weise berührt.
- ☒ **Sonstige Rechte** — Die Lizenz hat keinerlei Einfluss auf die folgenden Rechte:
 - Die Rechte, die jedermann wegen der Schranken des Urheberrechts oder aufgrund gesetzlicher Erlaubnisse zustehen (in einigen Ländern als grundsätzliche Doktrin des **fair use** bekannt);
 - Die **Persönlichkeitsrechte** des Urhebers;
 - Rechte anderer Personen, entweder am Lizenzgegenstand selber oder bezüglich seiner Verwendung, zum Beispiel für **Werbung** oder Privatsphärenschutz.
- ☒ **Hinweis** — Bei jeder Nutzung oder Verbreitung müssen Sie anderen alle Lizenzbedingungen mitteilen, die für diesen Inhalt gelten. Am einfachsten ist es, an entsprechender Stelle einen Link auf diese Seite einzubinden.

Table of contents

1. Summary	1
2. Introduction	4
2.1 <i>Drosophila melanogaster</i> as a model organism	5
2.2 The <i>Drosophila</i> nervous system	7
2.3 Glial cells in <i>Drosophila</i>	8
2.4 The <i>Drosophila</i> neuromuscular junction (NMJ)	9
2.5 Glial cells at the <i>Drosophila</i> NMJ	13
2.6 Growth control at the <i>Drosophila</i> NMJ	14
2.7 Mlf1 adapter molecule (Madm)	15
2.8 Bunched A (BunA)	16
2.9 Myeloid leukemia factor (Mlf)	18
2.10 Aim of this thesis	20
3. Results	21
3.1 Introduction to results	22
3.2 Manuscript	23
3.2.1 Abstract	24
3.2.2 Introduction	24
3.2.3 Results	28
3.2.3.1 Presynaptic Madm is essential for synapse stability	28
3.2.3.2 Madm mutants display nerve bulges	31
3.2.3.3 Madm mutants display severe NMJ growth and morphology phenotypes	33
3.2.3.4 Madm synapse stability and morphology phenotype manifests during 3 rd instar larval stage	35
3.2.3.5 Madm localizes to larval brain, nerves and NMJs	36
3.2.3.6 Mlf1 and BunA modulate synaptic stability as well as morphology	37
3.2.3.7 Mlf and BunA genetically interact with Madm to modulate synaptic stability	38
3.2.4 Discussion	40
3.2.5 Acknowledgement	45
3.2.6 Author contributions	46
3.2.7 Figures	47
3.2.8 Supplementary figures	61
3.2.9 Material and Methods	72

3.2.9.1	Fly stocks.....	72
3.2.9.2	Generation of UAS-EGFP-Madm construct and transgenes.....	72
3.2.9.3	Generation of Madm antibody.....	72
3.2.9.4	Western blot.....	73
3.2.9.5	Larval dissections and immunohistochemistry.....	73
3.2.9.6	Image acquisition.....	74
3.2.9.7	Quantification of phenotypes.....	74
3.2.9.8	Statistical analysis	75
3.2.10	Abbreviations.....	76
3.2.11	References.....	76
3.3	Additional analysis of Madm	82
3.3.1	Presynaptic Madm controls NMJ stability as well as morphology and growth	82
3.3.2	The role of the postsynapse in <i>madm</i> mutants.....	86
3.3.3	Mlf and Bun genetically interact with Madm to modulate synaptic stability and morphology phenotype	91
3.3.3.1	Mlf & Madm.....	91
3.3.3.2	Bun A.....	94
3.3.4	Further attempts to identify additional Madm interaction partners	96
3.4	RNAi-based genetic screens for novel regulators of synapse development	97
3.4.1	Background information on RNAi screens.....	97
3.4.2	Hits of “cytoskeleton, cytoskeleton-associated and transport proteins” screen.....	98
3.4.2.1	Subsequent analysis of most promising candidates.....	98
3.4.3	Hits of “signaling pathways” screen.....	104
3.4.3.1	Subsequent analysis of most promising candidates.....	104
3.5	Characterization and localization of the Ankyrin2 isoforms & establishment of live-imaging	113
4.	Discussion.....	114
4.1	Additional analysis of Madm & outlook.....	115
4.1.1	Varicosities at nerves in Madm mutant animals	115
4.1.2	Additional data on Madm	115
4.1.3	Mlf and BunA genetically interact with Madm to modulate synaptic stability and morphology phenotype	117
4.2	Hits of RNAi-based genetic screens.....	119
5.	Material & Methods.....	122
5.1	Additional fly stocks used in this thesis.....	123

5.2	Additional antibody used for immunohistochemistry	124
5.3	Mosaic analysis with a repressible cell marker (MARCM).....	124
5.4	Image acquisition for quantification of synapse growth and morphology.....	125
5.5	Buffers & solutions	126
5.6	Chemicals, consumables & equipment	127
6.	Appendix	128
6.1	Supplementary Tables	129
6.1.1	Tables for figures of manuscript.....	129
6.1.2	Tables for supplementary figures of manuscript	136
6.1.3	Tables for additional analysis of Madm in thesis	143
6.1.4	Tables for RNAi-based genetic screens and hits of thesis.....	149
6.1.4.1	List of hits from “cytoskeleton, cytoskeleton-associated and transport proteins” RNAi screen	149
6.1.4.2	List of hits from “signaling pathways” RNAi screen.....	150
6.1.4.3	VDRC lines for “cytoskeleton, cytoskeleton-associated and transport proteins” RNAi screen.....	152
6.1.4.4	VDRC lines for signaling pathways RNAi screen	156
6.2	Abbreviations	161
6.3	References	164
6.4	Acknowledgement.....	171
6.5	Curriculum vitae.....	172

1. Summary

Every neuronal function relies on the formation of precise neuronal circuits. Accurate control of synaptic connectivity is essential both during development and plasticity of the nervous system. It enables efficient information transmission within the nervous system to execute appropriate behavior in response to changing sensory stimuli. In contrast, inappropriate connections are eliminated. Studies in vertebrate disease models have shown that a loss of synaptic connections is central to most if not all neurodegenerative diseases (Goda et al., 2003; Jontes et al., 2006). Little is still known regarding the molecular control of synapse formation, maintenance and refinement. The *Drosophila* neuromuscular junction (NMJ) represents an excellent model system to study these mechanisms. To identify novel regulatory molecules controlling synapse development and maintenance, I designed two RNAi-based genetic screens targeting 269 candidate genes. Two groups of proteins were analyzed: cytoskeleton, cytoskeleton-associated and transport proteins as well as signaling molecules from different conserved pathways. I focused on the analysis of a very promising candidate gene, the Mlf1 adapter molecule (Madm). In this study, we implicate for the first time a central role for Madm in the nervous system. Madm is a pseudo kinase which was previously shown to be an adaptor for unknown growth-related signaling pathways in *Drosophila* (Gluderer S. et al. 2010). We demonstrate that Madm controls multiple aspects of synapse development and refinement at the *Drosophila* neuromuscular junction (NMJ). First, *Drosophila madm* mutants displayed prominent synaptic stability and degeneration defects. Second, Madm mutant animals showed severe morphological alterations as well as reduced growth of NMJs. Third, nerves in Madm mutant animals displayed huge swellings and varicosities - a hallmark of neurodegenerative diseases in mammals and humans e.g. in Parkinson's and Alzheimer's disease. Fourth, Madm depletion resulted in the accumulation of the presynaptic marker Bruchpilot (BRP) in motoneuron axons. In addition, we could identify two genetic interaction partners of Madm - Myeloid leukemia factor (Mlf) and Bunched A (BunA). Mlf and BunA mutant animals showed similar tendencies of impaired synaptic stability and morphology. Using genetic interaction studies, we demonstrated that Mlf together with Madm normally promotes synaptic stability at the NMJ whereas BunA antagonizes synaptic instability caused by the loss of Madm.

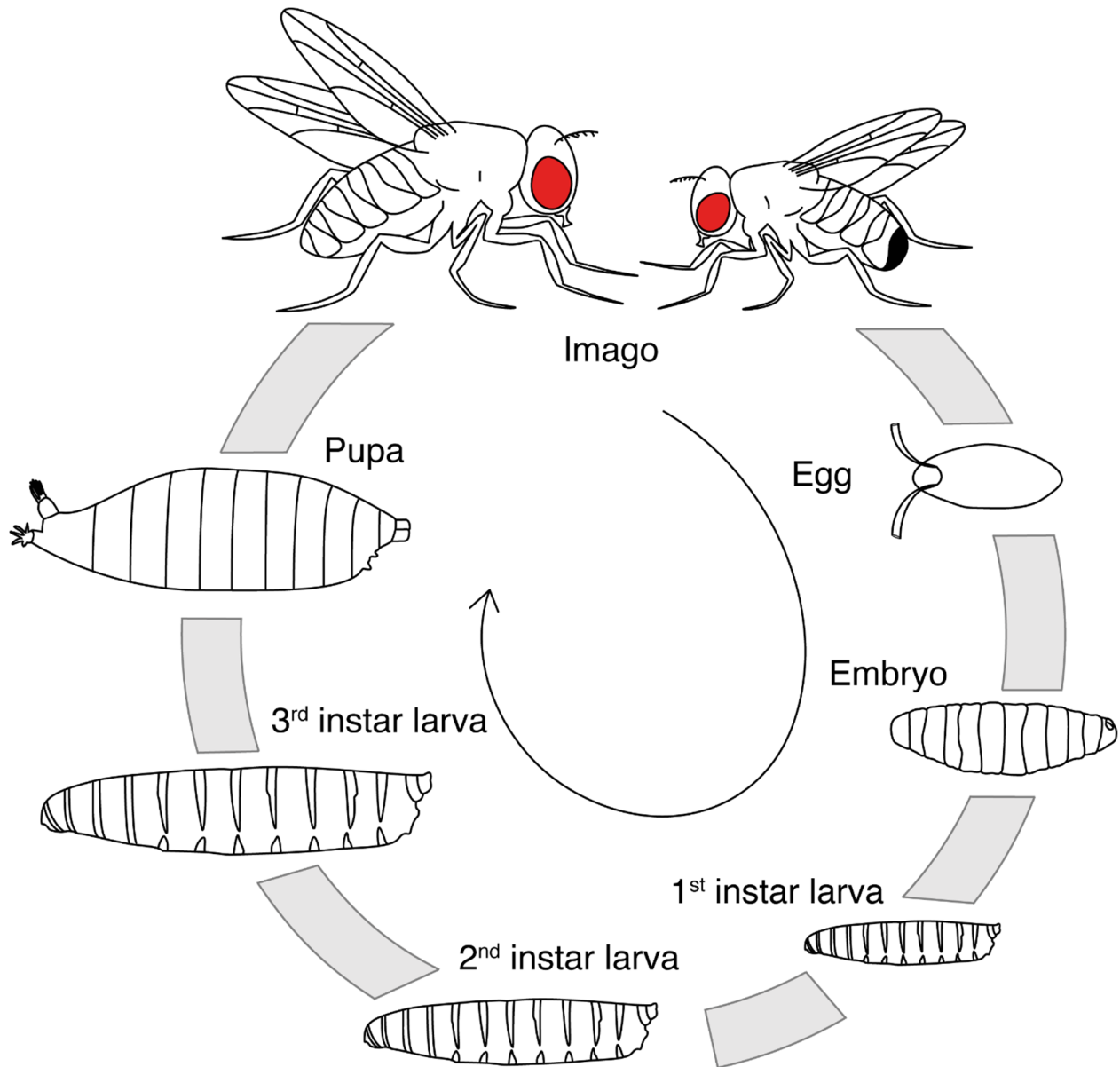
In conclusion, our findings support a model of Madm - together with BunA and Mlf - acting as a novel platform controlling different aspects of the normal development, growth and maintenance of synapses.

2. Introduction

2.1 *Drosophila melanogaster* as a model organism

Drosophila melanogaster belongs to the phylum *Arthropoda*, the class *Insecta*, the order *Diptera*, the family *Drosophilidae*, the genus *Drosophila*, the subgenus *Sophophora* and the species *melanogaster*. The advantages of *Drosophila melanogaster* as a model organism are numerous and formidable. Thus, *Drosophila* has a long history and tradition of being used in science. The American entomologist Charles W. Woodworth was the first to suggest the use of *Drosophila* in the laboratory at Harvard University (United States). Finally, the use of *Drosophila* in the lab was pioneered by Thomas Hunt Morgan in the 1910s (Rubin et al., 2000). He used the fruit flies to study heredity. In 1933, he received the Nobel Prize in Physiology or Medicine demonstrating that genes carried on chromosomes are the basis for heredity. Ever since, *Drosophila* was an important model system for the development and discoveries of modern genetics (Rubin et al., 2000). In 2000, the fruit fly was one of the first model organisms which genome was sequenced and annotated (at least to a high extend, see <http://flybase.org/>) (Adams et al., 2000). The genome is estimated to be composed of ~13,600 genes.

Drosophila melanogaster is a small animal. The handling of the fruit fly is relatively easy. The flies require little amount of food as well as laboratory space, making it possible to cultivate them in large quantity at relatively low cost. Flies have a short generation time with a well-defined lifecycle (see Thesis Fig. 1). Their fecundity is high. Genetic studies are facilitated by the two facts that male flies do not have meiotic recombination as well as the use of so-called balancer chromosomes (exhibiting multiple inverted repeats) also prevents recombination. Furthermore, an amazing tool set for genetic manipulation is available allowing site-directed and tissue-specific genetic analyses. For example, a huge armamentarium of genetic markers with easy visible phenotypes helps to control the outcome of crosses. Another example is the use of the UAS/Gal4 system derived from yeast (Brand et al., 1993). The yeast transcription activator protein Gal4 binds to the enhancer UAS (Upstream Activation Sequence) sequence and initiates the expression of any gene after the UAS sequence. As different enhancer and promoter regions can be combined with the Gal4 driver, the expression of the UAS-target gene construct can be controlled in a cell- and tissue-specific as well as temporal manner. In addition, Gal4 expression can be inhibited via Gal80 allowing even more precise control of the system.



Thesis Figure 1. The life cycle and developmental stages of *Drosophila melanogaster*.

At 25°C the fruit fly develops within 8 days from the embryo to an adult fly. After embryogenesis, *Drosophila* larvae hatch. In the next 4 days, the larvae develop and grow during three larval stages (1st, 2nd and 3rd instar larval stage) including two larval molts. During that developmental period, the larva increases massively in size and weight. Subsequently, the puparium is formed and the metamorphosis starts. After additional 4 days, the imago emerges.

There is a high degree of conservation between *Drosophila* and other species, including mammals. Fundamental signaling pathways like the insulin/mTOR (mammalian target of

rapamycin) pathway, for example, are highly conserved between *Drosophila* and mammals (Hietakangas et al., 2009). Hence, genes and molecules identified to play a role in a certain cellular process in *Drosophila* are likely to have conserved functions in other organisms. Furthermore, studies in mammals are often impeded by redundancy. Thus, the fruit fly provides a very fast and reliable model system to study developmental and disease aspects.

It is estimated that 75% of all genes which were associated with human diseases have a *Drosophila* ortholog (Reiter et al., 2001). For example, the fruit fly is used as neurodegenerative disease model. Neurodegenerative protein conformation diseases such as Huntington's disease display the formation of large protein aggregates (Marsh et al., 2004). Essential features of diseases can be well mimicked in *Drosophila* e.g. using the UAS/Gal4 system for transgene expression, helping to gain insight into disease processes (Marsh et al., 2004). In Huntington's disease, polyglutamine expansion mutations cause the abnormal aggregations of the Huntingtin protein which is also observed in the disease's fly model (Kazemi-Esfarjani et al., 2002).

2.2 The *Drosophila* nervous system

The central nervous system (CNS) in *Drosophila* develops from a bilaterally symmetrical neuroectoderm. This tissue gives rise to around 1,000 neuroblasts (neural stem cells) which asymmetrically divide to produce cells differentiating into various cell types needed for the CNS organization and architecture. The final CNS is composed of the brain and the ventral nerve cord (VNC) (Urbach et al., 2004).

The peripheral nervous system (PNS) consists of two distinct axonal classes:

- Afferent sensory axons which project into the CNS.
- Efferent motoneuron axons which project outwards from the CNS to muscle fibers in the periphery.

Sensory and motoneuron axons are kept separated in distinct axon fascicles which are wrapped by glial cells (see **Glial cells in *Drosophila***) (Stork et al., 2008).

2.3 Glial cells in *Drosophila*

It is likely that glial cells have very similar crucial functions in invertebrates as well as vertebrates. However, only very little is known about normal glia function and morphology in the *Drosophila* nervous system. In general, glial cells exert protective, insulating and nourishing functions as well as they modulate electric conductance and synaptic transmission (Barres, 2008; Nave et al., 2008; Zlokovic, 2008). To sum it up, glia provide the environment for neurons to function optimally (Freeman et al., 2006). There are different glial cell types in the *Drosophila* nervous system executing various functions (Pereanu et al., 2005; Freeman et al., 2006; Stork et al., 2008; Doherty et al., 2009; Schmidt et al., 2012). These glial cells are organized into layers (subsequently mentioned from outside to inside layers):

1. Extra cellular matrix (neural lamella) → surface glia
2. Perineurial layer → perineurial glia
3. Subperineurial layer → subperineurial glia
4. Final inner glial cell layer: generation of high potassium concentration in hemolymph which allows electrical conductance
 - PNS → wrapping glia
 - CNS → cortex glia (insulating neuronal cell bodies and initial segments of axons) & neuropile glia (surrounding axon fascicles and contacting synapses in dendritic compartments)

The surface, perineurial and subperineurial glia form the outer layers of the entire nervous system. They build the so-called blood-brain barrier (BBB) which is set up as a protective boundary between the brain and the rest of the body. Pleated septate junctions (pSJs) in the subperineurial layer ensure the paracellular tightness of the BBB, conferring barrier function. The perineurial as well as the neural lamella layer control the permeability for larger molecules e.g. proteins, conferring barrier selectivity. Thus, the uptake of ions, metabolites and particles of different size into the nervous system can tightly be controlled (Stork et al., 2008). In addition, the BBB is designed to protect the brain from bacterial or viral infections.

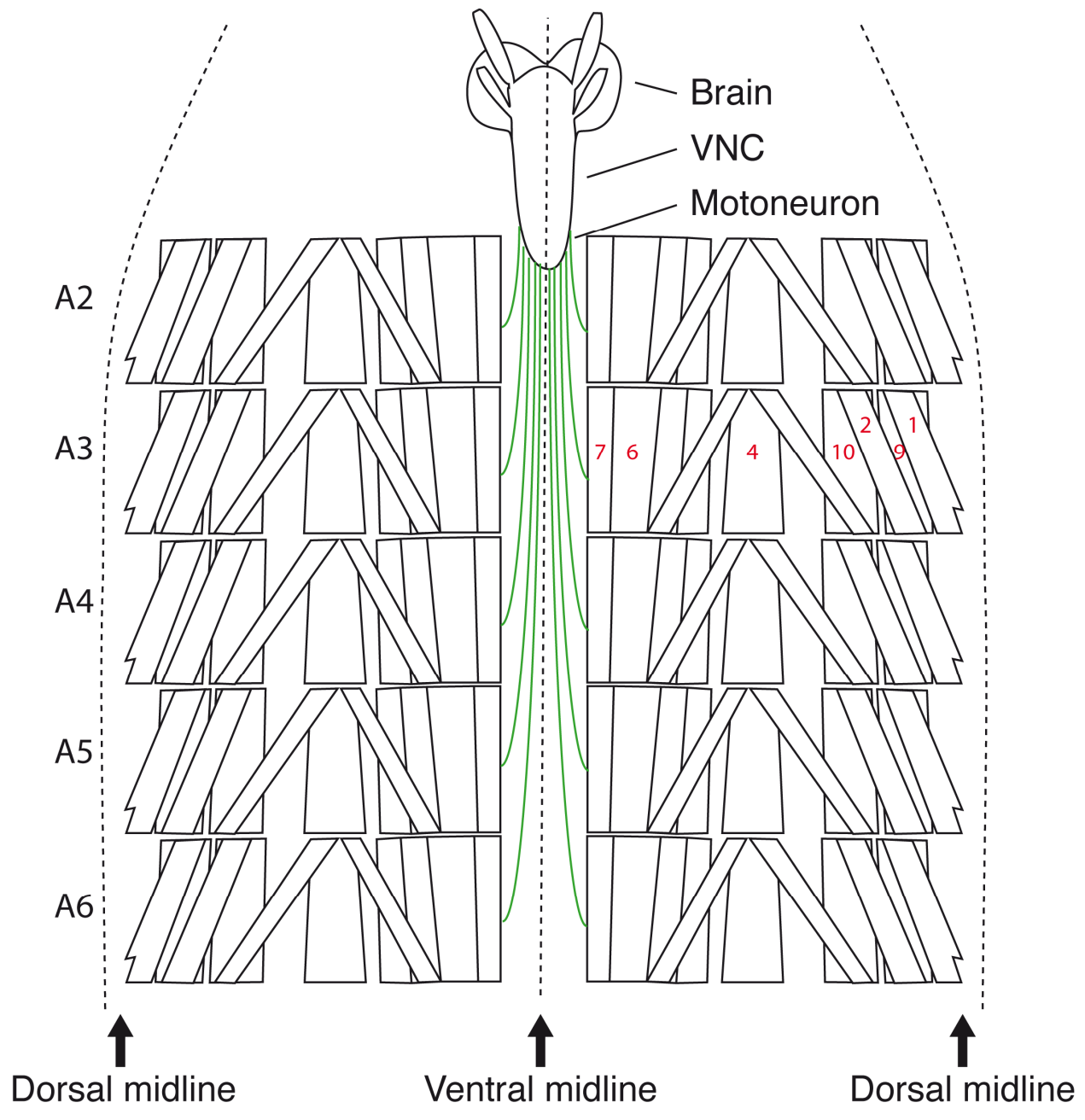
2.4 The *Drosophila* neuromuscular junction (NMJ)

Chemical synapses are specialized connections between neurons or neuron and muscle which transmit information via small molecules and/or peptides, referred to as neurotransmitters. Those synaptic connections are altered during a process called neuronal plasticity. Plasticity means the functional and structural change of neuronal connections (synapses) in response to neuronal activity. Plasticity occurs during development as well as during maturation and refinement of synapses - likely using the same fundamental mechanisms (Shen et al., 2010). Thus, the process of plasticity is involved in the changes of synaptic connectivity and activity necessary for all important cognitive functions including learning and memory (Menon et al., 2013).

The *Drosophila* NMJ is an excellent, well-studied genetic model for both developmental as well as functional plasticity (Menon et al., 2013). At the same time this arthropod NMJ is characterized by a stereotyped, robust pattern of connectivity of motoneurons innervating each abdominal hemisegment. While the vertebrate NMJ uses acetylcholine as neurotransmitter, the *Drosophila* larval NMJ uses glutamate. As in excitatory, glutamatergic synapses in the vertebrate nervous system, the *Drosophila* NMJ displays large protein complexes on the postsynaptic muscle side. They are enriched in ionotropic glutamate receptors (GluRs) homologous to AMPA-type GluRs in the mammalian brain. Because this features are similar to central excitatory synapses in mammals/vertebrates, the *Drosophila* NMJ represents an excellent model to study plasticity involved in development and maturation of excitatory, glutamatergic synapses (Menon et al., 2013).

On top of this similarities to the vertebrate system, *Drosophila* larval NMJs are relatively large and easy to access. This facilitates any form of manipulation or recording as well as visualization. The NMJs develop in a stereotypic pattern. Motoneurons as well as their postsynaptic muscle targets rise during embryogenesis and are individually specified. Motoneurons are formed in lineages from more than 10 different neuroblasts (Landgraf et al., 1997; Schmid et al., 1999). The NMJs are already defined in stage 13-15 during embryogenesis (Menon et al., 2013). The axons of the motoneurons grow out of the CNS to find their appropriate target muscles. When the axonal growth cone forms its initial contact with its postsynaptic target, specific molecules start to cluster on the muscle. These postsynaptic proteins involve for example GluRs as well as Discs

large (Dlg), the *Drosophila* ortholog of mammalian PSD-95 (postsynaptic density protein 95). The recruitment of proteins leads to the formation of the so-called subsynaptic reticulum (SSR). The SSR is a membranous structure of the muscle. The precise role of the SSR is still not exactly determined, but one of its proposed functions is glutamate uptake (Faeder et al., 1970). Furthermore, the SSR might also act as a local translation site of GluRs (Sigrist et al., 2000). The formation of the SSR also triggers the maturation of the presynaptic side into a well-defined terminal. The motoneuron axons which leave the CNS follow three distinct pathways: the segmental (SN), intersegmental (ISN) or transverse nerve (TN) and split up into further pathways in the periphery (Menon et al., 2013). By the end of embryogenesis, small NMJs are formed and the typical pattern of larval connections has been established (Menon et al., 2013). During the subsequent larval development the NMJs will grow and expand in size in order to keep up with muscular growth. The muscle surface area increases approximately 100-times during the development from embryo to late third instar larvae (Menon et al., 2013).



Thesis Figure 2. Schematic overview of the larval body wall muscle preparation.

The use of the *Drosophila* larval NMJ as model system was pioneered by Jan & Jan in the mid to late 1970s (Jan et al., 1976a, b; Jan et al., 1977; Jan et al., 1978). The preparation of *Drosophila* larval body wall muscles and their innervating motoneurons is relatively easy. The NMJs in these dissections are big with good access for manipulations or visualization. There are seven abdominal segments (A1-A7) in the larvae from anterior to posterior (only five segments are shown here). Each segment is divided into two hemisegments by the ventral midline. Each hemisegment consists of 30 multinucleated skeletal muscle fibers which are organized in a stereo-typed pattern. The motoneuron axons extended from the CNS and innervate the 30 muscles in each hemisegment (Menon et al., 2013). As the muscle pattern is invariant in all hemisegments the same type of NMJ can be localized and

subsequently analyzed in the same larva multiple times. Thus, variation and effects from anterior to posterior within the same animal can be monitored. The dorsal muscles 1/9 and 2/10, the muscle 4 and the ventral muscles 6/7 used for quantifications throughout this thesis are numbered in red.

A synaptic bouton is defined by multiple active zones, which are the sites of glutamate release on the presynaptic side, opposed by GluRs on the postsynaptic side. Thus, boutons are small units of connectivity and plasticity at the *Drosophila* NMJ.

During synapse refinement throughout larval development, boutons will be added and eliminated. The number of boutons will change up to a 10-fold and boutons grow in size together leading to an up to 10-fold increase in active zones per bouton (Atwood et al., 1993; Schuster et al., 1996). During metamorphosis, NMJs disassemble as muscles dissolve and the motoneurons subsequently innervate newly generated adult muscles (Liu et al., 2010). There are three different types of boutons at the *Drosophila* larval NMJ:

First, type-Ib and type-Is (type-I big and type-I small) motoneurons which are exclusively glutamatergic. Type Ib synaptic boutons are bigger than Is and differ in size, morphology, physiology and amount of surrounding SSR.

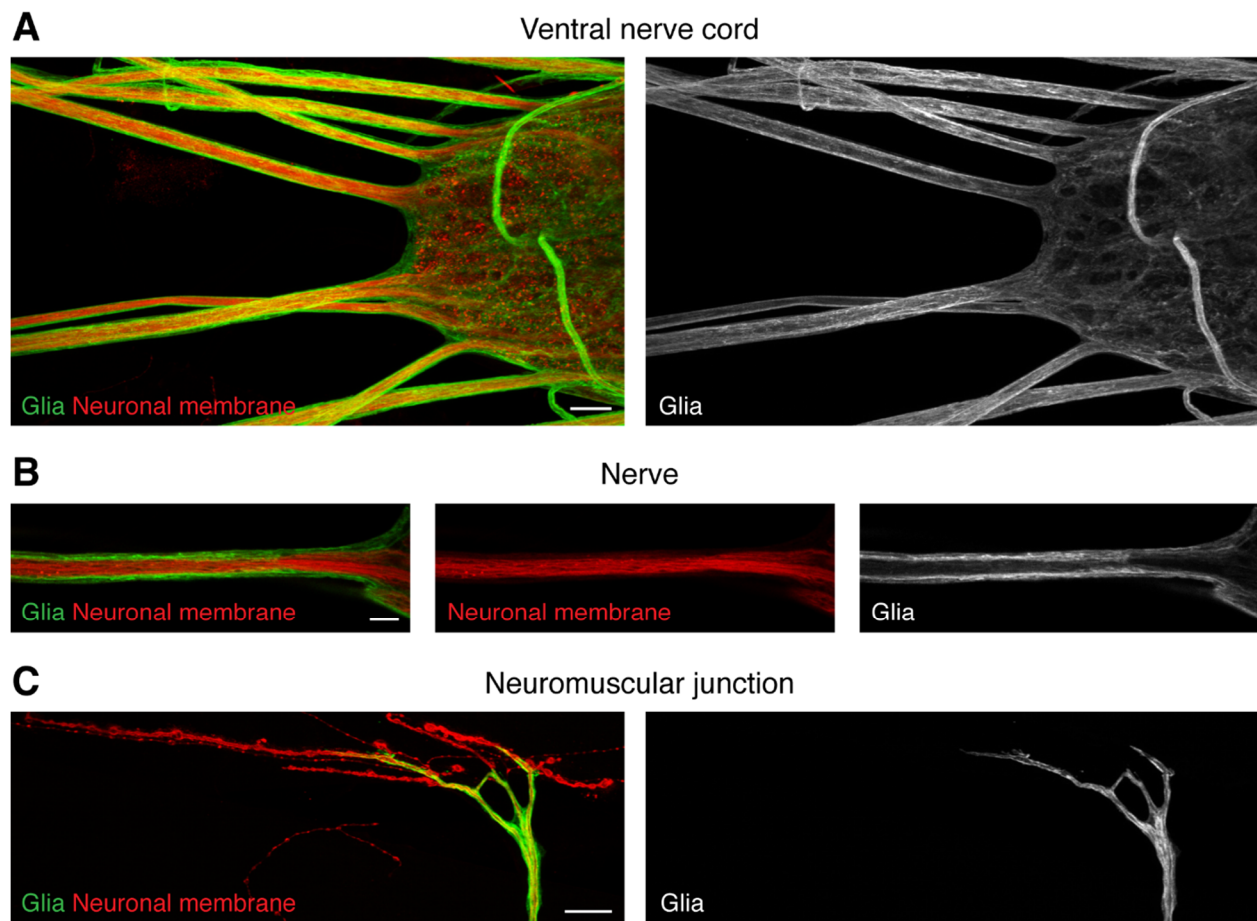
Second and third, type-II or type-III motoneurons which are neuromodulatory and therefore use the biogenic amine octopamine or different neuropeptides for synaptic transmission. Another difference is apparent: Only the presynaptic structure of type-I boutons is embedded into the SSR.

One of the first live-imaging studies examined the formation of new synaptic boutons at the NMJ using a GFP-tagged protein to target the SSR (Zito et al., 1999). The drawback of this study was that only postsynaptic type-Ib boutons could be visualized - leaving questions about the presynapse and synaptic destabilization unanswered. Nevertheless, three different modes of bouton formation could be monitored: asymmetric division from a mature bouton (similar to the budding in yeast), symmetric division of preexisting boutons as well as *de-novo* formation of a bouton from the axonal membrane.

2.5 Glial cells at the *Drosophila* NMJ

In vertebrates, Schwann cells ensheath the NMJ. In *Drosophila*, there are tripartite NMJs consisting of glia, neuron and SSR. The NMJ grows into the muscle. The muscle subsequently forms the SSR around the presynapse. Two types of glial cells are found at the NMJ: perineurial and subperineurial glia (Brink et al., 2012). Proximal to the first synaptic bouton, subperineurial glia surround the motoneuron axon and form a blood-nerve barrier (Brink et al., 2012). Perineurial glia reach out even further to the NMJ where they contact synaptic boutons as well as the muscle (Brink et al., 2012).

The glial processes at the NMJ are highly dynamic. It was demonstrated that they function in the removal of presynaptic debris (Jia et al., 1993; Sepp et al., 2000; Fuentes-Medel et al., 2009).



Thesis Figure 3. Glial cells at the VNC and the *Drosophila* NMJ.

(A) Glial cells at the ventral nerve cord were visualized by crossing the pan-glial driver REPO-Gal4 to a UAS-CD8GFP construct. Glial cells are marked in green. HRP - a marker for neuronal membranes - is displayed in red. Note that afferent and efferent nerves at the VNC are ensheathed by glial cells. **(B)** Higher magnification of a single nerve shows wrapping by glia in more detail. **(C)** Perineurial and subperineurial glial cells and their processes at the NMJ are visualized. Glial processes do not embed the entire NMJ. Scale bars: **(A)** 15 μm , **(B)** 7 μm , **(C)** 15 μm .

2.6 Growth control at the *Drosophila* NMJ

Different signaling networks as well as protein degradation pathways were shown to affect and regulate synaptic growth at the *Drosophila* NMJ (Menon et al., 2013). Parameters like synaptic bouton number and size or NMJ branching are altered upon perturbation of these networks.

The BMP/TGF- β (bone morphogenetic protein/transforming growth factor β) as well as insulin and mTOR signaling were shown to mediate *Drosophila* NMJ formation, growth and synaptic stability (Aberle et al., 2002; Eaton et al., 2005; Martin-Pena et al., 2006). For example, mutant animals of the TGF- β type II receptor Wishful thinking (Wit) of the BMP/TGF- β signaling cascade show reduced NMJ size together with synaptic instability (Aberle et al., 2002; Eaton et al., 2005). Furthermore, the TGF- β pathway shows a high level of crosstalk and interaction with *Wnt* (Wingless & Int-1) signaling. Interestingly, loss of function of the two components of the *Wnt* pathway *arrow (arr)* and *disheveled (dsh)* alter the microtubule (MT) cytoskeleton thus leading to a reduction of NMJ growth (Miech et al., 2008).

Studies on the pathways involved in NMJ growth regulation also helped to understand pathological mechanisms underlying neurological diseases. The current status of research is that BMP/TGF- β signaling seems to be reduced in amyotrophic lateral sclerosis (ALS), spinal muscular atrophy (SMA) and Huntington's disease (HD) while it increases in hereditary spastic paraplegia (HSP) and multiple sclerosis (MS) (Bayat et al., 2011).

In addition to signaling pathways, protein degradation is also crucial for NMJ growth (Menon et al., 2013). The ubiquitin-proteasome system (UPS) executes the degradation of ubiquitinated proteins. The anaphase-promoting complex/cyclosome (APC/C) is an E3 ubiquitin ligase complex necessary for this degradation. APC2 (*morula*), Cdc27 and Cdh1 are core or catalytic subunits of the APC/C complex known to affect NMJ formation and growth. One substrate of the APC/C

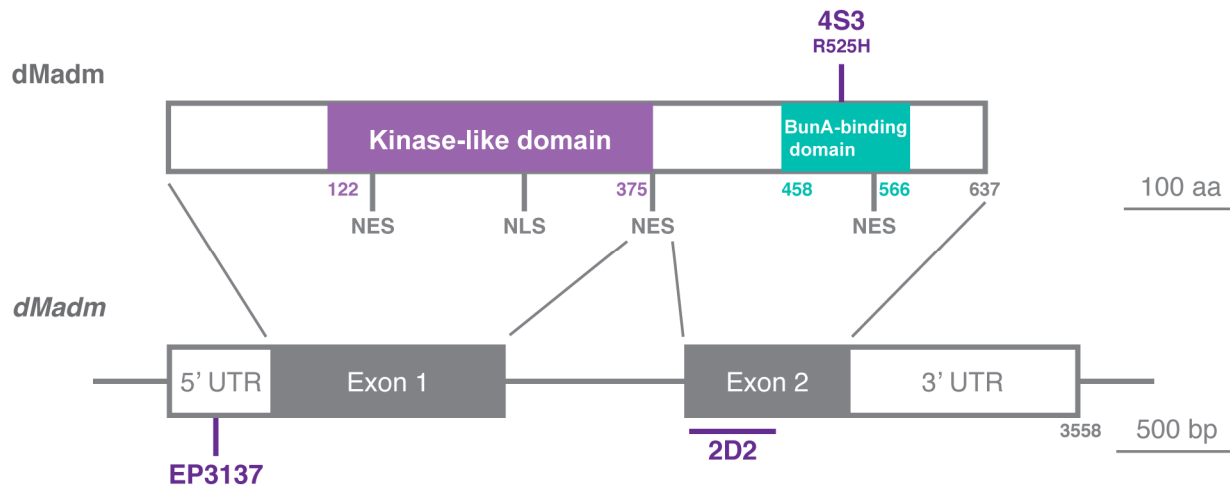
complex - DLiprin- α - is a scaffolding protein which promotes NMJ growth. In *apc2* mutants, DLiprin- α is not ubiquitinated. Thus, the protein accumulates at the NMJ leading to an increased synaptic bouton number. Highwire (Hiw) is an ubiquitin ligase of another E3 ubiquitin ligase complex. *Hiw* mutants show increased NMJ branching as well as increased synaptic bouton number and NMJ span while synaptic bouton size decreases. Highwire acts, at least partially, through the MAP (mitogen-activated protein) kinase signaling pathway (Collins et al., 2006).

2.7 Mlf1 adapter molecule (Madm)

Only very little is known about Madm. Madm represents a pseudo kinase lacking the adenosine triphosphate (ATP) -binding domain and was previously shown to be a positive regulator of growth (Gluderer S. *et al.* 2010). *Drosophila* Madm mutant animals displayed severe growth and developmental deficits. Cell number and size was reduced in these mutant animals, for example in the eye (Gluderer et al., 2010). It is unclear in which signaling cascade Madm acts. Thus, Madm was suggested to be an adaptor for an unknown growth-related signaling pathway (Gluderer S. *et al.* 2010).

Madm was previously implicated in Endoplasmic Reticulum (ER)-to-Golgi trafficking (De Langhe et al., 2002). In addition, Madm RNA-interference (RNAi) knockdown was shown to inhibit protein secretion (Bard et al., 2006; Brunner et al., 2007). In humans, Madm is named nuclear receptor binding protein (NRBP1) because of two putative nuclear receptor binding motifs (Hooper et al., 2000). However, so far no experimental proof for the binding to nuclear receptors has been reported. In mouse, Madm was shown to bind myeloid leukemia factor 1 (Mlf1) (Lim et al., 2002). Murine Madm was found to recruit an unknown kinase which phosphorylated serine residues of Madm (Lim et al., 2002). In addition, Madm was predicted to contain protein kinase C as well as casein kinase II phosphorylation sites (Lim et al., 2002).

In *Drosophila*, there is one *madm* locus (see Thesis Fig. 4). Madm has not yet been studied in nervous system development, which is the focus of my thesis.



Thesis Figure 4. The *Drosophila madm* locus (modified after (Gluderer et al., 2010)).

A set of mutations affecting the *madm* locus was generated previously via EMS (ethyl methanesulfonate) mutagenesis. For the manuscript and my thesis, I focused on the analysis of 3 different alleles: Madm 2D2, 4S3 and P(EP)3137. The Madm 2D2 allele is a genetic null allele. A deletion mutation leads to a frameshift and thereafter to a premature translational stop codon after additional 34 amino acids. In initial Madm studies, this amorphic mutation resulted in a strong small head phenotype referred to as “pinhead” and major growth and developmental deficits (Gluderer et al., 2010). Madm mutant larvae were found to be up to 10 days developmentally delayed. The Madm 4S3 allele is a point mutation changing an arginine to histidine (R525H). This mutation was previously associated with an intermediate pinhead phenotype and minor growth deficits. The P(EP)3137 element insertion is characterized for the first time in this thesis. The EP element resides within the 5’UTR of the *madm* locus.

Interestingly, beside the kinase-like domain Madm has one additional domain which mediates the binding to two protein interactors: Bunched A (BunA) and Myeloid leukemia factor (Mlf) (Lim et al., 2002). This interaction domain is affected in the Madm 4S3 mutant allele.

2.8 Bunched A (BunA)

Bunched A belongs to the TSC-22/Dip/Bun (transforming growth factor- β -stimulated clone 22/DSIP-immunoreactive peptide/Bunched) protein family of putative transcription factors as well as negative growth regulators and thus tumor suppressors. All family members have a TSC domain, which was shown to bind DNA *in vitro* (Ohta et al., 1996), and a leucine zipper motif for homo- and heterodimerization (Kester et al., 1999) at their C-termini. There are long and short isoforms of the protein characterized by alternative N-termini. Consistent with the role of TSC-22 as potential tumor suppressor, its upregulation was mostly found associated with growth

inhibition and/or the induction of apoptosis (Kawamata et al., 1998; Omotehara et al., 2000; Uchida et al., 2000). TSC-22 expression was found to be reduced in a variety of tumor types including liver (Iida et al., 2005), brain (Shostak et al., 2003), prostate (Rentsch et al., 2006) and salivary glands (Nakashiro et al., 1998).

Most of the studies on TSC-22 were done in cell culture and did not discriminate between long and short isoforms. In mammals, there are four different loci coding for the TSC-22 domain family (TSC-22D1-4) which are all supposed to generate different isoforms (Gluderer et al., 2008). Thus, a specific study of distinct isoforms, like the long isoform BunA, might be ruled out via redundancy and compensatory mechanisms between the different isoforms. Accordingly, the TSC-22 knockout mouse does not display any severe phenotype or tumor formation (Yu et al., 2009). Hence, *Drosophila* is an ideal model system to study TSC-22 domain family, respectively Bunched functions. Only one genomic locus encodes eight different protein isoforms: the three long A, F and G as well as the five short B to E and H isoforms (Gluderer et al., 2008). The long isoforms BunA and BunF are almost identical (Gluderer et al., 2008).

Originally, the *bunched* gene was identified in *Drosophila* in the development of the embryonic peripheral nervous system (Kania et al., 1995). Disruption of the *bunched* gene led to closely associated lateral chordotonal neurons. Thus, the gene was called *bunched*. In *Drosophila*, Bunched is furthermore required for the control of patterning processes in eye development (Treisman et al., 1995), egg shell development (Dobens et al., 1997; Dobens et al., 2000) as well as the development of α/β neurons in the mushroom body (Kim et al., 2009). Furthermore, Bun was shown to be induced in 3rd instar larvae upon starvation which indicates that it acts in growth regulation associated with the availability of nutrients (Zinke et al., 2002).

An *in vivo* study in *Drosophila* changed the view of all TSC-22/Dip/Bun protein family members acting as negative growth regulators and thus tumor suppressors. BunA was identified together with Madm in an unbiased screen for novel growth regulators to positively affect growth (Gluderer et al., 2008; Gluderer et al., 2010). Reduction of each protein individually resulted in the “pinhead” phenotype. EMS-induced recessive *bunA* mutants, like *madm* mutants, showed patterning defects, for example in the eye, as well as general growth deficits with flies being smaller and lighter (Gluderer et al., 2008; Gluderer et al., 2010). Again like *madm*, *bunA* mutants

displayed a reduction in cell number and size (Gluderer et al., 2008; Gluderer et al., 2010). Defects of strong *madm* alleles were observed to be even more severe than BunA defects (Gluderer et al., 2010). Co-overexpression of BunA and Madm resulted in enhanced organ growth, for example in the eye (Gluderer et al., 2010). Concomitant BunA and Madm loss even enhanced growth deficits observed in the individual Madm or BunA mutant animals (Gluderer et al., 2010). However, previous studies did not reveal a dominant genetic interaction between Madm and BunA in the analysed tissues - eyes and wings (Gluderer et al., 2010).

Only long isoforms, like BunA, and not short isoforms were found to be essential for growth (Gluderer et al., 2008). Short Bun isoforms even acted in a dominant negative manner on BunA function (Gluderer et al., 2008). Thus, the current hypothesis is that long and short Bun isoforms together regulate growth (Gluderer et al., 2008). Long isoforms seem to promote growth versus short isoforms might act like tumor suppressors inhibiting growth.

The signaling cascade in which BunA and Madm may act is still unclear. Both proteins were suggested to be essential in a novel growth-regulating complex (Gluderer et al., 2010).

Interestingly, there is evidence for BunA to control the activity of S6 kinase (dS6K) which acts downstream of the mTOR/insulin signaling pathway. Co-overexpression of BunA as well as the S6K enhanced growth (Gluderer et al., 2008).

Furthermore, BunA and Madm protein were found to co-localize *in vitro* in *Drosophila* S2 cells at the Golgi apparatus (Gluderer et al., 2010). Interestingly, long human TSC-22 isoforms were able to replace BunA function in flies (Gluderer et al., 2010). Thus, the growth-promoting effect of long TSC-22 isoforms seems to be highly conserved.

2.9 Myeloid leukemia factor (Mlf)

Myeloid leukemia factor 1 (Mlf 1) was first described in the mammalian system. In acute myeloid leukemia (AML) and myelodysplastic syndrome (MDS), a genetic translocation leads to the fusion with the nucleolar protein Nucleophosmin (NPM/B23) (Yoneda-Kato et al., 1996). The NPM-Mlf1 fusion protein is then targeted to the nucleus, the nucleolus respectively.

The myeloid leukemia factor (MLF) family is a small group of evolutionary conserved genes. The MLF family is poorly characterized. The family members lack significant homology with any known protein except from a 14-3-3 binding motif for protein interaction (Ohno et al., 2000). Mlf and Madm were previously identified to biochemically interact via this 14-3-3 binding motif (Lim et al., 2002).

In vertebrates, two paralogs are described. In *Drosophila*, there is one *mlf* gene which seems to encode four different dMlf isoforms generated via alternative RNA splicing (Martin-Lannere et al., 2006). dMlf protein can be localized to the nucleus as well as the cytoplasm depending on the developmental context (Martin-Lannere et al., 2006). It was shown that maternal Mlf contribution modulates lethality and phenotypes (Martin-Lannere et al., 2006). Furthermore, dMlf was implicated in the development of hematopoietic cells via Hedgehog and Wnt signaling (Fouix et al., 2003; Bras et al., 2012).

In another study, a possible link of Mlf to growth-regulating signaling pathways was shown (Killip et al., 2012). Interestingly, dMlf interacts with the transcription factor DREF (DNA replication-related element factor) (Ohno et al., 2000; Martin-Lannere et al., 2006). DREF mediates the upregulation of genes involved in DNA replication and proliferation e.g. DNA polymerase- α or dE2F (Hirose et al., 1993; Takahashi et al., 1996; Sawado et al., 1998). The transcription factor DREF was found to modulate growth downstream of the mTOR, but not the insulin/phosphatidylinositol 3-kinase (PI3K) signaling cascade. It was demonstrated that TOR controlled DREF mRNA levels. This transcriptional control was partially mediated via the transcription factor dMyc.

Finally, dMlf or hMlf was found to suppress neuronal toxicity of poly glutamine (poly Q) in neurodegenerative disease models (Kazemi-Esfarjani et al., 2002; Kim et al., 2005). Poly Q expansions are found in neurodegenerative diseases like Huntington's disease or different types of cerebellar ataxia.

2.10 Aim of this thesis

The control of synaptic formation and maintenance in the nervous system is of high importance for the development and function of neuronal circuits. Despite the fact that without refined connections between neurons and their target cells no meaningful neuronal function can be executed, the individual factors determining synapse formation, stabilization and/or degeneration remain largely unknown. The aim of this study was to identify novel molecular components involved in distinct steps of the formation and refinement of synaptic connectivity.

3. Results

3.1 Introduction to results

The result section is divided into four different parts. The first part contains a manuscript about the role of Mlf adapter molecule (Madm) and its interaction partners Myeloid leukemia factor (Mlf) and Bunched A (BunA) in synapse development and maintenance entitled “Madm Controls Synapse Development and Stability”. In the second part of the results section, data of additional analyses of Madm is shown. The third section summarizes the findings of two RNAi-based genetic screens which I performed in order to identify novel regulators of synapse formation and maintenance. The results section concludes with the brief description of an additional project. Fluorescently tagged Ankyrin 2 isoforms were generated with the intention to use them for live-imaging in *Drosophila*.

3.2 Manuscript

Madm Controls Synapse Development and Stability

Ingrid D. Kieweg, Victoria Bulat and Jan Pielage[#]

Friedrich Miescher Institute for Biomedical Research
Maulbeerstrasse 66
4058 Basel
Switzerland
Phone: +41 61 69 604 37
Fax: +41 61 69 739 76
Email: jan.pielage@fmi.ch

[#] to whom correspondence should be addressed

3.2.1 Abstract

The coordination of synaptic growth and maintenance is essential for the establishment of neuronal circuits and functional connectivity within the nervous system. To identify novel signaling and regulatory factors of synapse development, we performed forward genetic RNAi-based screens using the *Drosophila* neuromuscular junction (NMJ) as a model system. Here, we identify a central role for the Mlf1 adaptor molecule (Madm) in the control of synapse growth and stability. Loss of Madm results in severe alterations of NMJ growth and a progressive impairment of synaptic maintenance. We demonstrate that Madm is required presynaptically in a dose-dependent manner to coordinate synaptic morphology and maintenance. In addition, we show that mutations in two interacting proteins, Mlf1 and the TSC-22 homolog BunA also perturb synaptic growth but cause only minor impairments in synaptic stability. Using genetic interaction assays, we demonstrate antagonistic functions of these interaction partners with Mlf1 promoting and BunA preventing synapse stability. Our study provides first insights into synaptic functions of Madm-Mlf1-BunA and identifies the complex as a novel regulatory hub coordinating synaptic growth and maintenance.

3.2.2 Introduction

Every neuronal function relies on the formation of precise neuronal circuits. Accurate control of synaptic connectivity is essential both during development and plasticity of the nervous system. It enables efficient information transmission within the nervous system to execute appropriate behavior in response to changing sensory stimuli. In contrast, inappropriate connections are eliminated. Studies in vertebrate disease models have shown that a loss of synaptic connections is central to most if not all neurodegenerative diseases (Goda et al., 2003; Jontes et al., 2006). Therefore, a more detailed knowledge of mechanisms controlling synaptic development and stability is desirable.

During *Drosophila* embryogenesis, the initial contacts of motoneurons to muscles are formed and the typical pattern of innervation observed in larvae is established. During the subsequent larval development the NMJs will grow and expand in size in order to keep up with muscular growth

(Menon et al., 2013). The muscle surface area increases 100-times during the development from embryo to late third instar larvae. This dramatic size increase indicates the need for proper growth control.

So far, mainly three signaling pathways were shown to mediate growth control, morphology as well as synaptic stability at the *Drosophila* NMJ. These networks are the mTOR (mammalian target of rapamycin) pathway, insulin/PI3K (phosphatidylinositol 3-kinase) signaling and BMP (bone morphogenetic protein)/TGF- β (transforming growth factor β) signaling (Featherstone et al., 2000; McCabe et al., 2003; Rawson et al., 2003; Baines, 2004; Eaton et al., 2005; Martin-Pena et al., 2006; Collins et al., 2007; Goold et al., 2007; Cheng et al., 2011; Dimitroff et al., 2012; Fuentes-Medel et al., 2012; Natarajan et al., 2013).

In humans as well as in *Drosophila*, the protein kinase TOR associates with other proteins and forms two distinct TOR-containing complexes - TOR complex 1 and 2 (TORC1 and TORC2). TORC1 mediates its effects mainly through the control of protein synthesis via ribosomal S6 kinase (S6K). The small GTPase Rheb (Ras homolog enriched in brain) activates TOR by an unknown mechanism (Saucedo et al., 2003; Stocker et al., 2003; Tee et al., 2003). In turn, the tumor suppressors TSC1 and TSC2 (tuberous sclerosis complex 1 and 2) inhibit Rheb activity. They act as Rheb-GTPase-activating proteins (Rheb-GAP). Thus, Rheb hydrolyses its bound GTP and remains in its inactive GDP-bound state. In contrast, TCTP (translationally controlled tumor protein) might be a Rheb-GEF (guanine nucleotide exchange factor) activating Rheb (Hsu et al., 2007). Rheb links the mTOR to the insulin signaling pathway (Martin-Pena et al., 2006).

Studies of the pathways involved in NMJ growth regulation also helped to understand pathological mechanisms underlying neurological diseases. The current status of research is that BMP/TGF- β signaling seems to be reduced in amyotrophic lateral sclerosis (ALS), spinal muscular atrophy (SMA) and Huntington's disease (HD) while it increases in hereditary spastic paraplegia (HSP) and multiple sclerosis (MS) (Bayat et al., 2011).

To identify novel regulators of synapse development, growth and stability, we performed two RNA-interference (RNAi)-based forward genetic screens at the *Drosophila* neuromuscular junction (NMJ). We targeted 389 different candidates of *Drosophila* kinases and phosphatase (Bulat et al., 2014) as well as 133 selected molecules of the PTEN, mTOR, Hedgehog, JAK-STAT,

Non-canonical Wnt, Wnt/ β -Catenin, Notch, NF- κ B, Ras superfamily, EGFR and additional signaling pathways as well as the ESCRT machinery (endosomal sorting). In this screens, we identified one top candidate: Madm (Mlf1 adapter molecule). Upon presynaptic Madm knockdown, multiple aspects of synapse development and stability were affected. NMJs of presynaptic Madm knockdown animals displayed a very pronounced synaptic stability as well as growth and morphology defects. In addition, abnormal accumulations of presynaptic proteins within nerves were present. Because of these strong and penetrant phenotypes, I focused in this study on the analysis of Madm to identify its role for synaptic development and stability at the *Drosophila* NMJ.

Thus far, there is only little knowledge regarding the cellular function of Madm. Madm is a pseudo kinase lacking the conserved ATP-binding domain. Interestingly, in an unbiased screen Madm was identified to be a positive regulator of growth in *Drosophila* (Gluderer S. *et al.* 2010). Madm was previously implicated in ER-to-Golgi trafficking (De Langhe *et al.*, 2002) and Madm RNAi knockdown was shown to interfere with protein secretion (Bard *et al.*, 2006; Brunner *et al.*, 2007). In human, Madm is named nuclear receptor binding protein 1 (NRBP1) because of two putative nuclear receptor binding motifs (Hooper *et al.*, 2000). However, there was never any experimental proof for the binding to nuclear receptors. In this study, we implicate Madm for the first time in the development of the nervous system.

As it remains unclear in which signaling cascade Madm may act, we also searched for potential interaction partners of Madm to place it within potential signaling networks required for *Drosophila* NMJ development and maintenance. Interestingly, the Madm 4S3 mutation, a point mutation that does not decrease levels of Madm protein, caused the strongest synaptic stability and morphology defects of all analysed *madm* alleles. Strikingly, this point mutation resides in a domain of the Madm protein which was previously shown to selectively mediate the binding to two proteins: Myeloid leukemia factor 1 (Mlf1) and Bunched A (BunA). In mouse, Madm was shown to bind Mlf1 (Lim *et al.*, 2002). Later, Madm was shown to bind BunA through the same domain (Gluderer *et al.*, 2010).

In *Drosophila*, the *bunched* gene was originally shown to be essential for the development of the embryonic peripheral nervous system (Kania *et al.*, 1995). Disruption of the *bunched* gene led to

closely associated lateral chordotonal neurons. Thus, the gene was called *bunched*. Furthermore, Bunched was shown to be required for patterning processes during eye development (Treisman et al., 1995), egg shell development (Dobens et al., 1997; Dobens et al., 2000) as well as the development of α/β neurons in the mushroom body (Kim et al., 2009). Bunched belongs to the TSC-22/Dip/Bun (transforming growth factor- β -stimulated clone 22/DSIP-immunoreactive peptide/Bunched) protein family of putative transcription factors. In *in vitro* and cell culture studies, the TSC-22/Dip/Bun protein family was implied to act as negative growth regulators and thus tumor suppressors. Accordingly, transcriptional upregulation of TSC-22/Dip/Bun proteins was mostly found associated with growth inhibition and / or the induction of apoptosis (Kawamata et al., 1998; Omotehara et al., 2000; Uchida et al., 2000). Most of these studies on TSC-22 were done in cell culture and did not discriminate between long and short Bunched isoforms. Surprisingly, the first *in vivo* studies in *Drosophila* demonstrated that the long isoform BunA and Madm act together as positive regulators of growth (Gluderer S. *et al.* 2010). Reduction of each protein individually resulted in a small head phenotype referred to as “pinhead”. *BunA* as well as *madm* mutants showed patterning defects, for example in the eye, as well as general growth deficits with flies being smaller and lighter (Gluderer et al., 2008; Gluderer et al., 2010). Defects of strong *madm* alleles were observed to be even more severe than BunA defects. Both mutants also showed a reduction of cell number and size. In contrast, co-overexpression resulted in enhanced growth phenotypes. Concomitant BunA and Madm loss caused even stronger growth deficits. However, previous studies did not reveal a dominant genetic interaction between Madm and BunA in the analysed tissues - eyes and wings (Gluderer et al., 2010). Thus, both proteins were suggested to be essential in a novel growth-regulating complex (Gluderer et al., 2010).

Mlf 1, the second Madm interaction partner we identified at the *Drosophila* NMJ, was first described in the mammalian system to be involved in acute myeloid leukemia (AML) and myelodysplastic syndrome (MDS) (Yoneda-Kato et al., 1996). A genetic translocation leads to the formation of a fusion protein together with the nucleolar protein Nucleophosmin (NPM/B23). This fusion protein is then targeted to the nucleus, the nucleolus respectively.

The myeloid leukemia factor (MLF) family is a small group of evolutionary conserved proteins which are poorly characterized. They lack significant homology with any known protein except from a 14-3-3 binding motif for protein interaction (Ohno et al., 2000). There is one *mlf* gene in *Drosophila*. In vertebrates, two paralogs are described. It was shown that maternal contribution modulates lethality and phenotypes (Martin-Lannere et al., 2006).

In *Drosophila*, dMlf was implicated in the development of hematopoietic cells (Fouix et al., 2003; Bras et al., 2012) and the upregulation of genes involved in DNA replication and proliferation e.g. DNA polymerase- α or dE2F (Hirose et al., 1993; Takahashi et al., 1996; Sawado et al., 1998; Ohno et al., 2000; Martin-Lannere et al., 2006).

Here, we demonstrate essential roles of *Drosophila* Madm for the control of synaptic stability and morphology at the *Drosophila* NMJ. We show that Madm is required in the presynaptic motoneuron to coordinate synapse development and stability. Using genetic interaction assays, we demonstrate that Madm interacts with BunA or Mlf during synapse development and stability. Mlf promotes synaptic stability. Interestingly, the removal of BunA in the Madm mutant background was able to significantly alleviate the synaptic stability defects indicating antagonistic roles of Mlf and BunA. Together, our study provides first evidence for a role of Madm together with Mlf and BunA during synapse development and maintenance.

3.2.3 Results

3.2.3.1 Presynaptic Madm is essential for synapse stability

In *Drosophila* larvae, a stable wild-type NMJ is characterized by the precise and close opposition of the presynaptic active zone marker Bruchpilot (BRP) (the *Drosophila* ortholog of CAST) and postsynaptic glutamate receptor clusters (marker GLURIII) in all individual synapses which are organized in roundish boutons. The neuronal membranes which can be marked by HRP are continuously formed and intact. In case of destabilization, the retraction is designated by the gradual loss of the presynapse (BRP) leaving the postsynaptic profiles and markers behind (GLURIII). The presynaptic motoneuron membrane starts to get disconnected and subsequently degraded. Upon knockdown of genes essential for synapse maintenance, synaptic retractions can

be observed via these morphological changes. This *in vivo* assay allows to monitor changes at the resolution of single synapses. In wild-type animals, synaptic retractions are relatively rare events ($\leq 5\%$ of all NMJs).

Using this assay, a presynaptic network of molecules has previously been identified which mediates synapse formation and stability at the *Drosophila* NMJ. Among other components, this network consists of the cell-adhesion molecule Neuroglian (Enneking et al., 2013), the scaffolding molecules alpha- and beta-Spectrin (Pielage et al., 2005), the adaptor molecule Ankyrin2 (Ank2) (Koch et al., 2008; Pielage et al., 2008), the actin-capping molecule Hts/Adducin (Pielage et al., 2011), Dynactin for the transport along microtubules (Eaton et al., 2002) as well as LIM kinase (Eaton et al., 2005). The association of these proteins provides a link to the cytoskeleton and may represent a platform for signaling pathways to control different aspects of synapse development. In our RNAi-based genetic screens, we observed severe stability defects upon presynaptic Madm knockdown at larval NMJs throughout different muscle groups. In all cases, we observed between 42.5 and 57.8% synaptic retractions (Fig. 1 F, I and Fig. S1 D, F). In addition to the synaptic retraction frequency, we also quantified the severity of the defects. Four different classes of synaptic retraction severity were quantified. Shown are small retractions with only 1-2 distal boutons affected, medium retractions with 3-6 boutons missing and large retractions with 7 and more boutons affected. In addition, total eliminations of presynaptic nerve terminals were counted. Those can on top fall into each of the previous categories depending on the number of boutons affected and the size of the affected NMJ respectively. Complete eliminations are not observed in wild-type at any muscle group (Fig. 1 A, J and Fig. S1 C, E, G). In presynaptic Madm knockdown animals, large synaptic retractions occurred to a high extend (up to 29.7% on m1/9 & 2/10) (Fig. 1 D, E, J and Fig. 1S B, E, G) as well as total eliminations of nerve terminals appeared (Fig. 1 J and Fig. S1 E, G). Due to this pronounced synaptic stability defect, we went for further analysis of different *madm* alleles to verify the observed phenotype. Different recessive lethal EMS-induced mutations targeting Madm were previously published (Gluderer et al., 2010). We focused on three distinct *madm* mutations: 2D2 - a genetic null allele executed via a premature translational stop codon, 4S3 - a point mutation, and in addition the P(EP)3137 element insertion, here referred to as Madm EP. This EP element resides in the 5' UTR of the *madm* locus. Madm

2D2 and 4S3 alleles were analyzed as transheterozygous combination with the deficiency Df(3R)Exel7283, subsequently referred to as Madm Df. This deficiency was already used for analyses in previous studies (Gluderer et al., 2010). In contrast, the EP allele is homozygous viable. Thus, this genotype was analyzed as well. In all allelic combinations, pronounced synaptic stability defects were observed. Those defects were present throughout all muscle groups of the mutant animals (Fig. S1 B). Synaptic retraction frequencies as high as 77.5% in 4S3/Df mutant animals for the most dorsal muscle 1 were detected (Fig. 1 I). To analyze the synaptic stability of a larger group of muscles, dorsal muscles 1/9 & 2/10 were pooled. The synaptic retraction frequency was 80% (Fig. S1 D). In comparison, we also monitored synaptic retraction frequencies on the ventral muscles 6/7 to verify the effect throughout the animal. The frequency ranged from 26.3 to 65.0% (Fig. S1 F). Interestingly, the transheterozygous allelic combination 4S3/Df resulted in the highest synaptic retraction frequencies across all tested genotypes. Large retractions occurred in all mutant genotypes across all muscle groups (Fig. 1 J and Fig. S1, E, G). Total eliminations were observed only for the dorsal muscles (Fig. 1 J and Fig. S1, E). To verify that the synaptic stability defect is caused by the loss of Madm, we performed rescue experiments. A UAS-Madm construct was expressed under the control of the pan-neuronal elav-Gal4 driver in the different mutant backgrounds. In all cases, the synaptic retraction frequencies could be significantly reduced (2.5% - 17.5% on muscle 1, Fig. 1 I and 3.4% - 7.2% on muscles 1/9 & 2/10 as well as 6.3% - 17.5% on muscles 6/7, Fig. S1 D, F). Synaptic retraction frequencies could be even shifted back to mainly small and medium retraction events (Fig. 1 J and Fig. S1 E, G). Furthermore, no large synaptic retractions or total eliminations of nerve terminals were observed across all quantified muscles (Fig. 1 J and Fig. S1 E, G). As control, we expressed the UAS-Madm construct using the elav-Gal4 in a wild-type background. We did not observe any significant change of synaptic stability compared to controls (Fig. 1 I and Fig. S1 D, F). In addition, we expressed Madm under the control of the motoneuron-specific OK371-Gal4 driver (2D2/Df mutant background is shown). On all analyzed muscles, we observed significant rescue, but higher synaptic stability defects compared to elav-Gal4 driven rescues (Fig. 1 I and Fig. S1 D, F). OK371-Gal4 driven rescues did also not rescue the occurrence of large synaptic retractions as did

comparable elav-Gal4 driven rescues (Fig. 1 J and Fig. S1 E, G). Nevertheless, synaptic instability was significantly rescued compared to mutant animals in all cases.

To monitor the efficiency of the RNAi knockdown as well as to verify the molecular nature of the *madm* alleles, we generated a Madm antibody (Fig. 5 A, B, C) and analyzed larval brain extracts using Western blots (Fig. 1 B). We observed a significant decrease of Madm protein upon RNAi-mediated knockdown. In homozygous EP/EP animals, protein levels were reduced similar to changes upon RNAi-mediated knockdown. *In trans* to the deficiency, the presence of the EP allele almost completely abolished Madm protein levels. The transheterozygous combination of the point mutation 4S3 and the deficiency showed significant levels of Madm expression indicating that the mutant protein was still stable. In contrast, only a slight protein band was visible in the transheterozygous 2D2/Df sample. No additional band at a lower molecular weight - which would represent the truncated protein - could be detected (data not shown). Rescuing 2D2/Df mutant animals via elav-Gal4 re-expression of Madm restored protein expression. The faint double band of Madm that we observed on the Western blot might represent a phosphorylated version of Madm as was previously shown for murine Madm (Lim et al., 2002).

In this study, we characterized the previously described *madm*^{EP3137} allele in more detail (Gluderer et al., 2010). Thus, we could show that the EP element insertion in the 5'UTR of the *madm* gene has a strong effect on Madm protein expression. Detected levels of Madm protein on the Western blot are significantly reduced (Fig. 1 B). Hence, the EP *madm* allele seems to strongly reduce protein levels either via repression of transcription or translation.

3.2.3.2 Madm mutants display nerve bulges

In Madm mutant animals, we observed bulges or swellings of the nerves, mostly close to the ventral nerve cord (VNC), which we never found in control animals (Fig. 2 A, B). We quantified the occurrence of these varicosities in 2D2/Df mutant animals which are lacking the Madm protein. Varicosities were also present in other *madm* mutants (data not shown). On average, 4.3 nerves were affected per animal (out of an average of 14 nerves in total) (Fig. 2 D). This represented a frequency of 31.2% nerves with axonal bulges or swellings (Fig. 2 E). Expression of Madm using the elav-Gal4 driver in the transheterozygous 2D2/Df mutant background

completely rescued the phenotype (Fig. 2 D). Interestingly, trying to rescue the phenotype using the pan-glial REPO-Gal4 driver did not completely rescue but highly diminished the bulges (0.8 varicosities per animal; 5.2%) (Fig. 2 C, D, E). This indicates that *Madm* is normally expressed in the motoneuron as well as in the glial cells at the *Drosophila* NMJ or that *Madm* acting on either of these sides is sufficient to rescue the swelling phenotype and maybe restores normal interaction between motoneurons and glial cells.

Axonal swellings and varicosities are a hallmark of neurodegenerative diseases in mammals and humans e.g. in Parkinson's and Alzheimer's disease, multiple sclerosis or hereditary spastic paraplegias. In those affected axons, axonal transport is usually impaired. Thus, we wanted to address the molecular and functional identity of the observed bulges in the *Madm* mutant animals in more detail. We wanted to see whether this defect affects transport and related structures. Hence, we visualized microtubule bundles via Futsch - the invertebrate microtubule-associated protein 1B (MAP1B) homolog (Fig. 2 F). We observed that microtubules were not accurately organized in parallel, but displayed wavelike structures which might affect transport. Finally, we monitored if axonal cargos accumulated within the varicosities. We did not detect any increased accumulation of BRP or DVGlut (Fig. 2 G). Thus, the observed bulges did not seem to be sites of increased axonal cargo defects.

In contrast, we observed the accumulation of puncta of the active zone marker BRP within afferent and efferent nerves leaving the ventral nerve cord as well as motoneuron axons innervating the muscles in *madm* mutants (Fig. 1 D, E; Fig. S1 B and Fig. S2 B). We quantified these accumulations and found them highly significantly increased among all mutant genotypes (Fig. S2 D). Expression of *Madm* in the mutant background using *elav*-Gal4 efficiently rescued the BRP accumulations (Fig. S2 D). As control, *Madm* was overexpressed using *elav*-Gal4 in the wild-type background. No significant BRP puncta were observed (Fig. S2 D). To test if general transport was affected, we also assayed the occurrence of DVGlut-containing vesicles accumulations. This would indicate a general transport issue as vesicles are no longer properly transported along nerves and axons (Fuger et al., 2012). However, no significant accumulation of DVGlut was measured in *madm* mutants (Fig. S2 E). *Elav*-Gal4 driven *Madm* overexpression caused even slight

decrease of DVGlut signals (Fig. S2 E). Thus, the transport of axonal cargos seems not to be impaired in *Madm* mutant animals.

3.2.3.3 *Madm* mutants display severe NMJ growth and morphology phenotypes

In addition to the severe synaptic stability defect, we observed dramatic morphological changes upon loss of *Madm*. NMJs did not grow out over the muscle to the same extent as in wild-type. Thus, the mutant NMJs stay more compact and condensed. To analyze the key features of the observed phenotype, we defined four parameters for quantification: number of NMJ branches, number of synaptic boutons (type Ia and Ib), total length of all branches of the NMJ as well as the NMJ area related to the muscle area. We considered a precise analysis of NMJ growth correlated to the muscle growth as important. Thus, we could be sure that observed defects were not simply due to general growth deficits affecting larval and thus muscle size. This is especially important regarding the fact that *Madm* mutant larvae are up to 10 days developmentally delayed compared to control animals (Gluderer et al., 2010). Accordingly, we also show the variance in the different measured parameters (see box plots Fig. S3).

The four defined categories were quantified at the most dorsal muscle 1. The number of NMJ branches was significantly increased in all *madm* mutants (Fig. 3 B, C, G and Fig. S3 A). This parameter was not significantly altered in the presynaptic *Madm* knockdown animals compared to the control animals (Fig. 3 D, G and Fig. S3 A). Re-expression of *Madm* using again the pan-neuronal driver *elav-Gal4* did not significantly rescue the increase of branches in all transheterozygous *Madm* mutant animals (Fig. 3 E, F, G and Fig. S3 A). The rescue values were comparable to wild-type. Overexpression of *Madm* using *elav-Gal4* did not have any significant effect compared to wild-type (Fig. 3 G and Fig. S3 A). Subsequently, we counted the number of total synaptic boutons. We saw a significant decrease in the presynaptic knockdown and all mutants (Fig. 3 B, C, D, H and Fig. S3 B). In the transheterozygous 4S3/Df mutant animals, the number of synaptic boutons was almost cut in half (50.6%). Upon neuronal re-expression of *Madm* in the mutant backgrounds, there was a slight increase in bouton number - which was significant in the presynaptic 4S3/Df rescue (Fig. 3 E, F, H and Fig. S3 B). We also tested for potential effects of *Madm* overexpression and found the total number of synaptic boutons

reduced, as we previously observed in *Madm* mutant animals. In addition, the total NMJ length was highly significantly decreased in the presynaptic knockdown as well as in the mutant animals (Fig. 3, B, C, D, I and Fig. S3 C). Again the observed effect was greatest in 4S3/Df mutant animals where the NMJ length was reduced to 54%. A gradual difference was visible between the homozygous EP mutant animals (not significantly reduced) versus the EP/Df mutant animals. Pan-neuronal rescues significantly restored the NMJ length (Fig. 3 E, F, I and Fig. S3 C). *Madm* overexpression did not show a significant effect on this parameter (Fig. 3 I and Fig. S3 C). Finally, we correlated the area covered by the NMJ to the area and size of the corresponding muscle (depicted in %). We observed a reduction which was highly significant in the group of *madm* alleles over deficiency (Fig. 3 B, C, J and Fig. S3 D). Once more, the 4S3/Df allelic combination caused the strongest effect. The NMJs only covered about one third of the muscle area (35.1%) compared to control. This phenotype could be significantly rescued (Fig. 3 E, F, J and Fig. S3 D). Interestingly, presynaptic *Madm* overexpression showed an increased NMJ area (Fig. 3 J and Fig. S3 D).

Together, this data shows that NMJ morphology and growth is indeed drastically altered in *madm* mutants. The number of NMJ branches increased significantly, whereas the number of synaptic boutons, the total NMJ length and the NMJ area covering the muscle surface significantly decreased. Presynaptic re-expression of *Madm* in the different mutant backgrounds significantly rescued the observed defects except from the number of synaptic boutons where a slight increase was observed, but not significant (only the *elav* 4S3/Df rescue animals showed significant increase in synaptic bouton number). Interestingly, presynaptic *Madm* overexpression animals also showed a significant decrease of synaptic boutons. Furthermore, presynaptic *Madm* overexpression animals displayed significantly larger NMJ areas covering the muscle surface than *Madm* mutant animals or rescue animals. These results indicate that a precise control of *Madm* expression levels is important at the *Drosophila* larval NMJ to mediate development and morphology. While the loss of *Madm* caused significant morphological changes, re-expression or overexpression of *Madm* did not significantly restore morphology of controls. Thus, too high as well as too low *Madm* protein levels caused morphological defects.

3.2.3.4 Madm synapse stability and morphology phenotype manifests during 3rd instar larval stage

In order to assess the time course of the destabilization of synapses as well as to address at which developmental stage the morphology phenotype manifests, we analyzed second instar larvae. We focused on 4S3/Df mutant larvae which showed the strongest synaptic instability phenotype among all quantified muscle groups (Fig. 1 E, I and Fig. S1 B, D, F) as well as the most large synaptic retractions and total nerve terminal eliminations (Fig 1. J and Fig. S1 E, G). In second instar larvae, we did not detect any significant differences in synaptic stability between control animals and 4S3/Df mutant animals on the dorsal muscles 1 and 9 & 2 and 10 (Fig. 4 A, C, E). In addition, only small synaptic retractions affecting 1-2 boutons were observed (Fig. 4 F). While NMJ morphology of second instar animals was not significantly altered between control and 4S3/Df mutant animals, the 4S3/Df mutant NMJs were already undergrown in comparison to the control (Fig. 4 A, C). In third instar larvae, highly significant increases in synaptic instability were observed as previously described (Fig. 1 and Fig. S1). Comparing second to third instar larvae within the two genotypes, control as well as 4S3/Df mutant animals showed significant increases in synaptic instability (Fig. 4 A, B, C, D, E). Furthermore, the severity of retractions increased in third instar larvae (Fig. 4 F). Large synaptic retractions could be monitored in control as well as 4S3/Df mutant animals. In addition, eliminations of entire nerve terminals occurred in 4S3/Df mutant animals. The analysis of the most ventral muscles 6 and 7 revealed similar results (Fig. S4). In second instar larvae, again no significant difference was found between control and 4S3/Df mutant animals (Fig. S4 A). Only small synaptic retractions were discovered (Fig. S4 B). In third instar larvae, instability was highly significantly increased in 4S3/Df mutant animals compared to controls (Fig. S4 A). In addition, synaptic retraction severity was also increased (Fig. S4 B). Comparing second to third instar larvae, we observed increased synaptic instability within the control as well as the 4S3 larvae group (Fig. S4 A). Only this time, the increase of synaptic retraction frequency was not significant comparing second to third instar control larvae.

Thus, second instar larvae seem to be largely unaffected by instability, but there is a rapid, significant increase in stability defects during the development to third instar larval stage. In

contrast, clear alterations in growth and morphology were observed in second instar Madm mutant larvae. The span of these NMJs was obviously reduced compared to controls.

3.2.3.5 Madm localizes to larval brain, nerves and NMJs

To analyze the distribution of Madm within the nervous system, we generated an antibody. This Madm antibody specifically recognized Madm on Western blots of larval brain extracts (Fig. 1 B). In addition, this antibody recognized Madm *in situ* on larval brains. In wild-type animals, Madm was expressed throughout the larval brain and present in the ventral nerve cord as well as in the afferent and efferent nerves (Fig. 5 A). In 2D2/Df mutant animals, the Madm levels were strongly diminished compared to the control (also note varicosities along nerves) (Fig. 5 B). Pan-neuronal re-expression of Madm using *elav-Gal4* restored protein expression and localization (Fig. 5 C). Unfortunately, at the NMJ we observed unspecific background that did not allow us to detect endogenous protein levels. Thus, we generated N-terminal tagged UAS-EGFP-Madm constructs to monitor the localization of the protein at the NMJ. In presynaptic EGFP-Madm overexpression as well as presynaptic EGFP-Madm 2D2/Df rescue animals, Madm was clearly localized to all boutons throughout the larval presynaptic nerve terminal (Fig. 5 D, E). At the subcellular level, Madm was not located within nuclei. Cell body nuclei at the ventral nerve cord are spared from Madm protein (Fig. 5 D, E). In contrast, Madm was expressed throughout the nerve (Fig. S5 A, B) as already observed in the antibody staining (Fig. 5 A, C). To demonstrate that the expression of the EGFP-Madm construct reflects endogenous Madm expression, we tested for rescue ability of synaptic stability (Fig. S5 C, D). We observed a significant rescue of synaptic stability in presynaptic EGFP-Madm 2D2/Df rescue animals compared to 2D2/Df mutant animals (Fig. S5 C). Furthermore, synaptic retraction severities were reduced (Fig. S5 D). Next, we confirmed that overexpression of the UAS-Madm and the EGFP-Madm construct had similar effects on NMJ morphology (Fig. S5 E, F, G, H). Thus, the EGFP-Madm construct we used to demonstrate Madm localization to the *Drosophila* NMJ indeed acts like the endogenous Madm protein in synapse stability.

3.2.3.6 Mlf1 and BunA modulate synaptic stability as well as morphology

Interestingly, we observed the strongest synaptic stability and morphology defects in Madm 4S3/Df mutant animals. As we already demonstrated, this mutation does not affect protein levels, but it specifically affects the binding to the interaction partners Mlf and BunA. Therefore, we next analyzed the potential requirements of Mlf and BunA for NMJ stability and morphology. For Mlf, we analyzed the *mlfΔC1* allele. The *mlfΔC1* deletion allele was generated via imprecise excision of the P element of strain EU2490 (Kazemi-Esfarjani et al., 2002) in the first *mlf* intron (Martin-Lannere et al., 2006). The deletion represents a null allele (Martin-Lannere et al., 2006). Homozygous *mlfΔC1* mutant animals displayed synaptic retraction frequencies comparable to wild-type animals (4.2%, Fig. 6 D) on the dorsal muscles 1/9 & 2/10. As maternal effects were previously described for Mlf, we also analyzed *mlfΔC1* mutant animals lacking maternal contribution (here referred to as “mat. ctr.”). Those animals were derived from crosses of homozygous mutant *mlfΔC1/Df* or *mlfΔC1/mlfΔC1* virgin females to *mlfΔC1* males. In those animals, we saw an increased synaptic retraction frequency of 9.4% compared to 4.2% in zygotic, homozygous *mlfΔC1* mutant animals (Fig. 6 B, D). BunA was previously shown to positively regulate growth together with Madm (Gluderer et al., 2010). For the analysis of BunA for synaptic stability, we focused on the combination of the null allele *bun 200B* and the P-element insertion GE12327 in the *bunA* 5'UTR (Gluderer et al., 2008). The *bun 200B* allele is considered to be a null allele, since Bun proteins lacking the TSC-box as well as the leucine zipper should not be functional (Gluderer et al., 2008). In *bun 200B/GE* mutant animals, we observed 10.3% synaptic retractions on muscle 1/9 and 2/10 (Fig. 6 C, D). This minor synaptic instability effects were not significant compared to the control (Fig. 6 C). Maternally controlled *mlfΔC1* mutant as well as BunA mutant animals displayed more severe synaptic retractions compared to zygotic *mlfΔC1* mutant animals (Fig. 6. E). Similar tendencies were observed for synaptic stability on the ventral muscles 6/7 (Fig. S6). The synaptic retraction frequency of homozygous *mlfΔC1* mat. ctr. mutant animals was higher than in zygotic, homozygous *mlfΔC1* mutant animals (15% compared to 4.2%; Fig. S6 A). But the observed synaptic stability defects were not significant compared to controls. Maternally controlled *mlfΔC1* mutant as well as BunA mutant animals exhibited also a substantial

amount of medium synaptic retractions (3-6 boutons affected), whereas control and zygotic *mlfΔC1* mutants only had small synaptic retractions (Fig. S6 B).

Hence, Mlf and BunA mutant animals displayed a tendency towards synaptic instability. But none of the observed defects was significant compared to controls. Interestingly, synaptic instability effects were more pronounced in homozygous *mlfΔC1* mat. ctr. mutant animals versus zygotic, homozygous *mlfΔC1* mutant animals indicating that the maternal Mlf contribution is promoting synaptic stability at the *Drosophila* NMJ.

Subsequently, we wanted to determine the effect of Mlf and BunA on NMJ morphology and growth. We analyzed the morphology of *mlf* and *bunA* mutants. We found the number of NMJ branches, the total bouton number as well as the total length of all NMJ branches significantly decreased compared to control (Fig. 6 F, G, H, I, J, K). Thus, those mutants displayed similar features of the morphological changes observed in *Madm* mutant animals (Fig. 2 and Fig. S3). The parameter of the NMJ area covering the muscle area showed a tendency towards reduction as observed in *Madm* mutant animals (Fig. 6 L). This effect was not significant compared to control, but the mean value went down to 78.0% (1.87 ± 0.36 SEM for *mlfΔC1* mat. ctr. versus 2.40 ± 0.20 SEM for control). For the *bun 200B/GE* mutant animals, we observed no significant change in NMJ area compared to control animals (Fig. 6 L).

Furthermore, we observed in Mlf mutant animals substantial accumulations of the active zone marker BRP in nerves and motoneuron axons (Fig. S7 B) similar to the phenotype described for *madm* mutants (Fig. S2 D). We quantified the accumulation of BRP puncta in *mlfΔC1* mat. ctr. mutant animals and they were significantly increased to 167.4% compared to control (Fig. S7 C). Subsequently, we also monitored the DVGlut levels. We found a highly significant increase to 173.7% compared to control. This indicates that *mlf* mutants in contrast to *madm* mutants display a transport defect of axonal cargos.

3.2.3.7 Mlf and BunA genetically interact with Madm to modulate synaptic stability

Next, we used genetic interaction assays to test whether Mlf and BunA interact with Madm in the control of synaptic stability.

Single copies of the *mlfΔC1* allele or the *Madm* 2D2 allele did not have any significant effect on the synaptic retraction frequency at the dorsal muscles (Fig. 7 A). In transheterozygous *mlfΔC1* /+; 2D2/+ animals, we observed a small but significant increase of synaptic instability to 8.4% (Fig. 7 A). Similarly, removal of one copy of *Madm* (2D2/+) in the homozygous mutant *mlfΔC1* animals resulted in a significant increase of synaptic destabilization from 4.2% to 25.0% (Fig. 7 A). Furthermore, large synaptic retractions were observed which were not present in the homozygous *mlfΔC1* mutant animals (Fig. 7 B). We also tested the reverse interaction. Removal of one copy of *Mlf* (*mlfΔC1*/+) in the 2D2/Df mutant animals did not cause any significant increase in synaptic stability levels compared to 2D2/Df mutant animals (Fig. 7 A). Also the distribution of the different categories of synaptic retraction severities remained unaffected (Fig. 7 B). Similar effects and tendencies were also observed on muscles 6/7 (Fig. S8 A, B). Interestingly, the removal of one *madm* copy in homozygous *mlfΔC1* mat. ctr. mutant animals resulted in an increase of synaptic instability (15.0% to 20%, n.s.) (Fig. S8 A).

Subsequently, we tested for a potential interaction between *Madm* and *BunA*. The analysis of heterozygous *bun 200B* as well as *Madm* mutant animals did not reveal any changes compared to control (Fig. 7 C). Furthermore, there was no significant increase in synaptic instability in transheterozygous *bun 200B*/+; 2D2/+ animals (Fig. 7 C). However, the removal of one *madm* copy in *bun 200B/GE* mutant animals resulted in a decrease of synaptic retraction frequency from 10.3% to 5.0% (Fig. 7 C). In addition, the occurrence of large synaptic retractions disappeared (Fig. 7 D). Similarly, the removal of one *bun* copy (*bun 200B*/+) in *Madm* 2D2/Df mutant animals led to a significant reduction from 36.6% to 11.9% synaptic retraction frequency (Fig. 7 C). The occurrence of large retractions disappeared as well (Fig. 7 D). The same effect was observed on muscles 6/7 (Fig. S8 C). 2D2/Df mutant animals displayed 40.0% synaptic retractions compared to *bun 200B*/+; 2D2/Df mutant animals with 21.3% synaptic retractions (n.s.). This data indicates that *bunA* mutations antagonizes the destabilizing effect of *madm* mutants as the introduction of the mutant *bun 200B* allele into *madm* mutants caused an improvement in synaptic stability. In contrast, *Madm* mutant alleles in the *Mlf* mutant animals promoted synaptic instability. Thus, we have identified two genetic interaction partners of *Madm* - *Mlf* and *BunA* - working in opposite directions to modulate synapse stability.

3.2.4 Discussion

We demonstrate for the first time that presynaptic Madm is involved in fundamental aspects of synapse development and maintenance. We provide evidence that Madm contributes to the control of synapse stability, growth and morphology as well as certain aspects of axonal transport.

We used an allelic series of *madm* mutations to dissect the role of Madm at the *Drosophila* NMJ and in the nervous system in more detail. We demonstrated that the *madm*^{EP3137} allele caused a strong decrease of Madm protein levels and represents a hypomorphic allele. Furthermore, we used the Madm 2D2 null allele for analysis. Indeed, we did not detect any Madm protein in mutant 2D2/Df brain samples. In addition, we used the point mutation 4S3 which did not diminish Madm protein levels but likely affects essential protein-protein interactions.

In *madm* mutants, we observed severe synaptic stability and morphology defects. NMJs did not grow out to the same extent as in control animals, but remained entangled and condensed at the point of NMJ innervation. Furthermore, in Madm mutant animals the number of NMJ branches was increased, whereas synaptic bouton number, total NMJ length and NMJ area were significantly decreased. We observed that the precise control of Madm protein levels is crucial for the control of synaptic stability and morphology. The number of synaptic boutons was significantly decreased in Madm mutant animals. Presynaptic rescue experiments increased the number of synaptic boutons. However, with the exception of the 4S3/Df combination these values did not reach significance. Interestingly, presynaptic overexpression of Madm in wild type animals also caused a significant decrease of synaptic bouton number. Another example for the importance of tight control of Madm protein levels in the nervous system was the significant increase of NMJ area covering the muscle surface after presynaptic Madm overexpression in control animals. Thus, we can assume that the precise levels of Madm protein in the nervous system are crucial for the phenotypic outcome, as excess of Madm directly contributes to morphological defects. This assumption is also supported by the observation that hypomorphic alleles of Madm caused significantly weaker perturbations of synaptic morphology and stability. Hence, Madm levels in the nervous system must be tightly controlled in wild-type animals.

In addition, we tried to address the time course of the manifestation of the *Madm* mutant phenotype. Second instar larvae displayed only minor synaptic stability defects and the severity of the synaptic instability increased significantly from second to third instar larvae. This suggests that *Madm* is not required for initial synapse formation, but for long-term maintenance. A similar requirement for synaptic maintenance was previously demonstrated for Spectrins and Ankyrin2 at the *Drosophila* NMJ (Pielage et al., 2005; Pielage et al., 2008).

In second instar larvae, we also saw that the overall appearance and organization of control versus *Madm* mutant NMJs was very similar. However, the NMJs in *Madm* mutant animals were already smaller compared to control animals. Thus, it seems likely that *madm* mutants fail to grow out over the muscle surface in the first place, sharing less contact area with the muscle. This failure to appropriately innervate the muscle may contribute to the observed progressive loss of synaptic stability.

In addition to the NMJ defects, we observed the formation of large varicosities and swellings at nerves in *Madm* mutant animals. Interestingly, our rescue data suggests that *Madm* expression both in glia and neurons is sufficient to prevent formation of the nerve bulges. Thus two different scenarios are possible. First, *Madm* might act as a signal via an unidentified pathway from both sides to ensure glial wrapping of the axons. If this effect holds true it would be interesting to analyze this potential new signaling cascade in more details. Second and more likely, the pan-neuronal driver *elav-Gal4* used for rescues was already described to be partially expressed in embryonic glia (Berger et al., 2007). Thus, the rescue would be entirely executed via restoring *Madm* expression in glial cells.

We tried to determine the nature of these swellings by using a set of different cellular markers. Microtubule bundles, visualized via Futsch - the invertebrate MAP1B (microtubule-associated protein 1B) homolog, were less organized and formed sinuous structures. The linear, parallel bundling within the axon was lost. Although this might affect transport along these microtubules, we could not observe accumulation of BRP or DVGLuT inside the varicosities. Interestingly, a similar varicosity phenotype was previously reported as swelling of peripheral glia upon knockdown of the anterograde motor protein Kinesin heavy chain (*Khc*) (Schmidt et al., 2012). *Khc* seems to be crucial in subperineurial glia which are part of the blood-brain barrier (BBB).

Glia-specific knockdown resulted in swollen peripheral nerves with maldistributed mitochondria. This affected directed axonal transport in glia and suppressed neuronal excitability. Glial Khc depletion resulted in an opening of the BBB indicated by the mislocalization of the septate junction protein Neurexin IV (invertebrate homolog of mammalian Caspr) and spastic flies (adult hyperexcitation phenotype) (Schmidt et al., 2012). Based on the absence of synaptic vesicle accumulations in these regions, it is unlikely that related pathways are affected in *Madm* mutant flies.

In *Drosophila* larvae, few (perineurial and subperineurial) glia processes reach out to the NMJ (Brink et al., 2012). Those processes are highly dynamic. They are known to be involved in the removal of presynaptic debris (Jia et al., 1993; Sepp et al., 2000; Fuentes-Medel et al., 2009). It will be interesting to further evaluate potential glial defects at the NMJ of *Madm* mutant animals that may relate to the observed synaptic stability impairment.

In human and mammalian neurodegenerative diseases, nerve swellings usually indicate axonal transport defects (Coleman, 2005; De Vos et al., 2008). Thus, we analyzed *Madm* mutant animals for transport defects. Upon *Madm* depletion, no classical axonal transport defect characterized by an accumulation of axonal cargos like DVGluT could be observed. The monitored accumulation of BRP in the nerves and presynaptic motoneuron axon still indicates a specific axonal transport defect. Whether anterograde or retrograde transport is affected could not yet be determined. An alternative hypothesis would be that due to the synaptic stability defects present in *madm* mutants, BRP as an active zone component is actively transported back to the soma.

We next aimed to identify potential *Madm* interaction partners. The *Madm* 4S3/Df mutant animals displayed the strongest synaptic stability and morphology defects. The defects present in 4S3 mutants were even stronger than the defects caused by the null allele 2D2. Interestingly, the point mutation of the 4S3 allele specifically affects binding to BunA and Mlf (Lim et al., 2002; Gluderer et al., 2010). Hence, we investigated their potential role in the control of synapse stability and morphology. In contrast to *Madm* mutant animals, no significant impairment of synaptic stability was detected. However, synaptic morphology of Mlf and BunA mutant animals was altered compared to control animals with a significant decrease in the number of synaptic boutons.

We observed that depletion of the maternal contribution in *mlfΔC1* animals increased synaptic stability defects (on muscles 1/9 & 2/10 as well as muscles 6/7) (Fig. 6 and Fig. S6). The modulation of phenotypic strength as well as lethality via maternal contribution was previously described (Martin-Lannere et al., 2006).

We demonstrated that Mlf and BunA modulate synaptic stability defects caused by the loss of Madm. Although *mlf* or *bunA* mutants alone did not display significant synaptic instability phenotypes, they modulated synaptic stability defects in combination with Madm. The removal of a single copy of Mlf in the Madm mutant background significantly increased synaptic instability. Thus, Mlf seems to promote synaptic stability. In contrast, the removal of a single copy of BunA in the Madm mutant background was able to significantly antagonize the synaptic stability defects present in Madm mutant animals. Thus, BunA likely acts as antagonist to Madm in the control of synaptic stability. In our study, we provide first evidence for a role of Madm together with Mlf and BunA for synapse maintenance, although the exact mechanism or signaling network still has to be determined. But the pronounced defects observed with Madm 4S3 mutants indicate the specificity and importance of the interaction between Madm, Mlf and BunA for synapse development and stability.

Furthermore, we could show that *mlfΔC1* mutant animals lacking maternal contribution exhibit features of axonal transport defects (Fig. S7). BRP and DVGluT puncta get stuck in the nerves as well as axons and accumulate. Again this might also be linked to the synaptic instability and morphological changes observed in these animals. BRP is one of the first markers to withdraw from instable synaptic boutons (data not shown). Thus, BRP might be transported in a retrograde manner for degradation. Similarly, the morphological changes at the NMJ might lead to a reduced or delayed incorporation of synaptic proteins.

Still it is not clear, in which pathway Madm could function together with Mlf and BunA during the control of synapse development and maintenance. How can the observed synaptic stability and morphology defects upon Madm loss be linked to other pathways that have been implicated in these processes at the NMJ? Potential insights may come from signaling pathways previously described to display similar NMJ phenotypes.

The mTOR pathway component S6 kinase was found to regulate the development and size of the *Drosophila* NMJ including synaptic bouton size, active zone numbers and neurotransmitter release (Cheng et al., 2011). Upon S6K loss, the size of motoneuron cell bodies as well as motoneuron axons was reduced (Cheng et al., 2011). Interestingly, co-overexpression of BunA as well as the growth-promoting mTOR pathway component S6 kinase was demonstrated to enhance growth (Gluderer et al., 2008). Furthermore, mutants of the two mTOR pathway components TSC1 and TSC2 displayed increased synaptic growth as well as morphology defects at the NMJ (Dimitroff et al., 2012; Natarajan et al., 2013). Neuron-specific overexpression of Rheb led to increased synaptic growth (Dimitroff et al., 2012). One study showed that the TOR complex 2 (TorC2), but not the TOR complex 1 (TorC1), was involved in the control of growth at the *Drosophila* NMJ (Dimitroff et al., 2012). Initial testing of potential genetic interaction with S6K did not allow potential integration of Madm into this pathway. Further experiments with additional components of this pathway will be necessary to implicate or rule out direct regulation of Madm by the mTOR pathway.

Rheb links the mTOR to the insulin signaling pathway (Martin-Pena et al., 2006). The insulin-like peptides are hormones acting via the PI3K (phosphatidylinositol 3-kinase)/AKT (=PKB (protein kinase B)) pathway. Neuronal overexpression of PI3K resulted in increased synaptic growth at the NMJ (Dimitroff et al., 2012). Furthermore, PI3K was shown to regulate synapse number of *Drosophila* larval motoneurons (Martin-Pena et al., 2006), indicating a potential link to the growth promoting and stability promoting functions of Madm. We will use genetic interaction tests to analyze whether Madm may represent a downstream target of this pathway.

In addition, the BMP/TGF- β (bone morphogenetic protein/transforming growth factor β) pathway was shown to regulate NMJ formation and growth (Featherstone et al., 2000; Collins et al., 2007). Glass-bottom boat (Gbb) is released from the muscles and activated the TGF- β receptors Wishful thinking (Wit) and Saxophone (Sax) or Thick veins (Tkv) in motoneurons. This leads to the phosphorylation of Mad and its translocation to the nucleus. Subsequently, transcriptional regulation controls bouton growth and function (McCabe et al., 2003; Rawson et al., 2003; Baines, 2004; Goold et al., 2007; Fuentes-Medel et al., 2012). In addition, a local link of TGF- β in the control of synapse stability has been demonstrated (Eaton et al., 2005). Thus, at

least two pathways, insulin signaling and TGF- β signaling, have previously been implicated in the control of synapse stability and growth.

One mode of action of growth-regulating signaling pathways is the regulation of expression of metabolic genes via different transcription factors like Myc, FOXO (Forkhead box class 'O') and DREF (DNA replication related element binding factor) (Killip et al., 2012). Interestingly, Mlf was previously shown to interact with DREF (Ohno et al., 2000; Martin-Lannere et al., 2006).

Although the Madm protein has a nuclear localization signal, we did not find any indication for Madm being localized to the nucleus *in vivo* which would indicate for example that Madm might be involved in transcription directly. This was already proposed by Gluderer *et al.* (2010). Previously, only murine Madm was shown to faintly localize to the nucleus *in vitro* (Lim et al., 2002). But we could demonstrate for the first time that Madm is expressed *in vivo* in *Drosophila* larval brains, nerves and NMJs.

Thus, there are demonstrated links of the Madm-Mlf-BunA network to growth-regulating signaling cascades like the insulin/TOR network. We implicate Madm as well as Mlf for the first time in nervous system development. This study demonstrates a novel, important role of Madm together with Mlf and BunA during synapse development, growth and maintenance.

3.2.5 Acknowledgement

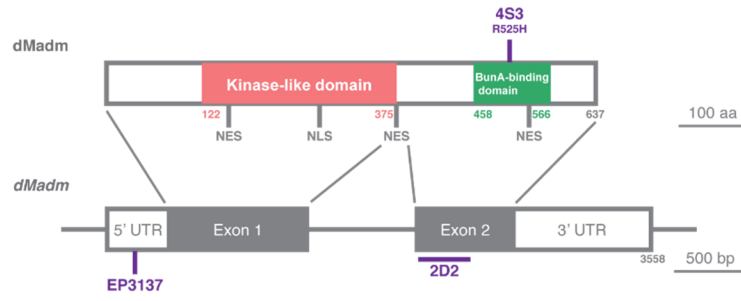
We like to thank Hugo Stocker (ETH Zürich, Switzerland) for the generous gift of Madm, Mlf and Bunched fly stocks. In addition, we like to thank the Vienna *Drosophila* RNAi Center (Vienna, Austria), the *Drosophila* Genomic Research Center (Indiana, USA) and the Developmental Studies Hybridoma Bank (Iowa, UAS) for fly stocks and cDNAs. Furthermore, we like to thank the imaging and microscopy facility at the Friedrich Miescher Institute (Basel, Switzerland) for the help with image acquisition as well as computational programming. Finally, we are thankful to the Life Imaging Center (Freiburg, Germany), respectively software engineer Shaojun Jin, for providing us with the LIC macro to acquire our morphology dataset. Research in the lab of Jan Pielage was supported by the Friedrich Miescher Institute for Biomedical Research (Basel, Switzerland).

3.2.6 Author contributions

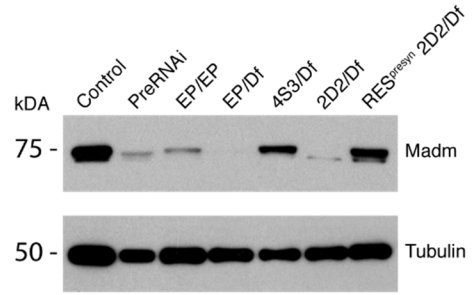
J.P. and I.D.K. designed the experiments. V.B. identified Madm as potential candidate. I.D.K. performed all experiments and quantifications. J.P. and I.D.K. wrote the paper with input from all authors.

3.2.7 Figures

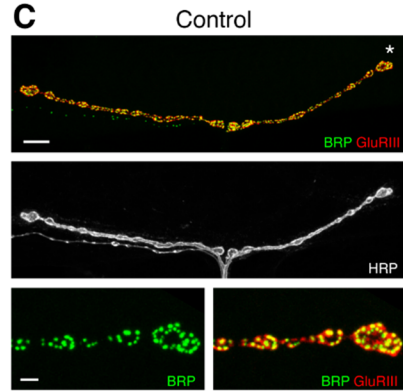
A



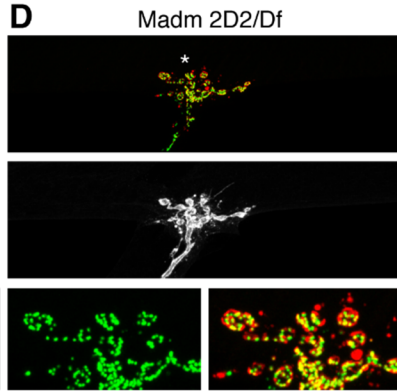
B



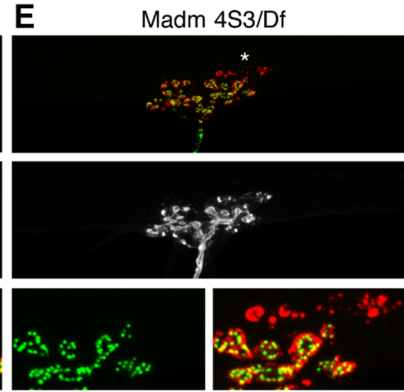
C



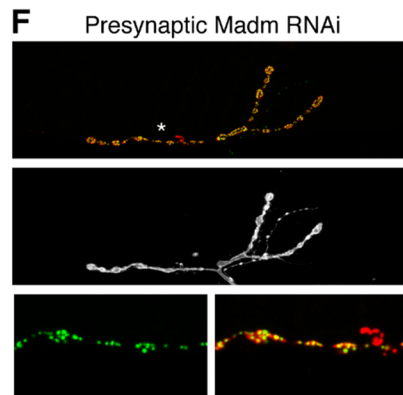
D



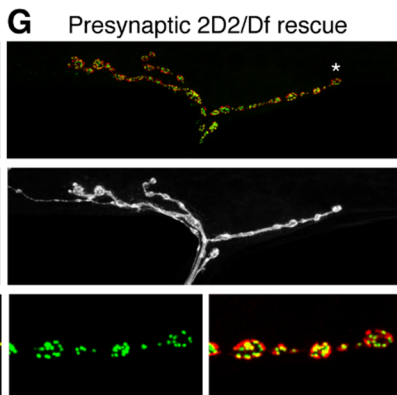
E



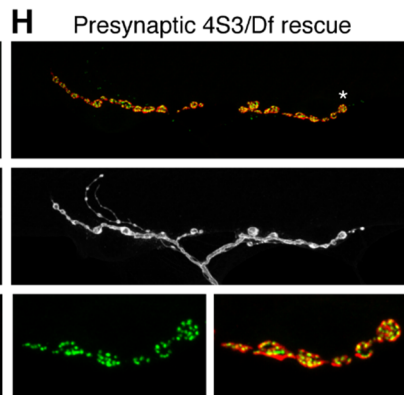
F



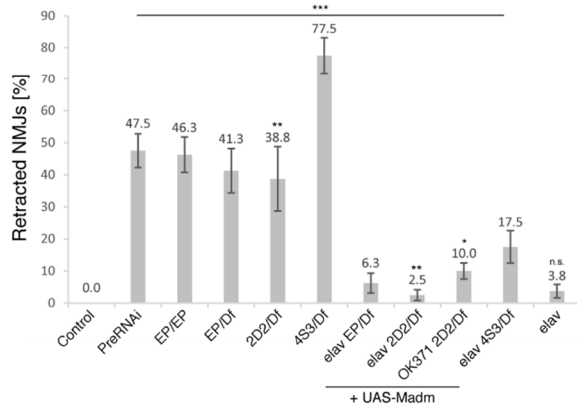
G



H



I



J

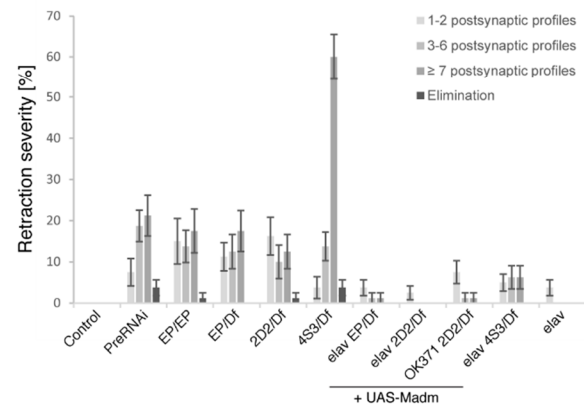


Figure 1. Presynaptic Madm is essential for synapse stability.

(A) The *Drosophila madm* locus. It is a single locus with two exons giving rise to one protein isoform of 637 amino acids (modified after (Gluderer et al., 2010)). Madm represents a non-functional kinase. The kinase-like domain is lacking the ATP-binding domain. The protein has three nuclear export signals (NES) and one nuclear localization signal (NLS). Different recessive lethal *madm* alleles were generated via EMS mutagenesis (Gluderer et al., 2010). Their allelic strength was monitored combining them with a deficiency (Df(3R)Exel7283). The same deficiency is used throughout this study. Originally, the degree of the small pinhead phenotype as well as larval growth deficits observed were rated. The Madm 2D2 allele was classified as a strong allele, 4S3 as an intermediate allele and the P{EP}3137 element insertion, we use in this study, was previously uncharacterized. The 2D2 allele is a deletion causing a frameshift after 385 amino acids. It leads to a premature translational stop codon after additional 34 amino acids. The 4S3 allele is a point mutation changing arginine to histidine (R525H). The P{EP}3137 element insertion resides in the 5'UTR. The initiation of prepupal stages in Madm mutant animals was two to ten days delayed. Interestingly, the BunA-binding domain of Madm is also the binding domain for Mlf (Lim et al., 2002). This interaction domain is affected in the Madm 4S3 allele. **(B)** Analysis of Madm knockdown, alleles and presynaptic rescue experiments on Western blot with larval brain samples. Madm protein was detected at ~ 75kDa size and showed double band. Tubulin served as loading control. n = 2 - 3.8 brains per lane. **(C)** NMJ of control did not display synaptic instability. A precise opposition of the presynaptic active zone marker BRP (green) and the postsynaptic GluRIII receptors (red) was observed. Neuronal membrane was continuously formed (HRP, white). **(D-E)** Madm mutant animals displayed strong synaptic stability defects. Postsynaptic footprints (red) were left behind unopposed by presynapse (green). Neuronal membrane started to get degraded (HRP in white). **(F)** Presynaptic Madm knockdown resulted in synaptic instability. **(G-H)** Presynaptic Madm re-expression in Madm 2D2/Df or 4S3/Df background rescued synaptic instability. **(C-H)** Scale bars: main panels 7 μ m, enlarged panels 1.5 μ m. **(I-J)** Quantification of synaptic retraction frequency and severity on muscle 1. n = 10 animals of each genotype. Error bars represent SEM.

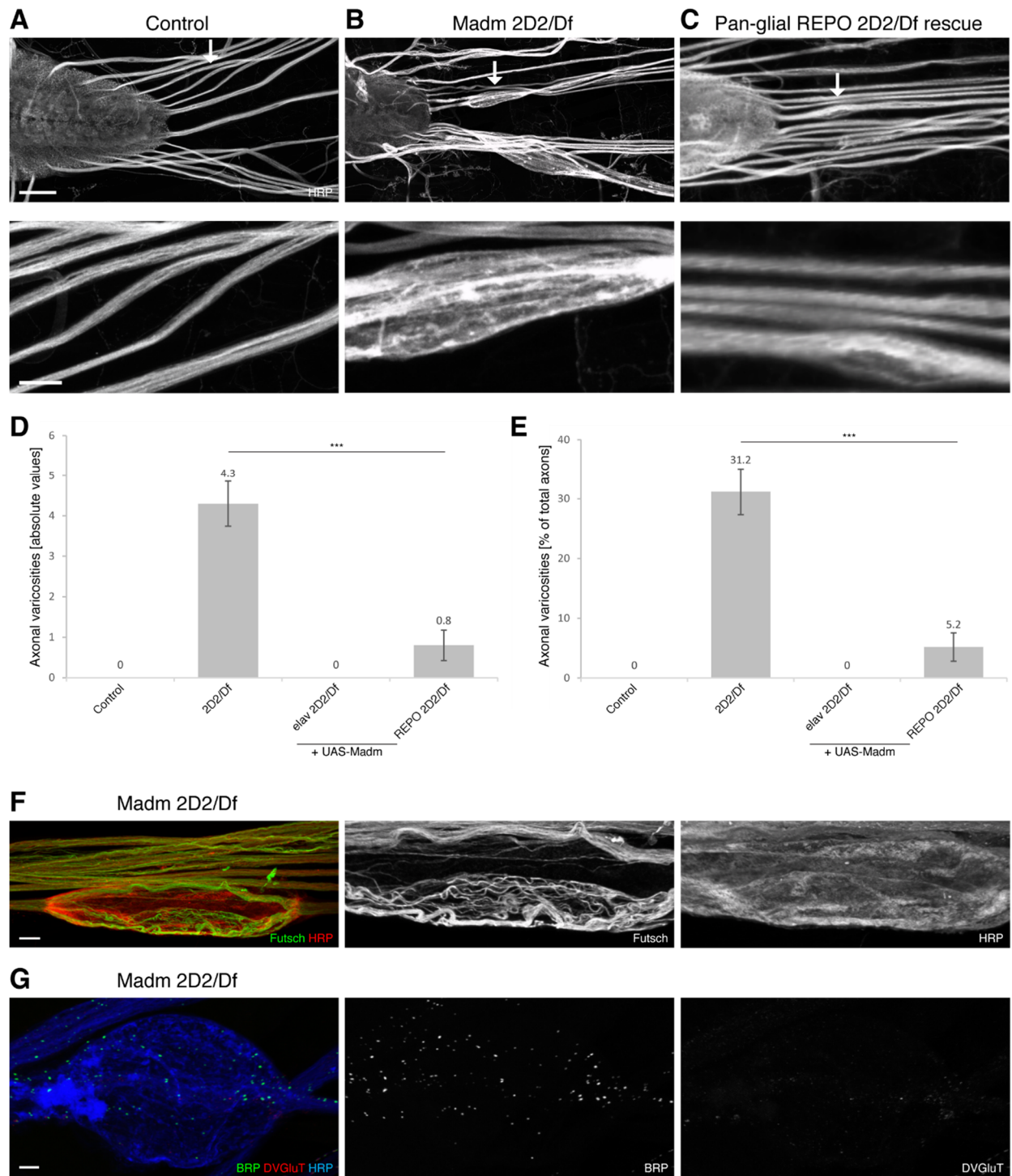


Figure 2. *Madm* mutants display nerve bulges.

(A) Neuronal membranes were marked by HRP (white). In control animals, nerves after the VNC were uniformly thick and shaped. **(B)** In *Madm* 2D2/Df mutant animals, nerves displayed bulges after the VNC (indicated by ↓). **(C)** Upon pan-gliial re-expression of *Madm* in the mutant animals, no prominent swellings were observed. **(A-C)** Scale bars:

main panels 60 μm , enlarged panels 7 μm . **(D-E)** Quantification of varicosities (absolute values and normalized to control). Bulges were not observed in control animals. In *Madm* mutant 2D2/Df animals, swellings were highly significantly increased. Upon pan-neuronal re-expression of *Madm* in mutant background using *elav-Gal4*, no bulges were observed. Also the pan-glial rescue experiment using *REPO-Gal4* highly significantly reduced the occurrence of varicosities. $n = 5 - 6$ animals of each genotype representing 76 - 86 nerves per animal. Error bars represent SEM. **(F)** Visualization of microtubules within bulges via Futsch (the homolog of mammalian MAB1B). Microtubules formed wavelike structures. Scale bar: 10 μm . **(G)** No accumulation of transported BRP particles or DVGLuT vesicles within varicosities was observed. Scale bar: 6 μm .

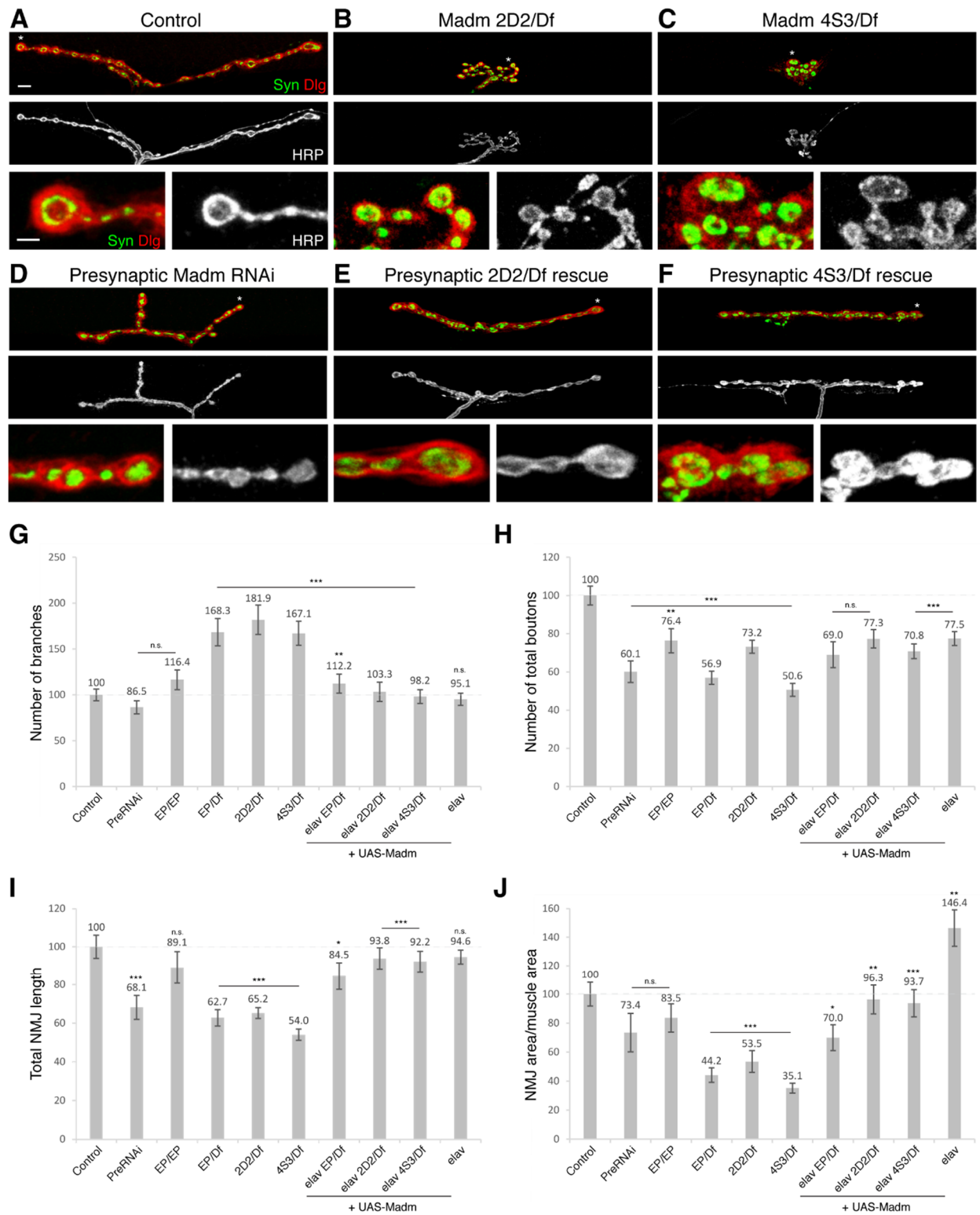


Figure 3. *Madm* mutants display severe NMJ growth and morphology phenotypes.

(A) Morphology of NMJs was visualized using the presynaptic marker Syn (green) and the postsynaptic marker Dlg (red). Neuronal membrane was marked by HRP (white). NMJs on muscle 1 of control animals covered substantial area over the muscle. Pre- and postsynaptic markers were well opposed and precisely organized. **(B-C)** In Madm mutant 2D2/Df and 4S3/Df animals, NMJs stayed more condensed and individual NMJ branches were more entangled. Morphological features were altered compared to control. **(D)** Upon presynaptic Madm knockdown, NMJ size was also diminished. **(E-F)** Pan neuronal, presynaptic re-expression of Madm in Madm mutant animals, restored normal features of NMJ morphology. **(A-F)** Scale bars: main panels 7 μm , enlarged panels 1.5 μm . **(G-J)** Quantification of four morphological NMJ parameters normalized to control. $n = 17 - 24$ NMJs on muscle 1 in 6 different animals per genotype. Error bars represent SEM. For range of values see box plots of Fig. S3. **(G)** Quantification of number of NMJ branches. This parameter was highly significantly increased in Madm mutant over Df animals. Presynaptic rescue experiments highly significantly reduced increased branch number. NMJs of presynaptic Madm knockdown, Madm EP/EP and presynaptic Madm overexpression animals were not significantly altered compared to control. **(H)** Quantification of number of total synaptic boutons. Quantified were type Ia and Ib boutons. Synaptic bouton number was highly significantly decreased in presynaptic Madm knockdown, mutant and presynaptic Madm overexpression animals. The number of synaptic boutons could be highly significantly restored upon Madm re-expression in the 4S3/Df mutant animals. **(I)** Quantification of total NMJ length. The length was highly significantly reduced in presynaptic Madm knockdown as well as Madm mutant over Df animals. Presynaptic rescue experiments significantly restored normal NMJ length. NMJs of presynaptic Madm overexpression animals were not significantly altered compared to control. **(J)** Quantification of NMJ area covering muscle area. NMJ area was highly significantly reduced in Madm mutant animals over deficiency (35.1% in 4S3/Df compared to control). Upon presynaptic Madm re-expression, NMJ area was significantly increasing. NMJs of presynaptic Madm overexpression animals were significantly larger.

To address at which developmental stage stability as well as morphology defects of *madm* mutants manifest, 2nd and 3rd instar larvae of control and *Madm* 4S3/Df animals were compared. **(A)** In control animals, NMJs of 2nd instar larvae were smaller than their 3rd instar counterparts. **(B)** No significant synaptic instability could be observed for 2nd or 3rd instar control larvae. **(C)** *Madm* 4S3/Df mutant 2nd instar larvae had smaller NMJs than control animals of the same stage. No significant synaptic stability defect was present. **(D)** NMJs of 4S3/Df 3rd instar larvae displayed severe synaptic stability and morphology defects. **(A-D)** Scale bars: main panels 5 μm , enlarged panels 3 μm . **(E-F)** Quantification of synaptic retraction frequency and severity on muscles 1/9 & 2/10. Highly significant synaptic stability defect was present in *Madm* 4S3/Df mutant larvae at 3rd instar stage, but not at 2nd instar stage. 3rd instar 4S3/Df mutant animals also showed most severe synaptic retractions. Comparing 2nd to 3rd instar larvae of each genotype individually, synaptic instability also significantly increased within the group over time. $n = 10$ animals of each genotype. Error bars represent SEM.

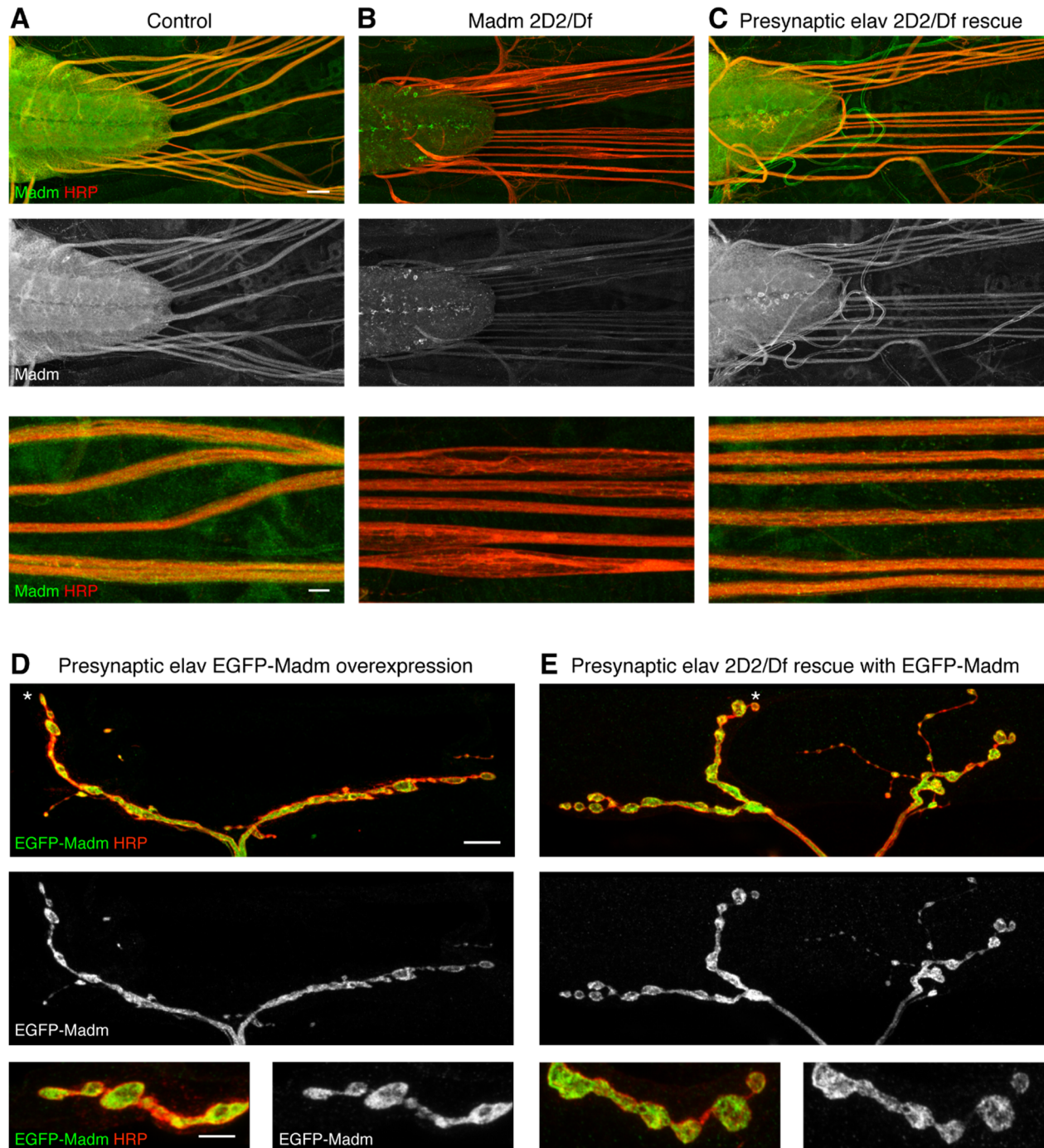


Figure 5. Madm localizes to larval brain, nerves and NMJs.

(A) Larval brains were stained *in situ* for Madm signal. Control animals showed Madm expression in the brain, the VNC and the nerves. Cell bodies in the brain did not express Madm. **(B)** Madm expression was clearly reduced in Madm mutant 2D2/Df animals. The Madm 2D2 mutation is a null allele caused by deletion. **(C)** Presynaptic Madm re-expression using elav-Gal4 restored Madm signals. **(A-C)** Scale bars: main panels 30 μm , enlarged panels 15 μm . **(D-F)** Madm localized to the NMJ and each individual synaptic bouton respectively. As the Madm antibody signal at

the NMJ was very faint, the NMJs of animals with presynaptic EGFP-Madm expression as well as presynaptic EGFP-Madm rescue of 2D2/Df animals are displayed. The expression of the EGFP-Madm construct significantly rescued synaptic stability defects in 2D2/Df mutant animals. Furthermore, the EGFP-Madm construct behaved equal in effects on synaptic stability and morphology to an untagged UAS-Madm construct (see Fig. S5). Scale bars: main panels 7 μm , enlarged panels 3 μm .

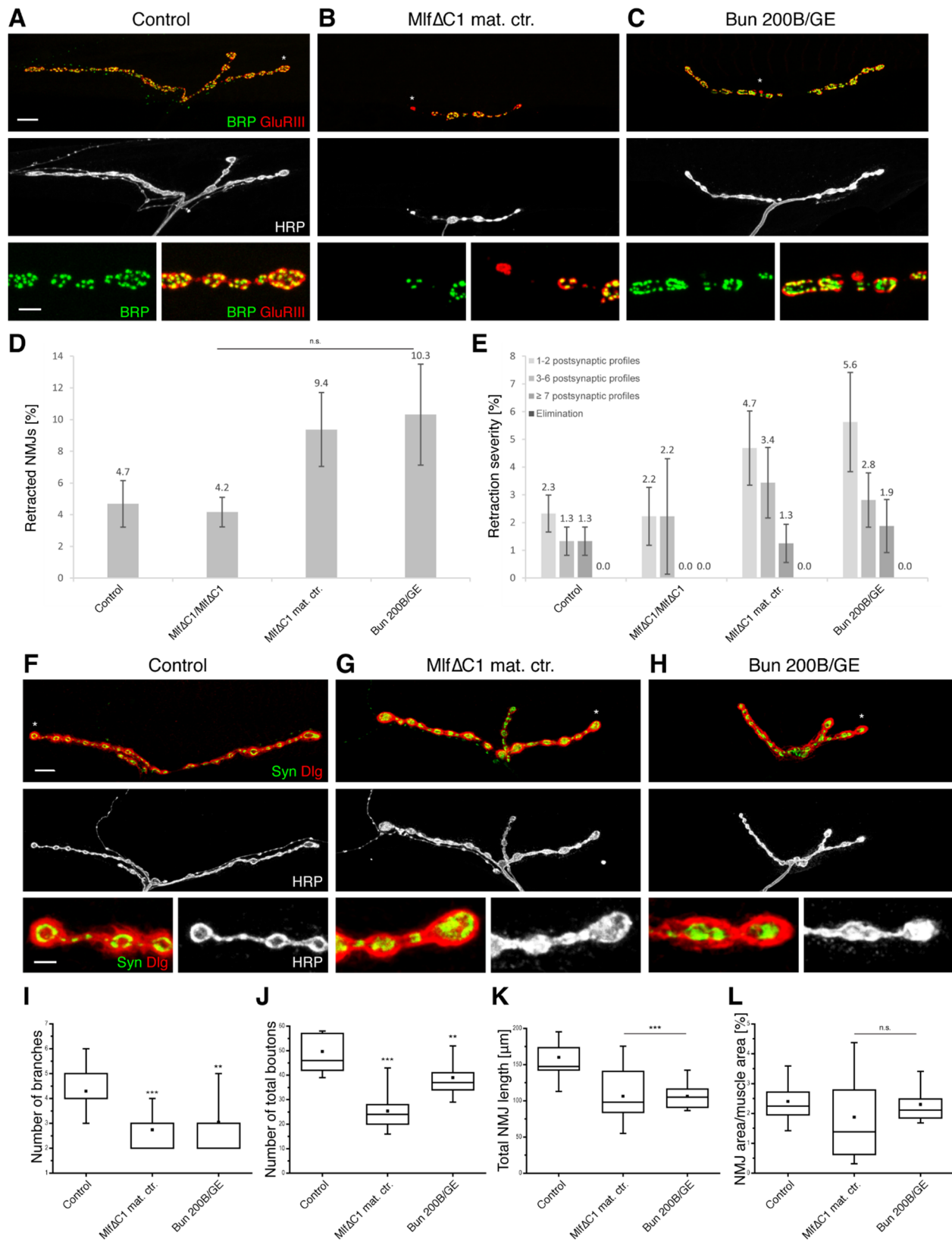


Figure 6. Mlf1 and BunA modulate synaptic stability as well as morphology.

The *mlfΔC1* deletion allele affects the first *mlf* intron. Thus, the deletion represents a null allele. Larvae controlled for the maternal contribution (mat. ctr.) were obtained by crossing homozygous mutant *MlfΔC1/MlfΔC1* or *MlfΔC1/Df* virgin females to heterozygous *MlfΔC1* mutant males. Thus, the genotype of *MlfΔC1/MlfΔC1* mat. ctr. animals is *MlfΔC1/MlfΔC1* or *MlfΔC1/Df*. The null allele *bun 200B* (affecting all Bunched isoforms) and the P-element insertion GE12327 (subsequently referred to as GE for simplicity) in the *bunA* 5'UTR are combined for analysis. **(A)** NMJ on muscle 1 of control animals did not show synaptic stability defects. Presynapse (BRP, green) and postsynapse (GluRIII, red) were present and in close opposition. Neuronal membrane was continuously formed (HRP, white). **(B)** *MlfΔC1* mutant animals lacking maternal contribution (mat. ctr.) only showed minor synaptic stability defects. **(C)** *Bun 200B/GE* mutant animals displayed synaptic stability defects. **(A-C)** Scale bars: main panels 7 μm, enlarged panels 3 μm. **(D-E)** Quantification of synaptic retraction frequency and severity on muscles 1/9 & 2/10. Control animals displayed same level of synaptic retraction frequency as zygotic *MlfΔC1/MlfΔC1* mutant animals. In *MlfΔC1/MlfΔC1* mat. ctr. mutant animals, the synaptic retraction frequency was more than doubled (4.2% to 9.4%) and retraction severity increased. The highest synaptic retraction frequency was present in *Bun200B/GE* animals. Mutant animals showed a tendency toward synaptic instability, but observed synaptic retraction frequencies were not significant compared to the control animals. n = 10 animals of each genotype, except *MlfΔC1/MlfΔC1* are 3 animals. Error bars represent SEM. **(F)** Morphology and growth was visualized on a NMJ on muscle 1 using Syn (presynapse, green) and Dlg (postsynapse, red). Neuronal membrane was marked by HRP (white). **(G)** *MlfΔC1/MlfΔC1* mat. ctr. mutant animals were used for analysis, as they showed more pronounced synaptic stability defects than zygotic *MlfΔC1/MlfΔC1* mutant animals. NMJ appeared smaller compared to control. **(H)** NMJ of *Bun 200B/GE* mutant animal was undergrown compared to control. **(F-H)** Scale bars: main panels 7 μm, enlarged panels 3 μm. **(I-L)** Quantification of four morphological NMJ parameters compared to control. The variance of the absolute values of the four different measured parameters for NMJ size and morphology on muscle 1 (see Fig. 2) is displayed via box blots. Boxes display 25-75 percentile, whiskers represent 5 - 95% range, the mean is depicted by □ and the median is shown via the horizontal line crossing the box. n = 17 - 23 NMJs on muscle 1 in 6 different animals per genotype. **(I)** Quantification of number of NMJ branches. The number of NMJ branches was significantly reduced in *MlfΔC1/MlfΔC1* mat. ctr. mutant as well as *Bun 200B/GE* mutant animals compared to control animals. **(J)** Quantification of number of total synaptic boutons. The total synaptic boutons were significantly reduced in *MlfΔC1/MlfΔC1* mat. ctr. mutant and *Bun 200B/GE* mutant animals. **(K)** Quantification of total NMJ length. The total length of the NMJs was highly significantly reduced in both mutants compared to control NMJs. **(L)** Quantification of NMJ area covering muscle area. The NMJ area covering the muscle surface was not significantly altered in *MlfΔC1/MlfΔC1* mat. ctr. mutant and *Bun 200B/GE* mutant animals. Note that this parameter displayed a bigger variance for *MlfΔC1/MlfΔC1* mat. ctr. NMJs compared to other categories.

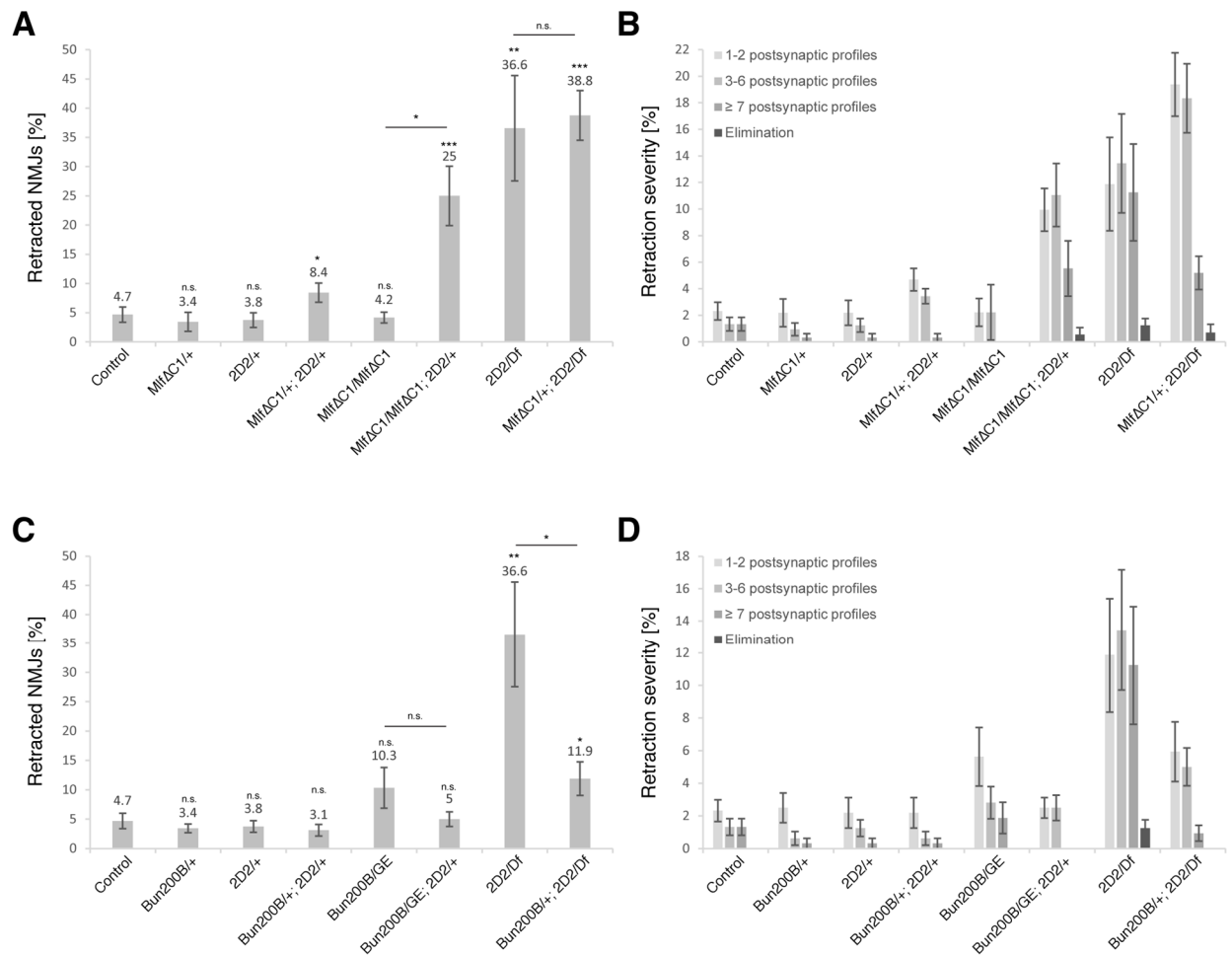


Figure 7. Mlf and BunA genetically interact with Madm to modulate synaptic stability.

The genetic interaction of Madm with Mlf or BunA was tested. Displayed are the effects on synaptic stability. **(A-B)** Quantification of synaptic retraction frequency and severity for genetic interaction of Madm and Mlf on dorsal muscles 1/9 & 2/10. Heterozygous MlfΔC1/+ as well as Madm 2D2/+ animals did not show significant increase of synaptic retraction frequency and severity. Transheterozygous MlfΔC1/+; 2D2/+ animals displayed a significant increase in synaptic instability with an almost doubled retraction frequency compared to control animals (8.4% compared to 4.7%). Zygotic MlfΔC1/MlfΔC1 mutant animals did not display significant synaptic stability defect. But the removal of one *madm* copy (2D2/+) in the zygotic MlfΔC1/MlfΔC1 mutant animals resulted in significant increase of synaptic instability (4.2% to 25%). Furthermore, the synaptic retraction severity was increased. Vice versa, the removal of one *mlf* copy (*mlf*ΔC1/+) did not increase synaptic instability of Madm 2D2/Df mutant animals. n = 10 animals of each genotype, except zygotic MlfΔC1/MlfΔC1 are 3 animals and MlfΔC1/MlfΔC1; 2D2/Df are 6 animals. Error bars represent SEM. **(C-D)** Quantification of synaptic retraction frequency and severity for genetic interaction of Madm and BunA on dorsal muscles 1/9 & 2/10. Heterozygous Bun 200B/+ and Madm 2D2/+ animals as well as transheterozygous Bun 200B/+; 2D2/+ animals did not show significant increase of synaptic retraction frequency and severity compared to control animals. Bun 200B/GE mutant animals and Bun 200B/GE; 2D2/+ animals did not display significant synaptic stability defects. But the removal of one *madm* copy in the Bun 200B/GE mutant animals reduced the synaptic retraction frequency more than half. Observed synaptic retractions were also less severe.

However, when one *bun* copy was removed in the 2D2/Df mutant animals, synaptic retraction frequency was significantly reduced. In addition, synaptic retraction severity was also reduced. n = 10 animals of each genotype. Error bars represent SEM.

3.2.8 Supplementary figures

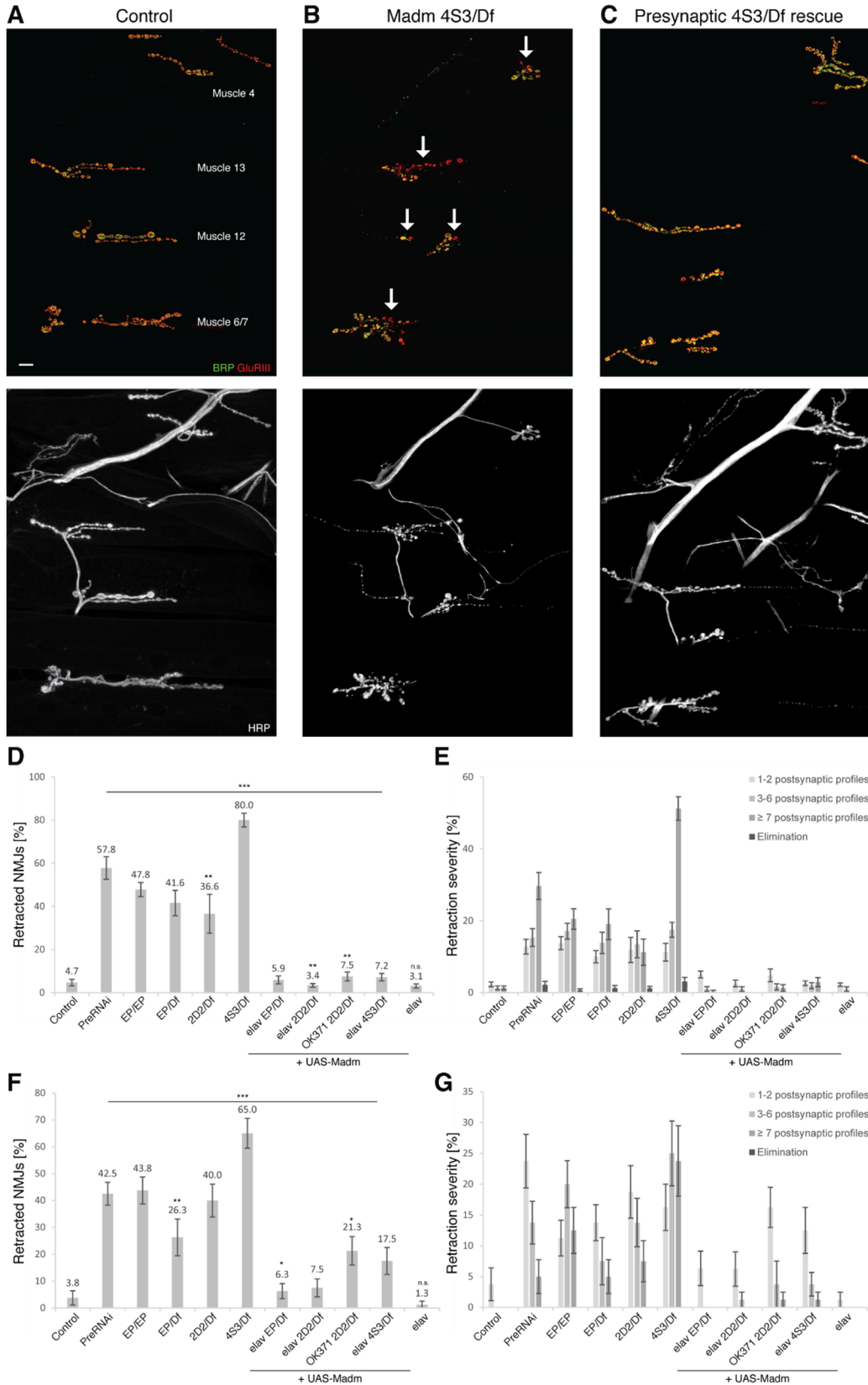


Figure S1. Synapse stability defect in *madm* mutants throughout larval segments.

(A) In control animals, ventral to middle parts of segments (m 6/7 towards m 4) are shown. No signs of synaptic instability were visible. **(B)** In *Madm* 4S3/Df mutant animals, segments were largely affected by synaptic instability (indicated by ↓). Postsynaptic profiles (GluRIII, red) were left behind by the retracting presynapse (BRP, green). Also note puncta of BRP in motoneurons and axons which were not present in control and rescue animals. **(C)** Pan-neuronal, presynaptic re-expression of *Madm* in *Madm* mutant animals resulted in higher synaptic stability throughout the segment. **(A-C)** Scale bar: 20 μm. **(D-E)** Quantification of synaptic retraction frequency and severity on dorsal muscle group 1/9 & 2/10. **(F-G)** Quantification of synaptic retraction frequency and severity on ventral muscles 6/7. **(D-G)** *Madm* 4S3/Df mutant animals displayed the highest synaptic instability among all muscles as well as the most severe synaptic retractions. Synaptic instability could be rescued upon presynaptic re-expression of *Madm* for all mutant animals. n = 10 animals of each genotype. Error bars represent SEM.

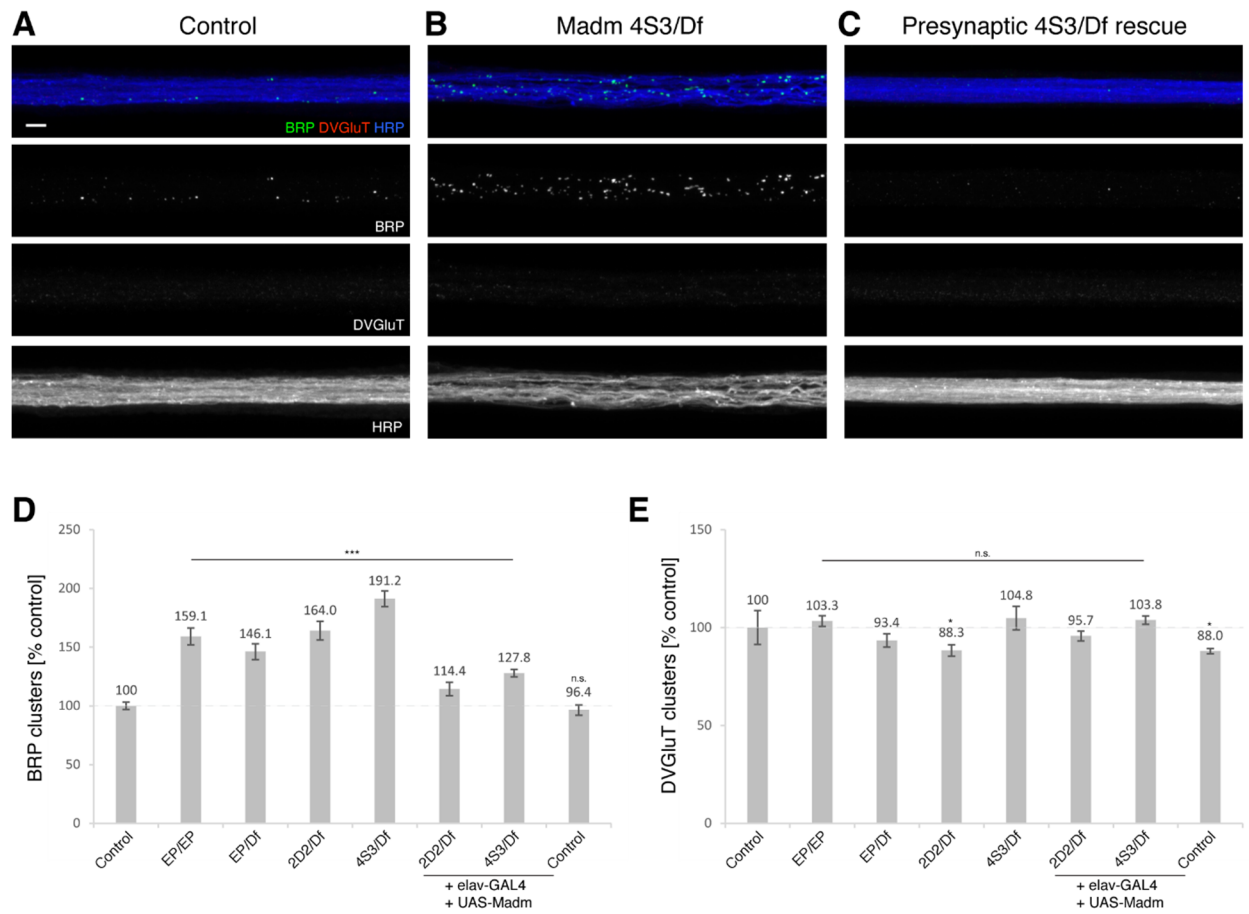


Figure S2. Accumulation of the active zone marker BRP within nerves.

(A) Nerve of control animal at height of larval segment A3. There were small BRP particles visible, but no specific DVGluT signals. **(B)** Upon Madm loss, BRP was accumulating within the nerves. There was no accumulation of DVGluT signals, which would have indicated impairment of vesicle transport along axons. **(C)** Presynaptic rescue animals did not show BRP accumulation any more. As expected, no increase in DVGluT signals was observed. **(A-C)** Scale bar: 3 μ m. **(D)** Quantification of BRP cluster intensities normalized to control. Highly significant increase was measured in all Madm mutant animals. This increase of BRP accumulations could be highly significantly rescued upon presynaptic Madm re-expression. Presynaptic Madm overexpression did not cause BRP accumulations. **(E)** Quantification of DVGluT cluster intensities normalized to control. No significant increase compared to control animals was observed in any genotype. DVGluT signals in animals with presynaptic Madm overexpression were significantly decreased. **(D-E)** n = 5 animals of each genotype. Error bars represent SEM.

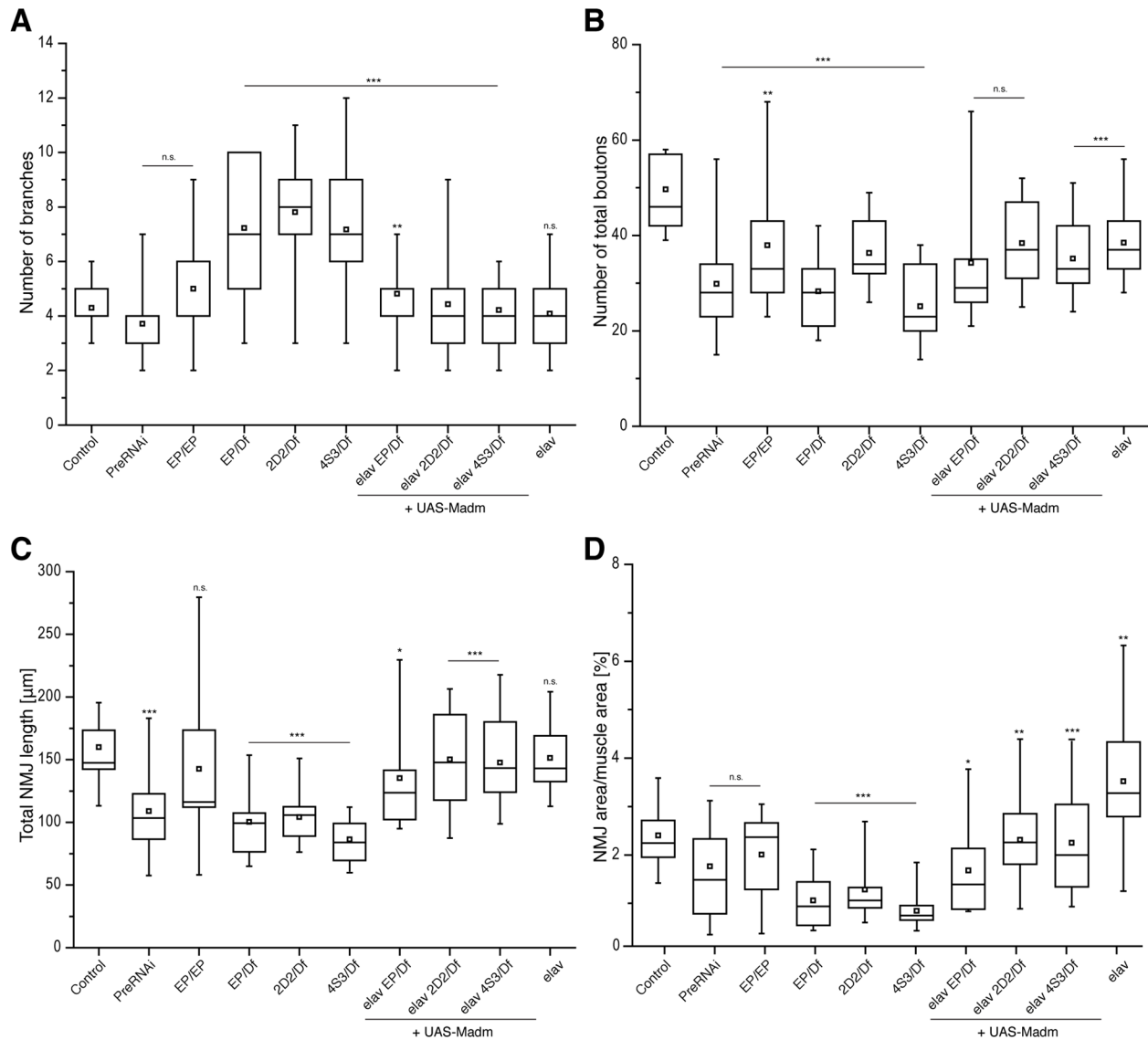


Figure S3. Variance of NMJ growth and morphology phenotypes in Madm mutant and presynaptic knockdown animals.

(A-D) The variance of the absolute values of the four different measured parameters for NMJ size and morphology on muscle 1 (see Fig. 2) is displayed via box blots. Boxes display 25-75 percentile, whiskers represent 5 - 95% range, the mean is depicted by \square and the median is shown via the horizontal line crossing the box. Note that the range of the values in the control animals is smaller and more compact than those of the Madm mutant and rescue genotypes. $n = 17 - 24$ NMJs on muscle 1 in 6 different animals per genotype. **(A)** Quantification of number of NMJ branches. **(B)** Quantification of number of total synaptic boutons. **(C)** Quantification of total NMJ length. **(D)** Quantification of NMJ area covering muscle area.

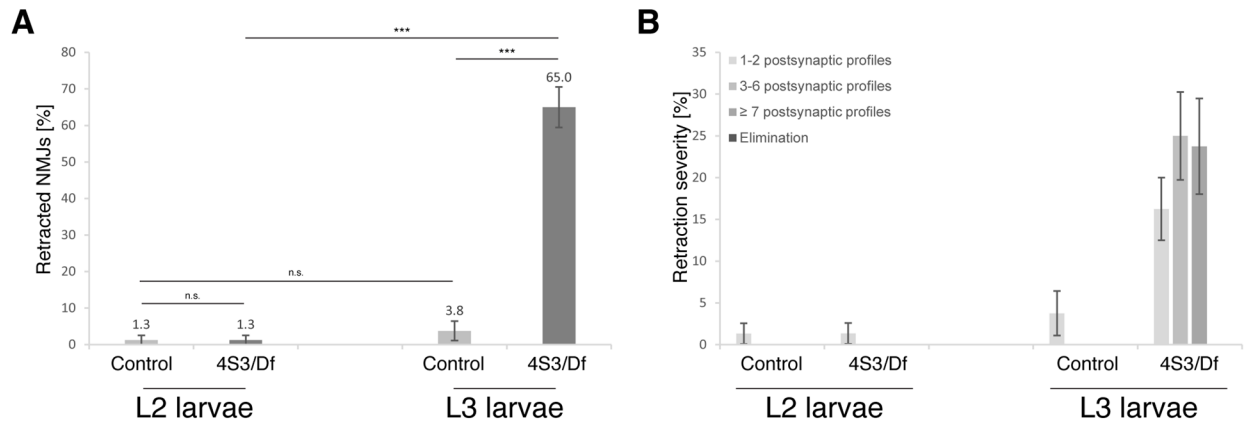
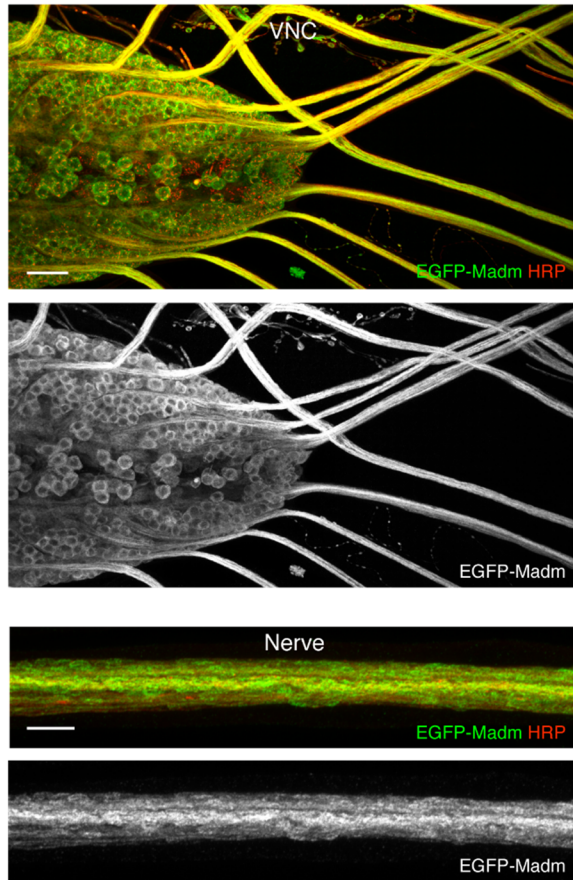


Figure S4. Madm synaptic stability and morphology phenotype manifests during 3rd instar larval stage throughout larvae.

In addition to the quantification of NMJs on muscles 1/9 & 2/10, the ventral muscles 6/7 were also monitored. Similar effects were observed. **(A-B)** Quantification of synaptic retraction frequency and severity on muscles 6/7. 3rd instar Madm 4S3/Df mutant larvae, but not 2nd instar larvae, displayed highly significant synaptic stability defects. Furthermore, 4S3/Df mutant animals at 3rd instar stage also showed most severe synaptic retractions. At 2nd instar larval stage, there was no difference between control and Madm 4S3/Df mutant animals. In control animals, synaptic instability of NMJs did not significantly increase between 2nd and 3rd instar larval stage. n = 10 animals of each genotype. Error bars represent SEM.

A Presynaptic EGFP-Madm overexpression



B Presynaptic 2D2/Df rescue with EGFP-Madm

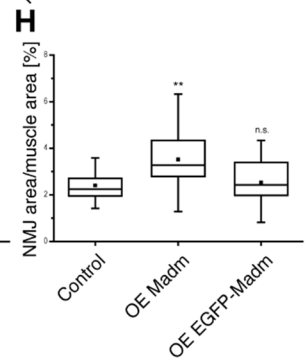
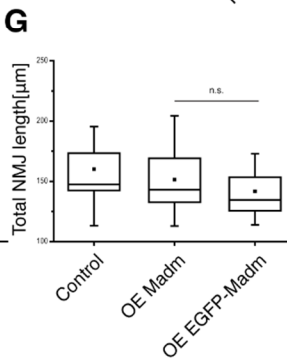
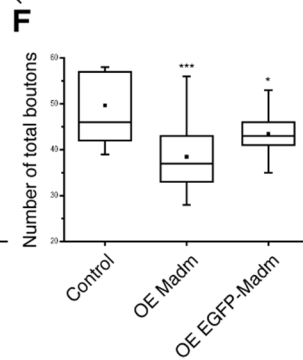
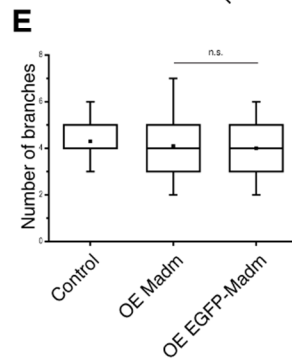
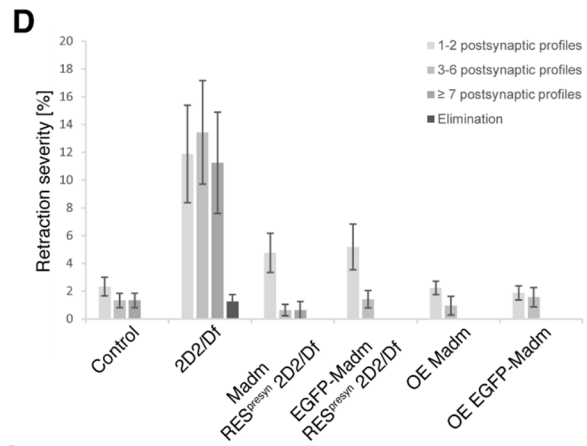
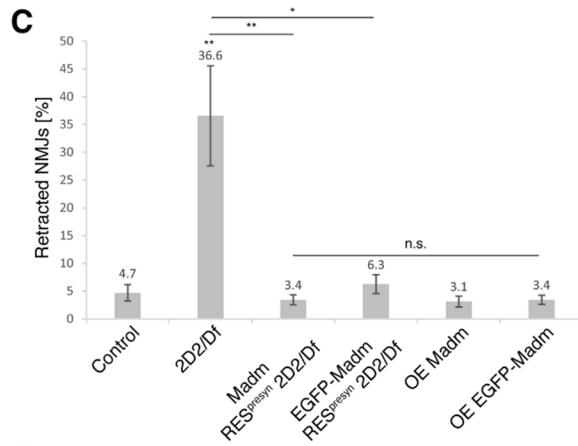
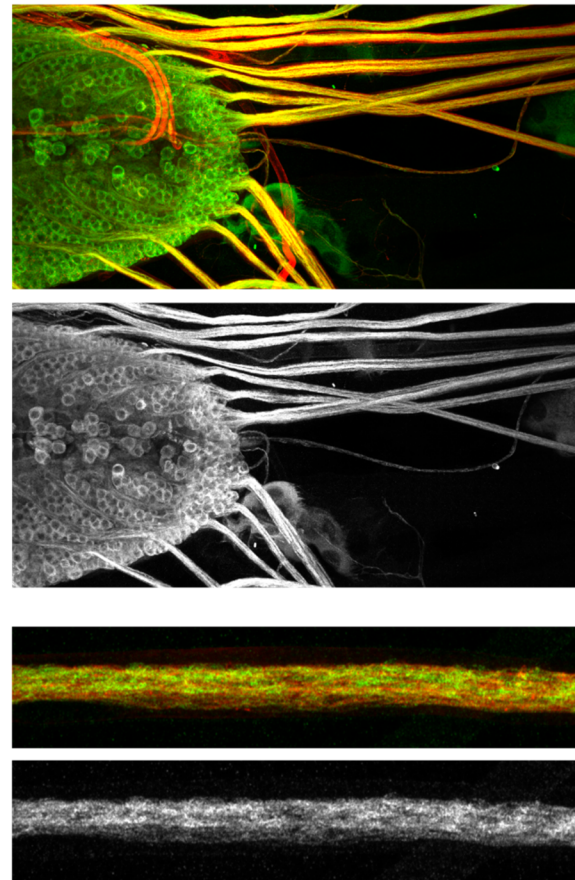


Figure S5. Cellular and subcellular Madm expression and localization.

(A-B) In animals with presynaptic EGFP-Madm expression as well as animals of the presynaptic 2D2/Df rescue, EGFP-Madm was localized at larval VNCs as well as nerves. Cell bodies of the larval brains did not show significant EGFP-Madm expression. Thus, Madm was not located within nuclei. Scale bars: VNC 20 μm , nerve 5 μm . **(C-D)** Quantification of synaptic retraction frequency and severity on muscles 1/9 & 2/10. The use of EGFP-Madm to rescue the synaptic instability observed in 2D2/Df mutant animals resulted in a significant decrease of synaptic instability. Presynaptic overexpression as well as presynaptic rescues using a UAS-Madm versus an UAS-EGFP-Madm construct behaved similarly. No significant increases of synaptic retraction frequency as well as severity compared to control were observed. $n = 10$ animals of each genotype, except EGFP-Madm $\text{RES}^{\text{presyn}}$ 2D2/Df are 7 animals. Error bars represent SEM. **(E-H)** Quantification of four morphological NMJ parameters on muscle 1 of presynaptic UAS-Madm versus UAS-EGFP-Madm overexpression experiments compared to control. Note that both overexpression genotypes showed similar morphological tendencies. Variance of values in each category is displayed by box plots. Boxes display 25-75 percentile, whiskers represent 5 - 95% range, the mean is depicted by \square and the median is shown via the horizontal line crossing the box. $n = 17 - 24$ NMJs on muscle 1 in 6 different animals per genotype. **(E)** Quantification of number of NMJ branches. **(F)** Quantification of number of total synaptic boutons. **(G)** Quantification of total NMJ length. **(H)** Quantification of NMJ area covering muscle area.

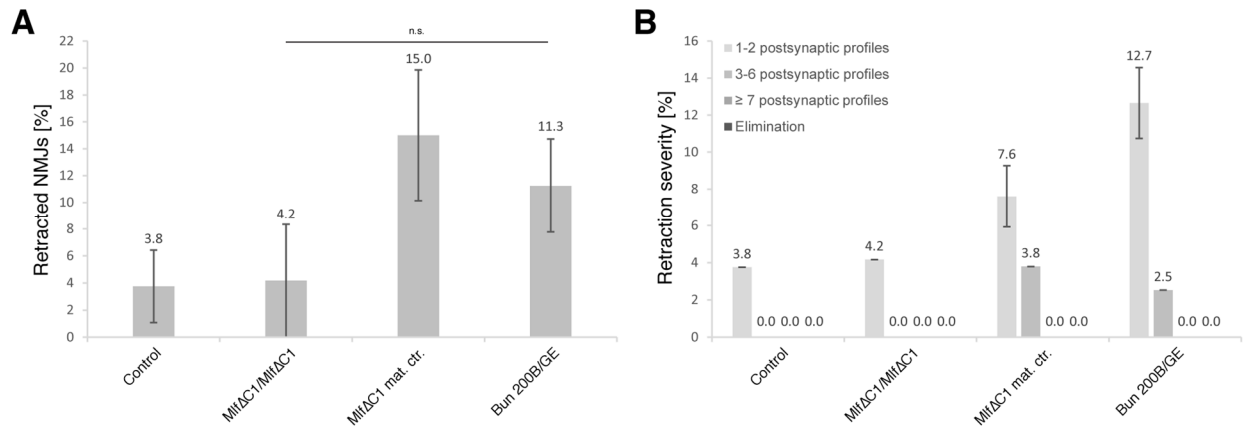


Figure S6. Mlf1 and BunA effects on synapse stability on ventral muscles 6/7.

In addition to the quantification of synaptic stability defect on muscles 1/9 & 2/10, quantifications were done for muscles 6/7. **(A-B)** Quantification of synaptic retraction frequency and severity on muscles 6/7. Synaptic retraction frequency of MlfΔC1/MlfΔC1 mutant animals was slightly higher than of control animals. As already observed for NMJs on muscles 1/9 & 2/10, MlfΔC1/MlfΔC1 mat. ctr. mutant animals, which were controlled for the maternal Mlf contribution, had a higher synaptic retraction frequency compared to zygotic MlfΔC1/MlfΔC1 mutant animals. Value was almost quadrupled (4.2% to 15.0%). In addition, their synaptic retraction severity was increased. The NMJs of Bun200B/GE mutant animals showed almost the triple synaptic retraction frequency compared to NMJs of control animals. The mutant animals displayed a tendency for synaptic stability defects, but observed synaptic retraction frequencies were not significant compared to the control animals. n = 10 animals of each genotype, except MlfΔC1/MlfΔC1 are 3 animals. Error bars represent SEM.

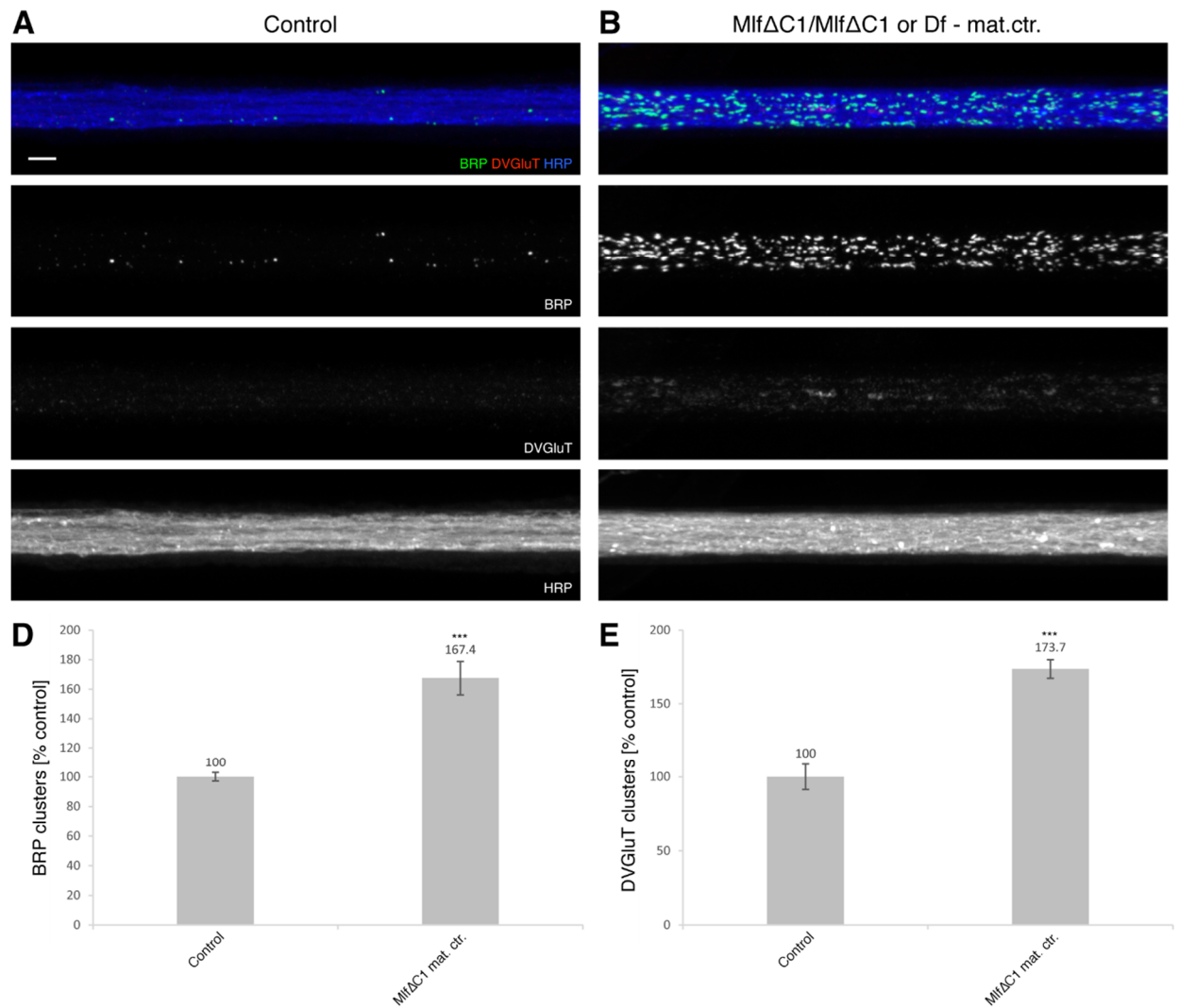


Figure S7. *Mlf* mutants have a transport defect of axonal cargos.

(A) Shown is a nerve of control animal at the height of larval segment A3. Only small BRP particles were present. No specific DVGlut signals or accumulations were visible. **(B)** Upon *Mlf* depletion, the active zone marker BRP was accumulating within the nerves. In addition, DVGlut signals accumulated, which indicated an impairment of vesicle transport along the axons. **(A-B)** Scale bar: 3 μ m. **(C)** Quantification of BRP cluster intensities normalized to control. A highly significant increase was measured in *MlfΔC1/MlfΔC1* mat. ctr. mutant animals. **(D)** Quantification of DVGlut cluster intensities normalized to control. As with BRP signals, there was also a highly significant increase in DVGlut clusters compared to control animals. Thus, the transport of cargos and vesicles along the nerves was affected. **(C-D)** $n = 5$ animals of control (45 nerves) and 7 animals of *MlfΔC1/MlfΔC1* mat. ctr. (62 nerves). Error bars represent SEM.

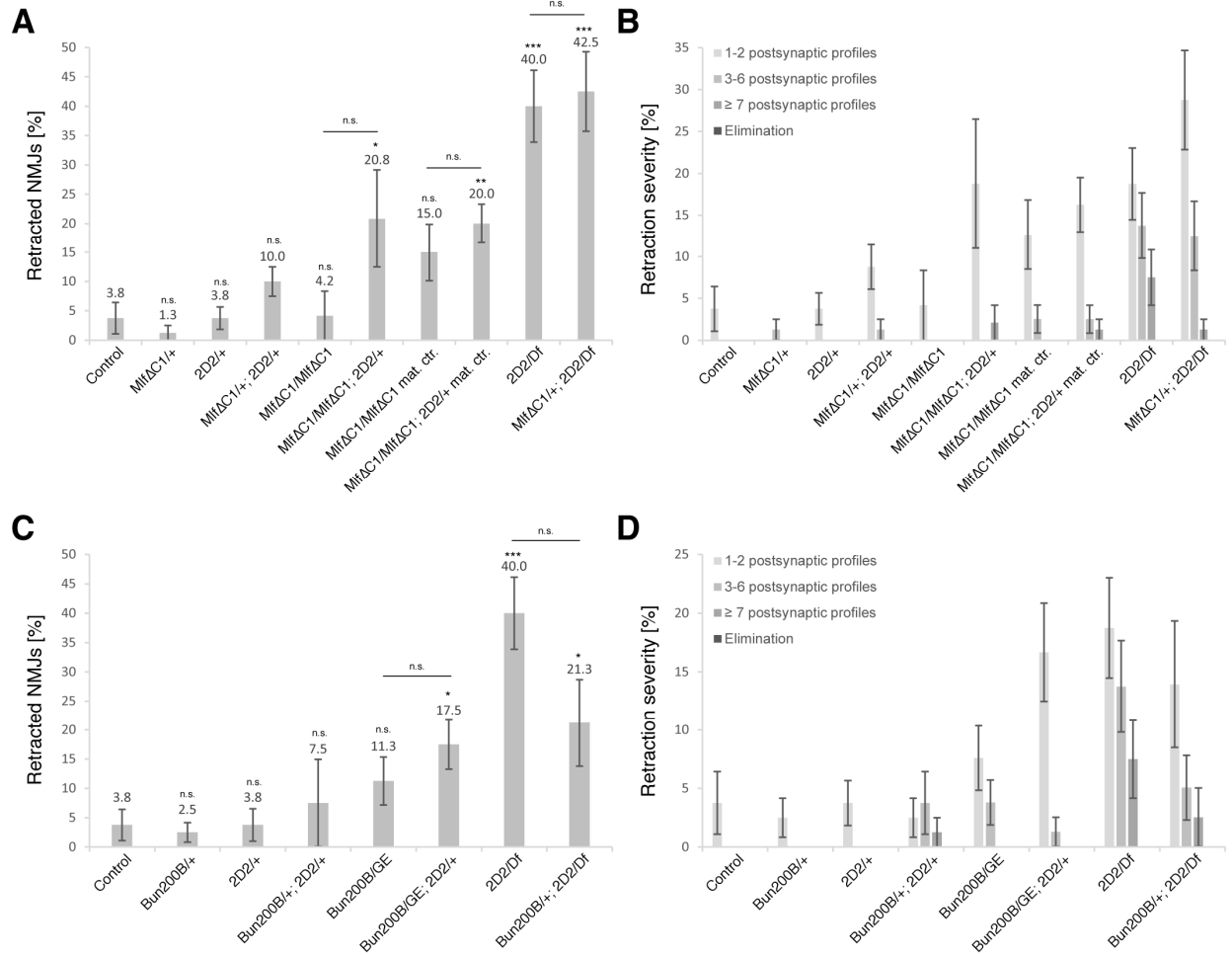


Figure S8. Effects on synaptic stability of Mlf and BunA with Madm on ventral muscles 6/7.

The genetic interaction of Madm with Mlf or BunA was tested. In addition to the quantification of synaptic stability defects on muscles 1/9 & 2/10, quantifications were done for muscles 6/7. Similar effects were observed. **(A-B)** Quantification of synaptic retraction frequency and severity for genetic interaction of Madm and Mlf on ventral muscles 6/7. Heterozygous MlfΔC1/+ and Madm 2D2/+ animals, transheterozygous MlfΔC1/+; 2D2/+ animals and zygotic MlfΔC1/MlfΔC1 mutant animals did not show significant increase of synaptic retraction frequency and severity. But the removal of one *madm* copy (2D2/+) in the zygotic MlfΔC1/MlfΔC1 mutant animals significantly increased synaptic instability compared to controls. The effect was not significant compared to zygotic MlfΔC1/MlfΔC1 mutant animals. Similarly, the removal of one *madm* copy in MlfΔC1/MlfΔC1 mat. ctr. mutant animals lacking maternal Mlf contribution resulted in a significant increase of synaptic instability compared to controls. This effect was also not significant compared to MlfΔC1/MlfΔC1 mat. ctr. mutant animals. In both cases, upon removal of one *madm* copy also the retraction severity increased. The reverse interaction, removing one *mlf* copy (*mlf*ΔC1/+) in the 2D2/Df mutant animals, led to a highly significant synaptic stability defect. This defect was not significantly increased compared to 2D2/Df mutant animals. n = 10 animals of each genotype, except zygotic MlfΔC1/MlfΔC1 are 3 animals and MlfΔC1/MlfΔC1; 2D2/+ are 6 animals. Error bars represent SEM. **(C-D)** Quantification of synaptic retraction frequency and severity for genetic interaction of Madm and BunA on ventral muscles 6/7. Heterozygous Bun 200B/+ and Madm 2D2/+ animals as well as transheterozygous

Bun 200B/+; 2D2/+ animals did not show significant increase of synaptic retraction frequency and severity compared to control animals. But synaptic retraction frequency of transheterozygous Bun 200B/+; 2D2/+ animals was almost doubled compared to control animals. Synaptic retraction severity was increased. In Bun 200B/GE mutant animals, synaptic retraction frequency was almost tripled compared to control animals, but not significantly altered. The removal of one *madm* copy (2D2/+) in the Bun 200B/GE mutant animals resulted in significantly increased synaptic stability defects. Synaptic retraction severity was not increased. The observed synaptic stability defect was not significant comparing Bun 200B/GE to Bun 200B/GE; 2D2/+ mutant animals. However, the removal of one *bun* copy (*bun 200B/+*) in the *Madm 2D2/Df* mutant animals clearly reduced synaptic instability, although not significantly. n = 10 animals of each genotype. Error bars represent SEM.

3.2.9 Material and Methods

3.2.9.1 Fly stocks

All fly stocks were maintained on standard fly food. All crosses were performed at 25°C, except the Madm RNAi crosses were raised at 29°C. Crosses for the RNAi-based genetic screens were set up at 27°C. Fly strains used in this study: w1118 (as wild-type) - crossed to Gal4-driver lines as controls, *elav^{C155}-Gal4*, *OK371-Gal4*, *REPO-Gal4*, *UAS-CD8GFP*, *Madm Df(3R)Exel7283*, *P(EP).madm^{EP3137}*, *Mlf Df(2R)BSC482*, *Mlf Df(2R)Exel7138* (all Bloomington *Drosophila* Stock Center), *madm^{2D2}*, *madm^{4S3}*, *UAS-Madm* (all (Gluderer et al., 2010)), *bun^{200B}*, *bun^{GE12327}* (all (Gluderer et al., 2008)), and *mJfΔC1* (Martin-Lannere et al., 2006). RNAi lines were obtained from the VDRC Vienna *Drosophila* RNAi Center. Madm RNAi: transformant ID 101758 with 0 off targets.

3.2.9.2 Generation of UAS-EGFP-Madm construct and transgenes

The full length Madm ORF was amplified from cDNA LD28657 obtained from the *Drosophila* Genomic Research Center (Indiana, USA) using the following primers: 5'-CACCATGTCAAATAGCCAAGCGAATG-3' and 5'-TCAATTGCTCGTCGTGCC-3'. The ORF was cloned into pENTR using TOPO cloning (Invitrogen). Then it was shuffled into the pUASattB-10xUAS destination vector with N-terminal EGFP tag (Enneking et al., 2013). Constructs were verified via sequencing (FMI sequencing facility) and subsequently injected into attP40 genomic landing site (BestGene Inc, California, USA).

3.2.9.3 Generation of Madm antibody

The full length Madm ORF was amplified from cDNA LD28657 obtained from the *Drosophila* Genomic Research Center (Indiana, USA). N-terminal 6xHis-tagged full-length Madm constructs were generated using the Gateway system (pDEST17 vector) (Invitrogen). As the protein was insoluble, further purification was performed under denaturing conditions using SpinTrap Columns (GE Healthcare). Polyclonal rabbit anti-Madm antibodies were generated and purified

by David's Biotechnologie (Regensburg, Germany). Presera of rabbits were checked before immunization.

3.2.9.4 Western blot

Larval brains were dissected in standard dissection saline with protease inhibitor added. Isolated larval brains were transferred into 20 µl of a NP40-based lysis buffer with protease inhibitor, mashed using a pipette tip and incubated on ice for 30 min. Samples were spun down for 10 min, 13,000 rpm, 4°C. Supernatant was recovered into fresh tube and mixed with the same volume of 2x sample buffer (Invitrogen). Samples were denatured for 10 min at 95°C. They were spun down again briefly before loading for analysis on NuPage gels (Invitrogen) according to standard procedures. Subsequently, protein was transferred to Invitrolon PVDF membranes (Invitrogen) again following standard procedures. After blocking, membranes were incubated with primary rabbit anti-Madm (1:500; generated by David's Biotechnologie (Regensburg, Germany) & ourselves) or mouse anti-Tubulin (1:1,000; Developmental Studies Hybridoma Bank) antibody at 4°C overnight. Incubation with secondary HRP-conjugated anti-rabbit or anti-mouse antibodies (Jackson ImmunoResearch), used at 1:10,000, was done for 2 h at RT. Protein was detected by chemiluminescence using ECL substrate (SuperSignal West Pico Kit, Thermo Scientific) and film (Fujifilm).

3.2.9.5 Larval dissections and immunohistochemistry

Standard body wall muscle preparations were performed. Wandering third instar larvae were dissected in cold standard dissection saline. Preparations were subsequently fixed for 3 min with Bouin's fixative (Sigma-Aldrich). Larval fillets were washed in standard PBST buffer. Primary antibodies were incubated overnight at 4°C. The following primary antibodies were used at the given concentrations: anti-Bruchpilot (nc82) 1:250, anti-Synapsin (3c11) 1:100, anti-Futsch (22c10) 1:500 (all obtained from Developmental Studies Hybridoma Bank), rabbit anti-Dlg 1:20,000, rabbit anti-GluRIII 1:2,000 (Pielage et al., 2011), rabbit anti-DVGlut 1:20,000, rabbit anti-GFP 1:1,000 (Invitrogen) and rabbit anti-Madm 1:500 (generated by David's Biotechnologie (Regensburg, Germany) & ourselves). During incubation with primary antibodies, neuronal

membranes were stained with anti-HRP directly conjugated with Alexa or Cy-dye used at 1:250 or 1:400. Larval preparations were washed again with PBST to remove unbound or excess antibody. Subsequently, the dissected larvae were incubated with Alexa-conjugated secondary antibodies (Invitrogen) diluted 1:1,000 for 2 h at room temperature. Again preparations were washed with PBST. Finally, larval preparations were mounted using Prolong Gold (Invitrogen). Mounting media was allowed to harden at least for 3 days before subsequent analysis. Images of dissected larvae were taken at room temperature with a Leica SPE or a Zeiss LSM700 confocal microscope.

3.2.9.6 Image acquisition

Images of dissected larvae were taken at room temperature with a Leica SPE or a Zeiss LSM700 confocal microscope. All images were no other adjusted than for brightness, contrast or levels using Imaris (Bitplane) and Adobe Photoshop.

3.2.9.7 Quantification of phenotypes

Synapse stability defect

Synapse stability was analyzed for 10 animals of each genotype (unless otherwise indicated) stained with presynaptic BRP, postsynaptic GluRIII and HRP (neuronal membranes). Different muscles or muscle groups (muscles 1/9 & 2/10 and muscles 6/7) were analyzed for stability defects from abdominal segments A3 to A6. Severity of synaptic retractions was classified by counting individual synaptic boutons missing presynaptic BRP signal. Classification of severity based on destabilized boutons was: 1-2 synaptic boutons, 3-6 synaptic boutons, ≥ 7 synaptic boutons as well as additional category of total elimination (can fall into the three previous categories on top - depending on number of synaptic boutons at this NMJ). Subsequent analysis see *Statistical analysis*.

Synapse morphology and growth

Larvae were stained with presynaptic Syn, postsynaptic Dlg and HRP (neuronal membranes). 6 animals of each genotype were imaged using the LIC macroLib Zen2012 (Life Imaging Center,

Freiburg, Germany) at a Zeiss LSM700 confocal microscope. Overview images of animals on slide were obtained for navigation. Subsequently, tile scans of muscles were obtained for later muscle dimension quantification. Muscle tiles were stitched together using XUV Tools Profiles and custom-written Fiji (ImageJ) applications. NMJs (muscle 1 or muscles 6/7) were imaged in abdominal segments A3 and A4 which show smallest growth variance in control. Muscle dimensions as well as different NMJ parameters were subsequently measured by hand. Values were extracted using a custom-written Fiji macro. Data of muscles and NMJs was combined using a custom-written MATLAB (The MathWorks) application and Microsoft Office Excel. Additional NMJ parameter “NMJ area” was calculated using MATLAB. Subsequent analysis see *Statistical analysis*.

Transport defect

Larval preparations were stained with presynaptic BRP and DVGluT as well as HRP (neuronal membranes). Confocal images were taken of motoneuron axons of 5 animals at the height of abdominal segment A3 to A4. A custom-written Fiji application was then used to measure BRP and DVGluT puncta intensities (Enneking et al., 2013). Subsequent analysis see *Statistical analysis*.

Nerve varicosity phenotype

HRP images of VNC and nerves of 6 animals (unless otherwise indicated) were obtained. Varicosities of nerves were then counted. Subsequent analysis see *Statistical analysis*.

3.2.9.8 Statistical analysis

Statistical analyses were performed using Microsoft Office Excel combined with an online source for unpaired Student's *t* test (<http://studentsttest.com>) (homoscedastic two-tailed Student's *t* test with equal variances). P-values for the different measured phenotypical categories and genotypes are given in supplementary tables. Significance levels were defined as following: *** $p \leq 0.001$, ** $p \leq 0.01$; * $p \leq 0.05$ and n.s. (not significant) $p > 0.05$. Madm, Mlf or BunA mutant allelic combination as well as protein overexpression experiments were always compared to the

control. Rescues were compared to the corresponding mutant condition. Exceptions would be indicated especially. Graphs were created using Microsoft Office Excel, box plots were drawn with Origin (OriginLab).

3.2.10 Abbreviations

ALS, amyotrophic lateral sclerosis; AML, acute myeloid leukemia; BMP, bone morphogenetic protein; BRP, Bruchpilot; BunA, Bunched A; Cdk, Cyclin-dependent kinase; CML, chronic myeloid leukemia; Df, deficiency; Dip, DSIP-immunoreactive peptide; Dlg, Disc-large; DVGluT, *Drosophila* vesicular glutamate transporter; EGFP, enhanced green fluorescent protein; EGFR, epidermal growth factor receptor; ESCRT machinery, endosomal sorting complexes required for transport machinery; FOXO, Forkhead box class 'O'; GAP, GTPase-activating proteins; Gbb, Glass bottom boat; GLuRIII, glutamate receptors subunit III; HD, Huntington's disease; HRP, horseradish peroxidase; HSP, hereditary spastic paraplegia; JAK-STAT, Janus kinases & signal transducers and activators of transcription; Khc, Kinesin heavy chain; m, muscle; Madm, Mlf1 adapter molecule; MAP1B, microtubule-associated protein 1B; MDS, myelodysplastic syndrome; Mlf, myeloid leukemia factor; MS, multiple sclerosis; mTOR, mammalian target of rapamycin; NF- κ B, nuclear factor 'kappa-light-chain-enhancer' of activated B-cells; NMJ, neuromuscular junction; NPM/B23, Nucleophosmin; PI3K, phosphatidylinositol 3-kinase; PTEN, phosphatase and tensin homolog; Ras, rat sarcoma; Rheb, Ras homolog enriched in brain; RNAi, ribonucleic acid (RNA) interference; S6K, S6 kinase; Sax, Saxophone; SEM, standard error of mean; SMA, spinal muscular atrophy; Syn, Synapsin; TCTP, translationally controlled tumor protein; Tkv, Thick veins; TORC1 and 2, TOR complex 1 and 2; TSC1 and 2, tuberous sclerosis complex 1 and 2; TSC-22, transforming growth factor- β -stimulated clone 22; Wit, Wishful thinking; Wnt, Wingless & Int-1; DREF, DNA replication related element binding factor;

3.2.11 References

Baines, R.A. (2004). Synaptic strengthening mediated by bone morphogenetic protein-dependent retrograde signaling in the *Drosophila* CNS. *The Journal of neuroscience : the official journal of the Society for Neuroscience* 24, 6904-6911.

- Bard, F., Casano, L., Mallabiabarrena, A., Wallace, E., Saito, K., Kitayama, H., Guizzunti, G., Hu, Y., Wendler, F., Dasgupta, R., *et al.* (2006). Functional genomics reveals genes involved in protein secretion and Golgi organization. *Nature* *439*, 604-607.
- Bayat, V., Jaiswal, M., and Bellen, H.J. (2011). The BMP signaling pathway at the *Drosophila* neuromuscular junction and its links to neurodegenerative diseases. *Current opinion in neurobiology* *21*, 182-188.
- Berger, C., Renner, S., Luer, K., and Technau, G.M. (2007). The commonly used marker ELAV is transiently expressed in neuroblasts and glial cells in the *Drosophila* embryonic CNS. *Developmental dynamics : an official publication of the American Association of Anatomists* *236*, 3562-3568.
- Bras, S., Martin-Lannere, S., Gobert, V., Auge, B., Breig, O., Sanial, M., Yamaguchi, M., Haenlin, M., Plessis, A., and Waltzer, L. (2012). Myeloid leukemia factor is a conserved regulator of RUNX transcription factor activity involved in hematopoiesis. *Proceedings of the National Academy of Sciences of the United States of America* *109*, 4986-4991.
- Brink, D.L., Gilbert, M., Xie, X., Petley-Ragan, L., and Auld, V.J. (2012). Glial processes at the *Drosophila* larval neuromuscular junction match synaptic growth. *PLoS one* *7*, e37876.
- Brunner, E., Ahrens, C.H., Mohanty, S., Baetschmann, H., Loevenich, S., Potthast, F., Deutsch, E.W., Panse, C., de Lichtenberg, U., Rinner, O., *et al.* (2007). A high-quality catalog of the *Drosophila melanogaster* proteome. *Nature biotechnology* *25*, 576-583.
- Bulat, V., Rast, M., and Pielage, J. (2014). Presynaptic CK2 promotes synapse organization and stability by targeting Ankyrin2. *The Journal of cell biology* *204*, 77-94.
- Cheng, L., Locke, C., and Davis, G.W. (2011). S6 kinase localizes to the presynaptic active zone and functions with PDK1 to control synapse development. *The Journal of cell biology* *194*, 921-935.
- Coleman, M. (2005). Axon degeneration mechanisms: commonality amid diversity. *Nature reviews Neuroscience* *6*, 889-898.
- Collins, C.A., and DiAntonio, A. (2007). Synaptic development: insights from *Drosophila*. *Current opinion in neurobiology* *17*, 35-42.
- De Langhe, S., Haataja, L., Senadheera, D., Groffen, J., and Heisterkamp, N. (2002). Interaction of the small GTPase Rac3 with NRBP, a protein with a kinase-homology domain. *International journal of molecular medicine* *9*, 451-459.
- De Vos, K.J., Grierson, A.J., Ackerley, S., and Miller, C.C. (2008). Role of axonal transport in neurodegenerative diseases. *Annual review of neuroscience* *31*, 151-173.
- Dimitroff, B., Howe, K., Watson, A., Campion, B., Lee, H.G., Zhao, N., O'Connor, M.B., Neufeld, T.P., and Selleck, S.B. (2012). Diet and energy-sensing inputs affect TorC1-mediated axon misrouting but not TorC2-directed synapse growth in a *Drosophila* model of tuberous sclerosis. *PLoS one* *7*, e30722.
- Dobens, L.L., Hsu, T., Twombly, V., Gelbart, W.M., Raftery, L.A., and Kafatos, F.C. (1997). The *Drosophila* bunched gene is a homologue of the growth factor stimulated mammalian TSC-22 sequence and is required during oogenesis. *Mechanisms of development* *65*, 197-208.
- Dobens, L.L., Peterson, J.S., Treisman, J., and Raftery, L.A. (2000). *Drosophila* bunched integrates opposing DPP and EGF signals to set the operculum boundary. *Development* *127*, 745-754.
- Eaton, B.A., and Davis, G.W. (2005). LIM Kinase1 controls synaptic stability downstream of the type II BMP receptor. *Neuron* *47*, 695-708.
- Eaton, B.A., Fetter, R.D., and Davis, G.W. (2002). Dynactin is necessary for synapse stabilization. *Neuron* *34*, 729-741.
- Enneking, E.M., Kudumala, S.R., Moreno, E., Stephan, R., Boerner, J., Godenschwege, T.A., and Pielage, J. (2013). Transsynaptic coordination of synaptic growth, function, and stability by the L1-type CAM Neuroglian. *PLoS biology* *11*, e1001537.
- Featherstone, D.E., and Broadie, K. (2000). Surprises from *Drosophila*: genetic mechanisms of synaptic development and plasticity. *Brain research bulletin* *53*, 501-511.

- Fouix, S., Martin-Lannere, S., Sanial, M., Morla, L., Lamour-Isnard, C., and Plessis, A. (2003). Over-expression of a novel nuclear interactor of Suppressor of fused, the *Drosophila* myelodysplasia/myeloid leukaemia factor, induces abnormal morphogenesis associated with increased apoptosis and DNA synthesis. *Genes to cells : devoted to molecular & cellular mechanisms* 8, 897-911.
- Fuentes-Medel, Y., Ashley, J., Barria, R., Maloney, R., Freeman, M., and Budnik, V. (2012). Integration of a retrograde signal during synapse formation by glia-secreted TGF-beta ligand. *Current biology : CB* 22, 1831-1838.
- Fuentes-Medel, Y., Logan, M.A., Ashley, J., Ataman, B., Budnik, V., and Freeman, M.R. (2009). Glia and muscle sculpt neuromuscular arbors by engulfing destabilized synaptic boutons and shed presynaptic debris. *PLoS biology* 7, e1000184.
- Fuger, P., Sreekumar, V., Schule, R., Kern, J.V., Stanchev, D.T., Schneider, C.D., Karle, K.N., Daub, K.J., Siegert, V.K., Flotenmeyer, M., *et al.* (2012). Spastic paraplegia mutation N256S in the neuronal microtubule motor KIF5A disrupts axonal transport in a *Drosophila* HSP model. *PLoS genetics* 8, e1003066.
- Gluderer, S., Brunner, E., Germann, M., Jovaisaite, V., Li, C., Rentsch, C.A., Hafen, E., and Stocker, H. (2010). Madm (Mlf1 adapter molecule) cooperates with Bunched A to promote growth in *Drosophila*. *Journal of biology* 9, 9.
- Gluderer, S., Oldham, S., Rintelen, F., Sulzer, A., Schutt, C., Wu, X., Raftery, L.A., Hafen, E., and Stocker, H. (2008). Bunched, the *Drosophila* homolog of the mammalian tumor suppressor TSC-22, promotes cellular growth. *BMC developmental biology* 8, 10.
- Goda, Y., and Davis, G.W. (2003). Mechanisms of synapse assembly and disassembly. *Neuron* 40, 243-264.
- Goold, C.P., and Davis, G.W. (2007). The BMP ligand Gbb gates the expression of synaptic homeostasis independent of synaptic growth control. *Neuron* 56, 109-123.
- Hirose, F., Yamaguchi, M., Handa, H., Inomata, Y., and Matsukage, A. (1993). Novel 8-base pair sequence (*Drosophila* DNA replication-related element) and specific binding factor involved in the expression of *Drosophila* genes for DNA polymerase alpha and proliferating cell nuclear antigen. *The Journal of biological chemistry* 268, 2092-2099.
- Hooper, J.D., Baker, E., Ogbourne, S.M., Sutherland, G.R., and Antalis, T.M. (2000). Cloning of the cDNA and localization of the gene encoding human NRBP, a ubiquitously expressed, multidomain putative adapter protein. *Genomics* 66, 113-118.
- Hsu, Y.C., Chern, J.J., Cai, Y., Liu, M., and Choi, K.W. (2007). *Drosophila* TCTP is essential for growth and proliferation through regulation of dRheb GTPase. *Nature* 445, 785-788.
- Jia, X.X., Gorczyca, M., and Budnik, V. (1993). Ultrastructure of neuromuscular junctions in *Drosophila*: comparison of wild type and mutants with increased excitability. *Journal of neurobiology* 24, 1025-1044.
- Jontes, J.D., and Phillips, G.R. (2006). Selective stabilization and synaptic specificity: a new cell-biological model. *Trends in neurosciences* 29, 186-191.
- Kania, A., Salzberg, A., Bhat, M., D'Evelyn, D., He, Y., Kiss, I., and Bellen, H.J. (1995). P-element mutations affecting embryonic peripheral nervous system development in *Drosophila melanogaster*. *Genetics* 139, 1663-1678.
- Kawamata, H., Nakashiro, K., Uchida, D., Hino, S., Omotehara, F., Yoshida, H., and Sato, M. (1998). Induction of TSC-22 by treatment with a new anti-cancer drug, vesnarinone, in a human salivary gland cancer cell. *British journal of cancer* 77, 71-78.
- Kazemi-Esfarjani, P., and Benzer, S. (2002). Suppression of polyglutamine toxicity by a *Drosophila* homolog of myeloid leukemia factor 1. *Human molecular genetics* 11, 2657-2672.
- Killip, L.E., and Grewal, S.S. (2012). DREF is required for cell and organismal growth in *Drosophila* and functions downstream of the nutrition/TOR pathway. *Developmental biology* 371, 191-202.

- Kim, J., Lee, S., Hwang, M., Ko, S., Min, C., and Kim-Ha, J. (2009). Bunched specifically regulates alpha/beta mushroom body neuronal cell proliferation during metamorphosis. *Neuroscience* 161, 46-52.
- Koch, I., Schwarz, H., Beuchle, D., Goellner, B., Langegger, M., and Aberle, H. (2008). Drosophila ankyrin 2 is required for synaptic stability. *Neuron* 58, 210-222.
- Lim, R., Winteringham, L.N., Williams, J.H., McCulloch, R.K., Ingley, E., Tiao, J.Y., Lalonde, J.P., Tsai, S., Tilbrook, P.A., Sun, Y., *et al.* (2002). MADM, a novel adaptor protein that mediates phosphorylation of the 14-3-3 binding site of myeloid leukemia factor 1. *The Journal of biological chemistry* 277, 40997-41008.
- Martin-Lannere, S., Lasbleiz, C., Sanial, M., Fouix, S., Besse, F., Tricoire, H., and Plessis, A. (2006). Characterization of the Drosophila myeloid leukemia factor. *Genes to cells : devoted to molecular & cellular mechanisms* 11, 1317-1335.
- Martin-Pena, A., Acebes, A., Rodriguez, J.R., Sorribes, A., de Polavieja, G.G., Fernandez-Funez, P., and Ferrus, A. (2006). Age-independent synaptogenesis by phosphoinositide 3 kinase. *The Journal of neuroscience : the official journal of the Society for Neuroscience* 26, 10199-10208.
- McCabe, B.D., Marques, G., Haghghi, A.P., Fetter, R.D., Crotty, M.L., Haerry, T.E., Goodman, C.S., and O'Connor, M.B. (2003). The BMP homolog Gbb provides a retrograde signal that regulates synaptic growth at the Drosophila neuromuscular junction. *Neuron* 39, 241-254.
- Menon, K.P., Carrillo, R.A., and Zinn, K. (2013). Development and plasticity of the Drosophila larval neuromuscular junction. *Wiley interdisciplinary reviews Developmental biology* 2, 647-670.
- Natarajan, R., Trivedi-Vyas, D., and Wairkar, Y.P. (2013). Tuberous sclerosis complex regulates Drosophila neuromuscular junction growth via the TORC2/Akt pathway. *Human molecular genetics* 22, 2010-2023.
- Ohno, K., Takahashi, Y., Hirose, F., Inoue, Y.H., Taguchi, O., Nishida, Y., Matsukage, A., and Yamaguchi, M. (2000). Characterization of a Drosophila homologue of the human myelodysplasia/myeloid leukemia factor (MLF). *Gene* 260, 133-143.
- Omotehara, F., Uchida, D., Hino, S., Begum, N.M., Yoshida, H., Sato, M., and Kawamata, H. (2000). In vivo enhancement of chemosensitivity of human salivary gland cancer cells by overexpression of TGF-beta stimulated clone-22. *Oncology reports* 7, 737-740.
- Pielage, J., Bulat, V., Zuchero, J.B., Fetter, R.D., and Davis, G.W. (2011). Hts/Adducin controls synaptic elaboration and elimination. *Neuron* 69, 1114-1131.
- Pielage, J., Cheng, L., Fetter, R.D., Carlton, P.M., Sedat, J.W., and Davis, G.W. (2008). A presynaptic giant ankyrin stabilizes the NMJ through regulation of presynaptic microtubules and transsynaptic cell adhesion. *Neuron* 58, 195-209.
- Pielage, J., Fetter, R.D., and Davis, G.W. (2005). Presynaptic spectrin is essential for synapse stabilization. *Current biology : CB* 15, 918-928.
- Rawson, J.M., Lee, M., Kennedy, E.L., and Selleck, S.B. (2003). Drosophila neuromuscular synapse assembly and function require the TGF-beta type I receptor saxophone and the transcription factor Mad. *Journal of neurobiology* 55, 134-150.
- Saucedo, L.J., Gao, X., Chiarelli, D.A., Li, L., Pan, D., and Edgar, B.A. (2003). Rheb promotes cell growth as a component of the insulin/TOR signalling network. *Nature cell biology* 5, 566-571.
- Sawado, T., Hirose, F., Takahashi, Y., Sasaki, T., Shinomiya, T., Sakaguchi, K., Matsukage, A., and Yamaguchi, M. (1998). The DNA replication-related element (DRE)/DRE-binding factor system is a transcriptional regulator of the Drosophila E2F gene. *The Journal of biological chemistry* 273, 26042-26051.
- Schmidt, I., Thomas, S., Kain, P., Risse, B., Naffin, E., and Klambt, C. (2012). Kinesin heavy chain function in Drosophila glial cells controls neuronal activity. *The Journal of neuroscience : the official journal of the Society for Neuroscience* 32, 7466-7476.

- Sepp, K.J., Schulte, J., and Auld, V.J. (2000). Developmental dynamics of peripheral glia in *Drosophila melanogaster*. *Glia* 30, 122-133.
- Stocker, H., Radimerski, T., Schindelholz, B., Wittwer, F., Belawat, P., Daram, P., Breuer, S., Thomas, G., and Hafen, E. (2003). Rheb is an essential regulator of S6K in controlling cell growth in *Drosophila*. *Nature cell biology* 5, 559-565.
- Takahashi, Y., Yamaguchi, M., Hirose, F., Cotterill, S., Kobayashi, J., Miyajima, S., and Matsukage, A. (1996). DNA replication-related elements cooperate to enhance promoter activity of the *Drosophila* DNA polymerase alpha 73-kDa subunit gene. *The Journal of biological chemistry* 271, 14541-14547.
- Tee, A.R., Manning, B.D., Roux, P.P., Cantley, L.C., and Blenis, J. (2003). Tuberous sclerosis complex gene products, Tuberin and Hamartin, control mTOR signaling by acting as a GTPase-activating protein complex toward Rheb. *Current biology : CB* 13, 1259-1268.
- Treisman, J.E., Lai, Z.C., and Rubin, G.M. (1995). Short sighted acts in the decapentaplegic pathway in *Drosophila* eye development and has homology to a mouse TGF-beta-responsive gene. *Development* 121, 2835-2845.
- Uchida, D., Kawamata, H., Omotehara, F., Miwa, Y., Hino, S., Begum, N.M., Yoshida, H., and Sato, M. (2000). Over-expression of TSC-22 (TGF-beta stimulated clone-22) markedly enhances 5-fluorouracil-induced apoptosis in a human salivary gland cancer cell line. *Laboratory investigation; a journal of technical methods and pathology* 80, 955-963.
- Yoneda-Kato, N., Look, A.T., Kirstein, M.N., Valentine, M.B., Raimondi, S.C., Cohen, K.J., Carroll, A.J., and Morris, S.W. (1996). The t(3;5)(q25.1;q34) of myelodysplastic syndrome and acute myeloid leukemia produces a novel fusion gene, NPM-MLF1. *Oncogene* 12, 265-275.

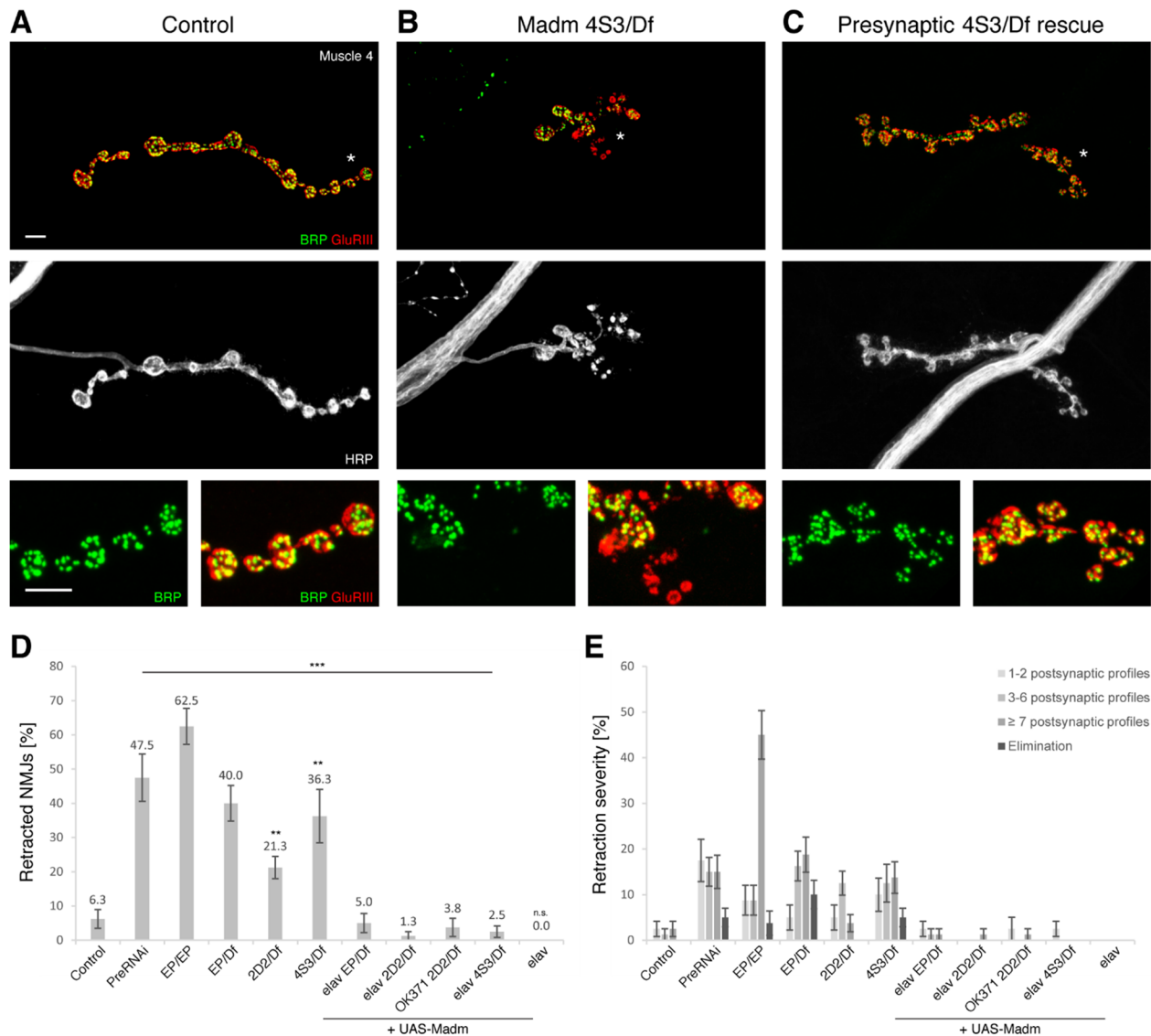
3.3 Additional analysis of Madm

3.3.1 Presynaptic Madm controls NMJ stability as well as morphology and growth

This results section summarizes additional experiments which I performed to investigate the role of Madm at the *Drosophila* larval NMJ. For discussion of the subsequent findings please see the discussion section of the manuscript as well as the additional discussion within this thesis. In the latter section, I will also explain where a more detailed analysis of observed effects would be advisable and where additional experiments should be performed in the future to gain further insights regarding the role of Madm.

In addition to the synaptic stability defects observed on the most dorsal muscle group 1/9 and 2/10 and the most ventral muscles m6/7, I also analyzed the synaptic stability defect upon Madm depletion on additional muscle groups. For example, I also quantified synaptic retraction frequencies observed on muscle 4. In the *Drosophila* larvae, this muscle lies in between the two muscle groups described in the manuscript and is one of the standard muscles used for morphology quantifications. As observed throughout the entire animal (one hemisegment shown in Fig. S1 of the manuscript), muscle 4 was also highly affected by synaptic instability (Thesis Fig. 5). Upon Madm knockdown, synaptic stability defects affected on average 47.5% of all muscle 4 NMJs per animal (Thesis Fig. 5 D). Synaptic retraction frequencies observed in the different Madm mutant combinations ranged from 21.3% to 62.5% and were highly significant compared to controls (Thesis Fig. 5 B, D). The presynaptic re-expression of Madm in different Madm mutant animals using the pan-neuronal driver *elav-Gal4* significantly rescued the synaptic stability defects to wild-type levels (Thesis Fig. 5 C, D). Furthermore, the rescue experiment using the motoneuron-specific driver line *OK371-Gal4* resulted in a significant increase in synaptic stability (Thesis Fig. 5 D). Overexpression of Madm using *elav-Gal4* did not result in any synaptic stability defect (0.0%; Thesis Fig. 5 D). The substantial number of large synaptic retractions (affecting ≥ 7 boutons) as well as the total eliminations were completely absent under rescue conditions (Thesis Fig. 5 E). Please note that although the synaptic stability defect was completely rescued (Thesis Fig. 5 D), the morphology and organization of individual boutons was still slightly altered, indicating potentially different requirements of Madm levels for the control of synapse

morphology and stability (Thesis Fig. 5 C). In addition, the prominent accumulations of BRP in the motoneuron axon in the Madm mutant animals (Thesis Fig. 5 B) were rescued (Fig. 5 C).

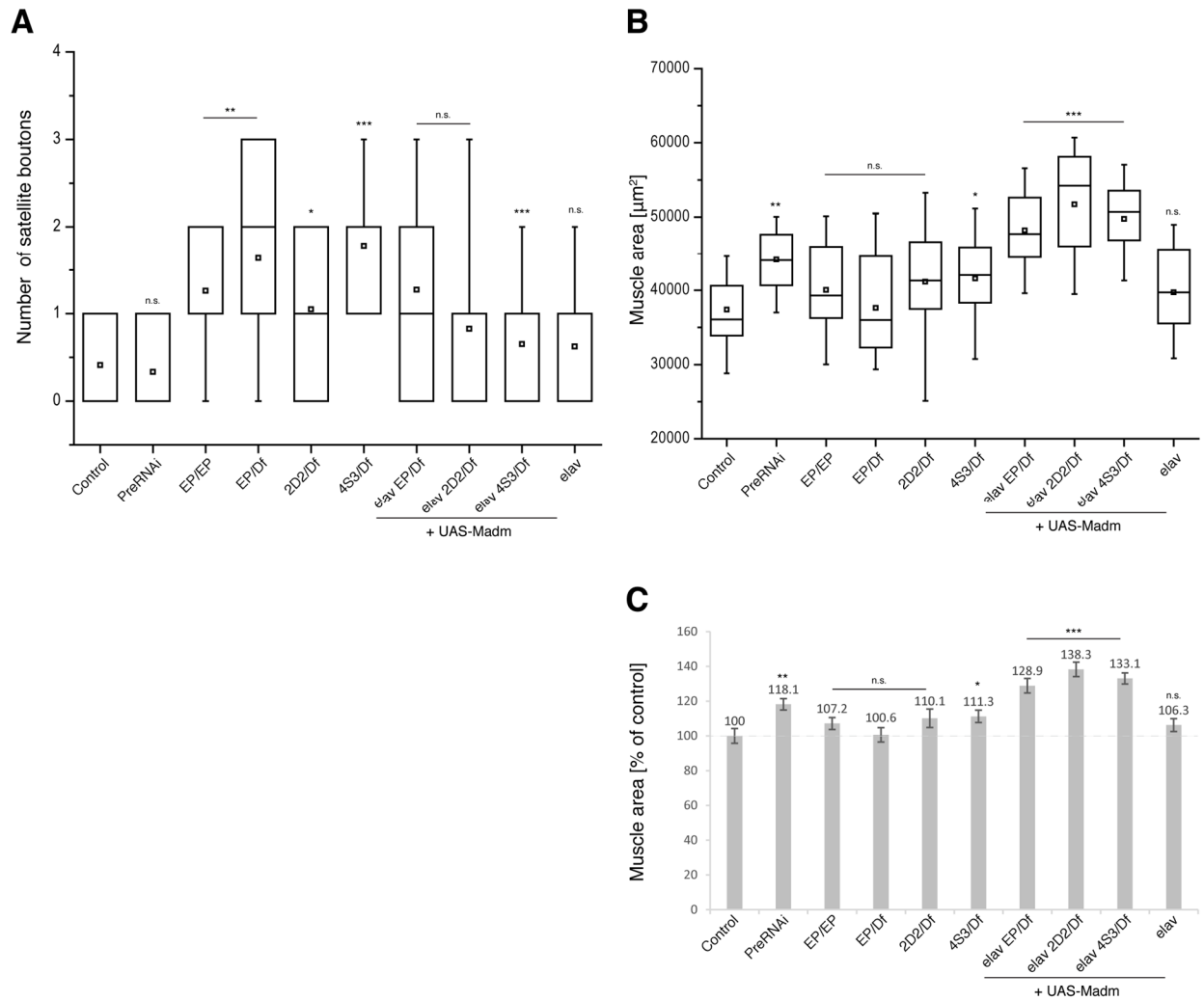


Thesis Figure 5. Presynaptic Madm is essential for synapse stability of NMJs on muscle 4.

(A) In control animals, a stable NMJ is characterized by precise opposition of the active zone marker BRP (green, presynapse) and the postsynaptic GluRIII clusters (red). The intact neuronal membrane is visualized by HRP (white). (B) A NMJ on muscle 4 in a Madm 4S3/Df mutant animal is showing severe stability defects. The presynapse is retracting, leaving the postsynapse behind. The neuronal membrane is discontinuous in some parts. Furthermore, BRP is accumulating in the motoneuron axon. (C) Upon presynaptic re-expression of Madm using elav-Gal4 in the 4S3/Df mutant background, synaptic stability was increased. Organization and morphology of synaptic boutons was still altered compared to controls. (A-C) Scale bars: main panels 5 μ m, enlarged panels 5 μ m. (D-E) Quantification of synaptic retraction frequency and severity on muscle 4. Synaptic instability was highly significantly increased in

presynaptic Madm knockdown and mutant animals. Large synaptic retractions as well as total eliminations of presynaptic nerve terminals were observed. Presynaptic rescue experiments, in which Madm was re-expressed presynaptically, highly significantly rescued synaptic stability defects. Synaptic retraction frequency as well as severity were rescued. The use of the motoneuron-specific OK371-Gal4 driver in comparison to the pan-neuronal elav-Gal4 driver was less efficient in restoring synaptic stability. But the effect was also highly significant. The presynaptic Madm overexpression animals did not show any signs of synaptic instability at all. n = 10 animals of each genotype. Error bars represent SEM.

For the description of the morphological and growth related alterations observed in *madm* mutants, I selected four categories to display the phenotype in the manuscript: number of NMJ branches, number of total (I_s and I_b) synaptic boutons, total NMJ length of all branches and the percentage of NMJ area covering the muscle surface. However, I also tested additional parameters. One of those was the category “satellite boutons”. Satellite boutons are defined as additional, small “satellite” boutons which are budding and pinching off from a central bouton of normal appearance (Torroja et al., 1999). These boutons can also arise on neuronal processes connecting two boutons. Satellite boutons can be found on type I_s as well as type I_b NMJ branches. These boutons are immunopositive for presynaptic markers such as Synapsin or Synaptotagmin and display T-bar shaped active zones in electron microscopy images. The satellite boutons are surrounded by postsynaptic SSR, indicating that these boutons are likely functional. Satellite boutons are rarely present in wild-type animals. If at all, only one satellite bouton was observed per NMJ in my studies (Thesis Fig. 6 A). While RNAi knockdown of Madm did not show a significant increase in the number of satellite boutons (Thesis Fig. 6 A), we observed a significant increase in *madm* mutants (Thesis Fig. 6 A). We observed up to three satellite boutons per NMJ (EP/Df; Thesis Fig. 6 A). It is important to note that this is a relatively weak feature of the Madm mutant phenotype. The number of satellite boutons observed in other published mutants or disease models are dramatically higher. For example, the overexpression of β -Amyloid precursor protein to mimic Alzheimer’s disease resulted in one third of all boutons being satellites at these NMJs (Torroja et al., 1999). Pan-neuronal re-expression of Madm in the Madm mutant animals using elav-Gal4 could reduce the occurrence of satellite boutons, but only in case of the 4S3/Df rescue experiment reached significance (Thesis Fig. 6 A).



Thesis Figure 6. Additional categories to describe NMJ growth and morphology phenotypes in *madm* mutants.

Additional parameters were also tested to reflect the phenotypes observed in *madm* mutants. Two more categories are depicted. **(A-B)** The variance of the absolute values of these parameters for NMJs on muscle 1 is displayed via box blots. Boxes display 25-75 percentile, whiskers represent 5 - 95% range, the mean is depicted by \square and the median is shown via the horizontal line crossing the box. $n = 17 - 24$ NMJs on muscle 1 in 6 different animals per genotype. **(A)** Quantification of the number of satellite boutons. Those boutons are additional, smaller boutons which bud of from normal boutons or which bud of from neuronal processes connecting two boutons. Upon presynaptic Madm knockdown, the number of satellite boutons was not altered compared to controls. But in all Madm mutant animals, there was a significant increase of these boutons. Presynaptic re-expression of Madm in the various mutant backgrounds significantly reduced satellite boutons. In case of the 4S3/Df rescue, this decrease was highly significant. Presynaptic overexpression of Madm did not alter the occurrence of satellite boutons compared to controls. **(B)** Depicted is the variance of the muscle 1 area for all tested genotypes. **(C)** The muscle 1 area is displayed normalized to control. Upon presynaptic Madm knockdown, muscle area was significantly increased. There was no significant change for Madm mutant animals except for 4S3/Df mutant animals, in which the muscle size was significantly increased. Rescue experiments via presynaptic re-expression of Madm in the various mutant backgrounds resulted in highly significant larger muscles. Presynaptic overexpression of Madm did not affect muscle size. $n = 17 - 24$ NMJs on muscle 1 in 6 different animals per genotype.

Furthermore, I monitored the general growth in the larvae and measured muscle sizes. This parameter was correlated to the NMJ area covering the corresponding muscles. When I analyzed muscle sizes individually, I observed a slight increase (maximum of 111.3%) in *Madm* mutant animals (Thesis Fig. 6 B, C). The effect on muscles in *Madm* knockdown animals was even a bit higher (118.1%; Thesis Fig. 6 B, C). Subsequently, I found a highly significant increase of muscle size in all pan-neuronal rescue experiments (Thesis Fig. 6 B, C). Muscle sizes increased to around 130% compared to controls (see discussion section). Control animals with overexpression of *Madm* showed no increase in muscle size (Thesis Fig. 6 B, C).

All morphological parameters were also tested on the ventral muscles 6/7. The analysis of this muscles showed similar tendencies as observed for the dorsal muscle 1 (data not shown). Due to the stereotypic appearance, I focused my main analysis on the NMJ on muscle 1.

3.3.2 The role of the postsynapse in *madm* mutants

Interestingly, we also observed phenotypes and defects upon postsynaptic *Madm* knockdown.

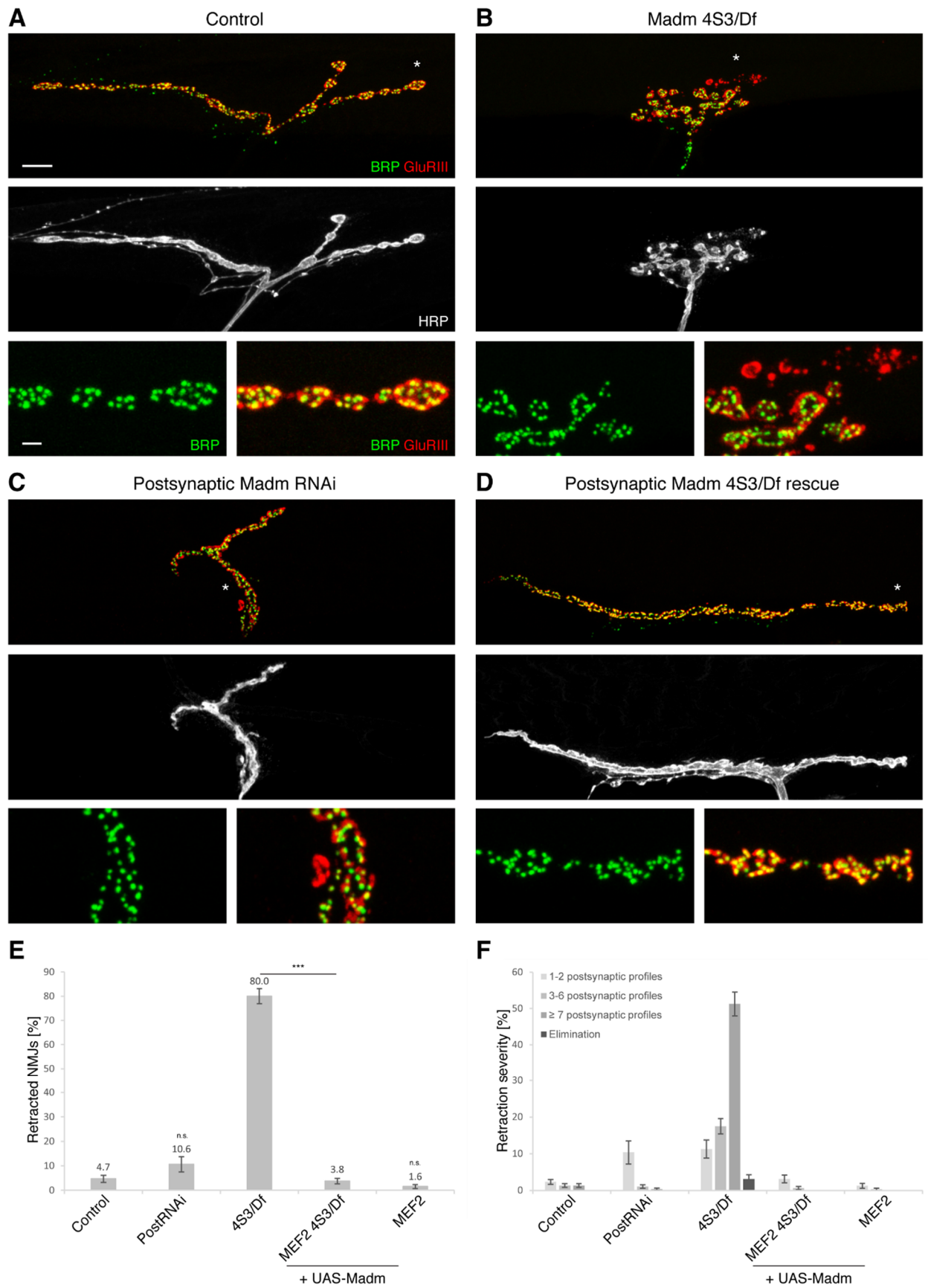
First, I knocked down *Madm* using the same RNAi construct as before but using a postsynaptic driver line. Upon postsynaptic *Madm* knockdown, I observed a small increase in synaptic retractions compared to controls on the dorsal muscles 1/9 & 2/10 (10.6% to 4.7%, Thesis Fig. 7 A, C, E). However, this effect was not significant. On the ventral muscles 6/7, I observed the same increase of synaptic retraction frequency to 12.5% compared to 3.8% in control animals. Again the effect was not significant.

To analyze the role of the postsynapse in more detail, I tried to rescue the synaptic stability defects present in *4S3/Df* mutant animals by re-expression of *Madm* using the muscle-specific MEF2-Gal4 driver. The *4S3* allele combined with a deficiency caused the strongest synaptic stability defects of all allelic combinations on all analyzed muscle groups (Thesis Fig. 7 B, E and Thesis Fig. 8 A). In the muscle-specific rescue experiments, I could significantly rescue the synaptic stability defects on all muscles (Thesis Fig. 7 D, E and Thesis Fig. 8 A). The severity of the synaptic retractions was also reduced, e.g. no eliminations were present (Thesis Fig. 7 F and

Thesis Fig. 8 B). As control, I expressed Madm using the same MEF2-Gal4 driver line in a wild-type background. This did not result in any significant change of synaptic stability (Thesis Fig. 7 E and Thesis Fig. 8 B).

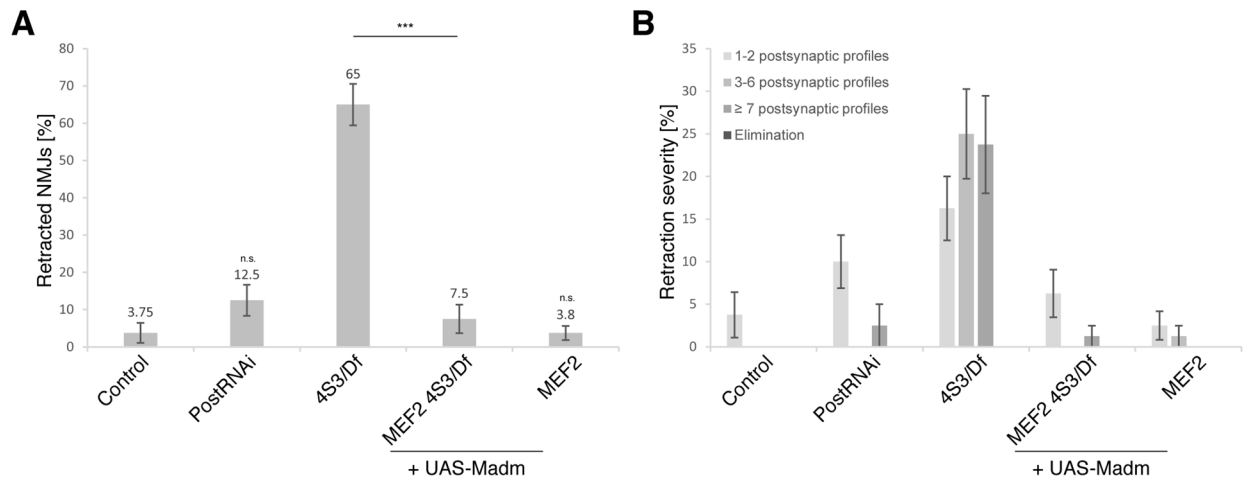
Subsequently, I also studied the role of postsynaptic Madm for NMJ morphology. I analyzed the four previously defined categories: number of NMJ branches, total number of synaptic boutons, total NMJ length and NMJ area covering the muscle surface on muscle 1. Again, I tried to rescue the strong morphology defects observed in 4S3/Df mutant animals (Thesis Fig. 9 B). Upon MEF2-Gal4-driven muscle-specific re-expression of Madm in this mutant background, all defects could be significantly rescued (Thesis Fig. 9 C, D, E, F, G). The number of NMJ branches decreased back to wild-type levels (Thesis Fig. 9 D). The NMJs displayed more synaptic boutons, were longer in total and covered a larger area of the muscle (Thesis Fig. 9 E, F, G).

A potential caveat of these experiments is that the used UAS-Madm construct may be leaky and may partially restore presynaptic Madm levels even in the absence of a specific driver line. Further control experiments are necessary to address this issue.



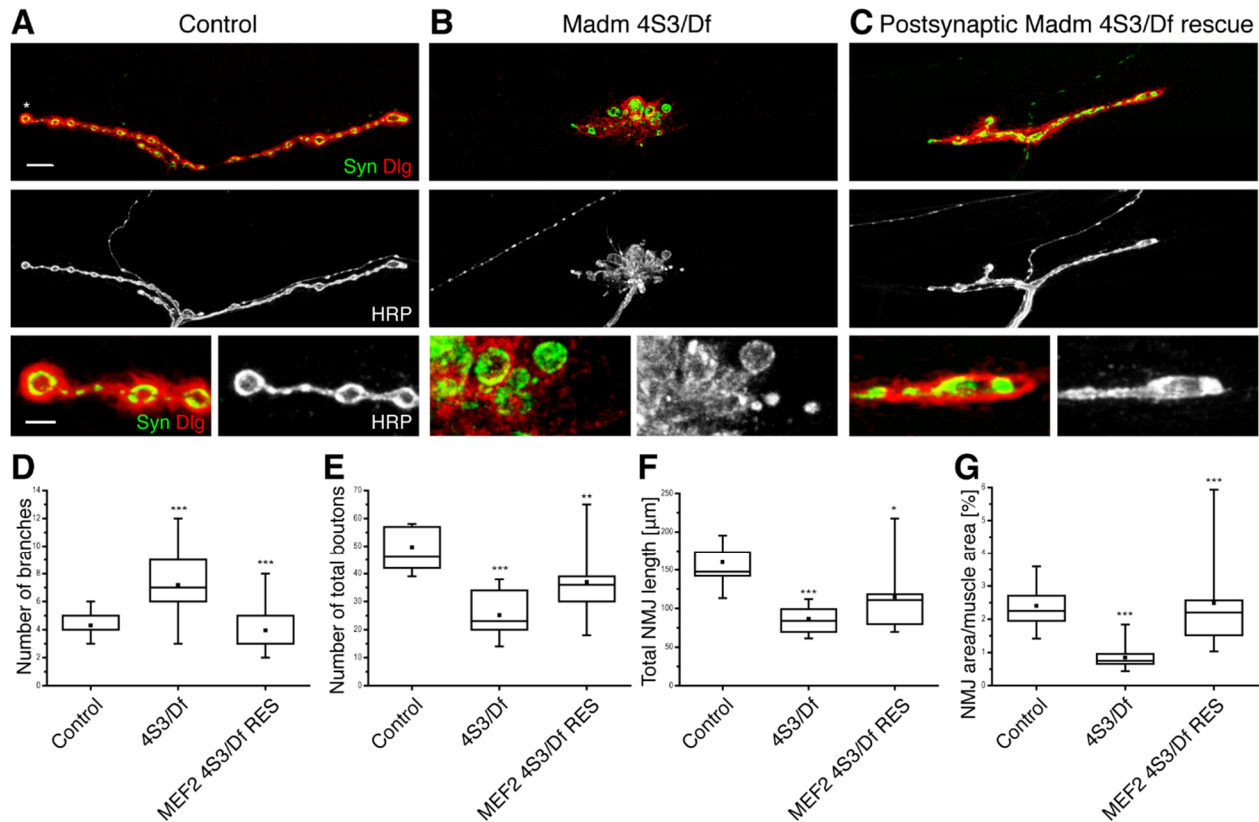
Thesis Figure 7. The role of the postsynapse on synaptic stability in *madm* mutants on muscle 1/9 & 2/10.

(A) A stable control NMJ on muscle 1 is displayed. There are no signs of synaptic retraction. The neuronal membrane is continuous. **(B)** In *Madm* 4S3/Df mutant animals, severe synaptic instability was observed. The postsynapse (GluRIII, red) was left behind unopposed by the presynapse (BRP, green). The neuronal membrane got fragmented (HRP, white). In addition, BRP was accumulating in the motoneuron axon. **(C)** Upon postsynaptic *Madm* knockdown, minor synaptic instability was observed. Furthermore, synaptic boutons appeared to be altered in organization and were less roundish. **(D)** Upon postsynaptic re-expression of *Madm* using the muscle-specific MEF2-Gal4 driver in 4S3/Df mutant animals, NMJs were more stable. Synaptic bouton organization was still changed. NMJ looked like long, fused stretch of synaptic boutons. **(A-D)** Scale bars: main panels 7 μ m, enlarged panels 1.5 μ m. **(E-F)** Quantification of synaptic retraction frequency and severity on muscles 1/9 & 2/10. Upon postsynaptic *Madm* knockdown, the synaptic stability frequency was more than doubled compared to control, but not significant. Postsynaptic re-expression of *Madm* in the mutant 4S3/Df animals highly significantly reduced synaptic instability. The severity of observed synaptic retractions was also reduced. Muscle-specific overexpression of *Madm* did not significantly increase synaptic instability. n = 10 animals of each genotype. Error bars represent SEM.



Thesis Figure 8. The role of the postsynapse on synapse stability in *madm* mutants on muscles 6/7.

In addition to the synaptic stability defects on the dorsal muscles 1/9 & 2/10, synaptic instability was also monitored for the ventral muscles 6/7. Similar effects were observed. **(A-B)** Quantification of synaptic retraction frequency and severity. Upon postsynaptic *Madm* knockdown, the synaptic stability frequency was more than tripled compared to control, but this effect was not significant. Postsynaptic re-expression of *Madm* using MEF2-Gal4 in mutant 4S3/Df animals reduced frequency as well as severity of the synaptic instability events significantly. Muscle-specific overexpression of *Madm* via MEF2-Gal4 did not significantly increase synaptic instability. n = 10 animals of each genotype. Error bars represent SEM.



Thesis Figure 9. The role of the postsynapse on morphology in *madm* mutants.

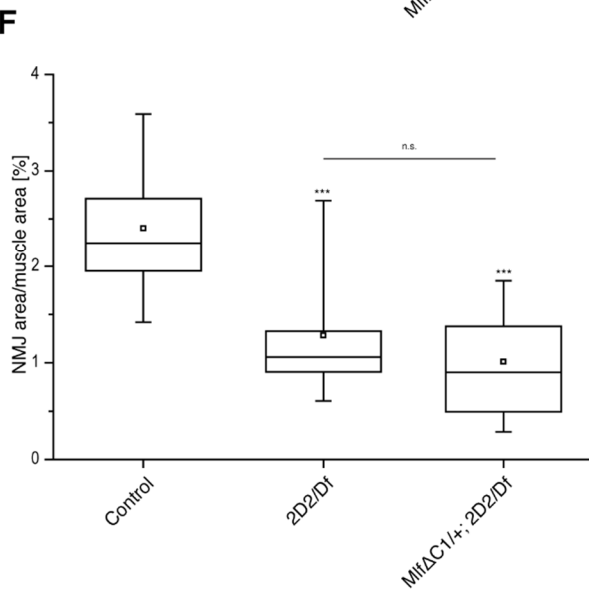
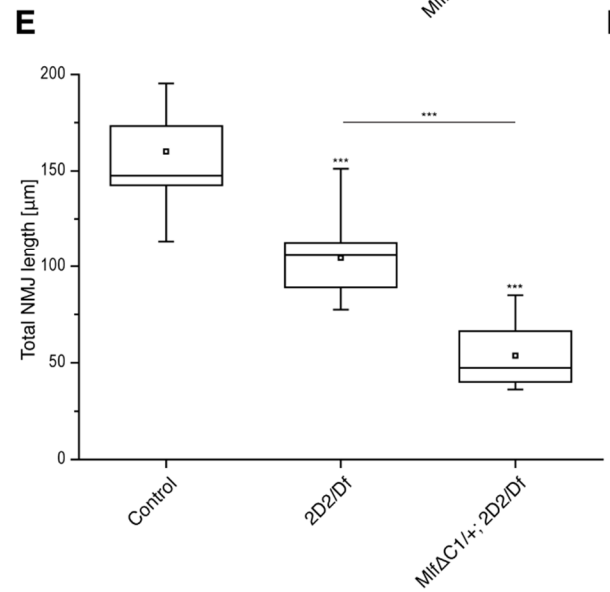
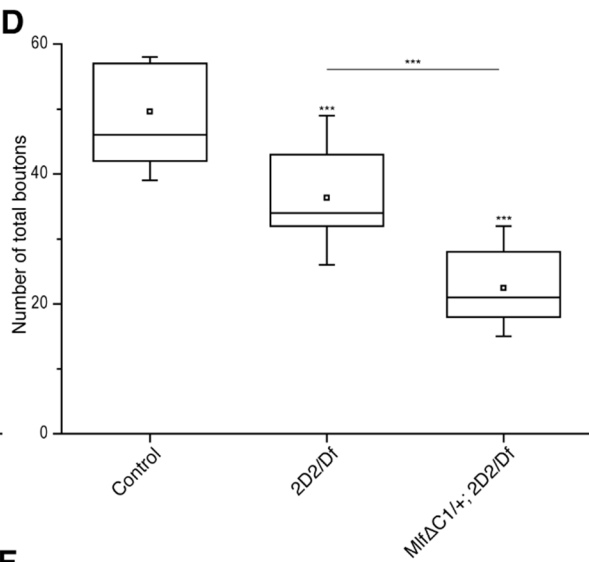
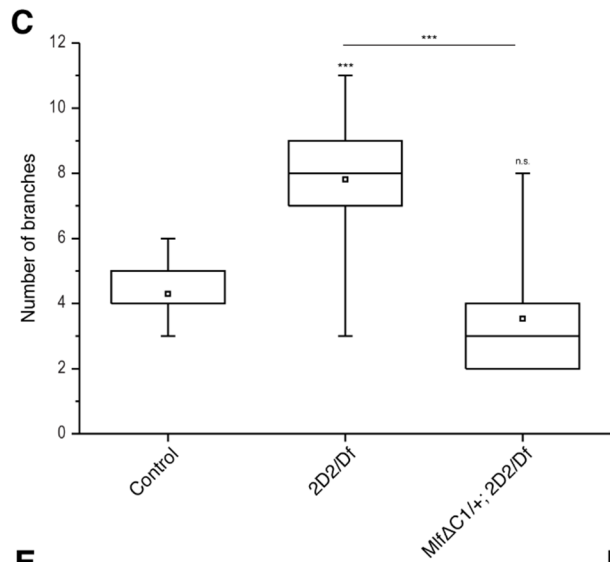
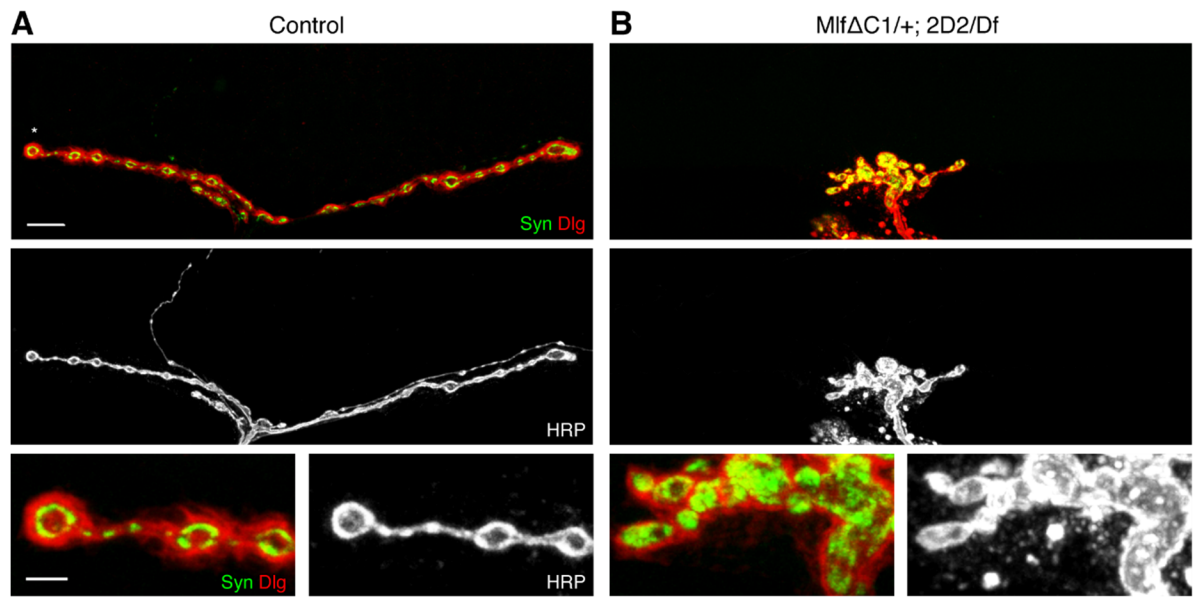
(A) The morphology and growth of a NMJ on muscle 1 in a control animal is monitored via the presynaptic marker Syn (green) and the postsynaptic marker Dlg (red). The neuronal membrane is visualized with HRP (white). (B) NMJs of *Madm* 4S3/Df mutant animals displayed severe synaptic growth and morphology deficits. (C) Upon postsynaptic re-expression of *Madm* using the muscle-specific MEF2-Gal4 driver in 4S3/Df mutant animals, normal NMJ growth and morphology was largely restored. (A-C) Scale bars: main panels 7 μm, enlarged panels 3 μm. (D-G) Quantification of four different morphological categories for NMJs. The variance of the absolute values of the four different measured parameters on muscle 1 is displayed via box blots. Boxes display 25-75 percentile, whiskers represent 5 - 95% range, the mean is depicted by □ and the median is shown via the horizontal line crossing the box. n = 17 - 23 NMJs on muscle 1 in 6 different animals per genotype. (D) Quantification of the number of NMJ branches. This parameter was highly significantly increased in 4S3/Df mutants. It could be highly significantly rescued upon postsynaptic re-expression of *Madm* using MEF2-Gal4 in 4S3/Df mutant animals. (E) Quantification of number of total synaptic boutons. The number of total synaptic boutons was highly significantly reduced in 4S3/Df mutant animals. This parameter was significantly rescued upon postsynaptic re-expression of *Madm* in the 4S3/Df mutant animals. (F) Quantification of total NMJ length. In 4S3/Df mutant animals, the total length of NMJs was highly significantly reduced. Postsynaptic re-expression of *Madm* in this mutant background significantly increased NMJ length. (G) Quantification of NMJ area covering muscle area. This category was highly specifically reduced in 4S3/Df mutant animals. NMJs covered less area over the muscle surface. This effect was highly significantly reverted upon postsynaptic re-expression of *Madm* in 4S3/Df mutant animals.

3.3.3 Mlf and Bun genetically interact with Madm to modulate synaptic stability and morphology phenotype

3.3.3.1 Mlf & Madm

In the manuscript of our paper, we demonstrate that Mlf and Madm interact genetically in the control of synapse stability. We demonstrated that the removal of one *madm* copy (2D2/+) in zygotic, homozygous *mlfΔC1* mutants resulted in increased synaptic instability (retraction frequency of 25.0% compared to 4.2%) (Fig. 7 A in manuscript). In addition, the severity of the observed synaptic retractions was increased (Fig. 7 B in manuscript).

Subsequently, I tested whether Mlf and Madm also interact to modulate morphology defects. Here, I show the four morphological categories analyzed on muscle 1. Indeed, I found a genetic interaction of Mlf and Madm. When one copy of Mlf (*mlfΔC1/+*) was removed in 2D2/Df mutant animals, the number of NMJ branches was significantly decreased (Thesis Fig. 10 B, C). However, the reduction in total synaptic boutons as well as total NMJ length was enhanced when one copy of Mlf was removed in this genetic background (Thesis Fig. 10 B, D, E). These effects were highly significant compared to controls as well as to 2D2/Df mutants. The NMJ area covering the muscle was highly significantly decreased compared to the control (Thesis Fig. 10 B, F), but this effect was not significant compared to 2D2/Df mutants. Together, these results show that removal of one *mlf* copy in the 2D2/Df mutant background led to an enhanced reduction of synaptic bouton number and NMJ length but did not further enhance the reduced NMJ area phenotype.



Thesis Figure 10. Mlf genetically interacts with Madm to modulate morphology phenotype.

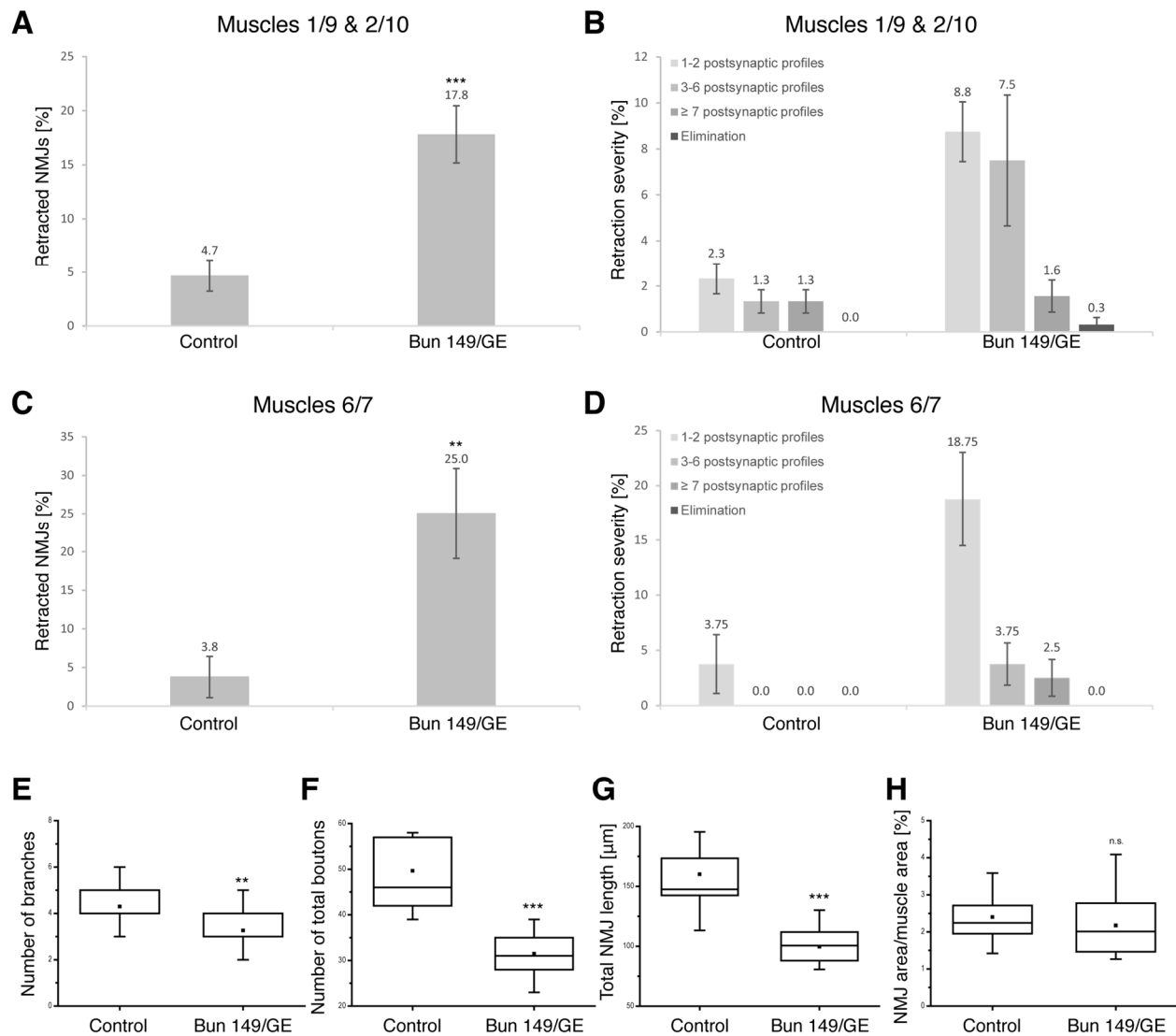
(A) A control NMJ on muscle 1 with the presynaptic marker Syn (green) and the postsynaptic marker Dlg (red). Neuronal membrane is visualized by HRP (white). **(B)** *Mlf Δ C1/+*; 2D2/Df mutant animals appeared to have even stronger morphology phenotype compared to *Madm* 2D2/Df mutant animals. **(A-B)** Scale bars: main panels 7 μ m, enlarged panels 3 μ m. **(C-F)** Quantification of four different morphological categories for NMJs. The variance of the absolute values of the four different measured parameters on muscle 1 is displayed via box blots. Boxes display 25-75 percentile, whiskers represent 5 - 95% range, the mean is depicted by \square and the median is shown via the horizontal line crossing the box. n = 17 - 21 NMJs on muscle 1 in 6 different animals per genotype. **(C)** Quantification of the number of NMJ branches. This parameter was highly significantly increased in 2D2/Df mutant animals. The removal of one *mlf* copy (*mlf Δ C1/+*) in 2D2/Df mutant animals resulted in a highly significant rescue. **(D)** Quantification of number of total synaptic boutons. The number of total synaptic boutons was highly significantly reduced in 2D2/Df mutant animals. The removal of one *mlf* copy (*mlf Δ C1/+*) in 2D2/Df mutant animals resulted in an even stronger reduction of synaptic boutons. This effect was also highly significant compared to 2D2/Df mutant animals. **(E)** Quantification of total NMJ length. In 2D2/Df animals, the total length of NMJs was highly significantly reduced. Removal of one *mlf* copy in this genetic background reduced the length even more significantly, also in comparison to 2D2/Df mutant animals. **(F)** Quantification of NMJ area covering muscle area. This category was highly specifically reduced in 2D2/Df mutant animals. This reduction was unaffected by the removal of one *mlf* copy in the *Madm* 2D2/Df mutant animals.

3.3.3.2 Bun A

As the *bun200B* allele affects all of the six different Bunched isoforms present in *Drosophila*, I also performed an analysis of *bun* alleles affecting only the isoform BunA. I analyzed the *bun*^{A-149B} allele which I will refer to as *bun149*. This allele was previously described to affect the long isoforms A and F (Gluderer et al., 2008). I combined the *bun149* allele with the *bun GE*¹²³²⁷ (referred to as *bun GE* for simplicity). This allele was also previously described as a P element insertion in the 5'UTR of the Bun A isoform and an intron of the Bun F isoform (Gluderer et al., 2008).

Compared to control animals, synaptic retraction frequencies were significantly increased on dorsal muscles 1/9 & 2/10 as well as on ventral muscles 6/7 (Thesis Fig. 11 A, C). In addition, the severity of synaptic retractions was increased (Thesis Fig. 11 B, D). Furthermore, the synaptic retraction frequencies on all muscles were higher when comparing the *bun 149/GE* animals to *bun 200B/GE* mutant animals. Morphological defects monitored on muscle 1 revealed that the synaptic bouton number, total NMJ length as well as NMJ area covering the muscle area were more reduced in *bun 149/GE* compared to *bun 200B/GE* mutant animals (data not shown in direct comparison). Compared to control, the number of NMJ branches and synaptic boutons as well as the total NMJ length was significantly reduced (Thesis Fig. 11 E, F, G). The NMJ area correlated to the muscle size was not significantly altered. (Thesis Fig. 11 H).

Interestingly, this data shows even stronger defects in synaptic stability and morphology as compared to the *bun 200B/GE* allelic combination. But the *bun 149* allele was created via imprecise excision of the GE element. Thus, common genetic background mutations could be responsible for the stronger phenotypes. As a consequence, I only included the analysis of the cleaner genetic combination *bun 200B/GE* in the manuscript even though the *bun 149/GE* combination was used for previous studies of growth-related phenotypes (Gluderer et al., 2008).



Thesis Figure 11. *Bun 149/GE* mutants display synaptic stability and morphology phenotype.

The *bun 149* allele was generated via imprecise excision of the GE element. Thus, both mutations should specifically target BunA. But background hits affecting other genes caused by the imprecise excision cannot be excluded. **(A-B)** Quantification of synaptic retraction frequency and severity on dorsal muscles 1/9 & 2/10. Bun 149/GE mutant animals displayed highly significant increase in synaptic instability compared to control animals. Total eliminations of nerve terminals were observed. **(C-D)** Quantification of synaptic retraction frequency and severity on ventral muscles 6/7. Synaptic retractions monitored in Bun 149/GE mutant animals were significantly increase in frequency as well as severity compared to control animals. **(A-D)** n = 10 animals of each genotype. Error bars represent SEM. **(E-H)** Quantification of four different morphological parameters to describe NMJ morphology. The variance of the absolute values of the four different measured parameters on muscle 1 is displayed via box blots. Boxes display 25-75 percentile, whiskers represent 5 - 95% range, the mean is depicted by □ and the median is shown via the horizontal line crossing the box. n = 17 - 19 NMJs on muscle 1 in 6 different animals per genotype. **(E)** Quantification of the number of NMJ branches. This parameter was significantly decreased in Bun 149/GE mutant animals.

(F) Quantification of number of total synaptic boutons. The number of total synaptic boutons was highly significantly reduced in Bun 149/GE mutant animals. **(G)** Quantification of total NMJ length. In Bun 149/GE mutant animals, the total length of NMJs was highly significantly reduced. **(H)** Quantification of NMJ area covering muscle area. This parameter was not altered in Bun 149/GE mutant animals compared to control animals.

3.3.4 Further attempts to identify additional Madm interaction partners

Finally, I also tested additional candidates from networks and signaling pathways implicated in growth control like e.g. the mTOR/insulin signaling network and prior proposed potential interacting candidates (see PhD thesis Gluderer S., 2009). Those candidates included Mlf, Elongin-B, CSN5, S6 kinase, Stat92E, mTOR, Akt and 4E-BP1. Elongin-B, CSN5, S6 kinase and Stat92E were tested for potential genetic interaction (data not shown). Pending on the availability of fly lines the following analyses were performed: Mutants were analyzed in homozygous conditions but also in combination with *madm* alleles. The effect of overexpression using a corresponding UAS-construct was monitored. Co-overexpression experiments of candidate UAS-construct together with a UAS-Madm construct were performed. Rescue experiments by expression of Madm in the candidate mutant background and vice versa were tested.

From these analyses, only Mlf was identified as being a putative Madm interaction partner. No additional, definite Madm interaction partner could be identified, but a more detailed quantitative analyses e.g. of synapse morphology would be advisable for some cases.

3.4 RNAi-based genetic screens for novel regulators of synapse development

In order to identify novel regulators of synapse development and maintenance, I performed two large-scale RNA interference (RNAi) - based genetic screens. I screened 269 candidate genes based on their affiliation to cytoskeleton, cytoskeleton-associated and transport proteins as well as signaling molecules (QueryBuilder of FlyBase) and literature searches.

Following the RNAi-based screens, mutations of the most promising candidate genes were tested and analyzed in detail to verify the screen hit and its phenotype. For embryonic lethal mutations, I performed MARCM (Mosaic analysis with a repressible cell marker) analysis which allowed me to investigate homozygous mutant motoneuron clones in an otherwise wild-type background.

The main part of my thesis focuses on the identification and characterization of Madm (**Mlf1 adapter molecule**), identified in collaboration with Victoria Bulat.

In this part of the result section, I want to focus on additional prominent hits I found in my RNAi-based genetic screens. Hereafter, I want to briefly summarize the findings and results of those analyses.

3.4.1 Background information on RNAi screens

A presynaptic network of molecules has previously been identified which mediates synapse formation and stability at the *Drosophila* NMJ. This network consists of the cell-adhesion molecule Neuroglian (Enneking et al., 2013), the scaffolding molecules alpha- and beta-Spectrin (Pielage et al., 2005), the adaptor molecule Ankyrin2 (Ank2) (Pielage et al., 2008) and the actin-capping molecule Hts/Adducin (Pielage et al., 2011). The association of these proteins provides a link to the cytoskeleton and may represent a platform for signaling pathways to control different aspects of synapse development. The aim of my unbiased RNAi screens was to identify further regulators of synapse development and maintenance and to ideally fit them into this previously identified network at the NMJ.

In *Drosophila*, (almost) every gene can be specifically knocked down using RNAi. A genome-wide RNAi library was established for this purpose (Dietzl et al., 2007). Long double-stranded RNA

hairpins can be expressed in a temporal and spatial manner using the UAS/Gal4-system. This RNA hairpins will be processed inside the cell and mediate RNAi in a cell autonomous fashion (Kennerdell et al., 2000; Martinek et al., 2000; Van Roessel et al., 2002).

3.4.2 Hits of “cytoskeleton, cytoskeleton-associated and transport proteins” screen

The 139 candidates of this screen were selected based on the following different features: microtubule-binding, actin-binding, motor-activity, GTPase activity, signal transducer activity, ubiquitin-protein ligase activity, and connections extracellular matrix (ECM) - actin cytoskeleton. For an overview of all candidates please see Table 69.

I identified 10 genes displaying a phenotype at the NMJ upon presynaptic knockdown (7.2%) as well as 10 hits showing an alteration of the postsynaptic features. For an overview of the hits please see Table 65 and 66.

3.4.2.1 Subsequent analysis of most promising candidates

1. Formin 3 (Thesis Fig. 12)

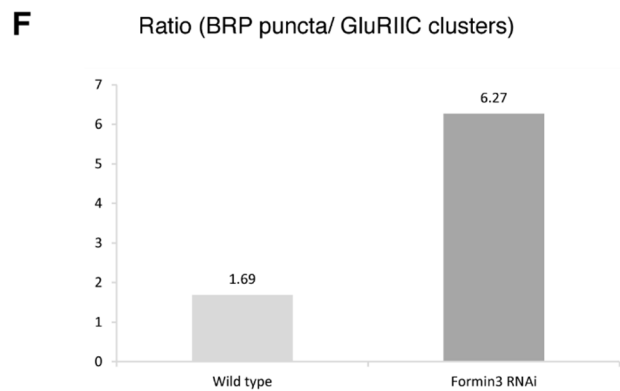
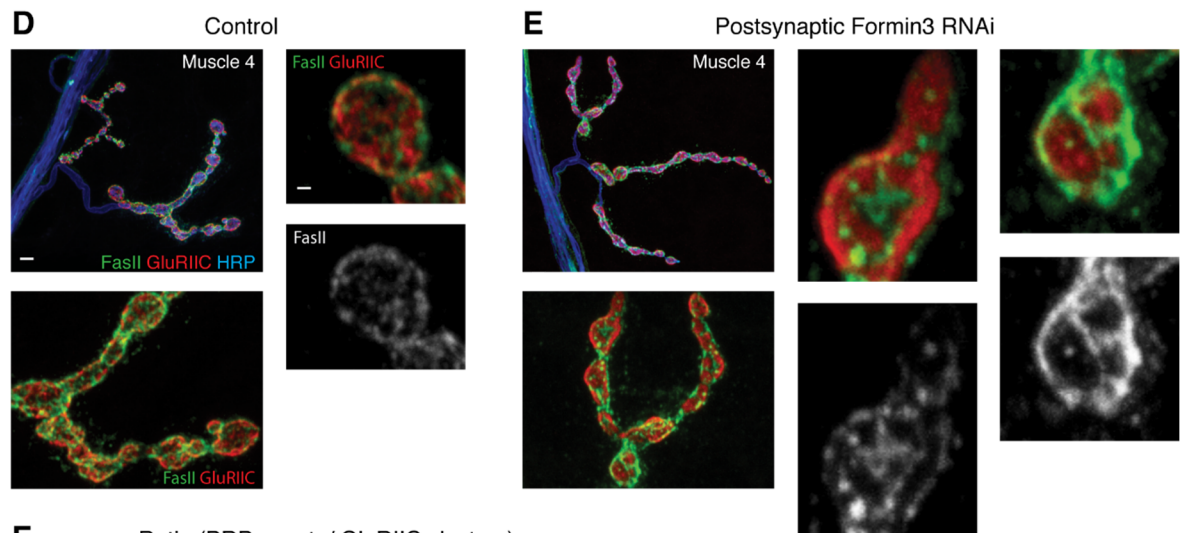
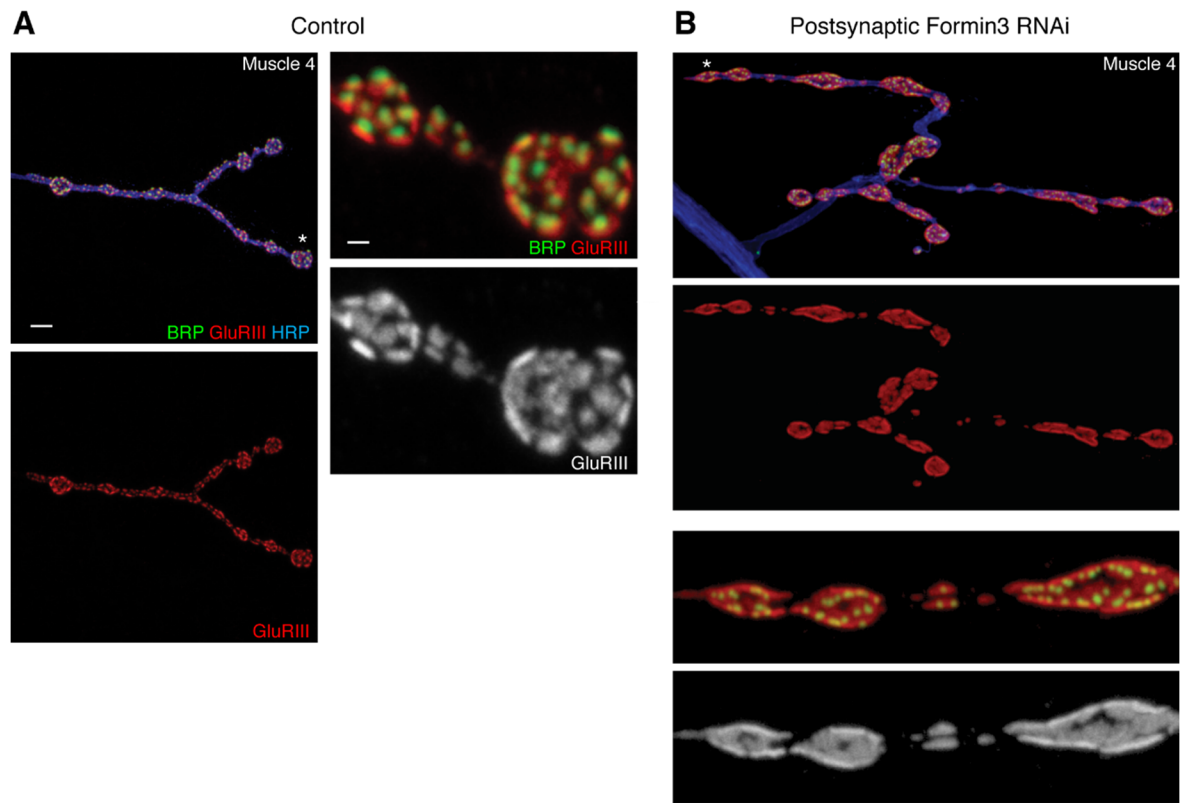
One of the most prominent hits and phenotypes was observed after postsynaptic knockdown of Formin 3 - a potential actin-binding protein. Upon postsynaptic knockdown of this protein, the precise arrangement of the postsynaptic glutamate receptors was strongly altered. The receptors were no longer forming distinct units at the synapse but fused to large aggregations (Thesis Fig. 12 B, E). I was able to confirm the phenotype using two additional RNAi lines. I quantified the observed glutamate receptor cluster phenotype upon postsynaptic Formin 3 knockdown. There were 1.69 BRP puncta per GluRIII cluster in wild-type animals, whereas there were 6.27 BRP puncta opposing the larger and fused GluRIII clusters in the knockdown animals. Unfortunately, analysis of previously published Formin 3 mutants (Tanaka et al., 2004) did not verify this phenotype.

2. KLHL18 (Kelch-like protein 18) (Thesis Fig. 13)

Knockdown of KLHL18 protein led to a prominent synaptic retraction phenotype which I quantified and analyzed. Interestingly, this synaptic stability defect was most pronounced on the ventral muscles 6/7 (Thesis Fig. 13 B, C). The synaptic retraction frequency pooled for the muscles 6/7, 12, 13 and 4 was 12.5% (data not shown). Unfortunately, there were no mutants or P elements available for further analysis and verification of this striking phenotype. Thus, we decided not to focus on this hits.

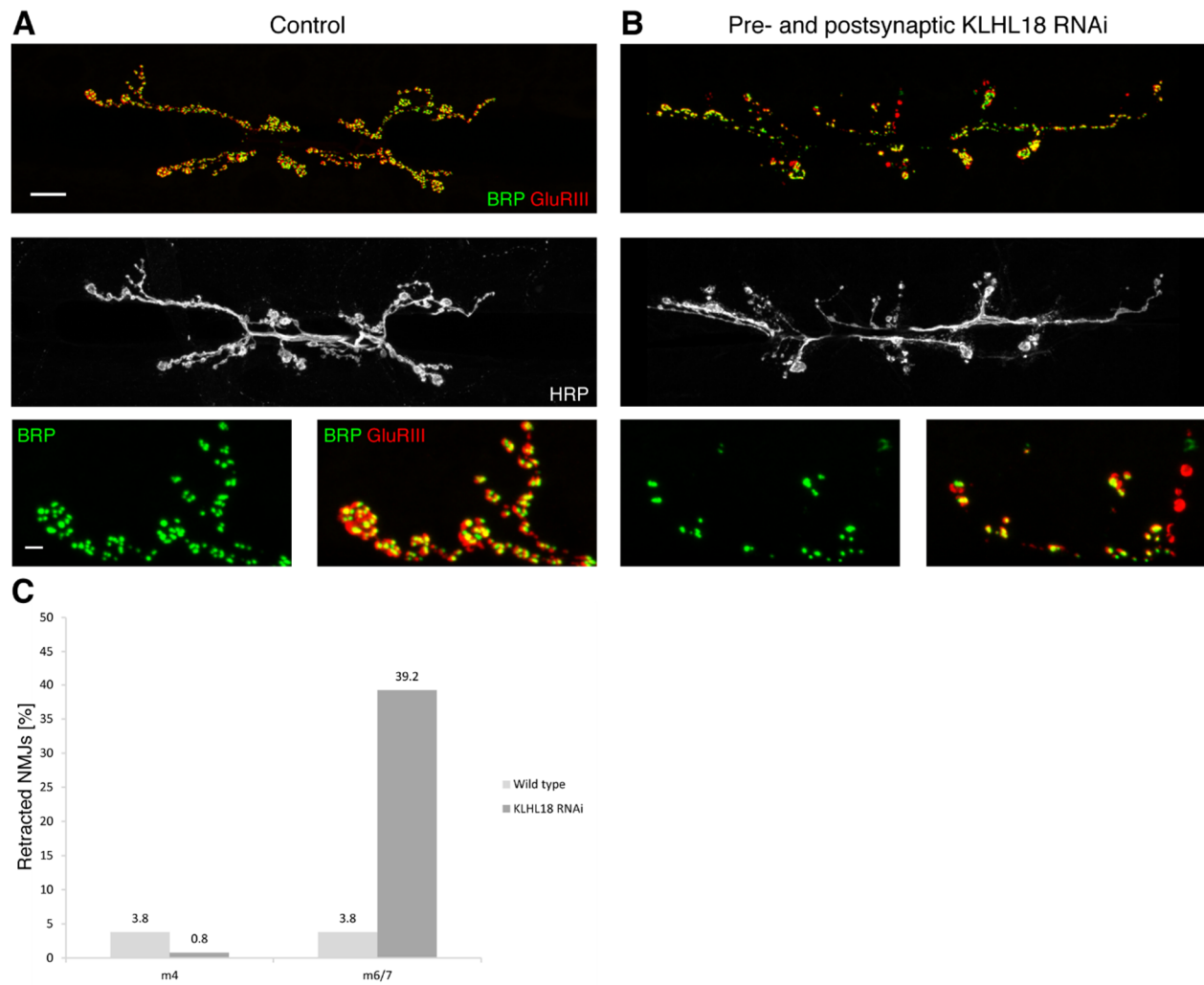
3. Chd64 (Calponin-like protein 64) (Thesis Fig. 14)

Presynaptic knockdown of this candidate resulted in an extended ventral nerve cord. The candidate was analyzed for potential central nervous system defects in the Reichert Lab at the University of Basel but did not reveal a specific patterning phenotype.



Thesis Figure 12. Postsynaptic Formin 3 RNAi knockdown caused fused clusters of glutamate receptors.

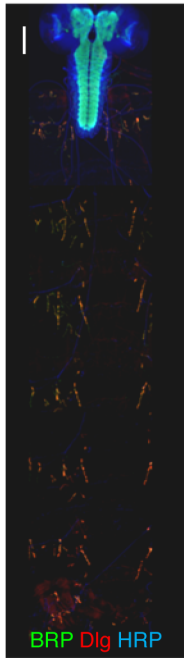
(A) A wild-type NMJ at muscle 4 is shown. The presynapse is marked by the active zone protein BRP (green) and the postsynapse by GluRIII glutamate receptor clusters (red). The neuronal membrane is visualized by HRP (blue and white in larger panels). Synaptic boutons are accurately organized. **(B)** Upon postsynaptic Formin 3 knockdown, the postsynaptic organization was altered. GluRIII clusters were fused and “donut-shaped”. **(A-B)** Scale bars: main panels 6 μm , enlarged panels 2 μm . **(C)** A wild-type NMJ on muscle 4 is stained for the synaptic cell adhesion molecule Fasciclin II (green). This molecule usually forms honeycomb-like structures within synaptic boutons. **(D)** Upon postsynaptic Formin 3 knockdown, the accurate organization of synaptic boutons was altered and GluRIII clusters got more predominant. **(C-D)** Scale bars: main panels 4 μm , enlarged panels 1 μm . **(E)** Quantification of the ratio of BRP puncta to GluRIII clusters. In postsynaptic Formin 3 animals, GluRIII clusters got bigger. Thus, more active zones visualized via BRP were observed per GluRIII cluster. $n = 5$ NMJs on muscle 4 of each genotype, representing 1,533 BRP puncta in wild-type and 1,604 BRP puncta in postsynaptic Formin3 knockdown animals.



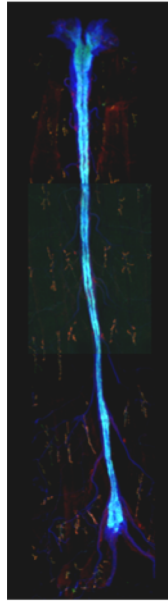
Thesis Figure 13. Pre- and postsynaptic KLHL18 RNAi knockdown caused synaptic stability defects.

(A) Displayed is a stable wild-type synapse on the ventral muscles 6/7. **(B)** Upon pre- and postsynaptic knockdown of KLHL18, synaptic stability defects were observed dispersed all over the NMJ at muscles 6/7. **(A-B)** Scale bars: main panels 10 μ m, enlarged panels 3 μ m. **(C)** Quantification of synaptic stability defects on muscles 4 and 6/7. There was no significant synaptic stability defect on muscle 4 in KLHL18 knockdown animals. But on muscles 6/7 synaptic instability was highly increased compared to wild-type animals. n = 9 wild-type animals and 12 KLHL18 knockdown animals.

A Control



B Presynaptic Chd64 RNAi



Thesis Figure 14. Presynaptic Chd64 RNAi knockdown caused elongated larval ventral nerve cord (VNC).

(A) The VNC and the NMJs in a wild-type larvae are visualized using BRP, Dlg and HRP. **(B)** Upon presynaptic Chd64 knockdown, the VNC was drastically elongated compared to wild-type animals. **(A-B)** Scale bar: 100 μ m.

3.4.3 Hits of “signaling pathways” screen

The second screen targeted 130 signaling molecules dissecting the following pathways: EGFR, ESCRT machinery (endosomal sorting), PTEN, mTOR, Hippo, Hedgehog, JAK-STAT, Non-canonical Wnt, Wnt/ β -Catenin, Notch, NF- κ B, Ras superfamily, and additional candidates. For an overview of all candidates please see Table 70. 12 of the screened proteins showed a phenotype after depletion in the motoneuron (9.2%), whereas 8 candidates displayed a phenotype after muscle-specific knockdown (6.2%). For an overview of the hits please see Table 67 and 68.

3.4.3.1 Subsequent analysis of most promising candidates

1. **Rab11 (Ras-related protein 11) (Thesis Fig. 15)**

Presynaptic knockdown of Rab11 via RNAi led to strong synapse formation and morphology defects at *Drosophila* NMJs. NMJs displayed significant overgrowth and a “bunch of grapes” morphology characterized by increased branching and smaller and less well-organised synaptic boutons (satellite boutons). Unfortunately, the Rab11 phenotype was previously identified and published by a different group (Khodosh et al., 2006).

2. **TSC1 & TSC2 (Tuberous sclerosis complex) (Thesis Fig. 16)**

These two signaling components of the insulin/mTOR signaling pathway showed strong growth and morphology defects as well as slight synaptic stability defects. Unfortunately, an analysis of TSC1 and TSC2 was published while I was working on the verification of the phenotype (Dimitroff et al., 2012; Natarajan et al., 2013).

3. **Rab5 (Ras-related protein 5) (Thesis Fig. 17)**

The presynaptic RNAi-caused phenotype of Rab5 was characterized by prominent synaptic stability defects as well as synaptic disorganization. I was able to verify the morphology phenotype of the candidate using the hypomorphic *rab5¹* allele (Wucherpennig et al., 2003). We aimed to analyze null mutants using MARCM. With this technique, homozygous mutant clones of embryonic lethal mutations can be generated in an otherwise wild-type background. An initial

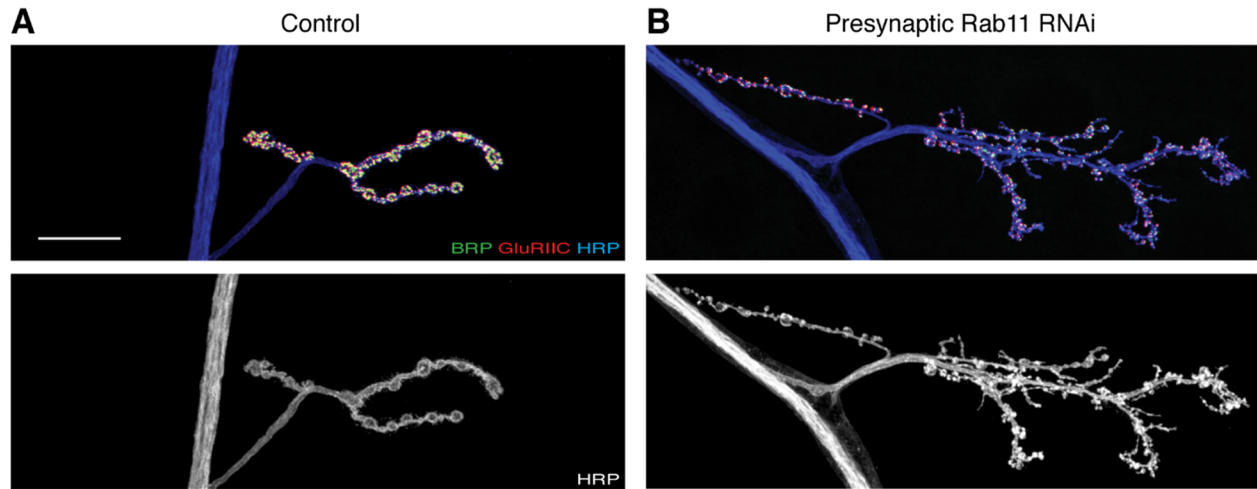
attempt failed because of incorrect MARCM stocks. Rab5 represents a strong candidate for further analysis using MARCM approaches.

4. Stat92E (Signal-transducer and activator of transcription protein at 92E) (Thesis Fig. 18)

Presynaptic knockdown of this JAK-STAT (Janus kinases & signal transducers and activators of transcription) signaling component caused synaptic stability, morphology, growth (undergrowth) and transport defects. I performed an analysis of different mutant alleles. Unfortunately, the loss-of-function phenotype of hypomorphic Stat92E alleles did not reveal as promising phenotypes as the RNAi knockdown phenotype. However, it would still be necessary to perform an analysis of *stat92E* null mutants that are embryonic lethal using the MARCM technique.

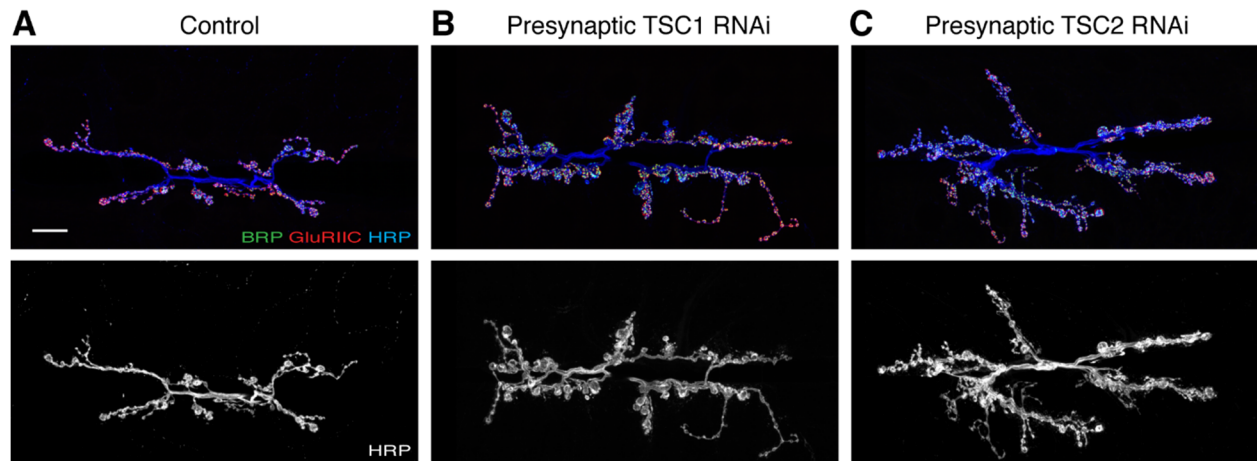
5. Myc = Diminutive (Thesis Fig. 19, 20, 21)

Myc was one of the most exciting hits from my screen as it would have been the first time to implicate a transcription factor in NMJ maintenance. Upon presynaptic Myc knockdown, I observed severe synaptic stability defects (55.8%) at larval NMJs as well as axonal transport defects and overgrowth. In order to verify the phenotype, I started to work with a subset of different mutations (plus mutants of the interaction partners Mnt and Max). Unfortunately, I was only able to partially confirm the RNAi-knockdown phenotype. Hypomorphic mutants showed only mild formation and morphology defects but no impairments in synapse stability. However, MARCM analysis of an embryonic lethal null allele failed to show any pronounced phenotype at all. While we still believe that there could be an acute requirement of Myc for synapse stability, it is very challenging to work against null-mutant phenotypes that might be compensated by redundant systems. Thus, we decided to focus instead on the analysis of Madm.



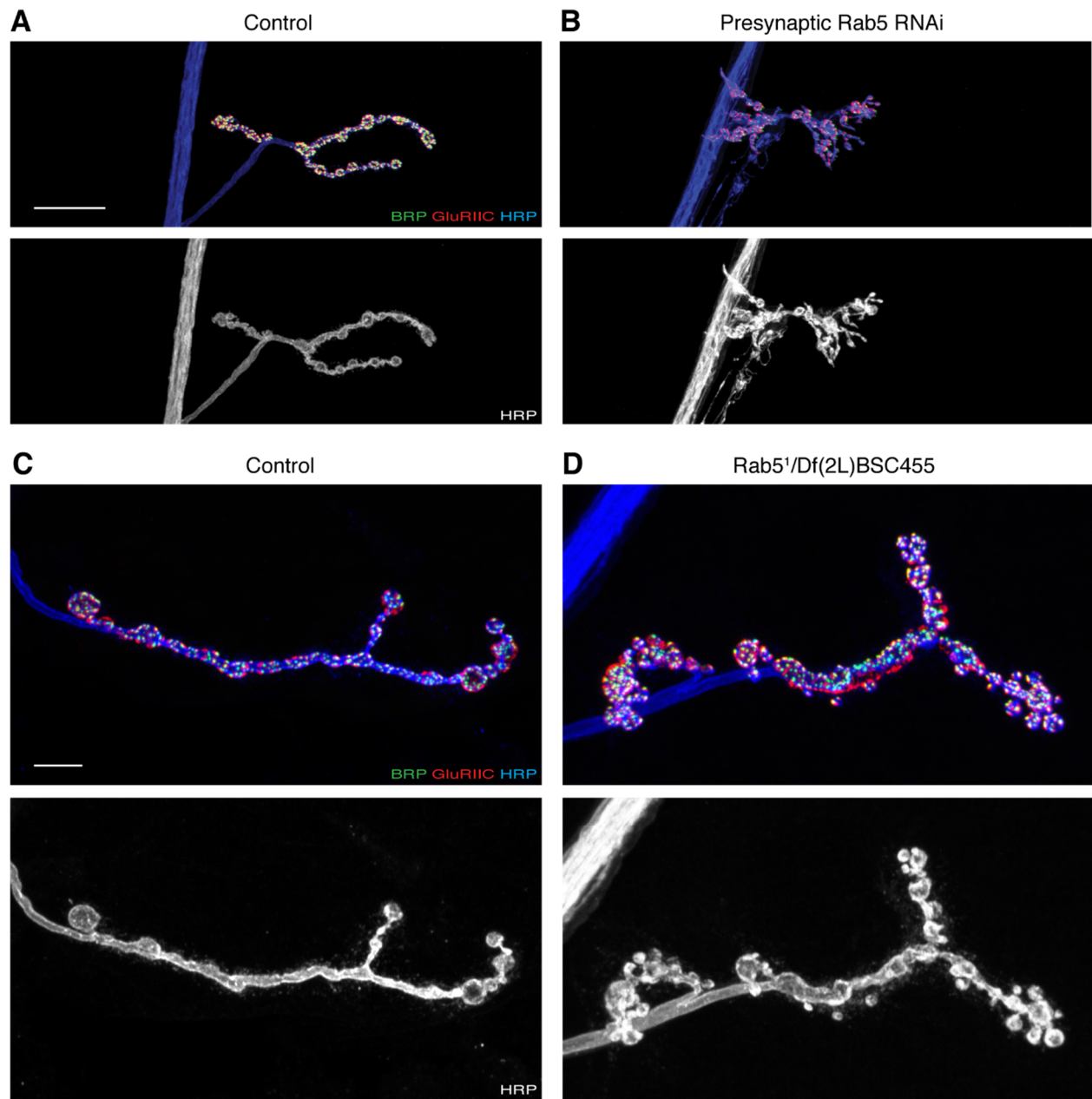
Thesis Figure 15. Presynaptic Rab11 RNAi knockdown caused morphology defects.

(A) A wild-type NMJ on muscle 4 is shown. **(B)** Upon presynaptic Rab11 knockdown, NMJ overgrowth as well as increased branching with altered “bunch of grapes” bouton morphology were observed. This results were consistent with previously published data (Khodosh et al., 2006). **(A-B)** Scale bar: 20 μ m.



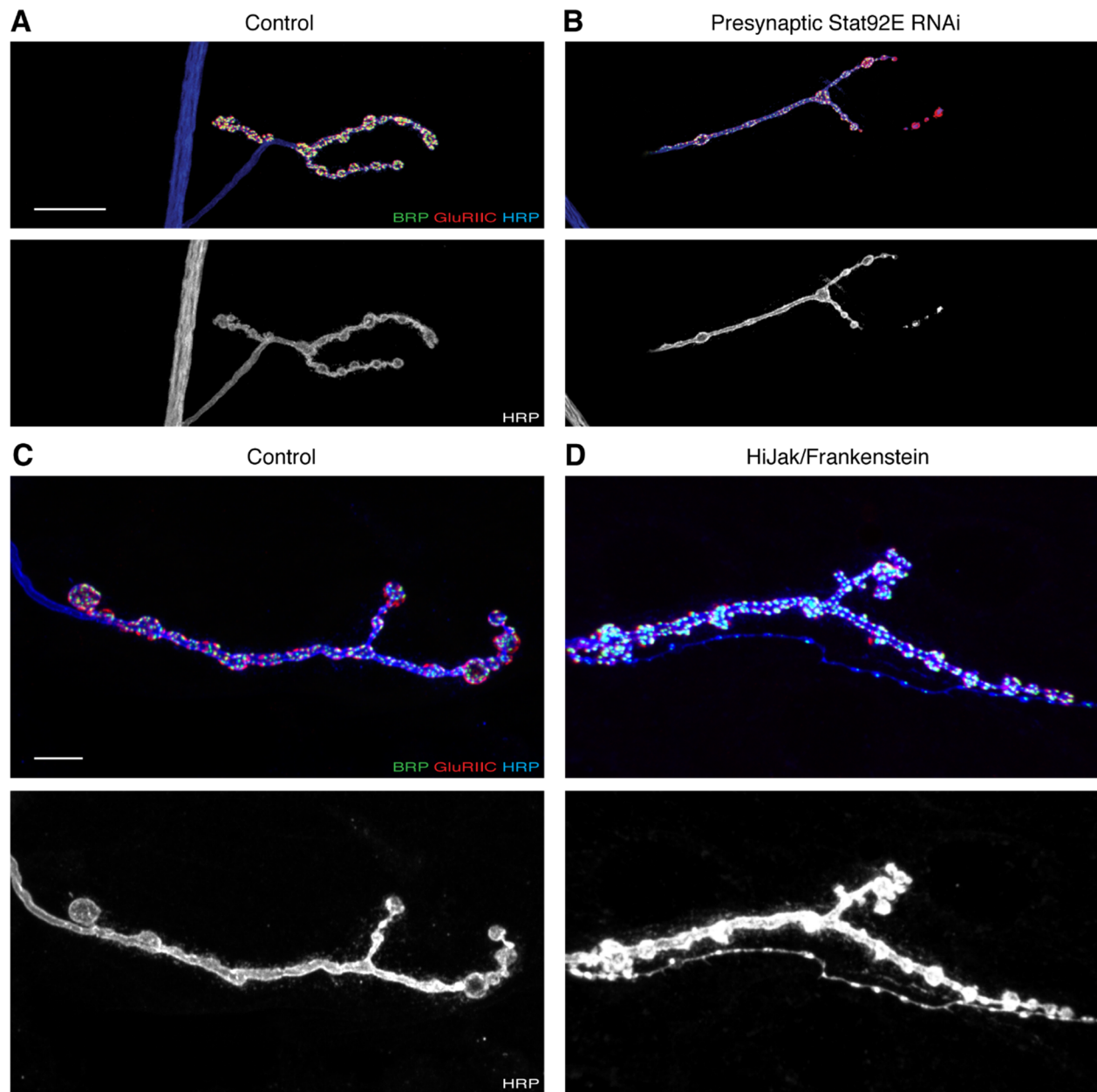
Thesis Figure 16. Presynaptic TSC1 & TSC2 RNAi knockdown caused growth and morphology defects.

(A) Displayed is a wild-type NMJ on muscles 6/7. **(B-C)** Upon presynaptic TSC1 and TSC2 knockdown, NMJ growth and morphology were highly altered. Synaptic bouton organization was affected. BRP and GluRIIC signals seemed more dispersed. NMJs appeared to be overgrown, forming more NMJ branches and more synaptic boutons. **(A-C)** Scale bar: 10 μ m.



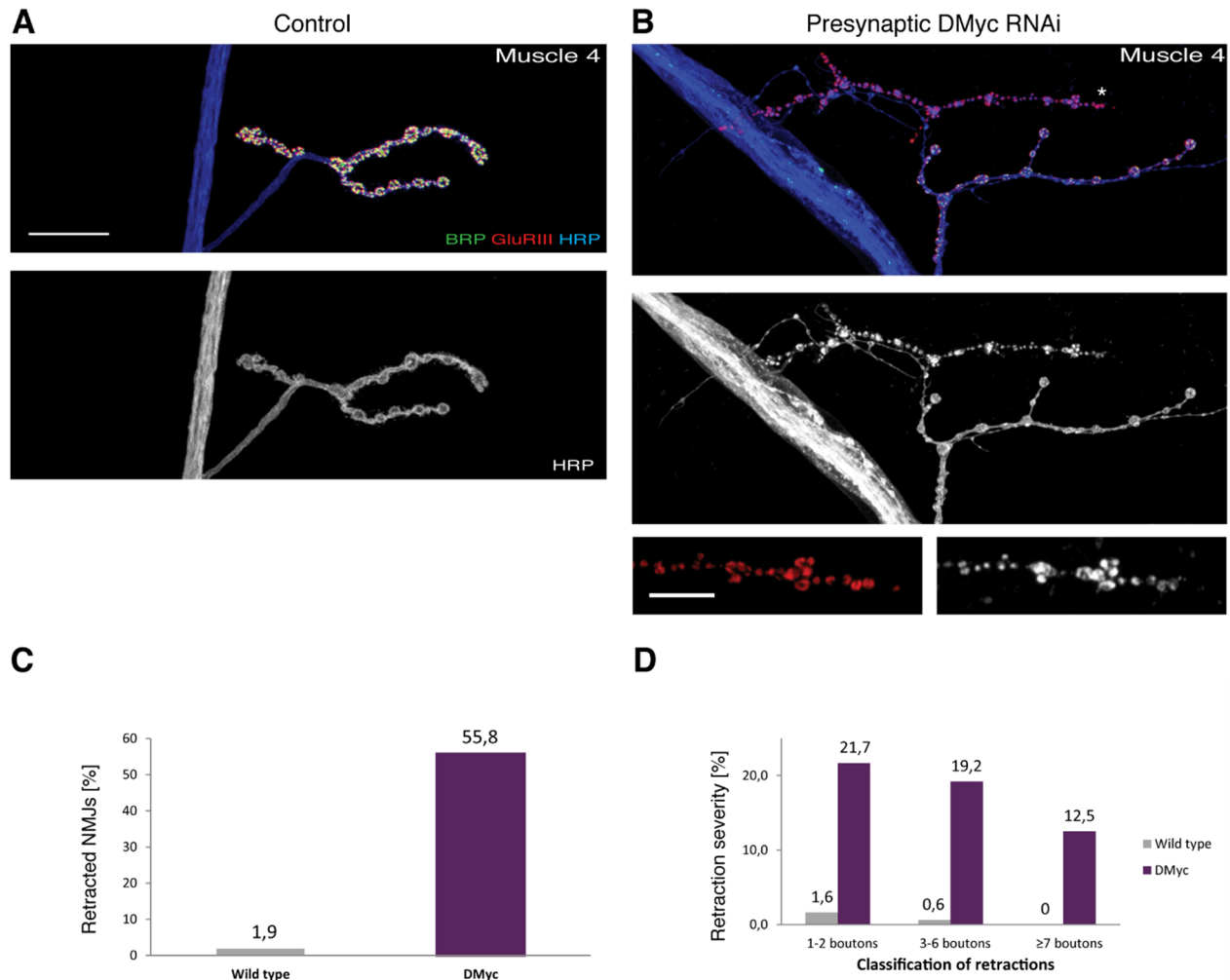
Thesis Figure 17. Presynaptic Rab5 RNAi knockdown caused synapse organization defects.

(A) A wild-type NMJ on muscle 4 is shown with precise synaptic organization. **(B)** Upon presynaptic Rab5 knockdown, NMJ morphology and synaptic bouton organization were highly altered. NMJ displayed more branches and was slightly undergrown. **(A-B)** Scale bar: 20 μ m. **(C)** Displayed is a wild-type NMJ on muscle 4. **(D)** The RNAi knockdown phenotype was verified in Rab5¹/Df animals. **(C-D)** Scale bar: 7 μ m.



Thesis Figure 18. Presynaptic Stat92E RNAi knockdown caused synaptic stability, morphology, growth and transport defects.

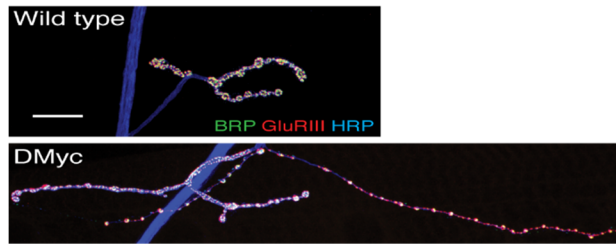
(A) A stable wild-type NMJ on muscle 4 with precise opposition of presynapse (BRP, green) and postsynapse (GluRIIC, red). The neuronal membrane was intact (HRP, white). **(B)** Upon presynaptic Stat92E knockdown, synaptic instability occurred at the NMJs. The presynapse was retracting leaving the postsynapse behind. The neuronal membrane got fragmented and partially degraded. Furthermore, BRP accumulations within axons were observed (data not shown). **(A-B)** Scale bar: 20 μm . **(C)** A wild-type NMJ of muscle 4. **(D)** In animals of the Stat92E HiJak/Frankenstein mutant background, bouton morphology was altered. **(C-D)** Scale bar: 7 μm .



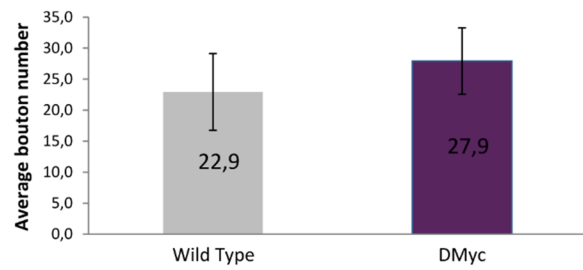
Thesis Figure 19. Presynaptic Myc RNAi knockdown caused synaptic stability, growth and transport defects.

(A) Displayed is a stable, precisely organized NMJ of muscle 4. **(B)** Upon presynaptic Myc knockdown, severe synaptic instability was observed. The presynapse was completely eliminated in the upper part of the NMJ (*). Furthermore, a transport defect, marked by the accumulation of BRP in the axon, was observed. **(A-B)** Scale bars: main panels 20 μm , enlarged panels 5 μm . **(C-D)** Quantification of synaptic retraction frequency and severity of NMJs on muscles 6/7, 12, 13 and 4. Presynaptic Myc RNAi knockdown resulted in a synaptic retraction frequency more than 29-times higher than in wild-type animals. The severity of the observed synaptic retractions was also increased, as a substantial amount of medium (3 - 6 boutons affected) and large (≥ 7 boutons affected) retractions were observed. $n = 320$ NMJs of wild-type and 120 NMJs of Myc knockdown animals.

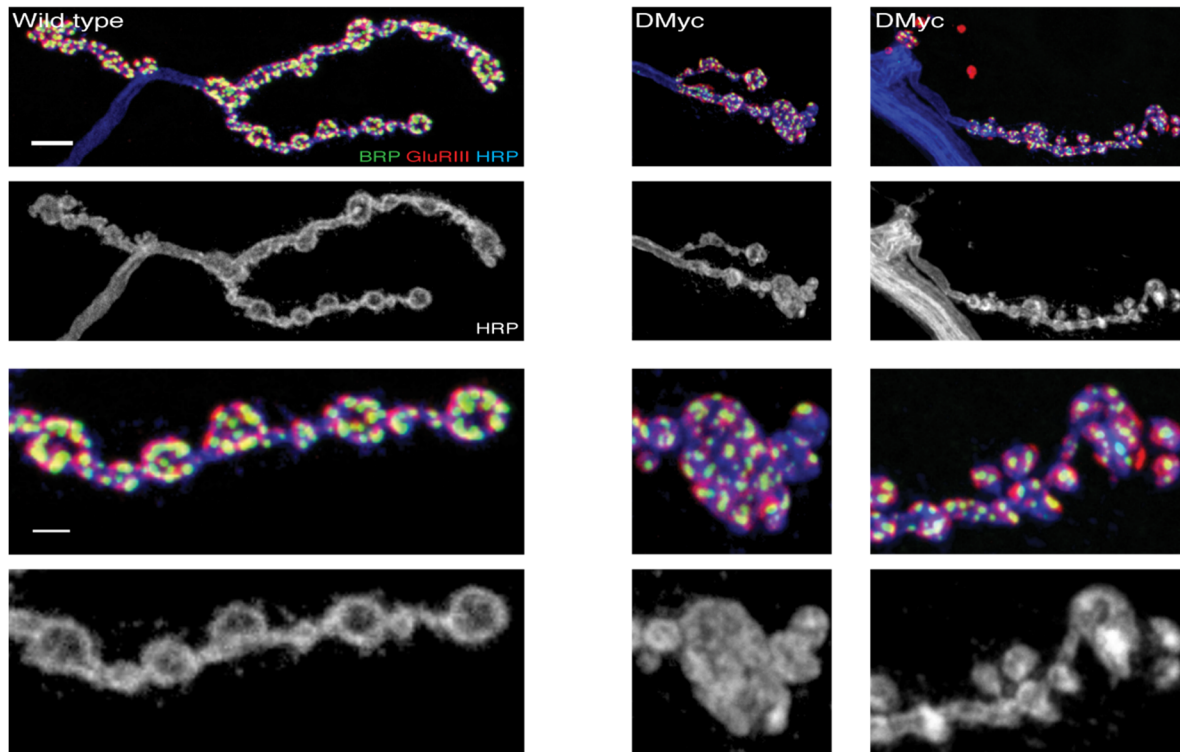
A Hypomorphic mutants - Overgrowth phenotype



B Quantification overgrowth phenotype



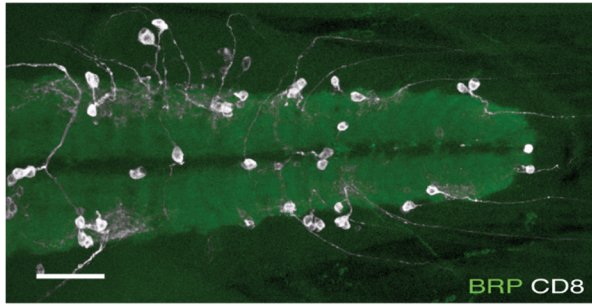
C Hypomorphic mutants - Bouton morphology & stability defects



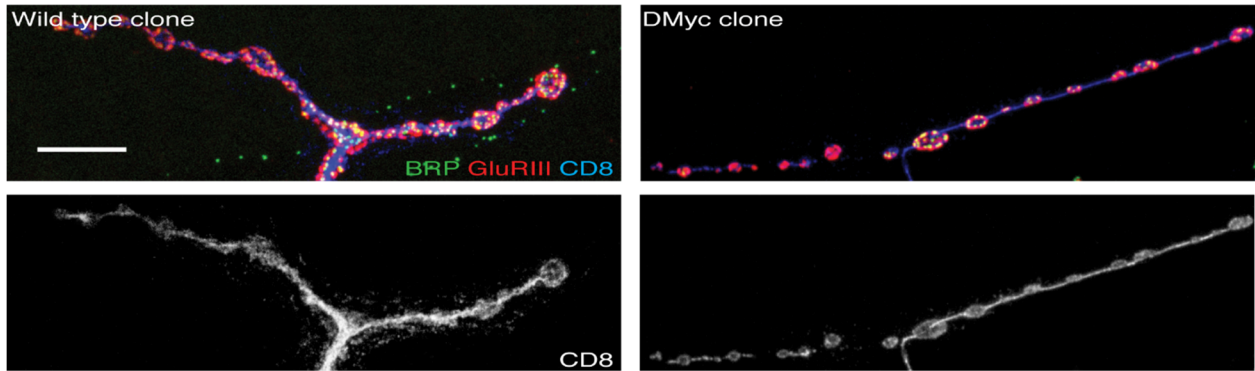
Thesis Figure 20. *Myc* hypomorph mutants caused synaptic stability, growth and morphology defects.

(A) Hypomorphic *myc* mutants displayed overgrowth phenotype compared to wild-type. Scale bar: 20 μm . **(B)** Quantification of synaptic bouton number to describe overgrowth phenotype. Average synaptic bouton number per NMJ on muscle 4 was increased. $n = 36$ NMJs (type Ib, segment A3-A5) of wild-type and 35 NMJs of *Myc* hypomorph animals. Error bars represent SEM. **(C)** Hypomorphic *myc* mutants displayed mild synaptic stability and bouton morphology defects. Scale bars: main panels 5 μm , enlarged panels 2 μm .

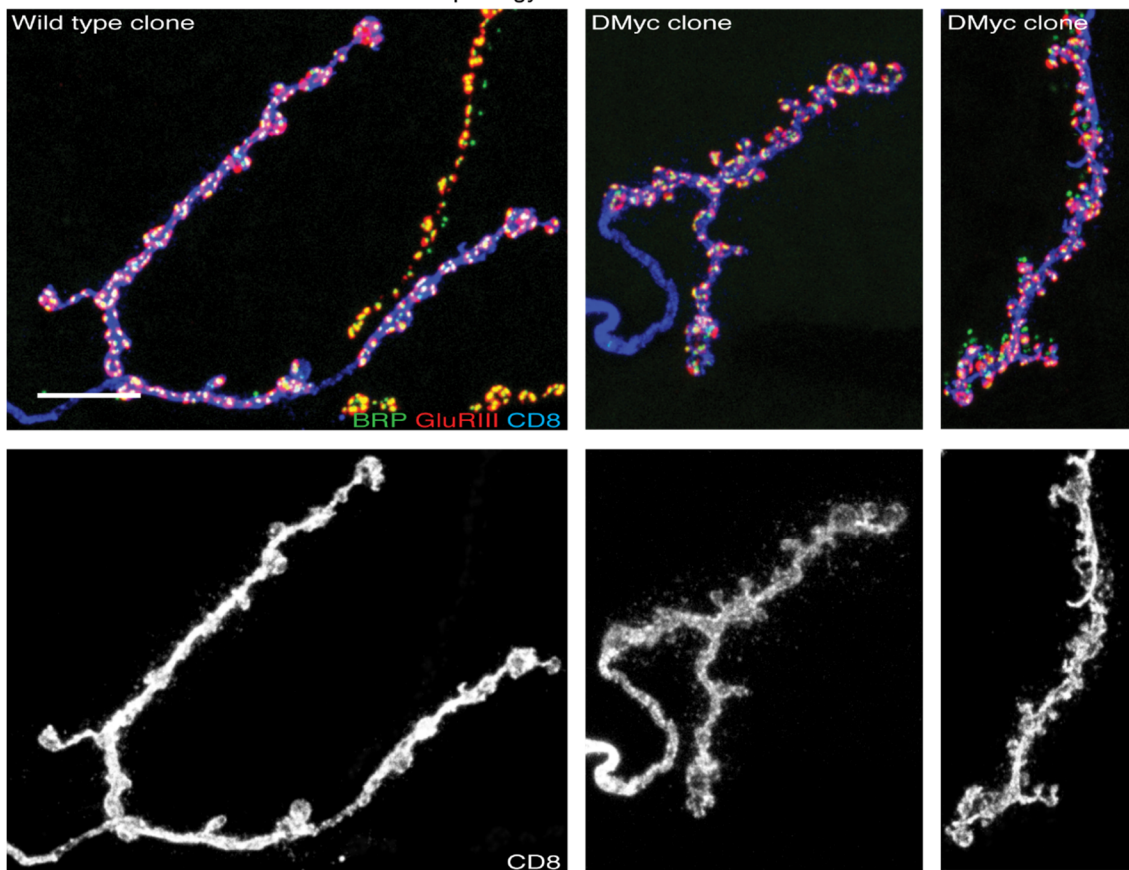
A Myc null allele MARCM clones



B Motoneuron clones - Stability defect



C Motoneuron clones - Bouton morphology



Thesis Figure 21. MARCM analysis of an embryonic lethal *myc* null allele did not show any pronounced phenotype.

(A) Homozygous mutant MARCM clones of *myc* null allele marked by CD8 (white) in central nervous system (CNS). Neuropile is visualized by BRP. Scale bar: 50 μm . **(B)** In homozygous *Myc* mutant motoneuron clones, I observed mainly minor synaptic retractions and mild synaptic bouton morphology defects. Scale bar: 10 μm . **(C)** The motoneuron clones displayed only slightly altered synaptic bouton morphology compared to controls. Scale bar: 10 μm .

3.5 Characterization and localization of the Ankyrin2 isoforms & establishment of live-imaging

Ankyrin 2 (Ank2) is an adaptor molecule for the cytoskeleton and other molecules at the *Drosophila* NMJ and mediates stability on the presynaptic side (Pielage et al., 2008). In order to investigate when and where different Ankyrin 2 (Ank2) isoforms are involved in synapse formation, maintenance and retraction, I cloned different fluorescently tagged Ank2 isoforms (Venus, Cerulean, RFP, td-EosFP (for photoconversion)). As the *ank2* locus is larger than 90 kb, I used BAC cloning & recombineering (P[acman] system; (Venken et al., 2006; Venken et al., 2009)). A main part of this work was to set-up and fine tune the recombination protocol to obtain the tagged molecules. Subsequently, I injected the generated constructs into flies to create transgenic animals expressing the constructs.

To gain insights into the cellular dynamics underlying synapse retractions, I started to set up the parameters and equipment to establish live-imaging in *Drosophila* larvae for the lab. Unfortunately, the expression levels of the tagged Ank2 isoforms in the transgenic animals were too low to perform live-imaging. Therefore, I stopped to work on this projects.

4. Discussion

4.1 Additional analysis of Madm & outlook

Please also see the discussion section of the manuscript.

4.1.1 Varicosities at nerves in Madm mutant animals

I already tried to assess the nature of the observed varicosities present at nerve bundles of *madm* mutants in more detail. Despite the presence of microtubule alterations at these sites, I did not observe any evidence for severely impaired axonal transport. Perineurial and subperineurial glial processes are present at the *Drosophila* larval NMJ (Brink et al., 2012). Thus, it might be worth to determine the type of glia around the varicosities. For this purpose, different Gal4 drivers could be used - like c527-Gal4 for perineurial glia, SPG-Gal4 or Gli-Gal4 for subperineurial glia or Mz97-Gal4 specifically for wrapping, subperineurial glia - to visualize subsets and - types of glia that may be specifically affected (Schmidt et al., 2012). In addition, rescue experiment using these specific set of driver lines could be tested. Even though it has to be said that it seems unlikely that re-expression of Madm only in a subset of glial cells could revert the phenotype. But as we still know very little about the functions and interactions of glial cells at *Drosophila* axons and at the NMJ, these experiments might result in new insights. Furthermore, a similar varicosity phenotype was observed upon Kinesin heavy chain (Khc) knockdown (Schmidt et al., 2012). In this case, maldistributed mitochondria and mislocated septate junction proteins were observed within the swellings. Hence, the accumulation of mitochondria and septate junction proteins in the bulges of the Madm mutant animals should be monitored.

4.1.2 Additional data on Madm

When analyzing the muscle size, I observed an increase of around 130% compared to control in all of my pan-neuronal rescue experiment using elav-Gal4. This effect might be explained by the following considerations. As those animals display a rather complete rescue of synaptic stability defects and have synaptic stability frequencies comparable to controls, they simply have larger,

more functional NMJs. As the development of the NMJ as well as of the corresponding muscle is depending on activity, the enlarged muscles might be explained via positive feedback between the pre- and postsynaptic side. In addition, compensatory mechanisms might act in order to overcome the functional consequences on Madm mutant NMJs as also Madm mutant animals display slight increases in muscle size. Furthermore, as Madm might be simply involved in growth control in general (Harvey, 2010), manipulation of Madm levels might have an impact on growth rates per se.

The accumulation of the active zone marker BRP in nerves and axons could be investigated in more detail. I prepared fly stocks which can be used for live-imaging experiments to monitor the rate of Synaptotagmin (vesicles are transported along microtubules) and BRP transport in axons of control and Madm mutant animals. These experiments could also help to answer the question, whether BRP accumulates due to defects of anterograde or retrograde transport. It could also be the case that BRP has to be transported in a retrograde manner from retracting nerve terminals in order to be degraded or recycled.

It would be interesting to perform electrophysiological recordings at Madm mutant larval NMJs to analyze whether the morphology and synaptic stability defects have an impact on NMJ functionality. This approach is limited by the fact, that the observed morphological as well as synaptic stability defects are more pronounced on the dorsal muscles. In contrast, electrophysiological records are usually performed on ventral muscles like muscles 6/7. Nevertheless, it might be worth testing how the observed changes at the Madm mutant NMJ relate to its functionality.

In order to understand the mode of action of Madm at the NMJ better, its specific functions and interactions on the pre- and postsynaptic side should be determined in more detail. Upon postsynaptic expression of Madm in Madm mutant animals, we observed a significant rescue of synaptic stability and morphology defects. However, it has to be excluded that any observed rescue was caused by a basal level of expression of the UAS-Madm construct even in the absence of a Gal4 driver ("leaky expression") which would explain the partial rescue observed in these animals.

4.1.3 Mlf and BunA genetically interact with Madm to modulate synaptic stability and morphology phenotype

In *mlf* mutants, I observed stronger axonal transport defects compared to *Madm* mutant animals. BRP as well as DVGluT-containing vesicles accumulated in axons of *mlf* mutants. Thus, it would be interesting to analyze this axonal transport using live-imaging approaches.

We found genetic evidence that the interaction between *Mlf* and *Madm* contributes to the control of synapse stability. When one copy of *Madm* (*2D2/+*) was removed in homozygous, zygotic *mlfΔC1* mutant animals, the frequency and severity of synaptic retractions increased significantly (4.2% to 25.0%; Fig. 7 in manuscript). In addition to the analysis of synapse stability, I also performed an analysis of morphological phenotypes. Again, I could observe an interaction between the two genes. Upon removal of one *mlf* copy (*mlfΔC1/+*) in the *Madm* mutant animals, the number of synaptic boutons as well as the total NMJ length further decreased significantly. The NMJ area was slightly reduced, but not significantly. I already started a morphological analysis of different mutant *Mlf* and *Madm* combinations to check for further interactions. This analysis should be completed in future to allow conclusions on how *Mlf* and *Madm* interact to modulate NMJ morphology.

As the *bun 200B* allele affects all of the six Bunched isoforms present in *Drosophila*, the analyses of additional combinations of *bun* alleles will tell if the observed effects are specifically caused by the long BunA isoform. I already tried to address this question using the combination of *Bun 149/GE*. This combination was previously used for the analysis of growth-related defects (Gluderer et al., 2008). The *bun 149* allele was generated via imprecise excision of the GE P element. Thus, it cannot be excluded that there are background hits in this genetic combination affecting other genes. So, unfortunately no confident conclusions can be drawn from this experiments regarding the specific effects of BunA. Thus, I included the analysis of the *bun 200B/GE* combination into the paper manuscript.

The morphological analysis of the interaction between BunA and Madm is still missing. This data should be included into the final manuscript to make a valid and complete statement about the genetic interaction of Madm and BunA regarding synapse morphology.

For the detailed analysis of Madm, I did not only perform pre- and postsynaptic rescue experiments. In addition, I also tried to rescue the Madm phenotype in all tissues except the nervous system. For these experiments, I used a Gal80 construct under the control of the elav promoter. The elavGal80 construct was combined with da-Gal4 which drives ubiquitous expression of UAS constructs throughout the entire animal. Synaptic stability as well as BRP transport defects in those animals were improved (not quantified, data not shown). The morphological defect was only slightly rescued (not quantified, data not shown). Again, potentially leaky expression of the used UAS-Madm construct has to be excluded before we can make final statements regarding the requirements of Madm outside the nervous system. Furthermore, I tried to rescue the Madm mutant phenotypes using ubiquitous da-Gal4 expression. However, I did not obtain any larvae in these crosses. Similarly, overexpression of Madm via da-Gal4 resulted in only few animals that died as first instar larvae. Hence, a precise control of Madm levels seems to be crucial - especially in the nervous system, as ubiquitous Madm expression seems to affect viability of the embryo or larvae.

4.2 Hits of RNAi-based genetic screens

Interestingly, there was one candidate which I hit in both of my screens using different RNAi lines. This candidate was Dishevelled Associated Activator of Morphogenesis (DAAM). Upon presynaptic knockdown of DAAM, minor morphology defects were observed at the NMJ. In addition, synaptic instability and accumulation of BRP in the motoneurons were observed. But the observed phenotype was mild in comparison to other candidates. Thus, I focused on the analyses of different molecules with more prominent RNAi-mediated phenotypes.

In the “cytoskeleton, cytoskeleton-associated and transport proteins” screen, Formin 3 was the most exciting hit. Upon RNAi-mediated Formin 3 knockdown, the organization of the postsynapse was dramatically altered and GluRIII clusters were fused together. As the exact mechanism for the organization of receptors in the postsynapse remains unknown, we aimed to clarify the role of Formin 3 in this process. Unfortunately, previously published *formin 3* null mutants (Tanaka et al., 2004) did not show any GluRIII cluster phenotype. For the Formin 3 VDRC RNAi line, one potential off target is described. This off target is an uncharacterized protein (CG42265) that belongs to the family of otopetrin transmembrane proteins which were shown to be involved in calcium homeostasis in structures of the inner ear of vertebrate and teleost fish (Hughes et al., 2007; Hughes et al., 2008). Potentially, this gene has a function at the arthropod NMJ.

Another explanation might be that there are different requirements for Formin 3 comparing the conditional knockdown to the mutant animals.

The availability of enough food and nutrients is a key determinant for animal growth. Two signaling pathways have been intensively studied for their role in organismal and cell growth in response to nutritional intake: the TOR kinase and the insulin/PI3K kinase signaling pathway. This insulin/mTOR signaling network is the main sensor and mediator of cellular nutrients (Hietakangas et al., 2009). Thus, this signaling network is a key regulator of cell size and proliferation as well as tissue growth (Hietakangas et al., 2009). One mode of action of these pathways is the regulation of expression of metabolic genes via different transcription factors like Myc, FOXO (Forkhead box class 'O') and DREF (DNA replication related element binding

factor) (Killip et al., 2012). Especially, the expression of genes for protein synthesis can be regulated (Killip et al., 2012). The protein kinase TOR mediates its effects mainly through the control of protein synthesis via ribosomal S6 kinase (S6K). For example, flies with limited access to food will have reduced body sizes. This effect can be as drastic as a reduction of more than half the normal body size (Hietakangas et al., 2009). The insulin-like peptides are hormones acting via the PI3K (phosphatidylinositol 3-kinase)/AKT (=PKB (protein kinase B)) pathway.

In *Drosophila*, the TOR pathway as well as the insulin/PI3K pathway were also previously shown to regulate NMJ growth and morphology (please see discussion section of manuscript). Interestingly, I hit many genes in my RNAi-based screen which are part of or are associated with this signaling network. In my screen, TSC1 and TSC2 as well as the transcription factor Myc displayed prominent phenotypes affecting NMJ morphology and synaptic stability. Unfortunately, the phenotype and effects of TSC1 and TSC2 at the *Drosophila* NMJ were published while I tried to verify them (Dimitroff et al., 2012; Natarajan et al., 2013). In contrast to the strong RNAi phenotype, the analysis of homozygous mutant motoneuron clones of an embryonic lethal *myc* null allele did not show pronounced alterations at the NMJ. This difference between acute and permanent loss of Myc could be potentially explained by redundancy and compensatory mechanisms taking over the important function of Myc within these cells.

Furthermore, I also observed a pronounced synaptic morphology phenotype upon presynaptic knockdown of phosphatidylinositol 4-kinase III alpha (PI4KIII alpha). PI4KIII alpha was already published to show NMJ growth defects in *Drosophila* (Khuong et al., 2010). PI4KIII alpha was shown to mediate localization and activation of presynaptic Wiscott-Aldrich syndrome protein/WASP (WSP). WASP is known to mediate actin dynamics (Vartiainen et al., 2004). In this study, a model was proposed that WSP and PI4KII alpha mediate signaling at the presynapse which results in the control of actin-dependent NMJ growth. This signaling cascade was suggested to be at least partially independent or parallel to TGF- β /BMP signaling, as PI4KIII alpha functions independent of the BMP signaling molecules Nervous wreck (NWK) and the TGF- β type II receptor Wishful thinking (Wit) which were shown to control NMJ growth as well as synaptic stability (Aberle et al., 2002; McCabe et al., 2003; Eaton et al., 2005).

To sum it up, I identified many promising hits in my RNAi-based genetic screens from different growth-regulating signaling pathways like the insulin/mTOR network. Unfortunately, some very promising candidates were published previously or while I was working on their verification. Thus, I focused my work mainly on the analysis of Madm.

5. Material & Methods

Please also see manuscript “Madm Controls Synapse Development and Stability”.

5.1 Additional fly stocks used in this thesis

Flies were maintained on standard fly food. RNAi lines were obtained from the Vienna *Drosophila* RNAi center. Fly stocks are listed in the appendix. Crosses with VDRC RNAi stocks for genetic screens were set up at 27°C, unless otherwise indicated. All other crosses were performed at 25°C.

The following fly stocks were used: da-Gal4, elav^{C155}-Gal4; sca-Gal4, MEF2-Gal4, BG57-Gal4, UAS-dicer2, UAS-CD8-GFP, P(neoFRT)19A (all obtained from the Bloomington *Drosophila* Stock Center) and elav-Gal80 (Sean Sweeney, University of York, UK).

In addition, the *bun*¹⁴⁹ (Gluderer et al., 2008) was used for analysis of BunA.

Verification of RNAi-based screen hits

- Formin 3: *form3*^{Em31} and *form3*^{Em41} (Tanaka et al., 2004);
- Rab5: *rab5*¹ (Wucherpfennig et al., 2003); *rab5*² FRT40A (Lu et al., 2005); Df(2L)BSC455 (Bloomington *Drosophila* Stock Center);
- Stat92E: *stat92E*⁰⁶³⁴⁶ (Perrimon et al., 1996); *stat92E*^{HJ} = Hijak (Yan et al., 1996); *stat92E*^F = Frankenstein (Baksa, 1997) (all Bloomington *Drosophila* Stock Center);
- Myc: *dm*¹; *dm*^{P0}; *dm*^[G0139]; *dm*^[BG02383]; Df(1)Exel6233 (all Bloomington *Drosophila* Stock Center); *dm*⁴ FRT19A (Steiger et al., 2008);

Test of putative Madm interactors

- Elongin-B: *elongin-B*^{EP3132}; *elongin-B*^{EY04022} (both Bloomington *Drosophila* Stock Center);
- CSN-5: *csn5*^{D148-5}; UAS-CSN5^{D148-5}; UAS-CSN5 (Wu et al., 2005);
- S6K: *s6k*^{l1}; *s6k*⁰⁷⁰⁸⁴; UAS-S6K(act) (Montagne et al., 1999);
- Stat92E: see above

5.2 Additional antibody used for immunohistochemistry

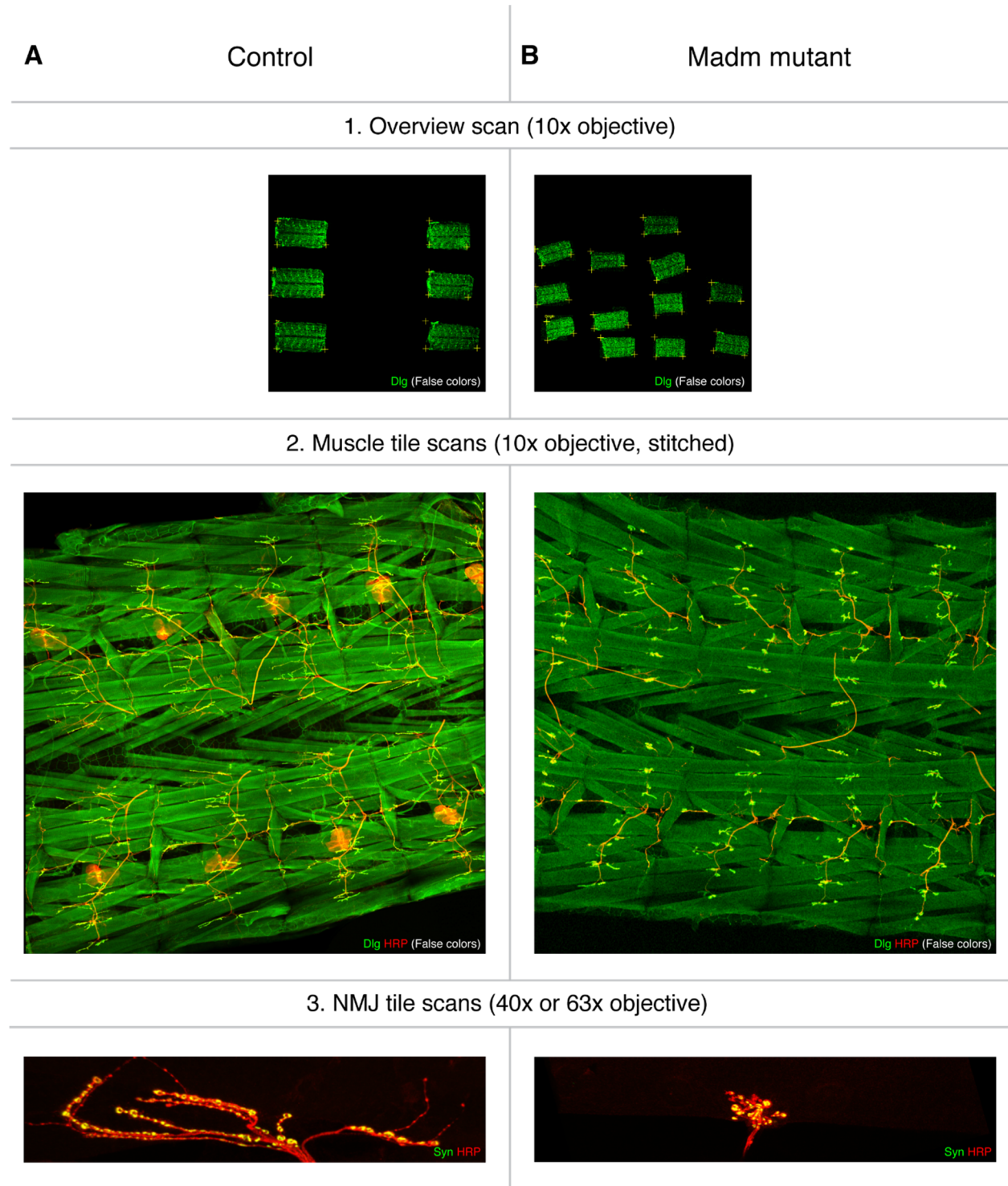
- rat anti-CD8, 1:1,000, Invitrogen
- anti-Fasciclin II (1D4), 1:10, Developmental Studies Hybridoma Bank, Iowa

5.3 Mosaic analysis with a repressible cell marker (MARCM)

Crosses were set up at 25°C with about 80 - 100 virgin females and about 30 males, 3 to 4 day in advance to the actual experiment. The P(hsFLP)1, P(neoFRT)19A, tubGal80; OK371-Gal4, UAS-CD8-GFP; MKRS, P(hsFLP)86E stock was crossed to FRT19A stock of mutant and P(neoFRT)19A stock as control in parallel. Flies were moved into fresh vial for 2.5 hours of egg laying at 25°C. Then embryos were aged for additional 2.5 hours at 25°C. A heat shock was applied for 1 hour at 38.5°C in a water bath. Embryos were transferred to 18°C incubator overnight. Subsequently, vials were put at 25°C.

5.4 Image acquisition for quantification of synapse growth and morphology

Please see material & methods section of the manuscript “Madm Controls Synapse Development and Stability”.



Thesis Figure 22. Image acquisition of synapse morphology and growth.

Images of different steps of acquisition are shown for controls (A) and Madm mutant animals (B). The LIC macroLib Zen2012 (Life Imaging Center, Freiburg, Germany) was used for image acquisition at a Zeiss LSM700 confocal microscope. (1) Overview scans of the larvae on the microscope slide were taken for navigation with a 10x air objective. (2) Tile scans were obtained also with a 10x air objective. For measurement of muscle dimensions, those muscle tile scans were stitched using XUV Tools Profiles together with custom-written Fiji (ImageJ) applications. (3) For final quantifications of synaptic morphology and growth, scans of *Drosophila* NMJs were done using oil lenses with 40x/1.4 NA and 63x/1.4 NA magnifications.

5.5 Buffers & solutions

Standard fly food (45 L): 195 g “Faden”-agar and 120 g USB-agar were boiled in 15 L water. Subsequently, 3210 g cornmeal, 720 g dry yeast, 405 g soy meal, 3210 g malt extract and 900 g treacle were added. All ingredients were mixed and cooked for 10 min. The mixture was chilled to 72 °C by adding 15 L of crashed ice. Water was added until the final volume of 45 L was reached. Finally, 160 ml propionic acid and 96 g nipagin in 500 ml ethanol were added. The mixture was stirred for 10 min and then filled into vials.

Dissection saline (without calcium) 1x (1 L): 4.0 g NaCl, 4.1 g MgCl₂ · 6H₂O, 0.36 g KCl, 1.2 g HEPES, 0.8 g NaHCO₃, 39.2 g sucrose and 40 ml EGTA (0.5 M) were dissolved in 900 ml of water. The pH was adjusted to 7.0. Solution was filled up with water to 1 L.

10xPBS (1 L): 76 g NaCl, 9.9 g Na₂HPO₄ and 4.1 g NaH₂PO₄ were dissolved in 900 ml water. After adjustment to pH = 7.3, volume was filled up to 1 L. Solution was filled into bottles and autoclaved. 1x PBS working concentration was obtained by dilution with bi-distilled water.

10xPBT (1 L): 1L 10xPBS solution was prepared and 10 ml Triton X-100 were added. The pH was adjusted to pH = 7.3. Solution was filled into bottles and autoclaved. 1x PBT working concentration was obtained by dilution with bi-distilled water.

NP-40 lysis buffer: A solution of 150 mM NaCl, 1% NP-40 and 50 mM Tris-HCl (pH = 7.5 - 8) was prepared and stored at 4°C. Before use, 1 tablet protease inhibitor (EDTA-free, Roche) was added to 10 ml of buffer. Solution was kept on ice during use.

5.6 Chemicals, consumables & equipment

These were used from the following companies:

- Agilent Technologies (Santa Clara, CA, USA)
- Bio-Rad Laboratories GmbH (Munich, Germany)
- Carl Roth GmbH (Karlsruhe, Germany)
- Carl Zeiss AG (Jena, Germany)
- Eppendorf (Hamburg, Germany)
- Fisher Scientific (Waltham, MA, USA)
- Greiner Bio-One GmbH (Frickhausen, Germany)
- Invitrogen (Paisley, UK)
- Leica Microsystems GmbH (Solms, Germany)
- MBI Fermentas (Vilnius, Lithuania)
- Millipore (Bedford, USA)
- New England Biolabs (Ipswich, USA)
- Promega (Madison, WI, USA)
- Roche Diagnostics GmbH (Mannheim, Germany)
- Sigma-Aldrich GmbH (Steinheim, Germany)
- VWR (Radnor, PA, USA)

6. Appendix

6.1 Supplementary Tables

Significance levels and p-values of analyzed parameters

Statistical analyses were performed using Microsoft Office Excel combined with an online source for unpaired Student's *t* test (<http://studentsttest.com>). P-values for the different measured phenotypical categories and genotypes are given below. Significance levels were defined as following: *** $p \leq 0.001$, ** $p \leq 0.01$; * $p \leq 0.05$ and n.s. (not significant) $p > 0.05$.

Madm, Mlf or BunA mutant allelic combination as well as protein overexpressions were always compared to the control. Rescues were compared to the corresponding mutant condition. Exceptions would be indicated especially.

6.1.1 Tables for figures of manuscript

Table 1. Madm - Retraction frequency on muscle 1 (ad Figure 1 I).

Genotype	Retraction frequency [%]	P-value	n [# animals]	n [# NMJs]
Control	0 ± 0		10	71
PreRNAi	47.5 ± 5.3	1.06E-08	10	73
EP/EP	46.3 ± 5.5	4.27E-08	10	74
EP/Df	41.3 ± 6.9	7.76E-06	10	75
2D2/Df	38.8 ± 10.1	0.00088	10	74
4S3/Df	77.5 ± 5.6	3.28E-11	10	78
elav EP/Df rescue	6.3 ± 3.1	0.00019	10	72
elav 2D2/Df rescue	2.5 ± 1.7	0.00172	10	78
OK371 2D2/Df rescue	10 ± 2.5	0.00999	10	77
elav 4S3/Df rescue	17.5 ± 5	1.85E-07	10	75
elav; UAS-Madm	3.8 ± 2.1	0.06583	10	74

Table 2. Madm - Retraction severity on muscle 1 (ad Figure 1 J).

Genotype	1-2 postsynaptic profiles	3-6 postsynaptic profiles	≥ 7 postsynaptic profiles	Elimination
Control	0 ± 0	0 ± 0	0 ± 0	0 ± 0
PreRNAi	7.5 ± 3.3	18.8 ± 3.8	21.3 ± 4.9	3.8 ± 1.9
EP/EP	15 ± 5.5	13.8 ± 3.9	17.5 ± 5.3	1.3 ± 1.3
EP/Df	11.3 ± 3.5	12.5 ± 4.2	17.5 ± 5	0 ± 0
2D2/Df	16.3 ± 4.6	10 ± 4.1	12.5 ± 4.2	1.3 ± 1.3
4S3/Df	3.8 ± 2.7	13.8 ± 3.5	60 ± 5.5	3.8 ± 1.9
elav EP/Df rescue	3.8 ± 1.9	1.3 ± 1.3	1.3 ± 1.3	0 ± 0

elav 2D2/Df rescue	2.5 ± 1.7	0 ± 0	0 ± 0	0 ± 0
OK371 2D2/Df rescue	7.5 ± 2.8	1.3 ± 1.3	1.3 ± 1.3	0 ± 0
elav 4S3/Df rescue	5 ± 2	6.3 ± 2.8	6.3 ± 2.8	0 ± 0
elav; UAS-Madm	3.8 ± 1.9	0 ± 0	0 ± 0	0 ± 0

Table 3. Madm - Nerve bulges (ad Figure 2 D and E).

Genotype	Absolute value	Normalized to control [%]	P-value	n [# animals]	n [# nerves]
Control	0 ± 0	0 ± 0		6	84
2D2/Df	4.3 ± 0.6	31.2 ± 3.9	1.05E-05	6	83
elav 2D2/Df rescue	0 ± 0	0 ± 0	1.05E-05	6	86
REPO 2D2/Df rescue	0.8 ± 0.4	5.2 ± 2.4	0.0004	5	76

Table 4. Madm - Morphological parameters on muscle 1 - Number of NMJ branches (ad Figure 3 G and S3 A).

Genotype	Absolute value	Normalized to control [%]	P-value	n [# animals]	n [# NMJs]
Control	4.3 ± 0.3	100 ± 6.2		6	17
PreRNAi	3.7 ± 0.3	86.5 ± 7.2	0.17647	6	21
EP/EP	5 ± 0.5	116.4 ± 10.8	0.23577	6	23
EP/Df	7.2 ± 0.6	168.3 ± 14.8	0.00047	6	22
2D2/Df	7.8 ± 0.7	181.9 ± 16	0.0001	6	21
4S3/Df	7.2 ± 0.6	167.1 ± 13.1	0.00019	6	23
elav EP/Df rescue	4.8 ± 0.4	112.2 ± 10.4	0.00346	6	22
elav 2D2/Df rescue	4.4 ± 0.5	103.3 ± 10.5	0.00015	6	23
elav 4S3/Df rescue	4.2 ± 0.3	98.2 ± 7.5	4.13E-05	6	23
elav; UAS-Madm	4.1 ± 0.3	95.1 ± 6.6	0.60485	6	24

Table 5. Madm - Morphological parameters on muscle 1 - Number of total boutons (ad Figure 3 H and S3 B).

Genotype	Absolute value	Normalized to control [%]	P-value	n [# animals]	n [# NMJs]
Control	49.6 ± 2.5	100 ± 5		6	17
PreRNAi	29.9 ± 2.8	60.1 ± 5.7	9.65E-06	6	21
EP/EP	37.9 ± 3.1	76.4 ± 6.3	0.00854	6	23
EP/Df	28.3 ± 1.7	56.9 ± 3.5	1.09E-08	6	22
2D2/Df	36.3 ± 1.7	73.2 ± 3.4	5.36E-05	6	21
4S3/Df	25.1 ± 1.7	50.6 ± 3.4	2.66E-10	6	23
elav EP/Df rescue	34.3 ± 3.4	69 ± 6.8	0.12086	6	22

elav 2D2/Df rescue	38.4 ± 2.4	77.3 ± 4.8	0.4957	6	23
elav 4S3/Df rescue	35.1 ± 1.9	70.8 ± 3.8	0.00031	6	23
elav; UAS-Madm	38.5 ± 1.8	77.5 ± 3.7	0.0006	6	24

Table 6. Madm - Morphological parameters on muscle 1 - Total NMJ length (ad Figure 3 I and S3 C).

Genotype	Absolute value	Normalized to control [%]	P-value	n [# animals]	n [# NMJs]
Control	160 ± 9.8	100 ± 6.1		6	17
PreRNAi	109 ± 9.8	68.1 ± 6.1	0.00087	6	21
EP/EP	142.6 ± 13.4	89.1 ± 8.4	0.33142	6	23
EP/Df	100.4 ± 6.8	62.7 ± 4.3	8.88E-06	6	22
2D2/Df	104.3 ± 4.5	65.2 ± 2.8	3.08E-06	6	21
4S3/Df	86.4 ± 4.6	54 ± 2.9	7.35E-09	6	23
elav EP/Df rescue	135.2 ± 11.2	84.5 ± 7	0.01131	6	22
elav 2D2/Df rescue	150.1 ± 9	93.8 ± 5.6	6.72E-05	6	23
elav 4S3/Df rescue	147.6 ± 8.7	92.2 ± 5.4	1.61E-07	6	23
elav; UAS-Madm	151.4 ± 5.9	94.6 ± 3.7	0.42968	6	24

Table 7. Madm - Morphological parameters on muscle 1 - NMJ area/muscle area (ad Figure 3 J and S3 D).

Genotype	Absolute value [%]	Normalized to control [%]	P-value	n [# animals]	n [# NMJs]
Control	2.4 ± 0.2	100 ± 8.3		6	17
PreRNAi	1.8 ± 0.3	73.4 ± 13.3	0.11729	6	21
EP/EP	2 ± 0.2	83.5 ± 9.8	0.22569	6	23
EP/Df	1.1 ± 0.1	44.2 ± 5.1	5.71E-07	6	22
2D2/Df	1.3 ± 0.2	53.5 ± 7.6	0.00019	6	21
4S3/Df	0.8 ± 0.1	35.1 ± 3.4	1.07E-09	6	23
elav EP/Df rescue	1.7 ± 0.2	70 ± 8.9	0.01606	6	22
elav 2D2/Df rescue	2.3 ± 0.2	96.3 ± 10	0.0016	6	23
elav 4S3/Df rescue	2.3 ± 0.2	93.7 ± 9.4	5.12E-07	6	23
elav; UAS-Madm	3.5 ± 0.3	146.4 ± 12.8	0.00839	6	24

Table 8. Madm - Time course of stability on muscles 1/9 & 2/10 - Retraction frequency (ad Figure 4 E).

Genotype	Retraction frequency [%]	P-value	n [# animals]	n [# NMJs]
Control - L2 larvae	0.6 ± 0.4		10	310
4S3xDf - L2 larvae	2.2 ± 1.4	0.082	10	240
Control - L3 larvae	4.7 ± 1.5		10	301
4S3xDf - L3 larvae	80 ± 3.1	1.28E-14	10	320
L3 compared to L2 larvae				
Control		0.00798		
4S3xDf		1.28E-14		

Table 9. Madm - Time course of stability on muscles 1/9 & 2/10 - Retraction severity (ad Figure 4 F).

Genotype	1-2 postsynaptic profiles	3-6 postsynaptic profiles	≥ 7 postsynaptic profiles	Elimination
Control - L2 larvae	0.6 ± 0.4	0 ± 0	0 ± 0	0 ± 0
4S3xDf - L2 larvae	2.2 ± 0.8	0 ± 0	0 ± 0	0 ± 0
Control - L3 larvae	2.3 ± 0.7	1.3 ± 0.5	1.3 ± 0.5	0 ± 0
4S3xDf - L3 larvae	11.3 ± 2.5	17.5 ± 2.1	51.3 ± 3.3	3.1 ± 1.1

Table 10. Mlf & BunA - Retraction frequency on muscles 1/9 & 2/10 (ad Figure 6 D).

Genotype	Retraction frequency [%]	P-value	n [# animals]	n [# NMJs]
Control	4.7 ± 1.5		10	301
MlfΔC1/MlfΔC1	4.2 ± 0.9	0.78278	3	90
MlfΔC1 mat. ctr.	9.4 ± 2.3	0.14412	10	297
Bun 200B/GE	10.3 ± 3.2	0.10595	10	283

Table 11. Mlf & BunA - Retraction severity on muscles 1/9 & 2/10 (ad Figure 6 E).

Genotype	1-2 postsynaptic profiles	3-6 postsynaptic profiles	≥ 7 postsynaptic profiles	Elimination
Control	2.3 ± 0.7	1.3 ± 0.5	1.3 ± 0.5	0 ± 0
MlfΔC1/MlfΔC1	2.2 ± 1	2.2 ± 2.1	0 ± 0	0 ± 0
MlfΔC1 mat. ctr.	4.7 ± 1.3	3.4 ± 1.3	1.3 ± 0.7	0 ± 0
Bun 200B/GE	5.6 ± 1.8	2.8 ± 1	1.9 ± 1	0 ± 0

Table 12. Mlf & BunA - Morphological parameters on muscle 1 - Number of NMJ branches (ad Figure 6 I).

Genotype	Absolute value	Normalized to control [%]	P-value	n [# animals]	n [# NMJs]
Control	4.3 ± 0.3	100 ± 6.2		6	17
MlfΔC1 mat. ctr.	2.7 ± 0.2	63.8 ± 4.4	2.03E-05	6	23
Bun 200B/GE	3 ± 0.3	71 ± 6.3	0.00267	6	21

Table 13. Mlf & BunA - Morphological parameters on muscle 1 - Number of total boutons (ad Figure 6 J).

Genotype	Absolute value	Normalized to control [%]	P-value	n [# animals]	n [# NMJs]
Control	49.6 ± 2.5	100 ± 5		6	17
MlfΔC1 mat. ctr.	25.3 ± 1.8	51.1 ± 3.6	6.27E-10	6	23
Bun 200B/GE	39 ± 2.2	78.6 ± 4.4	0.00261	6	21

Table 14. Mlf & BunA - Morphological parameters on muscle 1 - Total NMJ length (ad Figure 6 K).

Genotype	Absolute value	Normalized to control [%]	P-value	n [# animals]	n [# NMJs]
Control	160 ± 9.8	100 ± 6.1		6	17
MlfΔC1 mat. ctr.	106.3 ± 7.9	66.4 ± 4.9	0.00011	6	23
Bun 200B/GE	106.3 ± 3.8	66.4 ± 2.4	3.18E-06	6	21

Table 15. Mlf & BunA - Morphological parameters on muscle 1 - NMJ area/muscle area (ad Figure 6 L).

Genotype	Absolute value [%]	Normalized to control [%]	P-value	n [# animals]	n [# NMJs]
Control	2.4 ± 0.2	100 ± 8.3		6	17
MlfΔC1 mat. ctr.	1.9 ± 0.4	78 ± 15	0.25067	6	23
Bun 200B/GE	2.3 ± 0.2	95.8 ± 6.5	0.68805	6	21

Table 16. Mlf & Madm control stability - Retraction frequency on muscles 1/9 & 2/10 (ad Figure 7 A).

Genotype	Retraction frequency [%]	P-value	Compared to	P-value	Compared to	n [# animals]	n [# NMJs]
Control	4.7 ± 1.3					10	301
MlfΔC1/+	3.4 ± 1.6	0.54191	Control			10	300
2D2/+	3.8 ± 1.3	0.53279	Control			10	297
MlfΔC1/+; 2D2/+	8.4 ± 1.6	0.07759	Control			10	301

MlfΔC1/MlfΔC1	4.2 ± 0.9	0.78278	Control			3	24
MlfΔC1/MlfΔC1; 2D2/+	25 ± 5.1	0.00021	Control	0.02107	MlfΔC1/ MlfΔC1	6	181
2D2/Df	36.6 ± 9	0.00293	Control			10	320
MlfΔC1/+; 2D2/Df	38.8 ± 4.3	1.31E-07	Control	0.53717	2D2/Df	10	289

Table 17. Mlf & Madm control stability - Retraction severity on muscles 1/9 & 2/10 (ad Figure 7 B).

Genotype	1-2 postsynaptic profiles	3-6 postsynaptic profiles	≥ 7 postsynaptic profiles	Elimination
Control	2.3 ± 0.7	1.3 ± 0.5	1.3 ± 0.5	0 ± 0
MlfΔC1/+	2.2 ± 1	0.9 ± 0.5	0.3 ± 0.3	0 ± 0
2D2/+	2.2 ± 0.9	1.3 ± 0.5	0.3 ± 0.3	0 ± 0
MlfΔC1/+; 2D2/+	4.7 ± 0.8	3.4 ± 0.6	0.3 ± 0.3	0 ± 0
MlfΔC1/MlfΔC1	2.2 ± 1	2.2 ± 2.1	0 ± 0	0 ± 0
MlfΔC1/MlfΔC1; 2D2/+	9.9 ± 1.6	11 ± 2.4	5.5 ± 2.1	0.6 ± 0.5
2D2/Df	11.9 ± 3.5	13.4 ± 3.7	11.3 ± 3.6	1.3 ± 0.5
MlfΔC1/+; 2D2/Df	19.4 ± 2.4	18.3 ± 2.6	5.2 ± 1.3	0.7 ± 0.6

Table 18. BunA & Madm control stability - Retraction frequency on muscles 1/9 & 2/10 (ad Figure 7 C).

Genotype	Retraction frequency [%]	P-value	Compared to	P-value	Compared to	n [# animals]	n [# NMJs]
Control	4.7 ± 1.3					10	301
Bun200B/+	3.4 ± 0.7	0.33451	Control			10	307
2D2/+	3.8 ± 1	0.53279	Control			10	297
Bun200B/+; 2D2/+	3.1 ± 1	0.32974	Control			10	293
Bun200B/GE	10.3 ± 3.5	0.10595	Control			10	283
Bun200B/GE; 2D2/+	5 ± 1.3	0.94153	Control	0.10642	Bun200B/ GE	10	307
2D2/Df	36.6 ± 9	0.00293	Control			10	320
Bun200B/+; 2D2/Df	11.9 ± 2.9	0.01577	Control	0.02651	2D2/Df	10	282

Table 19. BunA & Madm control stability - Retraction severity on muscles 1/9 & 2/10 (ad Figure 7 D).

Genotype	1-2 postsynaptic profiles	3-6 postsynaptic profiles	≥ 7 postsynaptic profiles	Elimination
Control	2.3 ± 0.7	1.3 ± 0.5	1.3 ± 0.5	0 ± 0
Bun200B/+	2.5 ± 0.9	0.6 ± 0.4	0.3 ± 0.3	0 ± 0
2D2/+	2.2 ± 0.9	1.3 ± 0.5	0.3 ± 0.3	0 ± 0
Bun200B/+; 2D2/+	2.2 ± 0.9	0.6 ± 0.4	0.3 ± 0.3	0 ± 0
Bun200B/GE	5.6 ± 1.8	2.8 ± 1	1.9 ± 1	0 ± 0
Bun200B/GE; 2D2/+	2.5 ± 0.6	2.5 ± 0.8	0 ± 0	0 ± 0
2D2/Df	11.9 ± 3.5	13.4 ± 3.7	11.3 ± 3.6	1.3 ± 0.5
Bun200B/+; 2D2/Df	5.9 ± 1.8	5 ± 1.2	0.9 ± 0.5	0 ± 0

6.1.2 Tables for supplementary figures of manuscript

Table 20. Madm - Retraction frequency on muscles 1/9 & 2/10 (ad Figure S1 D).

Genotype	Retraction frequency [%]	P-value	n [# animals]	n [# NMJs]
Control	4.7 ± 1.5		10	301
PreRNAi	57.8 ± 5.2	1.38E-08	10	320
EP/EP	47.8 ± 3.3	1.99E-10	10	298
EP/Df	41.6 ± 5.9	9.16E-06	10	310
2D2/Df	36.6 ± 9	0.00293	10	320
4S3/Df	80 ± 3.1	2.47E-14	10	320
elav EP/Df rescue	5.9 ± 1.9	1.97E-05	10	299
elav 2D2/Df rescue	3.4 ± 0.9	0.00181	10	312
OK371 2D2/Df rescue	7.5 ± 2	0.00583	10	310
elav 4S3/Df rescue	7.2 ± 1.7	7.56E-14	10	306
elav; UAS-Madm	3.1 ± 1	0.29062	10	313

Table 21. Madm - Retraction severity on muscles 1/9 & 2/10 (ad Figure S1 E).

Genotype	1-2 postsynaptic profiles	3-6 postsynaptic profiles	≥ 7 postsynaptic profiles	Elimination
Control	2.3 ± 0.7	1.3 ± 0.5	1.3 ± 0.5	0 ± 0
PreRNAi	12.8 ± 2.1	15.3 ± 2.5	29.7 ± 3.8	2.2 ± 0.9
EP/EP	13.8 ± 1.8	17.1 ± 2.2	20.5 ± 2.9	0.7 ± 0.4
EP/Df	10 ± 1.7	13.9 ± 2.9	19 ± 4.3	1.3 ± 0.7
2D2/Df	11.9 ± 3.5	13.4 ± 3.7	11.3 ± 3.6	1.3 ± 0.5
4S3/Df	11.3 ± 2.5	17.5 ± 2.1	51.3 ± 3.3	3.1 ± 1.1
elav EP/Df rescue	5 ± 1	1 ± 0.7	0.3 ± 0.3	0 ± 0
elav 2D2/Df rescue	2.6 ± 0.9	1 ± 0.7	0 ± 0	0 ± 0
OK371 2D2/Df rescue	4.8 ± 1.8	1.6 ± 0.8	1.3 ± 1	0 ± 0
elav 4S3/Df rescue	2.6 ± 0.6	2 ± 0.8	2.9 ± 1.3	0 ± 0
elav; UAS-Madm	2.2 ± 0.5	1 ± 0.7	0 ± 0	0 ± 0

Table 22. Madm - Retraction frequency on muscles 6/7 (ad Figure S1 F).

Genotype	Retraction frequency [%]	P-value	n [# animals]	n [# NMJs]
Control	3.8 ± 2.7		10	80
PreRNAi	42.5 ± 4.2	4.03E-07	10	80
EP/EP	43.8 ± 5	1.44E-06	10	80
EP/Df	26.3 ± 6.8	6.64E-03	10	80
2D2/Df	40 ± 6.1	3.72E-05	10	80
4S3/Df	65 ± 5.5	9.22E-09	10	80

elav EP/Df rescue	6.3 ± 2.8	1.44E-02	10	79
elav 2D2/Df rescue	7.5 ± 3.3	0.00019	10	80
OK371 2D2/Df rescue	21.3 ± 5.3	0.03245	10	80
elav 4S3/Df rescue	17.5 ± 5	5.30E-06	10	80
elav; UAS-Madm	1.3 ± 1.3	0.40729	10	80

Table 23. Madm - Retraction severity on muscles 6/7 (ad Figure S1 G).

Genotype	1-2 postsynaptic profiles	3-6 postsynaptic profiles	≥ 7 postsynaptic profiles	Elimination
Control	3.8 ± 2.7	0 ± 0	0 ± 0	0 ± 0
PreRNAi	23.8 ± 4.4	13.8 ± 3.5	5 ± 2.8	0 ± 0
EP/EP	11.3 ± 2.9	20 ± 3.8	12.5 ± 3.7	0 ± 0
EP/Df	13.8 ± 2.9	7.5 ± 3.8	5 ± 2.8	0 ± 0
2D2/Df	18.8 ± 4.3	13.8 ± 3.9	7.5 ± 3.3	0 ± 0
4S3/Df	16.3 ± 3.8	25 ± 5.3	23.8 ± 5.7	0 ± 0
elav EP/Df rescue	6.3 ± 2.8	0 ± 0	0 ± 0	0 ± 0
elav 2D2/Df rescue	6.3 ± 2.8	1.3 ± 1.3	0 ± 0	0 ± 0
OK371 2D2/Df rescue	16.3 ± 3.3	3.8 ± 3.8	1.3 ± 1.3	0 ± 0
elav 4S3/Df rescue	12.5 ± 3.7	3.8 ± 1.9	1.3 ± 1.3	0 ± 0
elav; UAS-Madm	1.3 ± 1.3	0 ± 0	0 ± 0	0 ± 0

Table 24. Madm - Axonal transport - BRP puncta (ad Figure S2 D).

Genotype	Absolute value	Normalized to control [%]	P-value	n [# animals]	n [# nerves]
Control	12.5 ± 0.4	100 ± 3		5	45
EP/EP	19.9 ± 0.9	159.1 ± 7.2	6E-12	5	37
EP/Df	18.3 ± 0.8	146.1 ± 6.7	0.00000002	5	35
2D2/Df	20.5 ± 1	164 ± 7.9	1E-11	5	40
4S3/Df	23.9 ± 0.8	191.2 ± 6.7	1.50E-21	5	40
elav 2D2/Df rescue	14.3 ± 0.7	114.4 ± 5.7	0.000002	5	42
elav 4S3/Df rescue	16 ± 0.4	127.8 ± 3.1	1.4E-14	5	51
elav; UAS-Madm	12.1 ± 0.5	96.4 ± 4.4	0.51178	5	51

Table 25. Madm - Axonal transport - DVGluT puncta (ad Figure S2 E).

Genotype	Absolute value	Normalized to control [%]	P-value	n [# animals]	n [# nerves]
Control	15.3 ± 1.3	100 ± 8.6		5	45
EP/EP	15.8 ± 0.4	103.3 ± 2.7	0.56318	5	37

EP/Df	14.3 ± 0.5	93.4 ± 3.4	0.28109	5	35
2D2/Df	13.5 ± 0.4	88.3 ± 2.9	0.04241	5	40
4S3/Df	16 ± 0.9	104.8 ± 6	0.52372	5	40
elav 2D2/Df rescue	14.6 ± 0.4	95.7 ± 2.5	0.05895	5	42
elav 4S3/Df rescue	15.8 ± 0.3	103.8 ± 2.1	0.85949	5	51
elav; UAS-Madm	13.4 ± 0.2	88 ± 1.3	0.01056	5	51

Table. 26 Madm - Time course of stability on muscles 6/7 - Retraction frequency (ad Figure S4 A).

Genotype	Retraction frequency [%]	P-value	n [# animals]	n [# NMJs]
Control - L2 larvae	1.3 ± 1.3		10	76
4S3xDf - L2 larvae	1.3 ± 1.3	0.84372	10	75
Control - L3 larvae	3.8 ± 2.7		10	80
4S3xDf - L3 larvae	65 ± 5.5	9.22E-09	10	80
L3 compared to L2 larvae				
Control		0.51619		
4S3xDf		1.42E-09		

Table 27. Madm - Time course of stability on muscles 6/7 - Retraction severity (ad Figure S4 B).

Genotype	1-2 postsynaptic profiles	3-6 postsynaptic profiles	≥ 7 postsynaptic profiles	Elimination
Control - L2 larvae	1.3 ± 1.3	0 ± 0	0 ± 0	0 ± 0
4S3xDf - L2 larvae	1.3 ± 1.3	0 ± 0	0 ± 0	0 ± 0
Control - L3 larvae	3.8 ± 2.7	0 ± 0	0 ± 0	0 ± 0
4S3xDf - L3 larvae	16.3 ± 3.8	25 ± 5.3	23.8 ± 5.7	0 ± 0

Table 28. Madm - Comparison of UAS-EGFP-Madm & UAS-Madm construct - Retraction frequency on muscles 1/9 & 2/10 (ad Figure S5 C).

Genotype	Retraction frequency [%]	P-value	n [# animals]	n [# NMJs]
Control	4.7 ± 1.5		10	301
2D2/Df	36.6 ± 9	0.00293	10	320
elav 2D2/Df rescue	3.4 ± 0.9	0.00181	10	312
elav EGFP 2D2/Df rescue	6.3 ± 1.7	0.01476	7	212
elav; UAS-Madm	3.1 ± 1	0.29044	10	313

elav; UAS-EGFP-Madm	3.4 ± 0.8	0.35664	10	313
---------------------	-----------	---------	----	-----

Table 29. Madm - Comparison of UAS-EGFP-Madm & UAS-Madm construct - Retraction severity on muscles 1/9 & 2/10 (ad Figure S5 D).

Genotype	1-2 postsynaptic profiles	3-6 postsynaptic profiles	≥ 7 postsynaptic profiles	Elimination
Control	2.3 ± 0.7	1.3 ± 0.5	1.3 ± 0.5	0 ± 0
2D2/Df	11.9 ± 3.5	13.4 ± 3.7	11.3 ± 3.6	1.3 ± 0.5
elav 2D2/Df rescue	4.8 ± 1.4	0.6 ± 0.4	0.6 ± 0.6	0 ± 0
elav EGFP 2D2/Df rescue	5.2 ± 1.7	1.4 ± 0.6	0 ± 0	0 ± 0
elav; UAS-Madm	2.2 ± 0.5	1 ± 0.7	0 ± 0	0 ± 0
elav; UAS-EGFP-Madm	1.9 ± 0.5	1.6 ± 0.7	0 ± 0	0 ± 0

Table 30. Madm - Comparison of UAS-EGFP-Madm & UAS-Madm construct - Morphological parameters on muscle 1 - Number of NMJ branches (ad Figure S5 E).

Genotype	Absolute value	Normalized to control [%]	P-value	n [# animals]	n [# NMJs]
Control	4.3 ± 0.3	100 ± 6.2		6	17
elav; UAS-Madm	4.1 ± 0.3	95.1 ± 6.6	0.60485	6	24
elav; UAS-EGFP-Madm	4 ± 0.4	93.2 ± 8.4	0.52358	6	19

Table 31. Madm - Comparison of UAS-EGFP-Madm & UAS-Madm construct - Morphological parameters on muscle 1 - Number of total boutons (ad Figure S5 F).

Genotype	Absolute value	Normalized to control [%]	P-value	n [# animals]	n [# NMJs]
Control	49.6 ± 2.5	100 ± 5		6	17
elav; UAS-Madm	38.5 ± 1.8	77.5 ± 3.7	0.0006	6	24
elav; UAS-EGFP-Madm	43.5 ± 1.3	87.6 ± 2.6	0.02821	6	19

Table 32. Madm - Comparison of UAS-EGFP-Madm & UAS-Madm construct - Morphological parameters on muscle 1 - Total NMJ length (ad Figure S5 G).

Genotype	Absolute value	Normalized to control [%]	P-value	n [# animals]	n [# NMJs]
Control	160 ± 9.8	100 ± 6.1		6	17
elav; UAS-Madm	151.4 ± 5.9	94.6 ± 3.7	0.42968	6	24
elav; UAS-EGFP-Madm	141.7 ± 7.7	88.6 ± 4.8	0.14745	6	19

Table 33. Madm - Comparison of UAS-EGFP-Madm & UAS-Madm construct - Morphological parameters on muscle 1 - NMJ area/muscle area (ad Figure S5 H).

Genotype	Absolute value	Normalized to control [%]	P-value	n [# animals]	n [# NMJs]
Control	2.4 ± 0.2	100 ± 8.3		6	17
elav; UAS-Madm	3.5 ± 0.3	146.4 ± 12.8	0.00839	6	24
elav; UAS-EGFP-Madm	2.5 ± 0.3	105.4 ± 10.7	0.69713	6	19

Table. 34 Mlf & BunA - Retraction frequency on muscles 6/7 (ad Figure S6 A).

Genotype	Retraction frequency [%]	P-value	n [# animals]	n [# NMJs]
Control	3.8 ± 2.7		10	80
MlfΔC1/MlfΔC1	4.2 ± 4.2	0.94007	3	24
MlfΔC1 mat. ctr.	15 ± 4.9	0.05746	10	79
Bun 200B/GE	11.3 ± 3.5	0.09655	10	79

Table 35. Mlf & BunA - Retraction severity on muscles 6/7 (ad Figure S6 B).

Genotype	1-2 postsynaptic profiles	3-6 postsynaptic profiles	≥ 7 postsynaptic profiles	Elimination
Control	3.8 ± 2.7	0 ± 0	0 ± 0	0 ± 0
MlfΔC1/MlfΔC1	4.2 ± 4.2	0 ± 0	0 ± 0	0 ± 0
MlfΔC1 mat. ctr.	7.6 ± 4.2	3.8 ± 1.7	0 ± 0	0 ± 0
Bun 200B/GE	12.7 ± 2.8	2.5 ± 1.9	0 ± 0	0 ± 0

Table 36. Mlf - Axonal transport - BRP puncta (ad Figure S7 D).

Genotype	Absolute value	Normalized to control [%]	P-value	n [# animals]	n [# nerves]
Control	12.5 ± 0.4	100 ± 3		5	45
MlfΔC1 mat. ctr.	20.9 ± 1.4	167.4 ± 11.4	3.00E-06	7	62

Table 37. Mlf - Axonal transport - DVGluT puncta (ad Figure S7 E).

Genotype	Absolute value	Normalized to control [%]	P-value	n [# animals]	n [# nerves]
Control	15.3 ± 1.3	100 ± 8.6		5	45
MlfΔC1 mat. ctr.	26.5 ± 1	173.7 ± 6.3	3.75E-14	7	62

Table 38. Mlf & Madm control stability - Retraction frequency on muscles 6/7 (ad Figure S8 A).

Genotype	Retraction frequency [%]	P-value	Compared to	P-value	Compared to	n [# animals]	n [# NMJs]
Control	3.8 ± 2.7					10	80
MlfΔC1/+	1.3 ± 1.3	0.40729	Control			10	79
2D2/+	3.8 ± 1.9	1	Control			10	80
MlfΔC1/+; 2D2/+	10 ± 2.5	0.10456	Control	0.10456	Control	10	80
MlfΔC1/MlfΔC1	4.2 ± 4.2	0.94007	Control			3	24
MlfΔC1/MlfΔC1; 2D2/+	20.8 ± 8.3	0.03259	Control	0.22418	MlfΔC1/MlfΔC1	6	48
MlfΔC1/MlfΔC1 mat. ctr.	15 ± 4.9	0.05746	Control			10	79
MlfΔC1/MlfΔC1; 2D2/+ mat. ctr.	20 ± 3.3	0.00129	Control	0.40729	MlfΔC1/MlfΔC1 mat. ctr.	10	80
2D2/Df	40 ± 6.1	3.72E-05	Control			10	80
MlfΔC1/+; 2D2/Df	42.5 ± 6.8	4.62E-05	Control	0.78731	2D2/Df	10	80

Table 39. Mlf & Madm control stability - Retraction severity on muscles 6/7 (ad Figure S8 B).

Genotype	1-2 postsynaptic profiles	3-6 postsynaptic profiles	≥ 7 postsynaptic profiles	Elimination
Control	3.8 ± 2.7	0 ± 0	0 ± 0	0 ± 0
MlfΔC1/+	0 ± 0	1.3 ± 1.3	0 ± 0	0 ± 0
2D2/+	3.8 ± 1.9	0 ± 0	0 ± 0	0 ± 0
MlfΔC1/+; 2D2/+	8.8 ± 2.7	1.3 ± 1.3	0 ± 0	0 ± 0
MlfΔC1/MlfΔC1	4.2 ± 4.2	0 ± 0	0 ± 0	0 ± 0
MlfΔC1/MlfΔC1; 2D2/+	18.8 ± 7.7	0 ± 0	2.1 ± 2.1	0 ± 0
MlfΔC1/MlfΔC1 mat. ctr.	12.7 ± 4.2	2.5 ± 1.7	0 ± 0	0 ± 0
MlfΔC1/MlfΔC1; 2D2/+ mat. ctr.	16.3 ± 3.3	2.5 ± 1.7	1.3 ± 1.3	0 ± 0
2D2/Df	18.8 ± 4.3	13.8 ± 3.9	7.5 ± 3.3	0 ± 0
MlfΔC1/+; 2D2/Df	28.8 ± 5.9	12.5 ± 4.2	1.3 ± 1.3	0 ± 0

Table 40. BunA & Madm control stability - Retraction frequency on muscles 6/7 (ad Figure S8 C).

Genotype	Retraction frequency [%]	P-value	Compared to	P-value	Compared to	n [# animals]	n [# NMJs]
Control	3.8 ± 2.7					10	80
Bun200B/+	2.5 ± 1.7	0.69577	Control			10	80

2D2/+	3.8 ± 2.8	1	Control			10	80
Bun200B/+; 2D2/+	7.5 ± 7.4	0.34191	Control			10	80
Bun200B/GE	11.3 ± 4.1	0.09655	Control			10	79
Bun200B/GE; 2D2/+	17.5 ± 4.2	0.01221	Control	0.2684	Bun200B/ GE	10	78
2D2/Df	40 ± 6.1	3.72E-05	Control			10	80
Bun200B/+; 2D2/Df	21.3 ± 7.4	0.03828	Control	0.06996	2D2/Df	10	79

Table 41. BunA & Madm control stability - Retraction severity on muscles 6/7 (ad Figure S8 D).

Genotype	1-2 postsynaptic profiles	3-6 postsynaptic profiles	≥ 7 postsynaptic profiles	Elimination
Control	3.8 ± 2.7	0 ± 0	0 ± 0	0 ± 0
Bun200B/+	2.5 ± 1.7	0 ± 0	0 ± 0	0 ± 0
2D2/+	3.8 ± 1.9	0 ± 0	0 ± 0	0 ± 0
Bun200B/+; 2D2/+	2.5 ± 1.7	3.8 ± 2.7	1.3 ± 1.3	0 ± 0
Bun200B/GE	7.6 ± 2.8	3.8 ± 1.9	0 ± 0	0 ± 0
Bun200B/GE; 2D2/+	16.7 ± 4.2	1.3 ± 1.3	0 ± 0	0 ± 0
2D2/Df	18.8 ± 4.3	13.8 ± 3.9	7.5 ± 3.3	0 ± 0
Bun200B/+; 2D2/Df	13.9 ± 5.4	5.1 ± 2.8	2.5 ± 2.5	0 ± 0

6.1.3 Tables for additional analysis of Madm in thesis

Table 42. Madm - Retraction frequency on muscle 4 (ad Thesis Figure 5 D).

Genotype	Retraction frequency [%]	P-value	n [# animals]	n [# NMJs]
Control	6.3 ± 2.8		10	80
PreRNAi	47.5 ± 6.9	2.09E-05	10	80
EP/EP	62.5 ± 5.3	1.51E-08	10	80
EP/Df	40 ± 5.2	1.28E-05	10	80
2D2/Df	21.3 ± 3.3	1.29E-03	10	80
4S3/Df	36.3 ± 7.8	1.36E-03	10	80
elav EP/Df rescue	5 ± 2.8	1.28E-05	10	79
elav 2D2/Df rescue	1.3 ± 1.3	1.94E-05	10	80
OK371 2D2/Df rescue	3.8 ± 2.7	0.00059	10	80
elav 4S3/Df rescue	2.5 ± 1.7	4.90E-04	10	79
elav; UAS-Madm	0 ± 0	0.08717	10	80

Table 43. Madm - Retraction severity on muscle 4 (ad Thesis Figure 5 E).

Genotype	1-2 postsynaptic profiles	3-6 postsynaptic profiles	≥ 7 postsynaptic profiles	Elimination
Control	2.5 ± 1.7	1.3 ± 1.3	2.5 ± 1.7	0 ± 0
PreRNAi	17.5 ± 4.6	15 ± 3.1	15 ± 3.6	5 ± 2
EP/EP	8.8 ± 3.3	8.8 ± 3.3	45 ± 5.3	3.8 ± 2.7
EP/Df	5 ± 2.8	16.3 ± 3.3	18.8 ± 3.8	10 ± 3.1
2D2/Df	5 ± 2.8	12.5 ± 2.6	3.8 ± 1.9	0 ± 0
4S3/Df	10 ± 3.6	12.5 ± 4.2	13.8 ± 3.5	5 ± 2
elav EP/Df rescue	2.5 ± 1.7	1.3 ± 1.3	1.3 ± 1.3	0 ± 0
elav 2D2/Df rescue	0 ± 0	0 ± 0	1.3 ± 1.3	0 ± 0
OK371 2D2/Df rescue	2.5 ± 2.5	0 ± 0	1.3 ± 1.3	0 ± 0
elav 4S3/Df rescue	2.5 ± 1.7	0 ± 0	0 ± 0	0 ± 0
elav; UAS-Madm	0 ± 0	0 ± 0	0 ± 0	0 ± 0

Table 44. Madm - Morphological parameters on muscle 1 - Satellite boutons (ad Thesis Figure 6 A).

Genotype	Absolute value [%]	Normalized to control [%]	P-value	n [# animals]	n [# NMJs]
Control	0.4 ± 0.1	100 ± 36.4		6	17
PreRNAi	0.3 ± 0.1	81 ± 25.6	0.66312	6	21
EP/EP	1.3 ± 0.2	306.2 ± 57.6	0.00832	6	23
EP/Df	1.6 ± 0.3	397.4 ± 68.8	0.0012	6	22
2D2/Df	1 ± 0.2	254.4 ± 45.8	0.01526	6	21

4S3/Df	1.8 ± 0.2	432.9 ± 45.7	3.91E-06	6	23
elav EP/Df rescue	1.3 ± 0.2	309.1 ± 58	0.33211	6	22
elav 2D2/Df rescue	0.8 ± 0.3	200.6 ± 69.4	0.52939	6	23
elav 4S3/Df rescue	0.7 ± 0.2	158.4 ± 44.8	9.63E-05	6	23
elav; UAS-Madm	0.6 ± 0.2	151.8 ± 40.9	0.37317	6	24

Table 45. Madm - Morphological parameters on muscle 1 - Muscle area (ad Thesis Figure 6 B and C).

Genotype	Absolute value [%]	Normalized to control [%]	P-value	n [# animals]	n [#NMJs]
Control	37383.1 ± 1568.3	100 ± 4.2		6	17
PreRNAi	44167 ± 1224	118.1 ± 3.3	0.0014	6	21
EP/EP	40065.8 ± 1276.4	107.2 ± 3.4	0.18888	6	23
EP/Df	37615.1 ± 1546.6	100.6 ± 4.1	0.91794	6	22
2D2/Df	41169.3 ± 1965.3	110.1 ± 5.3	0.15443	6	21
4S3/Df	41594.4 ± 1334.6	111.3 ± 3.6	0.04749	6	23
elav EP/Df rescue	48186.9 ± 1566	128.9 ± 4.2	2.01E-05	6	22
elav 2D2/Df rescue	51699.5 ± 1542.2	138.3 ± 4.1	0.00012	6	23
elav 4S3/Df rescue	49742.5 ± 1198.3	133.1 ± 3.2	4.29E-05	6	23
elav; UAS-Madm	39720.9 ± 1396.9	106.3 ± 3.7	0.27716	6	24

Table 45. Madm - Effects of the postsynapse - Retraction frequency on muscles 1/9 & 2/10 (ad Thesis Figure 7 E).

Genotype	Retraction frequency [%]	P-value	n [# animals]	n [# NMJs]
Control	4.7 ± 1.5		10	301
PostRNAi	10.6 ± 3.1	8.02E-02	10	290
4S3/Df	80 ± 3.1	2.47E-14	10	320
MEF2 4S3/Df rescue	3.8 ± 1.1	9.12E-15	10	314
UAS-Madm; MEF2	1.6 ± 0.8	5.58E-02	10	289

Table 46. Madm - Effects of the postsynapse - Retraction severity on muscles 1/9 & 2/10 (ad Thesis Figure 7 F).

Genotype	1-2 postsynaptic profiles	3-6 postsynaptic profiles	≥ 7 postsynaptic profiles	Elimination
Control	2.3 ± 0.7	1.3 ± 0.5	1.3 ± 0.5	0 ± 0
PostRNAi	10.3 ± 3.2	1 ± 0.5	0.3 ± 0.3	0 ± 0
4S3/Df	11.3 ± 2.5	17.5 ± 2.1	51.3 ± 3.3	3.1 ± 1.1
MEF2 4S3/Df rescue	3.1 ± 1	0.6 ± 0.4	0 ± 0	0 ± 0
UAS-Madm; MEF2	1.3 ± 0.7	0.3 ± 0.3	0 ± 0	0 ± 0

Table 47. Madm - Effects of the postsynapse - Retraction frequency on muscles 6/7 (ad Thesis Figure 8 A).

Genotype	Retraction frequency [%]	P-value	n [# animals]	n [# NMJs]
Control	3.8 ± 2.7		10	80
PostRNAi	12.5 ± 4.2	9.39E-02	10	80
4S3/Df	65 ± 5.5	9.22E-09	10	80
MEF2 4S3/Df rescue	7.5 ± 3.8	9.25E-08	10	80
UAS-Madm; MEF2	3.8 ± 1.9	1.00E+00	10	80

Table 48. Madm - Effects of the postsynapse - Retraction severity on muscles 6/7 (ad Thesis Figure 8 B).

Genotype	1-2 postsynaptic profiles	3-6 postsynaptic profiles	≥ 7 postsynaptic profiles	Elimination
Control	3.8 ± 2.7	0 ± 0	0 ± 0	0 ± 0
PostRNAi	10 ± 3.1	0 ± 0	2.5 ± 2.5	0 ± 0
4S3/Df	16.3 ± 3.8	25 ± 5.3	23.8 ± 5.7	0 ± 0
MEF2 4S3/Df rescue	6.3 ± 2.8	0 ± 0	1.3 ± 1.3	0 ± 0
UAS-Madm; MEF2	2.5 ± 1.7	1.3 ± 1.3	0 ± 0	0 ± 0

Table 49. Madm - Effects of the postsynapse - Morphological parameters on muscle 1 - Number of NMJ branches (ad Thesis Figure 9 D).

Genotype	Absolute value	Normalized to control [%]	P-value	n [# animals]	n [# NMJs]
Control	4.3 ± 0.3	100 ± 6.2		6	17
4S3/Df	7.2 ± 0.6	167.1 ± 13.1	0.00019	6	23
MEF2 4S3/Df rescue	4 ± 0.5	92 ± 10.7	9.15E-05	6	20

Table 50. Madm - Effects of the postsynapse - Morphological parameters on muscle 1 - Number of total boutons (ad Thesis Figure 9 E).

Genotype	Absolute value	Normalized to control [%]	P-value	n [# animals]	n [# NMJs]
Control	49.6 ± 2.5	100 ± 5		6	17
4S3/Df	25.1 ± 1.7	50.6 ± 3.4	2.66E-10	6	23
MEF2 4S3/Df rescue	37 ± 3.1	74.5 ± 6.2	0.00116	6	20

Table 51. Madm - Effects of the postsynapse - Morphological parameters on muscle 1 - Total NMJ length (ad Thesis Figure 9 F).

Genotype	Absolute value	Normalized to control [%]	P-value	n [# animals]	n [# NMJs]
Control	160 ± 9.8	100 ± 6.1		6	17
4S3/Df	86.4 ± 4.6	54 ± 2.9	7.35E-09	6	23
MEF2 4S3/Df rescue	114.7 ± 10.5	71.7 ± 6.6	0.01347	6	20

Table 52. Madm - Effects of the postsynapse - Morphological parameters on muscle 1 - NMJ area/muscle area (ad Thesis Figure 9 G).

Genotype	Absolute value	Normalized to control [%]	P-value	n [# animals]	n [# NMJs]
Control	2.4 ± 0.2	100 ± 8.3		6	17
4S3/Df	0.8 ± 0.1	35.1 ± 3.4	1.07E-09	6	23
MEF2 4S3/Df rescue	2.5 ± 0.4	103.6 ± 15.2	3.04E-05	6	20

Table 53. Mlf & Madm control morphology - Morphological parameters on muscle 1 - Number of NMJ branches (ad Thesis Figure 10 C).

Genotype	Absolute value	Normalized to control [%]	P-value	n [# animals]	n [# NMJs]
Control	4.3 ± 0.3	100 ± 6.2		6	17
2D2/Df	7.8 ± 0.7	181.9 ± 16	0.0001	6	21
MlfΔC1/+; 2D2/Df	3.5 ± 0.4	82.1 ± 9.8	0.14366	6	19

Table 54. Mlf & Madm control morphology - Morphological parameters on muscle 1 - Number of total boutons (ad Thesis Figure 10 D).

Genotype	Absolute value	Normalized to control [%]	P-value	n [# animals]	n [# NMJs]
Control	49.6 ± 2.5	100 ± 5		6	17
2D2/Df	36.3 ± 1.7	73.2 ± 3.4	5.36E-05	6	21
MlfΔC1/+; 2D2/Df	22.5 ± 1.3	45.3 ± 2.7	1.26E-11	6	19

Table 55. Mlf & Madm control morphology - Morphological parameters on muscle 1 - Total NMJ length (ad Thesis Figure 10 E).

Genotype	Absolute value	Normalized to control [%]	P-value	n [# animals]	n [# NMJs]
Control	160 ± 9.8	100 ± 6.1		6	17
2D2/Df	104.3 ± 4.5	65.2 ± 2.8	3.08E-06	6	21
MlfΔC1/+; 2D2/Df	53.7 ± 4.2	33.6 ± 2.6	4.91E-12	6	19

Table 56. Mlf & Madm control morphology - Morphological parameters on muscle 1 - NMJ area/muscle area (ad Thesis Figure 10 F).

Genotype	Absolute value	Normalized to control [%]	P-value	n [# animals]	n [# NMJs]
Control	2.4 ± 0.2	100 ± 8.3		6	17
2D2/Df	1.3 ± 0.2	53.5 ± 5.3	1.90E-04	6	21
MlfΔC1/+; 2D2/Df	1 ± 0.2	42.2 ± 3.7	1.07E-05	6	19

Table 57. Bun 149/GE - Retraction frequency on muscles 1/9 & 2/10 (ad Thesis Figure 11 A).

Genotype	Retraction frequency [%]	P-value	n [# animals]	n [# NMJs]
Control	4.7 ± 1.5		10	301
Bun 149/GE	17.8 ± 2.6	0.00028	10	304

Table 58. Bun 149/GE - Retraction severity on muscles 1/9 & 2/10 (ad Thesis Figure 11 B).

Genotype	1-2 postsynaptic profiles	3-6 postsynaptic profiles	≥ 7 postsynaptic profiles	Elimination
Control	2.3 ± 0.7	1.3 ± 0.5	1.3 ± 0.5	0 ± 0
Bun 149/GE	8.8 ± 1.3	7.5 ± 2.8	1.6 ± 0.7	0.3 ± 0.3

Table 59. Bun 149/GE - Retraction frequency on muscles 6/7 (ad Thesis Figure 11 C).

Genotype	Retraction frequency [%]	P-value	n [# animals]	n [# NMJs]
Control	3.8 ± 2.7		10	80
Bun 149/GE	25 ± 5.9	0.00411	10	80

Table 60. Bun 149/GE - Retraction severity on muscles 6/7 (ad Thesis Figure 11 D).

Genotype	1-2 postsynaptic profiles	3-6 postsynaptic profiles	≥ 7 postsynaptic profiles	Elimination
Control	3.8 ± 2.7	0 ± 0	0 ± 0	0 ± 0
Bun 149/GE	18.8 ± 4.3	3.8 ± 1.9	2.5 ± 1.7	0 ± 0

Table 61. Bun 149/GE - Morphological parameters on muscle 1 - Number of NMJ branches (ad Thesis Figure 11 E).

Genotype	Absolute value	Normalized to control [%]	P-value	n [# animals]	n [#NMJs]
Control	4.3 ± 0.3	100 ± 6.2		6	17
Bun 149/GE	3.3 ± 0.2	76 ± 4.7	0.00363	6	19

Table 62. Bun 149/GE - Morphological parameters on muscle 1 - Number of total boutons (ad Thesis Figure 11 F).

Genotype	Absolute value	Normalized to control [%]	P-value	n [# animals]	n [#NMJs]
Control	49.6 ± 2.5	100 ± 5		6	17
Bun 149/GE	31.5 ± 1.4	63.4 ± 2.8	1.48E-07	6	19

Table 63. Bun 149/GE - Morphological parameters on muscle 1 - Total NMJ length (ad Thesis Figure 11 G).

Genotype	Absolute value	Normalized to control [%]	P-value	n [# animals]	n [#NMJs]
Control	160 ± 9.8	100 ± 6.1		6	17
Bun 149/GE	99.6 ± 3.9	62.2 ± 2.4	9.72E-07	6	19

Table 64. Bun 149/GE - Morphological parameters on muscle 1 - NMJ area/muscle area (ad Thesis Figure 11 H).

Genotype	Absolute value [%]	Normalized to control [%]	P-value	n [# animals]	n [#NMJs]
Control	2.4 ± 0.2	100 ± 8.3		6	17
Bun 149/GE	2.2 ± 0.2	90.5 ± 9.6	0.46296	6	19

6.1.4 Tables for RNAi-based genetic screens and hits of thesis

6.1.4.1 List of hits from “cytoskeleton, cytoskeleton-associated and transport proteins” RNAi screen

It was stated that candidates had transport defects if BRP was accumulating in nerves and axons. The different Gal4-driver lines, which the VDRC stocks were crossed to, are indicated and the observed phenotypes upon RNAi knockdown are described.

Abbreviations for stocks:

- ed: elav^{C155}-Gal4; UAS-dicer2
- esd: elav^{C155}-Gal4; scabrous-Gal4, UAS-dicer2
- BG57: BG57-Gal4
- dB: UAS-dicer2; BG-57-Gal4

A subjective ranking of the observed phenotypes is also shown ranging from:

- No ranking or (!) for weak and subtle phenotypes to
- !! for very prominent phenotypes which are also very consistent in all analyzed animals.

Phenotypes of Roadblock, PTEN, Shibire and Msp300 were previously published and served as positive controls (see results).

Table 65. “Cytoskeleton, cytoskeleton-associated and transport proteins” RNAi screen - Hits upon presynaptic RNAi knockdown.

#	Name	Transformant ID	Phenotype	Ranking
1	PI4K	15993	esd: morphology defects	(!) or !
2	Chd64	5654	esd: elongated ventral nerve cord; morphology defects, mostly † L2	!!
3	DAAM	24885	esd: mild morphology phenotype	(!) or !
4	Kinesin light chain	39583	esd: † L2/3, ed: muscle phenotype, stability and morphology defects	! or !!
5	Arp11	31710	esd: satellite boutons, morphology and mild stability defects	! or !!
6	Mini spindles	21982	esd: †; ed: mild morphology and stability defects	(!)
7	Roadblock	22760	esd: stability and transport defects	!!

8	Paramyosin	33615	esd: satellite boutons and morphology defects	!
9	PTEN	35731	esd: morphology defects	! or !!
10	Shibire	3798	esd: †	

Table 66. “Cytoskeleton, cytoskeleton-associated and transport proteins” RNAi screen - Hits upon postsynaptic RNAi knockdown.

#	Name	Transformant ID	Phenotype	Ranking
1	Formin3	42302	morphology defects - fused GluRIII clusters	!!
2	α-Actinin	7760	morphology defects	!!
3	Elongation factor 1α100E	40156	muscle and morphology defects	!!
4	Tropomyosin 2	42008	muscle and morphology defects, dB: † as pupae	!!
5	Bent	46252	BG57: † early L2	
6	Muscle-specific protein 300	50192	major muscle defect and stability defects	!!
7	Chd64	5654	BG57: mostly † L2	
8	KLHL18	43777	morphology defects	!
9	Integrin	29619	BG57: † L1/L2	
10	Talin	40399	BG57: † L3 / pupae	

6.1.4.2 List of hits from “signaling pathways” RNAi screen

Phenotypes of Rab11 and AP-2σ were previously published and served as positive controls (see results).

Table 67. “Signaling pathways” RNAi screen - Hits upon presynaptic RNAi knockdown.

#	Name	Transformant ID	Phenotype	Ranking	Pathway
1	DAAM	103921	esd: satellite boutons and morphology, stability, growth, transport and slight muscle defects	(!)	noncan Wnt
2	Rab11	108382	esd: † very little size L2 as pupae; other Gal4 drivers cause growth and morphology defects	!!	Notch
3	Stat92E	43866	esd: morphology, stability, growth and transport defects	!	JAK-STAT
4	Roc1	32399	esd: morphology, stability, growth and transport defects	! or !!	HH

5	TSC2	103417	esd: morphology ("gnarled tree") and transport defects	!!	PTEN
6	Rab5	103945	esd: stability and morphology defects	!!	Ras superfamily
7	HH	1403	esd: stability, morphology and slight transport defects	!	HH
8	Rhomboid	51952	esd: mild stability and muscle defects, transport defects	(!)	EGFR
9	TSC1	22252	esd: mild stability defects, morphology defects - "bunch of grapes" NMJs	(!)	PTEN
10	AP-2 σ	34148	esd: morphology defects	!	noncan Wnt
11	RhoA	109420	esd: morphology and growth defects	(!)	Ras superfamily
12	Myc	2948	esd: stability and transport defects	!!	Transcription factor

Table 68. "Signaling pathways" RNAi screen - Hits upon postsynaptic RNAi knockdown.

#	Name	Transformant ID	Phenotype	Ranking	Pathway
1	MRLC - Myosin light chain 2	104621	BG57: very little, † as pupae, no flies		noncan Wnt
2	Rab11	108382	dB: muscle phenotype, morphology defects		Notch
3	Roc1	32399	dB: major muscle phenotype, morphology defects		HH
4	Stat92E	43866	dB: stability and morphology defects	!	JAK-STAT
5	TRAF6	16125	dB: muscle phenotype, major stability and morphology defects	!!	NF- κ B
6	Myo62F	49345	dB: muscle phenotype, stability and growth defects	!(!)	Notch
7	Fz	43077	dB: muscle phenotype, stability, morphology and growth defects	!	noncan Wnt
8	Rhomboid	51952	dB: prominent muscle phenotype	!	EGFR

6.1.4.3 VDRC lines for “cytoskeleton, cytoskeleton-associated and transport proteins” RNAi screen

Table 69. List of candidates for “cytoskeleton, cytoskeleton-associated and transport proteins” RNAi screen.

Symbol	Names & Synonyms	Annotation	Transformant ID
Sep5	septin 5	CG2916	25454
Actr13E	Acrp, Actin-related protein 13E	CG11678	17242
		CG17150	35625
		CG13930	17753
		CG11659	16258
Mre11	meiotic recombination 11	CG16928	30474
Klp38B	KIF14, Kinesin-like protein at 38B, mothra, nebbish, tiovivo	CG10718	31329
		CG6300	27576
Robl	roadblock	CG10751	22760
Sry-α	serendipity alpha	CG17957	23954
Mical		CG33208	46096
Formin3	ah1644, formin/DIA-like	CG33556	42302
Dyn	dynactin, dynactin-subunit-p25, dyn-p25, p25 subunit	CG10846	8058
Fhos		CG32030	34034
MyoII	myosin 2, NMM, non-muscle myosin II, sgh, spaghetti squash	CG3595	7916
TnC	tnC4, TpnC4, TpnC41F, TpnC IIIb	CG12408	51740
		CG15609	43406
Mp20	Muscle protein 20, myophilin, Tpn	CG4696	40554
		CG11063	38442
Dhc	dynein-related heavy chain, kl5, Lms4, male fertility factor kl5	CG40444	32964
Kl3	gamma-dynein heavy chain, kl3, kl-4, Lms3, male fertility factor kl3	CG17629	32971
Msp-300,	Muscle-specific protein 300, Nesprin, Spec25CD	CG33715	50192
KIF23	Mitotic kinesin-like protein 1, Mklp1, pav, pavarotti	CG1258	46134
CEN190	Centrosomal Protein 190, Map190, Rb188	CG6384	35077
Myo10A	Myosin XV, Sisyphus, Syph, unconventional myosin class XV	CG2174	33486
Pat1	Protein interacting with APP tail-1	CG10695	27307
KLC	kinesin, kinesin I, kinesin light chain	CG5433	39583
DHC	beethoven, btv, DyneinHC, Dynein heavy chain 36D	CG15148	19323
Robl22E		CG10838	28289
		CG10859	27322

Gel	Gelsolin	CG1106	37865
Ald	6 biphosphate-aldolase A, fructose 1	CG6058	27541
		CG5022	8262
		CG6053	35052
		CG11289	45993
Mer	D Merlin, Emr2, Ezrin-moesin-radixin-2	CG14228	7161
Wave	scar	CG4636	21908
		CG14763	8271
		CG10971	16138
	CG11339, CG15566, LP8211	CG34347	18066
CdIc2	Cytoplasmic dynein light chain 2, dlc	CG5450	42113
	CG40016	CG17493	40080
	CG15097	CG15097	25188
PI4K	EG:BACR7C10.2	CG10260	15993
KIF21A	DmCG5300, DmKlp31D, DmKlp31E, Klp31E	CG5300	34983
Mir	mira, miranda	CG12249	51484
Chd64	Calponin-like protein 64, anon-EST:Liang-1.80, clone 1.80, CT34849	CG14996	5654
	CG15158	CG31802	18562
Dhc93AB	Dynein heavy chain at 93AB, dynein-related heavy chain polypeptide	CG3723	41947
Arm	armadillo, b-catenin, beta-cat	CG11579	7767
Bap55	Brahma associated protein 55kD, BRM-associated protein 55	CG6546	24703
MspS	Dis1, mini spindles, TOG, XMAP215	CG5000	21982
CYLD		CG5603	15340
Arp5	Actin-related protein 53D, Actr53D, arp53D	CG5409	22117
MLC-2	MRLC, muscle-specific myosin regulatory light chain, Myosin light chain 2	CG2184	51201
BetaH	beta-heavy-spectrin	CG12008	37074
		CG3339	41918
Anx B9	Annexin B9, Annexin IX	CG5730	27493
	BcDNA:AT15471, DmAAF51272	CG17237	51997
		CG1571	51846
Dbo	Diablo, Smac	CG6224	22476
Actn	alpha actinin, fliA, flightless A	CG4376	7760
Shi	shibire, shibiri, Ddyn, Ddyn3, Ddyn4, Dyn, dynamin	CG18102	3798
Arpc3A	ARC-P21	CG4560	26548
Mhc95F	95F myosin, jag, jaguar, jar, Myosin heavy chain at 95F, myosin VI	CG5695	37534
	anon-WO0140519.21, CG9489	CG31352	25750
		CGnone	40113

KIF20A	Double or nothing, Dub, mei-1794, sub, subito	CG12298	18754
		CG5023	34914
Tmod	CG11493, CG15540, sanpodo, spdo, tmod, tropomodulin	CG1539	32601
	BcDNA:GH08635, CG14908, late transcript	CG31275	49957
KIF10	cana, CENPana, Cenp-E, CENP-E ana, CG32955, CG4831, CP15516	CG33694	49776
eEF1alpha	EF-1, Efla2, elongation factor 1-alpha F2, F2	CG1873	40156
Bsh	MHC, muscle myosin-II, Not-upheld, Shrunken-thorax, Stuckup	CG17927	7164
	alpha-catenin related	CG2987	7182
Null0	BcDNA:RE47733	CG14426	17589
KLHL18	anon-WO0118547.179	CG3571	43777
NinaC	CG54125, myosin III, neither inactivation nor afterpotential C	CG5125	27359
Sep2	septin 2	CG4173	26413
DmnmII	cytoplasmic myosin II, E(br), Enhancer of broad, zip, zipper	CG15792	7819
c62E-11	CG1141, CG16764, villin-like	CG33232	18081
Sep1	Diff6, iby, innocent bystander, septin 1	CG1403	17344
DmV	myosin V, NMC7, 43CD	CG2146	44291
Incenp	anon-WO0118547.171, Inner centromere protein	CG12165	17044
		CG13465	49141
Aip1		CG10724	22851
	Filamin-like	CG5984	52489
Alpha-ctn	alphacat, alpha-catenin, Dalpha-cadherin	CG17947	19182
		CG10822	17005
Robl37BC		CG15171	41579
DAAM	DIA-like, Dishevelled associated activator of morphogenesis, Formin	CG14622	24885
	CG15780, CG17763	CG34435	35553
		CG16837	32751
Parvin	CG12533	CG32528	11670
Wsck		CG31127	1214
Kif3A	DmKlp64D, Kinesin-like protein at 64D, Klp4, klp64D	CG10642	45372
Beta3t	B3t, beta 3 tubulin	CG3401	34606
Grip84	gamma-tubulin ring protein 84, GCP2	CG3917	34731
Tektin A	anon-WO0140519.235, BG:DS02252.2	CG4767	21946
Qua	anon-WO0140519.71, female sterile(2)A12, fs(2)A12, Quail	CG6433	27623
Dhc36C	Dynein heavy chain at 36C, dynein-related heavy chain polypeptide	CG5526	27451
Mask	multiple ankyrin repeats single KH domain, CG18671, CG31138, CG6268, CG6313	CG33106	29541

Dhc62B	Dynein heavy chain at 62B, dynein-related heavy chain polypeptide, CG18613	CG15804	48542
mPM	miniparamyosin, Para, Prm	CG5939	33615
	MICAL-like, AAK93415	CG11259	17537
Arp11	Actin-related protein 11	CG12235	31710
Dlc90F	Dynein light chain 90F	CG12363	31749
PTEN	PTEN3	CG5671	35731
		CG13913	41514
	Debrin-like	CG10083	38330
P62 DYNAMACTIN		CG12042	31623
		CG15831	28582
	anon-EST:fe1E4, anon-fast-evolving-1E4, CG33352, CG9469	CG33558	46456
Klar	klarsicht, kls, marb, marbles	CG17046	32836
Fli	flightless, standby	CG1484	39528
Vin2EF	Vinculin at 2EF	CG3299	34586
KIF16A	Kinesin-like protein at 98A, Klp98A	CG5658	40603
Tm2	Tropomyosin 2, Troponin H	CG4843	42008
	BcDNA:GH23906, CG3950, CG3960	CG34417	34098
Cdk5	Cyclin-dependent kinase 5	CG8203	35855
Mlc-c	Myosin light chain cytoplasmic	CG3201	30035
	CG2159	CG32485	34565
Fs	fascin, singed, sn	CG32858	32579
Myo29D	myosin 29D, d, dachs	CG10595	12555
MEG1	PTP-meg, scc, split central complex, anon-WO0118547.211	CG1228	38651
p34	p34, anon-WO0118547.154, Arc-p34, Arpc2, ARPC2/p34	CG10954	45013
		CG1812	15491
	anon-WO0172774.98, CG13485, CG6807	CG32138	34412
f	forked	CG5424	33200
KIF10	CENP-E meta, cmet	CG6392	35081
p130CAS	CT1293	CG1212	41479
Cdep	i23, CG1283, CG2008	CG31536	25049
cTm	cytoplasmic tropomyosin, cytoskeletal Tropomyosin	CG4898	34119
Bent	Powell, myosin LCK, Projectin myosin light chain kinase, Tennessee-2, titin, twitchin	CG32019	46252
Talin	rhea, Talin	CG6831	40399
Vinculin	Vin2EF, vinc	CG3299	34585
Tensin		CG9379	22823
Integrin	MAB6G11	CG1560	29619
NCK	doc	CG3727	37525

6.1.4.4 VDRC lines for signaling pathways RNAi screen

Candidates without CG number and Transformant ID could not be screened because fly stocks were not available at that time. The TGF β (Transforming growth factor β) pathway is already extensively analyzed and was thus not included in my screen.

Table 70. List of candidates for “signaling pathways” RNAi screen.

Symbol	Names & Synonyms	Annotation	Transformant ID
EGFR			
Spitz	Spi	CG10334	3920
Gurken	s-Grk, CT32746, grk	CG17610	4332
Keren	s-krn, spitz2	CG32179	27111
Star	S	CG4385	109838
Rhomboid	rho	CG1004	51952
EGFR	pnt, top	CG10079	43268
PLC	Phospholipase C	CG4574	26558
SHC	SHC-adaptor	CG3715	40464
SOS	Son of sevenless	CG7793	106925
TACE	CT23908	CG7908	2733
ARGOS	rlt, roulette, strawberry	CG4531	47180
CHIP		CG5203	107447
Kekkon-1	NB1	CG12283	4761
Cbl	anon-WO0118547.68	CG7037	22335
Nedd8	Nedd8	CG10679	28444
TSG101	Tsg101	CG9712	23944
ESCRT machinery (endosomal sorting)			
TSG101		CG6637	21658
Larsen		CG9779	100295
PTEN			
FOXO	Q95V55, Afx	CG3143	106097
BAD			
TSC1	rocky, hamartin	CG6147	22252
TSC2	ME 109, gigas	CG6975	103417
Rheb			
Nedd4			

PCAF		CG4107	108943
p53		CG33336	103001
RAD51		CG7948	13362
mTOR			
4E-BP	Phas1, pp20, thor	CG8846	35439
GRB2	P1112, Su(sev)R1	CG6033	105498
TCTP		CG4800	45532
Raptor		CG4320	106491
mLST8			
Rictor			
SIN1	SAPK-interacting protein1	CG10105	18002
Paxillin	Pax	CG31794	25853
LKB1	PAR-4,STK11	CG9374	108356
Hedgehog			
Dally		CG4974	14136
Dispatched		CG2019	10004
Dlg			
Hedgehog	Mir, Mirabile, Moonrat	CG4637	1403
Ttv	P1.15, toutvelu	CG10117	4871
Botv	botv	CG15110	37185
Sotv	sister of tout-velu	CG8433	4902
Ihog	ihog	CG9211	29898
Boi	brother of ihog	CG32796	869
Smo	smooth	CG9218	108351
Ci	Cubitus interruptus	CG2125	51479
Sufu	su(fu), Suppressor of fused	CG6054	35055
PTC			
Engrailed	spermatheca, spt	CG9015	105678
HIB	rdx, roadkill	CG12537	107294
Cul3			
Pxb	baikal	CG33207	102240
Cul1			
Roc1	Rbx1, Rbx1/Roc	CG16982	32399
SCF-Slimb			
JAK-STAT			
Importin-alpha2	oho31	CG4799	102627
CRM1	Chromosomal region maintenance 1, embargoed, exportin	CG13387	3347

Stat92E	Marelle, mrl	CG4257	43866
Non-canonical Wnt			
Wnt	Sp, spade, spd ,Sternopleural, Wingless	CG4889	104579
Fz	frizzled, CG3646, DFz1	CG17697	43077
Dvl	dishevelled	CG18361	101525
AP-2σ	sigma2, AP-2sigma	CG6056	34148
Daam	anon-EST:Posey148, Dishevelled Associated Activator of Morphogenesis, Formin	CG14622	103921
Formin3	ah1644, CG14824, CG181	CG33556	45594
Profilin	chickadee, chic, sand, stranded	CG9553	102759
MRLC	muscle-specific myosin light chain 2	CG2184	104621
cJun	Jun-related antigen, AP-1, activator protein 1	CG2275	10835
PXN	peroxidasin	CG12002	15276
Dgo	diego	CG12342	108410
Fmi	stan, starry night, flamingo, serpentine cadherin	CG11895	51382
PLC	see EGFR pathway candidates; Phospholipase C	CG4574	26558
Cdc42	Cell division control protein 42	CG12530	100794
Armadillo	arm, beta-catenin	CG11579	107344
Rap1	Roughened, R	CG1956	20761
Filamin	jbug, jitterbug	CG30092	28471
FilaminA	shi kong, sko, cheerio	CG3937	107451
Futsch	Map1B		
Lgl	BCL9, legless	CG2041	105874
L2gl	lethal(2) giant larvae, p127	CG2671	51247
Axn	axin	CG7926	7748
Vang	Van Gogh, stb, strabismus	CG8075	100819
Fy	fuzzy	CG13396	30760
Wnt/β-Catenin			
Porc	poc, por	CG6205	100780
Wls	sprinter, srt, wls	CG6210	5215
LRP	arr, arrow	CG5912	6708
Cav	p55, 1G5	CG6219	15021
IDAX		CG9973	36188
Notch			
Notch	N, nd, n[fah], Nintra, Abruptex	CG3936	27229
Delta	Overflow	CG3619	109491
Serrate	Ripped wing, Rpw, ser	CG6127	108348
O-Fut1	neurotic ,ntc, nti	CG12366	44045
Furin 1	dFur1	CG10772	22853

Furin 2	DFur2	CG18734	1020
Fringe	D-Fng	CG10580	51977
Arrestin2	phosrestin-1	CG5962	40999
Deltex	dx	CG3929	7795
Contactin	cont	CG1084	28294
Neur	neuralized	CG11988	10662
Mib	mind bomb 1	CG5841	27526
Myo62F	Myo1B	CG9155	49345
Epsin	liquid facets-Related, CG13853, CG13854	CG42250	33799
Epsin	liquid facets	CG8532	107300
Rab11	Ras-related protein 11	CG5771	108382
Presenilin	pres	CG18803	101379
MAM	N-2G, SR2-4	CG8118	102091
CSL			
Sin3A		CG8815	105852
Crumbs	crb	CG6383	39178
NF-κB			
TLR	tlr, toll, Toll like receptor, 18 wheeler	CG8896	965
Tolkin	piranha, tldr1	CG6863	2656
MyD88	krapfen	CG2078	25402
TRIF			
IRAK			
RIP			
TRAF4	TNF-receptor-associated factor 4	CG3048	21214
TRAF6	TNF-receptor-associated factor 6	CG10961	16125
FADD	BG4	CG12297	100333
p100	Pep	CG6143	22246
p52	TFB2	CG7764	39069
p105	Caf1-10	CG12892	20270
p50	dynamitin, p50/Dmn	CG8269	23726
CYLD	cylindromatosis ortholog (H. sapiens)	CG5603	101414
BCR	RhoGAP1A, CG17617	CG00000	33029
Ras superfamily			
RhoA	Rho1	CG8416	109420
Cdc42	see non-canonical Wnt pathway	CG12530	100794
Rac1	Rac GTPase	CG2248	49246
Ras1	p21[Ras1]	CG9375	28129
Ras2	Ras oncogene at 64B	CG1167	6225
Rab5		CG3664	103945

RasGSP	Ras-GAP	CG6721	105383
GEF26	PDF-GEF Dizzy, dizzy	CG9491	105159
Additional e.g. Hippo pathway			
Mthl15	methuselah-like 15	CG31720	102865
DDB1		CG7769	44974
DDB1		CG7769	44976
Tankyrase		CG4719	21932
Tankyrase		CG4719	21930
Star	S.	CG4385	109838
Tensin		CG9379	22823
Crumbs		CG6383	39178
Myc	Diminutive	CG10798	2948
HDACs			
dHDACX		CG31119	108098
dHDAC1		CG7471	30600
dHDAC2		CG6170	108831
dHDAC3		CG2128	107073
dHDAC4		CG1770	20522

6.2 Abbreviations

4E-BP1	Eukaryotic initiation factor 4E (eIF-4E) binding protein-1
Akt	Protein kinase B
ALS	Amyotrophic lateral sclerosis
AML	Acute myeloid leukemia
AMPA	α -Amino-3-hydroxy-5-methyl-4-isoxazolepropionic acid
Ank2	Ankyrin 2
APC/C	Anaphase-promoting complex/cyclosome
Arr	Arrow
ATP	Adenosine triphosphate
BBB	Blood-brain barrier
BMP	Bone morphogenetic protein
BRP	Bruchpilot
BunA	Bunched A
cAMP	Cyclic adenosine monophosphate
Chd64	Calponin-like protein 64
CNS	Central nervous system
CREB	cAMP response element-binding protein
CSN5	COP9 signalosome complex subunit 5
DAAM	Dishevelled Associated Activator of Morphogenesis
Df	Deficiency
Dip	DSIP-immunoreactive peptide
Dlg	Discs large
DREF	DNA replication related element binding factor
Dsh	Disheveled
DVGLuT	<i>Drosophila</i> vesicular glutamate transporter
ECM	Extracellular matrix
EGFP	Enhanced green fluorescent protein
EGFR	Epidermal growth factor receptor
EMS	Ethyl methanesulfonate
ER	Endoplasmic reticulum
ESCRT machinery	Endosomal sorting complexes required for transport machinery
FasII	Fasciclin II
Fig.	Figure
FOXO	Forkhead box class 'O'
GAP	GTPase-activating protein

GEF	Guanine nucleotide exchange factor
GluR	Glutamate receptor
GluRIII	Glutamate receptor subunit III
GTP	Guanosine triphosphate
HD	Huntington's disease
Hiw	Highwire
HRP	Horseradish peroxidase
HSP	Hereditary spastic paraplegia
ISN	Intersegmental nerve
JAK-STAT	Janus kinases & signal transducers and activators of transcription
JNK	c-Jun N-terminal kinases
KHC	Kinesin heavy chain
Khc	Kinesin heavy chain
KLHL18	Kelch-like protein 18
m	Muscle
Madm	Mlf1 adapter molecule
MAP kinase	Mitogen-activated protein kinase
MAP1B	Microtubule-associated protein 1B
MARCM	Mosaic analysis with a repressible cell marker
MDS	Myelodysplastic syndrome
Mlf1	Myeloid leukemia factor 1
MS	Multiple Sclerosis
MT cytoskeleton	Microtubule cytoskeleton
mTOR	Mammalian target of rapamycin
mTORC1	Mammalian target of rapamycin complex 1, mechanistic target of rapamycin complex 1
mTORC2	Mammalian target of rapamycin complex 2, mechanistic target of rapamycin complex 2
NF-κB	Nuclear factor 'kappa-light-chain-enhancer' of activated B-cells
NMJ	Neuromuscular junction
NPM/B23	Nucleophosmin
NRBP1	Nuclear receptor binding protein
NWK	Nervous wreck
PI3K	Phosphatidylinositol 3-kinase
PI4K	Phosphatidylinositol 4-kinase
PKB	Protein kinase B
PNS	Peripheral nervous system
poly Q	Poly glutamine
PSD	Postsynaptic density
PSD-95	Postsynaptic density protein 95

pSJs	Pleated septate junctions
PTEN	Phosphatase and tensin homolog
Rab11	Ras-related protein 11
Rab5	Ras-related protein 5
RAS	Rat sarcoma
Rheb	Ras homolog enriched in brain
RNAi	Ribonucleic acid interference
S6K	S6 kinase
SEM	Standard error of mean
SMA	Spinal muscular atrophy
SN	Segmental nerve
SSR	Subsynaptic reticulum
Stat92E	Signal-transducer and activator of transcription protein at 92E
Syn	Synapsin
TGF- β	Transforming growth factor β
TN	Transverse nerve
TSC 1	Tuberous sclerosis complex 1
TSC2	Tuberous sclerosis complex 2
TSC-22	Transforming growth factor- β -stimulated clone 22
type-Ib bouton	Type-I big bouton
type-Is bouton	Type-I small bouton
UAS	Upstream activation sequence
UPS	Ubiquitin-proteasome system
VNC	Ventral nerve cord
Wit	Wishful thinking
Wnt	Wingless & Int-1
WSP	Wiscott-Aldrich syndrome protein/WASP

6.3 References

- Aberle, H., Haghighi, A.P., Fetter, R.D., McCabe, B.D., Magalhaes, T.R., and Goodman, C.S. (2002). wishful thinking encodes a BMP type II receptor that regulates synaptic growth in *Drosophila*. *Neuron* *33*, 545-558.
- Adams, M.D., Celniker, S.E., Holt, R.A., Evans, C.A., Gocayne, J.D., Amanatides, P.G., Scherer, S.E., Li, P.W., Hoskins, R.A., Galle, R.F., *et al.* (2000). The genome sequence of *Drosophila melanogaster*. *Science* *287*, 2185-2195.
- Atwood, H.L., Govind, C.K., and Wu, C.F. (1993). Differential ultrastructure of synaptic terminals on ventral longitudinal abdominal muscles in *Drosophila* larvae. *Journal of neurobiology* *24*, 1008-1024.
- Baines, R.A. (2004). Synaptic strengthening mediated by bone morphogenetic protein-dependent retrograde signaling in the *Drosophila* CNS. *The Journal of neuroscience : the official journal of the Society for Neuroscience* *24*, 6904-6911.
- Baksa, K., Parke, T., Dearolf, C.R. (1997). Frankenstein, a new mutation, shows temperature sensitive lethality over dSTAT. *A Dros Res Conf* *38* : 69A.
- Bard, F., Casano, L., Mallabiabarrena, A., Wallace, E., Saito, K., Kitayama, H., Guizzunti, G., Hu, Y., Wendler, F., Dasgupta, R., *et al.* (2006). Functional genomics reveals genes involved in protein secretion and Golgi organization. *Nature* *439*, 604-607.
- Barres, B.A. (2008). The mystery and magic of glia: a perspective on their roles in health and disease. *Neuron* *60*, 430-440.
- Bayat, V., Jaiswal, M., and Bellen, H.J. (2011). The BMP signaling pathway at the *Drosophila* neuromuscular junction and its links to neurodegenerative diseases. *Current opinion in neurobiology* *21*, 182-188.
- Berger, C., Renner, S., Luer, K., and Technau, G.M. (2007). The commonly used marker ELAV is transiently expressed in neuroblasts and glial cells in the *Drosophila* embryonic CNS. *Developmental dynamics : an official publication of the American Association of Anatomists* *236*, 3562-3568.
- Brand, A.H., and Perrimon, N. (1993). Targeted gene expression as a means of altering cell fates and generating dominant phenotypes. *Development* *118*, 401-415.
- Bras, S., Martin-Lannere, S., Gobert, V., Auge, B., Breig, O., Sanial, M., Yamaguchi, M., Haenlin, M., Plessis, A., and Waltzer, L. (2012). Myeloid leukemia factor is a conserved regulator of RUNX transcription factor activity involved in hematopoiesis. *Proceedings of the National Academy of Sciences of the United States of America* *109*, 4986-4991.
- Brink, D.L., Gilbert, M., Xie, X., Petley-Ragan, L., and Auld, V.J. (2012). Glial processes at the *Drosophila* larval neuromuscular junction match synaptic growth. *PloS one* *7*, e37876.
- Brunner, E., Ahrens, C.H., Mohanty, S., Baetschmann, H., Loevenich, S., Potthast, F., Deutsch, E.W., Panse, C., de Lichtenberg, U., Rinner, O., *et al.* (2007). A high-quality catalog of the *Drosophila melanogaster* proteome. *Nature biotechnology* *25*, 576-583.
- Bulat, V., Rast, M., and Pielage, J. (2014). Presynaptic CK2 promotes synapse organization and stability by targeting Ankyrin2. *The Journal of cell biology* *204*, 77-94.
- Cheng, L., Locke, C., and Davis, G.W. (2011). S6 kinase localizes to the presynaptic active zone and functions with PDK1 to control synapse development. *The Journal of cell biology* *194*, 921-935.
- Coleman, M. (2005). Axon degeneration mechanisms: commonality amid diversity. *Nature reviews Neuroscience* *6*, 889-898.
- Collins, C.A., and DiAntonio, A. (2007). Synaptic development: insights from *Drosophila*. *Current opinion in neurobiology* *17*, 35-42.
- Collins, C.A., Wairkar, Y.P., Johnson, S.L., and DiAntonio, A. (2006). Highwire restrains synaptic growth by attenuating a MAP kinase signal. *Neuron* *51*, 57-69.

- De Langhe, S., Haataja, L., Senadheera, D., Groffen, J., and Heisterkamp, N. (2002). Interaction of the small GTPase Rac3 with NRBP, a protein with a kinase-homology domain. *International journal of molecular medicine* 9, 451-459.
- De Vos, K.J., Grierson, A.J., Ackerley, S., and Miller, C.C. (2008). Role of axonal transport in neurodegenerative diseases. *Annual review of neuroscience* 31, 151-173.
- Dietzl, G., Chen, D., Schnorrer, F., Su, K.C., Barinova, Y., Fellner, M., Gasser, B., Kinsey, K., Oettel, S., Scheiblaue, S., *et al.* (2007). A genome-wide transgenic RNAi library for conditional gene inactivation in *Drosophila*. *Nature* 448, 151-156.
- Dimitroff, B., Howe, K., Watson, A., Campion, B., Lee, H.G., Zhao, N., O'Connor, M.B., Neufeld, T.P., and Selleck, S.B. (2012). Diet and energy-sensing inputs affect TorC1-mediated axon misrouting but not TorC2-directed synapse growth in a *Drosophila* model of tuberous sclerosis. *PLoS one* 7, e30722.
- Dobens, L.L., Hsu, T., Twombly, V., Gelbart, W.M., Raftery, L.A., and Kafatos, F.C. (1997). The *Drosophila* bunched gene is a homologue of the growth factor stimulated mammalian TSC-22 sequence and is required during oogenesis. *Mechanisms of development* 65, 197-208.
- Dobens, L.L., Peterson, J.S., Treisman, J., and Raftery, L.A. (2000). *Drosophila* bunched integrates opposing DPP and EGF signals to set the operculum boundary. *Development* 127, 745-754.
- Doherty, J., Logan, M.A., Tasdemir, O.E., and Freeman, M.R. (2009). Ensheathing glia function as phagocytes in the adult *Drosophila* brain. *The Journal of neuroscience : the official journal of the Society for Neuroscience* 29, 4768-4781.
- Eaton, B.A., and Davis, G.W. (2005). LIM Kinase1 controls synaptic stability downstream of the type II BMP receptor. *Neuron* 47, 695-708.
- Eaton, B.A., Fetter, R.D., and Davis, G.W. (2002). Dynactin is necessary for synapse stabilization. *Neuron* 34, 729-741.
- Enneking, E.M., Kudumala, S.R., Moreno, E., Stephan, R., Boerner, J., Godenschwege, T.A., and Pielage, J. (2013). Transsynaptic coordination of synaptic growth, function, and stability by the L1-type CAM Neuroglian. *PLoS biology* 11, e1001537.
- Faeder, I.R., and Salpeter, M.M. (1970). Glutamate uptake by a stimulated insect nerve muscle preparation. *The Journal of cell biology* 46, 300-307.
- Featherstone, D.E., and Broadie, K. (2000). Surprises from *Drosophila*: genetic mechanisms of synaptic development and plasticity. *Brain research bulletin* 53, 501-511.
- Fouix, S., Martin-Lannere, S., Sanial, M., Morla, L., Lamour-Isnard, C., and Plessis, A. (2003). Overexpression of a novel nuclear interactor of Suppressor of fused, the *Drosophila* myelodysplasia/myeloid leukaemia factor, induces abnormal morphogenesis associated with increased apoptosis and DNA synthesis. *Genes to cells : devoted to molecular & cellular mechanisms* 8, 897-911.
- Freeman, M.R., and Doherty, J. (2006). Glial cell biology in *Drosophila* and vertebrates. *Trends in neurosciences* 29, 82-90.
- Fuentes-Medel, Y., Ashley, J., Barria, R., Maloney, R., Freeman, M., and Budnik, V. (2012). Integration of a retrograde signal during synapse formation by glia-secreted TGF-beta ligand. *Current biology : CB* 22, 1831-1838.
- Fuentes-Medel, Y., Logan, M.A., Ashley, J., Ataman, B., Budnik, V., and Freeman, M.R. (2009). Glia and muscle sculpt neuromuscular arbors by engulfing destabilized synaptic boutons and shed presynaptic debris. *PLoS biology* 7, e1000184.
- Fuger, P., Sreekumar, V., Schule, R., Kern, J.V., Stanchev, D.T., Schneider, C.D., Karle, K.N., Daub, K.J., Siebert, V.K., Flotenmeyer, M., *et al.* (2012). Spastic paraplegia mutation N256S in the neuronal microtubule motor KIF5A disrupts axonal transport in a *Drosophila* HSP model. *PLoS genetics* 8, e1003066.

- Gluderer, S., Brunner, E., Germann, M., Jovaisaite, V., Li, C., Rentsch, C.A., Hafen, E., and Stocker, H. (2010). Madm (Mlf1 adapter molecule) cooperates with Bunched A to promote growth in *Drosophila*. *Journal of biology* 9, 9.
- Gluderer, S., Oldham, S., Rintelen, F., Sulzer, A., Schutt, C., Wu, X., Raftery, L.A., Hafen, E., and Stocker, H. (2008). Bunched, the *Drosophila* homolog of the mammalian tumor suppressor TSC-22, promotes cellular growth. *BMC developmental biology* 8, 10.
- Goda, Y., and Davis, G.W. (2003). Mechanisms of synapse assembly and disassembly. *Neuron* 40, 243-264.
- Goold, C.P., and Davis, G.W. (2007). The BMP ligand Gbb gates the expression of synaptic homeostasis independent of synaptic growth control. *Neuron* 56, 109-123.
- Harvey, K.F. (2010). Bunched and Madm: a novel growth-regulatory complex? *Journal of biology* 9, 8.
- Hietakangas, V., and Cohen, S.M. (2009). Regulation of tissue growth through nutrient sensing. *Annual review of genetics* 43, 389-410.
- Hirose, F., Yamaguchi, M., Handa, H., Inomata, Y., and Matsukage, A. (1993). Novel 8-base pair sequence (*Drosophila* DNA replication-related element) and specific binding factor involved in the expression of *Drosophila* genes for DNA polymerase alpha and proliferating cell nuclear antigen. *The Journal of biological chemistry* 268, 2092-2099.
- Hooper, J.D., Baker, E., Ogbourne, S.M., Sutherland, G.R., and Antalis, T.M. (2000). Cloning of the cDNA and localization of the gene encoding human NRBP, a ubiquitously expressed, multidomain putative adapter protein. *Genomics* 66, 113-118.
- Hsu, Y.C., Chern, J.J., Cai, Y., Liu, M., and Choi, K.W. (2007). *Drosophila* TCTP is essential for growth and proliferation through regulation of dRheb GTPase. *Nature* 445, 785-788.
- Hughes, I., Binkley, J., Hurle, B., Green, E.D., Program, N.C.S., Sidow, A., and Ornitz, D.M. (2008). Identification of the Otopetrin Domain, a conserved domain in vertebrate otopetrins and invertebrate otopetrin-like family members. *BMC evolutionary biology* 8, 41.
- Hughes, I., Saito, M., Schlesinger, P.H., and Ornitz, D.M. (2007). Otopetrin 1 activation by purinergic nucleotides regulates intracellular calcium. *Proceedings of the National Academy of Sciences of the United States of America* 104, 12023-12028.
- Iida, M., Anna, C.H., Holliday, W.M., Collins, J.B., Cunningham, M.L., Sills, R.C., and Devereux, T.R. (2005). Unique patterns of gene expression changes in liver after treatment of mice for 2 weeks with different known carcinogens and non-carcinogens. *Carcinogenesis* 26, 689-699.
- Jan, L.Y., and Jan, Y.N. (1976a). L-glutamate as an excitatory transmitter at the *Drosophila* larval neuromuscular junction. *The Journal of physiology* 262, 215-236.
- Jan, L.Y., and Jan, Y.N. (1976b). Properties of the larval neuromuscular junction in *Drosophila melanogaster*. *The Journal of physiology* 262, 189-214.
- Jan, Y.N., and Jan, L.Y. (1978). Genetic dissection of short-term and long-term facilitation at the *Drosophila* neuromuscular junction. *Proceedings of the National Academy of Sciences of the United States of America* 75, 515-519.
- Jan, Y.N., Jan, L.Y., and Dennis, M.J. (1977). Two mutations of synaptic transmission in *Drosophila*. *Proceedings of the Royal Society of London Series B, Containing papers of a Biological character Royal Society* 198, 87-108.
- Jia, X.X., Gorczyca, M., and Budnik, V. (1993). Ultrastructure of neuromuscular junctions in *Drosophila*: comparison of wild type and mutants with increased excitability. *Journal of neurobiology* 24, 1025-1044.
- Jontes, J.D., and Phillips, G.R. (2006). Selective stabilization and synaptic specificity: a new cell-biological model. *Trends in neurosciences* 29, 186-191.
- Kania, A., Salzberg, A., Bhat, M., D'Evelyn, D., He, Y., Kiss, I., and Bellen, H.J. (1995). P-element mutations affecting embryonic peripheral nervous system development in *Drosophila melanogaster*. *Genetics* 139, 1663-1678.

- Kawamata, H., Nakashiro, K., Uchida, D., Hino, S., Omotehara, F., Yoshida, H., and Sato, M. (1998). Induction of TSC-22 by treatment with a new anti-cancer drug, vesnarinone, in a human salivary gland cancer cell. *British journal of cancer* *77*, 71-78.
- Kazemi-Esfarjani, P., and Benzer, S. (2002). Suppression of polyglutamine toxicity by a *Drosophila* homolog of myeloid leukemia factor 1. *Human molecular genetics* *11*, 2657-2672.
- Kennerdell, J.R., and Carthew, R.W. (2000). Heritable gene silencing in *Drosophila* using double-stranded RNA. *Nature biotechnology* *18*, 896-898.
- Kester, H.A., Blanchetot, C., den Hertog, J., van der Saag, P.T., and van der Burg, B. (1999). Transforming growth factor-beta-stimulated clone-22 is a member of a family of leucine zipper proteins that can homo- and heterodimerize and has transcriptional repressor activity. *The Journal of biological chemistry* *274*, 27439-27447.
- Khodosh, R., Augsburger, A., Schwarz, T.L., and Garrity, P.A. (2006). Bchs, a BEACH domain protein, antagonizes Rab11 in synapse morphogenesis and other developmental events. *Development* *133*, 4655-4665.
- Khuong, T.M., Habets, R.L., Slabbaert, J.R., and Verstreken, P. (2010). WASP is activated by phosphatidylinositol-4,5-bisphosphate to restrict synapse growth in a pathway parallel to bone morphogenetic protein signaling. *Proceedings of the National Academy of Sciences of the United States of America* *107*, 17379-17384.
- Killip, L.E., and Grewal, S.S. (2012). DREF is required for cell and organismal growth in *Drosophila* and functions downstream of the nutrition/TOR pathway. *Developmental biology* *371*, 191-202.
- Kim, J., Lee, S., Hwang, M., Ko, S., Min, C., and Kim-Ha, J. (2009). Bunched specifically regulates alpha/beta mushroom body neuronal cell proliferation during metamorphosis. *Neuroscience* *161*, 46-52.
- Kim, W.Y., Fayazi, Z., Bao, X., Higgins, D., and Kazemi-Esfarjani, P. (2005). Evidence for sequestration of polyglutamine inclusions by *Drosophila* myeloid leukemia factor. *Molecular and cellular neurosciences* *29*, 536-544.
- Koch, I., Schwarz, H., Beuchle, D., Goellner, B., Langegger, M., and Aberle, H. (2008). *Drosophila* ankyrin 2 is required for synaptic stability. *Neuron* *58*, 210-222.
- Landgraf, M., Bossing, T., Technau, G.M., and Bate, M. (1997). The origin, location, and projections of the embryonic abdominal motoneurons of *Drosophila*. *The Journal of neuroscience : the official journal of the Society for Neuroscience* *17*, 9642-9655.
- Lim, R., Winteringham, L.N., Williams, J.H., McCulloch, R.K., Ingley, E., Tiao, J.Y., Lalonde, J.P., Tsai, S., Tilbrook, P.A., Sun, Y., *et al.* (2002). MADM, a novel adaptor protein that mediates phosphorylation of the 14-3-3 binding site of myeloid leukemia factor 1. *The Journal of biological chemistry* *277*, 40997-41008.
- Liu, Z., Chen, Y., Wang, D., Wang, S., and Zhang, Y.Q. (2010). Distinct presynaptic and postsynaptic dismantling processes of *Drosophila* neuromuscular junctions during metamorphosis. *The Journal of neuroscience : the official journal of the Society for Neuroscience* *30*, 11624-11634.
- Lu, H., and Bilder, D. (2005). Endocytic control of epithelial polarity and proliferation in *Drosophila*. *Nature cell biology* *7*, 1232-1239.
- Marsh, J.L., and Thompson, L.M. (2004). Can flies help humans treat neurodegenerative diseases? *BioEssays : news and reviews in molecular, cellular and developmental biology* *26*, 485-496.
- Martin-Lannere, S., Lasbleiz, C., Sanial, M., Fouix, S., Besse, F., Tricoire, H., and Plessis, A. (2006). Characterization of the *Drosophila* myeloid leukemia factor. *Genes to cells : devoted to molecular & cellular mechanisms* *11*, 1317-1335.
- Martin-Pena, A., Acebes, A., Rodriguez, J.R., Sorribes, A., de Polavieja, G.G., Fernandez-Funez, P., and Ferrus, A. (2006). Age-independent synaptogenesis by phosphoinositide 3 kinase. *The Journal of neuroscience : the official journal of the Society for Neuroscience* *26*, 10199-10208.

- Martinek, S., and Young, M.W. (2000). Specific genetic interference with behavioral rhythms in *Drosophila* by expression of inverted repeats. *Genetics* 156, 1717-1725.
- McCabe, B.D., Marques, G., Haghghi, A.P., Fetter, R.D., Crotty, M.L., Haerry, T.E., Goodman, C.S., and O'Connor, M.B. (2003). The BMP homolog *Gbb* provides a retrograde signal that regulates synaptic growth at the *Drosophila* neuromuscular junction. *Neuron* 39, 241-254.
- Menon, K.P., Carrillo, R.A., and Zinn, K. (2013). Development and plasticity of the *Drosophila* larval neuromuscular junction. *Wiley interdisciplinary reviews Developmental biology* 2, 647-670.
- Miech, C., Pauer, H.U., He, X., and Schwarz, T.L. (2008). Presynaptic local signaling by a canonical wingless pathway regulates development of the *Drosophila* neuromuscular junction. *The Journal of neuroscience : the official journal of the Society for Neuroscience* 28, 10875-10884.
- Montagne, J., Stewart, M.J., Stocker, H., Hafen, E., Kozma, S.C., and Thomas, G. (1999). *Drosophila* S6 kinase: a regulator of cell size. *Science* 285, 2126-2129.
- Nakashiro, K., Kawamata, H., Hino, S., Uchida, D., Miwa, Y., Hamano, H., Omotehara, F., Yoshida, H., and Sato, M. (1998). Down-regulation of TSC-22 (transforming growth factor beta-stimulated clone 22) markedly enhances the growth of a human salivary gland cancer cell line in vitro and in vivo. *Cancer research* 58, 549-555.
- Natarajan, R., Trivedi-Vyas, D., and Wairkar, Y.P. (2013). Tuberous sclerosis complex regulates *Drosophila* neuromuscular junction growth via the TORC2/Akt pathway. *Human molecular genetics* 22, 2010-2023.
- Nave, K.A., and Trapp, B.D. (2008). Axon-glia signaling and the glial support of axon function. *Annual review of neuroscience* 31, 535-561.
- Ohno, K., Takahashi, Y., Hirose, F., Inoue, Y.H., Taguchi, O., Nishida, Y., Matsukage, A., and Yamaguchi, M. (2000). Characterization of a *Drosophila* homologue of the human myelodysplasia/myeloid leukemia factor (MLF). *Gene* 260, 133-143.
- Ohta, S., Shimekake, Y., and Nagata, K. (1996). Molecular cloning and characterization of a transcription factor for the C-type natriuretic peptide gene promoter. *European journal of biochemistry / FEBS* 242, 460-466.
- Omotehara, F., Uchida, D., Hino, S., Begum, N.M., Yoshida, H., Sato, M., and Kawamata, H. (2000). In vivo enhancement of chemosensitivity of human salivary gland cancer cells by overexpression of TGF-beta stimulated clone-22. *Oncology reports* 7, 737-740.
- Pereanu, W., Shy, D., and Hartenstein, V. (2005). Morphogenesis and proliferation of the larval brain glia in *Drosophila*. *Developmental biology* 283, 191-203.
- Perrimon, N., Lanjuin, A., Arnold, C., and Noll, E. (1996). Zygotic lethal mutations with maternal effect phenotypes in *Drosophila melanogaster*. II. Loci on the second and third chromosomes identified by P-element-induced mutations. *Genetics* 144, 1681-1692.
- Pielage, J., Bulat, V., Zuchero, J.B., Fetter, R.D., and Davis, G.W. (2011). Hts/Adducin controls synaptic elaboration and elimination. *Neuron* 69, 1114-1131.
- Pielage, J., Cheng, L., Fetter, R.D., Carlton, P.M., Sedat, J.W., and Davis, G.W. (2008). A presynaptic giant ankyrin stabilizes the NMJ through regulation of presynaptic microtubules and transsynaptic cell adhesion. *Neuron* 58, 195-209.
- Pielage, J., Fetter, R.D., and Davis, G.W. (2005). Presynaptic spectrin is essential for synapse stabilization. *Current biology : CB* 15, 918-928.
- Rawson, J.M., Lee, M., Kennedy, E.L., and Selleck, S.B. (2003). *Drosophila* neuromuscular synapse assembly and function require the TGF-beta type I receptor saxophone and the transcription factor Mad. *Journal of neurobiology* 55, 134-150.
- Reiter, L.T., Potocki, L., Chien, S., Gribskov, M., and Bier, E. (2001). A systematic analysis of human disease-associated gene sequences in *Drosophila melanogaster*. *Genome research* 11, 1114-1125.

- Rentsch, C.A., Cecchini, M.G., Schwaninger, R., Germann, M., Markwalder, R., Heller, M., van der Pluijm, G., Thalmann, G.N., and Wetterwald, A. (2006). Differential expression of TGFbeta-stimulated clone 22 in normal prostate and prostate cancer. *International journal of cancer Journal international du cancer* 118, 899-906.
- Rubin, G.M., and Lewis, E.B. (2000). A brief history of Drosophila's contributions to genome research. *Science* 287, 2216-2218.
- Saucedo, L.J., Gao, X., Chiarelli, D.A., Li, L., Pan, D., and Edgar, B.A. (2003). Rheb promotes cell growth as a component of the insulin/TOR signalling network. *Nature cell biology* 5, 566-571.
- Sawado, T., Hirose, F., Takahashi, Y., Sasaki, T., Shinomiya, T., Sakaguchi, K., Matsukage, A., and Yamaguchi, M. (1998). The DNA replication-related element (DRE)/DRE-binding factor system is a transcriptional regulator of the Drosophila E2F gene. *The Journal of biological chemistry* 273, 26042-26051.
- Schmid, A., Chiba, A., and Doe, C.Q. (1999). Clonal analysis of Drosophila embryonic neuroblasts: neural cell types, axon projections and muscle targets. *Development* 126, 4653-4689.
- Schmidt, I., Thomas, S., Kain, P., Risse, B., Naffin, E., and Klambt, C. (2012). Kinesin heavy chain function in Drosophila glial cells controls neuronal activity. *The Journal of neuroscience : the official journal of the Society for Neuroscience* 32, 7466-7476.
- Schuster, C.M., Davis, G.W., Fetter, R.D., and Goodman, C.S. (1996). Genetic dissection of structural and functional components of synaptic plasticity. I. Fasciclin II controls synaptic stabilization and growth. *Neuron* 17, 641-654.
- Sepp, K.J., Schulte, J., and Auld, V.J. (2000). Developmental dynamics of peripheral glia in Drosophila melanogaster. *Glia* 30, 122-133.
- Shen, K., and Cowan, C.W. (2010). Guidance molecules in synapse formation and plasticity. *Cold Spring Harbor perspectives in biology* 2, a001842.
- Shostak, K.O., Dmitrenko, V.V., Garifulin, O.M., Rozumenko, V.D., Khomenko, O.V., Zozulya, Y.A., Zehetner, G., and Kavsan, V.M. (2003). Downregulation of putative tumor suppressor gene TSC-22 in human brain tumors. *Journal of surgical oncology* 82, 57-64.
- Sigrist, S.J., Thiel, P.R., Reiff, D.F., Lachance, P.E., Lasko, P., and Schuster, C.M. (2000). Postsynaptic translation affects the efficacy and morphology of neuromuscular junctions. *Nature* 405, 1062-1065.
- Steiger, D., Furrer, M., Schwinkendorf, D., and Gallant, P. (2008). Max-independent functions of Myc in Drosophila melanogaster. *Nature genetics* 40, 1084-1091.
- Stocker, H., Radimerski, T., Schindelholz, B., Wittwer, F., Belawat, P., Daram, P., Breuer, S., Thomas, G., and Hafen, E. (2003). Rheb is an essential regulator of S6K in controlling cell growth in Drosophila. *Nature cell biology* 5, 559-565.
- Stork, T., Engelen, D., Krudewig, A., Silies, M., Bainton, R.J., and Klambt, C. (2008). Organization and function of the blood-brain barrier in Drosophila. *The Journal of neuroscience : the official journal of the Society for Neuroscience* 28, 587-597.
- Takahashi, Y., Yamaguchi, M., Hirose, F., Cotterill, S., Kobayashi, J., Miyajima, S., and Matsukage, A. (1996). DNA replication-related elements cooperate to enhance promoter activity of the drosophila DNA polymerase alpha 73-kDa subunit gene. *The Journal of biological chemistry* 271, 14541-14547.
- Tanaka, H., Takasu, E., Aigaki, T., Kato, K., Hayashi, S., and Nose, A. (2004). Formin3 is required for assembly of the F-actin structure that mediates tracheal fusion in Drosophila. *Developmental biology* 274, 413-425.
- Tee, A.R., Manning, B.D., Roux, P.P., Cantley, L.C., and Blenis, J. (2003). Tuberous sclerosis complex gene products, Tuberin and Hamartin, control mTOR signaling by acting as a GTPase-activating protein complex toward Rheb. *Current biology : CB* 13, 1259-1268.

- Torroja, L., Packard, M., Gorczyca, M., White, K., and Budnik, V. (1999). The *Drosophila* beta-amyloid precursor protein homolog promotes synapse differentiation at the neuromuscular junction. *The Journal of neuroscience : the official journal of the Society for Neuroscience* *19*, 7793-7803.
- Treisman, J.E., Lai, Z.C., and Rubin, G.M. (1995). Short sighted acts in the decapentaplegic pathway in *Drosophila* eye development and has homology to a mouse TGF-beta-responsive gene. *Development* *121*, 2835-2845.
- Uchida, D., Kawamata, H., Omotehara, F., Miwa, Y., Hino, S., Begum, N.M., Yoshida, H., and Sato, M. (2000). Over-expression of TSC-22 (TGF-beta stimulated clone-22) markedly enhances 5-fluorouracil-induced apoptosis in a human salivary gland cancer cell line. *Laboratory investigation; a journal of technical methods and pathology* *80*, 955-963.
- Urbach, R., and Technau, G.M. (2004). Neuroblast formation and patterning during early brain development in *Drosophila*. *BioEssays : news and reviews in molecular, cellular and developmental biology* *26*, 739-751.
- Van Roessel, P., Hayward, N.M., Barros, C.S., and Brand, A.H. (2002). Two-color GFP imaging demonstrates cell-autonomy of GAL4-driven RNA interference in *Drosophila*. *Genesis* *34*, 170-173.
- Vartiainen, M.K., and Machesky, L.M. (2004). The WASP-Arp2/3 pathway: genetic insights. *Current opinion in cell biology* *16*, 174-181.
- Venken, K.J., Carlson, J.W., Schulze, K.L., Pan, H., He, Y., Spokony, R., Wan, K.H., Koriabine, M., de Jong, P.J., White, K.P., *et al.* (2009). Versatile P[acman] BAC libraries for transgenesis studies in *Drosophila melanogaster*. *Nature methods* *6*, 431-434.
- Venken, K.J., He, Y., Hoskins, R.A., and Bellen, H.J. (2006). P[acman]: a BAC transgenic platform for targeted insertion of large DNA fragments in *D. melanogaster*. *Science* *314*, 1747-1751.
- Wu, J.T., Lin, H.C., Hu, Y.C., and Chien, C.T. (2005). Neddylation and deneddylation regulate Cul1 and Cul3 protein accumulation. *Nature cell biology* *7*, 1014-1020.
- Wucherpennig, T., Wilsch-Brauninger, M., and Gonzalez-Gaitan, M. (2003). Role of *Drosophila* Rab5 during endosomal trafficking at the synapse and evoked neurotransmitter release. *The Journal of cell biology* *161*, 609-624.
- Yan, R., Luo, H., Darnell, J.E., Jr., and Dearolf, C.R. (1996). A JAK-STAT pathway regulates wing vein formation in *Drosophila*. *Proceedings of the National Academy of Sciences of the United States of America* *93*, 5842-5847.
- Yoneda-Kato, N., Look, A.T., Kirstein, M.N., Valentine, M.B., Raimondi, S.C., Cohen, K.J., Carroll, A.J., and Morris, S.W. (1996). The t(3;5)(q25.1;q34) of myelodysplastic syndrome and acute myeloid leukemia produces a novel fusion gene, NPM-MLF1. *Oncogene* *12*, 265-275.
- Yu, J., Ershler, M., Yu, L., Wei, M., Hackanson, B., Yokohama, A., Mitsui, T., Liu, C., Mao, H., Liu, S., *et al.* (2009). TSC-22 contributes to hematopoietic precursor cell proliferation and repopulation and is epigenetically silenced in large granular lymphocyte leukemia. *Blood* *113*, 5558-5567.
- Zinke, I., Schutz, C.S., Katzenberger, J.D., Bauer, M., and Pankratz, M.J. (2002). Nutrient control of gene expression in *Drosophila*: microarray analysis of starvation and sugar-dependent response. *The EMBO journal* *21*, 6162-6173.
- Zito, K., Parnas, D., Fetter, R.D., Isacoff, E.Y., and Goodman, C.S. (1999). Watching a synapse grow: noninvasive confocal imaging of synaptic growth in *Drosophila*. *Neuron* *22*, 719-729.
- Zlokovic, B.V. (2008). The blood-brain barrier in health and chronic neurodegenerative disorders. *Neuron* *57*, 178-201.

Additional Reference: Gluderer, S. (2009). BunA and Madm Co-operate to Promote Growth in *Drosophila*. PhD Thesis. ETH Zürich.

6.4 Acknowledgement

This work was performed in the Pielage Lab at the Friedrich Miescher Institute in Basel. I want to thank Jan for the opportunity to do my PhD in his lab. Furthermore, I would like to thank Jan for his support, guidance, inspiring scientific discussions and insights throughout my work.

I want to express my gratitude to my thesis committee, Prof. Silvia Arber and Prof. Heinrich Reichert, for their support throughout my PhD.

I would also like to thank the members of the Pielage Lab for the nice working atmosphere and many long, but cheerful hours in the lab.

Last but not least, I want to thank my family, partner and friends for their constant love and support.

6.5 Curriculum vitae

Ingrid Daniela Kieweg

Personal Information	
Address	Bärenfelsenstrasse 20, 4057 Basel, Switzerland
Nationality	Austrian
Date of birth	22.05.1984
Education & Academic Studies	
2009 - 2014	Degree: PhD in Neurobiology Friedrich Miescher Institute for Biomedical Research, Basel, Supervisor: Dr. Jan Pielage, Title: "Madm Controls Synapse Development and Stability"
2007 - 2008	Degree: Magistra of Natural Sciences Division of Neuronal Cell Biology, Center for Brain Research, Medical University of Vienna, Supervisor: O. Univ.-Prof. Dr. Michael Kiebler, Title: "Analysis and Characterisation of Five Novel Barentsz Interactors in the Context of Nonsense- mediated mRNA Decay"
2002 - 2008	Study "Molecular Biology" (A 490) University of Vienna, Specialisations: Genetics, Cell Biology & Neuroscience
1994 - 2002	Gymnasium with supplementary tuitions in Chemistry, Physics and Biology
Scientific Work Experiences & Traineeships	
03. – 04.2007	Internship "Neurobiology & Genetics" Medical University of Vienna, Center for Brain Research, Division of Neuronal Cell Biology, Supervisors: O. Univ.-Prof. Dr. Paolo Macchi and O. Univ.-Prof. Dr. Michael Kiebler
07. & 12.2006	Internship "Cell Biology" University of Vienna, Department of Molecular Cell Biology on the Campus Vienna Biocenter, Supervisors: Univ.-Ass. Mag. Dr. Christina Abrahamsberg and O. Univ.-Prof. Dr. Gerhard Wiche
12.2005	Internship "Neurobiology" Medical University of Vienna, Center for Brain Research, University course „Basics of Neuroscience“